UNIVERSITY OF SOUTHAMPTON

Optical characterisation and reflectance modelling in Case II waters: quantitative tools for investigations of coastal environments

by

Mark D. Dowell

Submitted in partial fulfilment of the requirements
for the Degree of Doctor of Philosophy

at

Department of Oceanography,
University of Southampton,
Southampton,
United Kingdom
October 1998

to Cristina

UNIVERSITY OF SOUTHAMPTON
ABSTRACT
FACULTY OF SCIENCE
OCEANOGRAPHY
Doctor of Philosophy

Optical characterisation and reflectance modelling in Case II waters: quantitative tools for investigations of coastal environments

by Mark Dowell

For over two decades, ocean colour remote sensing has provided an unprecedented perspective on the complex dynamics of biogeochemical processes in coastal waters. However, with the first generation of sensors this information could be only considered qualitatively in these regions. With the second generation of sensors, more advanced instrumental and theoretical experience, and extensive field datasets, the foundations now exist on which analytical and semi-analytical solutions can be sought to make a truly quantitative use of ocean colour imagery for coastal regions. These solutions will allow for the differentiation of multiple optically active components (Chlorophyll, Total Suspended Matter and Coloured Dissolved Organic Matter) and the generation of additional products such as individual pigment concentrations.

The inherent optical properties of the water column ultimately provide the theoretical link between the optically active components and the satellite measured radiances. Of these inherent optical properties, the absorption coefficient largely governs the spectral shape of the satellite-derived water leaving radiances. A study was thus made to establish the minimum number of absorbing component to adequately describe the total coefficient in coastal waters. It was shown that the co-variability of detrital and yellow substance absorption could not be assumed, and thus these two components need to be considered separately. The absorption budget itself was considered, in terms of the spectral variability and absolute magnitude, in an attempt to formulate improved spectral models of the individual absorption coefficients. A comparison of variance spectra between measured and modelled absorption coefficients showed that the proposed spectral models adequately reproduced the variability found in the field datasets, improving on traditional formulations.

A methodology is proposed here to satisfy a community requirement for a regional solution to developing algorithms in coastal waters. A three component model, which allows maximum variability of the non-chlorophyllous components, was developed. This model was then systematically applied to a range of input values of the forward model defined using lognormal distributions, yielding a dataset of reflectances for the studied area. A principal component analysis was then performed on the simulated dataset. A multiple regression was carried out on the resulting eigenvectors and the input values of the optically active components to define the algorithms for the chosen region for the retrieval of chlorophyll, total suspended matter and yellow substance.

A case study was made applying the method to the South Baltic and a validation dataset from the same region showed the capacity of this method to retrieve the concentrations of the individual optically active components to within the accuracy defined by NASA for Case I water chlorophyll retrieval. The sensitivity of the method, to inelastic processes and bottom reflectance, was considered. The study was made both through the influence on the absolute signal as well as the influence on the shape of the characteristic vectors that are retrieved from the simulated reflectance in an attempt to assess the impact on the algorithm development procedure. In both cases the influence is shown to be minimum for wavelengths below 650nm.

An alternative methodology is also presented (Direct Inversion Algorithm) which is based on the inversion of absolute reflectances for the retrieval of total absorption. This coefficient is then deconvolved into the individual constituents using the absorption model presented earlier in the study and ultimately the retrieval of multiple pigment concentration is achieved from the phytoplankton pigment absorption. This method was validated for an in-situ dataset and shown to retrieve chlorophyll "a" to within 30% accuracy. The applications of such a technique were considered in the context of primary production in coastal waters and chemotaxonomy.

Table of Contents

Abstract i
Table of Contents ii
List of Figures v
List of Tables vii
List of Appendixes vii
Acknowledgments viii
List of Symbols used ix
Glossary xv

Chapter 1: Introduction

1.1. Bio-optical Oceanography 2
1.2. Case I vs. Case II waters 4
1.3. Statement of the Problem 5
1.4. Comparative role of satellite and in-situ measurements 6
1.5. Objectives and Applications 9
1.6. Summary of the content of the main chapters 11

Chapter 2: Bio-optical characteristics of Case II waters: the significance and variability of the Non-Chlorophyllous components.

2.1. Introduction and background on Region of Interest 14
2.2. Datasets Used 15
2.2.1. Baltic dataset (ULISSE) 15
2.2.2. Adriatic dataset (CoASTS) 18
2.2.3. Tokyo Bay dataset 18
2.3. Measurements made 20
2.3.1. Geophysical measurements: Chlorophyll "a", TSM, DOC 20
2.3.2. Physical measurements-Conductivity, Temperature, Density, Beam attenuation 21
2.3.3. Measurement of AOPs (i.e. L_u E_d and calculation of R) 21
2.3.4. CDOM measurements (absorption, fluorescence, Quantum Yield) 22
2.3.5. In-vivo pigment measurements (a_{ph} and a_d) 24
2.3.6. Meteorological Measurements 25
2.4. Theory and Results 25
2.4.1. The co-variability of the non-chlorophyllous contributions to absorption 26
2.4.2. The spectral variability of absorption in Case II waters 29
2.4.3. The budget of absorption in Case II waters 31
2.5. Discussion 37

2.5.1. Absorption modelling and sources of variability 37
2.5.2. Spectral variability of pigment absorption, significance in forward modelling 50
2.5.3. An IOP classification and its significance in algorithm development 52
2.6. Conclusions 55

Chapter 3: A regional three component Reflectance R(λ) model.

3.1. Introduction 58
3.2. Reflectance Theory 60
3.3. Statistical Distributions of the OACs 63
3.4. Forward Model 66
3.4.1. Relationship between OACs and the IOPs 66
3.4.2. Inherent Optical Property parameterisation 68
3.4.2.1. Parameterisation of absorption 71
3.4.2.2. Parameterisation of the backscattering 76
3.4.3. Calculation of the proportionality factor (f) 81
3.4.4. Determination of the Q-factor 84
3.5. Inversion procedure 91
3.6. Discussion 97
3.6.1. Parameterisation of CDOM absorption 97
3.6.2. The two component model for scattering 101
3.6.3. Determination of f is the remote sensing context 102
3.6.4. Reproduced shape of reflectance 104
3.6.5. Adequacy of the spectral information from RS wavelengths for Case II waters 105
3.6.6. PCA inversion scheme and the geophysical algorithms 106
3.7. Conclusions 107

Chapter 4: Contamination of the elastic signal by transpectral processes and bottom reflectance

4.1. Introduction 110
4.2. Methodology and Theory 111
4.2.1. Determination of the surface light field 111
4.2.2. Modelisation of in-elastic processes and bottom reflectance 115
4.2.2.1. Modelisation of CDOM fluorescence 115
4.2.2.2. Modelisation of Chlorophyll "a" fluorescence 116
4.2.2.3. Modelisation of Phycoerythrin fluorescence 118
4.2.2.4. Modelisation of Raman Scattering 121
4.2.2.5. Modelisation of bottom reflectance 121
4.3. Results 122
4.3.1. Proportional contribution of inelastic processes to modelled 122

reflectance
4.3.2. Influence of in-elastic processes on calculated eigenvectors 125
4.4. Discussion 127
4.4.1. The contribution of inelastic processes to absolute reflectance 127
4.4.2. The importance of the in-elastic processes in the PCA inversion procedure 128
4.4.3. Partition of the visible spectral range by elastic and inelastic processes 132
4.5. Conclusions 134

Chapter 5: Retrieval of spectral absorption and multiple pigments from absolute reflectance: Direct Inversion Algorithm

5.1. Introduction 138
5.2. Methodology and Results 140
5.2.1. Estimation of the backscattering coefficient 141
5.2.2. Calculation of the proportionality factor 144
5.2.3. Evaluation of the total absorption coefficient 147
5.2.4. Deconvolution of the absorption coefficient 147
5.2.5. Calculation of multiple pigment concentrations 149
5.3. Discussion 152
5.3.1. Parameterisation of b_{bTOT} - a generic algorithm for TSM 152
5.3.2. Determination of f and possibility of replacing with f/Q 153
5.3.3. Considerations on band position and number on pigment retrieval accuracy 155
5.3.4. Globalisation of the algorithm suite 157
5.3.5. Application of presented algorithm 158
5.3.5.1. Primary production 160
5.3.5.2. Chemotaxonomy 163
5.4. Conclusions 164

Chapter 6: Summary and Conclusions

6.1. Summary of the Individual Chapters 168
6.2. Accomplishment of the Main goal and objectives 171
6.3. Applications of presented work 172
6.4. Future work 173

Bibliography 176

List of Figures

Chapter 1

Figure 1.1: Physical and biological ocean processes and space and time scales 8

Chapter 2

Figure 2.1: Station map for the ULISSE campaigns 17
Figure 2.2: Example CTD profiles from the ULISSE campaigns for April, August and September 19
Figure 2.3: Correlation plots for a_{ys} vs. S_{ys} and a_d vs. S_d 28
Figure 2.4: a-c absorption spectra for a_{ph}, a_d, a_{ys} 30
Figure 2.5: a-c normalised spectra of 2.4 32
Figure 2.6: a-c variance spectra calculated from 2.5 33
Figure 2.7: Total absorption coefficients and absorption budgets for individual contributions at the different sites (Baltic, Adriatic, Tokyo Bay) 35
Figure 2.8: Ternary plot of the spectrally averaged absorption coefficients of each constituent for all datasets considered 36
Figure 2.9: a first eigenvector for yellow substance and detritus for each dataset 39
b second eigenvector for yellow substance and detritus for each dataset 39
Figure 2.10: TFA residual analysis for a_d and a_{ys} 40
Figure 2.11: Exponential slopes as fits for the first eigenvectors for a_{ys} and a_d 42
Figure 2.12: Normalised $a_p'675$ and $a_{ph}'675$ spectra 44
Figure 2.13: a a_{tot} and a_{ys} spectra from deconvolution 45
b $a_{ys}412$ calculated against $a_{ys}412$ measured 45
Figure 2.14: a a_d spectra from deconvolution 46
b a_d412 calculated against a_d412 measured 46
Figure 2.15: a aph spectra from deconvolution 48
Figure 2.16: Spectral variance of ays and ad after TFA reconstruction 49
Figure 2.17: a a_{ph} spectra from Bricaud model 51
Figure 2.18: Classification scheme based on a ternary plot 54

Chapter 3

Figure 3.1: a) Figure from Sathyendranath and Platt 1997 their figure 1 62
b) Figure from Sathyendranath and Platt 1997 their figure 2 62
Figure 3.2: Probability distribution functions for the OACs in the Southern Baltic 65
Figure 3.3: Plot showing correlation between a_d440 and CHL, TSM variable 69
Figure 3.4: a) v_s versus TSM relationship 70
b) v_l versus CHL relationship 70
Figure 3.5: a) variability of $a^*_{ph}(\lambda)$ for Baltic ULISSE stations 72
b) modelled $a_{ph}(\lambda)$ spectra 72
Figure 3.6: Modelled spectra of $a_d(\lambda)$ 74
Figure 3.7: a) Graph showing S_{ys} versus $a_{ys}400$ relationships 75
b) Model $a_{ys}(\lambda)$ spectra 75
Figure 3.8: a) water absorption spectra after Pope and Fry (1997) 77

b) water backscatter spectra used in model 77
Figure 3.9: Mass specific volume scattering phase functions for small and large particles 78
Figure 3.10: a) modelled spectra for the backscattering by small particles 80
b) modelled spectra for the backscattering by large particles 80
Figure 3.11: a) modelled spectra of the total absorption coefficient 82
b) modelled spectra of the total backscattering coefficient 82
c) modelled spectra of normalised backscattering albedo 82
Figure 3.12: a) Values of f for ULISSE stations 85
b) Values of Q for ULISSE stations 85
Figure 3.13: a) simulated reflectance spectra at 1nm resolution and in-situ reflectance 87
b) Comparison for four spectra of modelled and in-situ reflectance 88
Figure 3.14: Simulated reflectance for 5 satellite bandsets 90
Figure 3.15: First four eigenvectors for a) satellite sensors and 93
b) in-situ data 94
Figure 3.16: Correlation between the OACs calculated through the developed algorithms and the measured values from the ULISSE datasets 96
Figure 3.17: Synchronous fluorescence spectra showing division between terrestrial and autochtonous inputs 100
Figure 3.18: Graph of f versus sun zenith angle in air 103

Chapter 4

Figure 4.1: a) spectral distribution of the aerosol transmittance 114
b) spectral distribution of downwelling irradiance 114
Figure 4.2: a) CDOM fluorescence emission spectra 117
b) Total absorption coefficient 117
c) CDOM absorption coefficient 117
Figure 4.3: a) Specific absorption coefficients for main photosynthetic pigments 120
b) Chlorophyll measured versus chlorophyll calculated 120
c) Calculated absorption spectra for PEB 120
Figure 4.4: Elastic reflectance spectra from chapter 3 model (at top) then two columns: left is inelastically modelled reflectance and right is contribution of inelastic to elastic signal. Processes considered in descending order are: bottom reflectance, CDOM, Chlorophyll, and PEB fluorescence and Raman Scattering. 123
Figure 4.5: Effect on the 1st and 2nd eigenvector of the addition of inelastic processes 126
Figure 4.6: Plot showing FS due to elastic processes versus those due to elastic + F_{ys} 130
Figure 4.7: The effect of chlorophyll SSF on eigenvectors at satellite wavelength 131
Figure 4.8: Relative spectral contributions of elastic and inelastic processes 133

Chapter 5

Figure 5.1: a) Eigenvectors calculated using different reflectance models 143
b) Calculated against measured TSM concentrations 143
Figure 5.2: Calculated spectral distribution of backscattering coefficient 145
Figure 5.3: a) spectral distribution of f calculated from Morel and Gentili 1991 146
b) f from Morel and Gentili (1991) versus f from Sathyendranath and Platt 146

Figure 5.4: Calculated spectral distribution of the total absorption coefficient 148
Figure 5.5: Measured against modelled phytoplankton absorption coefficients at three wavelengths (443,490,520) 150
Figure 5.6: a) Modelled spectral phytoplankton pigment absorption spectra 151
b) Individual pigment specific absorption spectra 151
c) Chlorophyll "a" calculated against measured 151
Figure 5.7: Chlorophyll calculated and measured using three different band combinations 156
Figure 5.8: Flowchart illustrating inputs outputs and processes of the proposed method 159

List of Tables

Chapter 2

Table 2.1: Correlation and covariance results from the a_{ys} a_d spectral properties 27
Table 2.2: First two eigenvectors for a_{ys} and a_d at SeaWiFS/ OCTS wavelengths 41

Chapter 3

Table 3.1: relationship between OACs and the IOPs 67
Table 3.2: Haltrin's coefficients for P_s and P_l 84
Table 3.3: Sensors and wavelengths considered in the inversion procedure 89
Table 3.4: Table showing coefficients resulting for each algorithms 95

Chapter 4

Chapter 5

Table 5.1: Table illustrating channels of the MERIS sensor and optimal band wavelengths of centres of gaussian peaks. 157

List of Appendices

Appendix 2.A: Ferrari et. al. 1996 (Marine Chemistry)

Appendix 2.B: Ferrari and Dowell 1998 (Estuarine, Coastal and Shelf Science)

Appendix 2.C: Dowell et. al. 1996 (Proc. Ocean Optics XIII)

Acknowledgements

To begin I would like to thank from the University of Southampton, Dr. S. R Boxall and Prof. M. B. Collins, who provided me the opportunity to embark on this thesis and who gave me the initial stimulus and direction. My supervisor, Dr. Boxall, in particular has been a constant point of reference throughout my thesis often taking time to visit the JRC to discuss the progress of my work with me.

I am also of course deeply indebted to Dr. Schlittenhardt the Head of the Marine Environment (ME) Unit at the JRC. Apart from offering sincere encouragement and showing a genuine interest in the topic of my work, he also helped secure funding for a Training and Mobility grant for me to stay at the JRC.

During the fieldwork undertaken at the beginning of my thesis I received help and support from the scientists of the Institute of Oceanology of the Polish Academy of Science and the crew of the *r.v. Oceania*. Also pertaining to the field activities, I have to thank Dott. Massimo Ferrari (ME Unit) who helped me get my footing with the measurement protocols and laboratory work and with whom I began some of the data analysis.

I subsequently had the good fortune to meet Dr. J-F Berthon (ME Unit) and it was discussions with him that directed my research interests more specifically to those subject of the presented thesis. Similarly, recent developments in the ME Unit's activities have provided a continuous source of information on various topics that have contributed positively to shaping the current thesis. Notably of these, is the "CAL/VAL team" co-ordinated by Dr. Giuseppe Zibordi (responsible for the Adriatic dataset used in Chapter 2). Also I feel indebted to Dr. B. Sturm (ME Unit) whose broad knowledge of the fields of radiative transfer theory and marine optics have been a constant input to the bio-optical modelling.

The greatest recognition, however, goes to Dr. Nicolas Hoepffner. Nick has been my closest "confident" since the second year of my thesis and he slowly first unofficially then officially took on the role of my supervision at the JRC. He has demonstrated a great deal of patience and comprehension helping me continuously on a one-to-one basis and has stimulated many of the ideas, which form the core chapters of the presented thesis.

Finally, my thanks go to my family and friends who have showed considerable moral support all throughout my thesis. My parents who particularly in the first years gave me support and encouragement and to my lovely wife Cristina who has been extremely patient with my sometimes irrational behaviour.

List of Symbols

$\tilde{b}_b$	Backscattering to scattering ratio
$\hat{L}_u$	Corrected/True upwelled spectral radiance
$\tilde{L}_u$	Measured upwelled spectral radiance
$[Lw]_N(\lambda)$	Normalised water leaving radiance
$A(\lambda)$	1st spectral constant from Bricaud et. al. 1995
$a(\lambda)$	Spectral absorption coefficient
$a^*_{a,b,c,car,phyc}$	Concentration specific absorption coefficient for individual pigments
a^*_c	Chlorophyll specific absorption coefficient
a^*_f	Concentration specific absorption coefficient for marine fulvic acid
a^*_h	Concentration specific absorption coefficient for marine humic acid
$a^*_{ph}(\lambda)$	Chlorophyll specific pigment absorption spectra
a, b, c, car, phyc	Individual pigment chlorophyll "a", chlorophyll "b", chlorophyll "c", carotenoids, phycoerythrin
$a'_p675(\lambda)$	Mean particle absorption coefficient normalised at 675
$a'_{ph}675(\lambda)$	Mean phytoplankton pigment absorption coefficient normalised at 675
$a_{d,ys,ph,w,tot}(\lambda)$	Absorption coefficients for: detritus, yellow substance , phytoplankton water and total
$a_p(\lambda)$	Spectral absorption coefficient for particles
$a_{qs}(\lambda)$	Absorption coefficient of quinine sulphate
$a_s(\lambda)$	Absorption coefficient of the sample
$a_{sub}(\lambda)$	absorption of all substance apart from water
$a_w(\lambda)$	Spectral absorption coefficient for water

a_x	Spectrally averaged absorption coefficient where x is each component
ϕ	Azimuth angle
$B(\lambda)$	2nd spectral constant from Bricaud et. al. 1995
$b(\lambda)$	Spectral scattering coefficient
$b_{b\ bs,bl,bw,tot}(\lambda)$	The spectral backscattering coefficient due to: small particles, large particles, water and total
$b_b(\lambda)$	Backward scattering coefficient
B_{chl}	Chlorophyll biomass concentration
$b_f(\lambda)$	Forward scattering coefficient
b_{min}	Part of the total scattering due to phytoplankton
b_r	Raman scattering coefficient
$b_u(\lambda)$	Upward scattering coefficient
C	Junge Particle Size Distribution amplitude factor
$c(\lambda)$	Spectral attenuation coefficient
C'	Coefficient related to phytoplankton absorption (Prieur and Sathyendranath 1981)
$C_{a,b,c,car,phyc}$	Concentration of the individual photosynthetic pigments
C_f	Concentration of marine fulvic acid
C_h	Concentration of marine humic acid
D	Day number
E^*_m	Dimensionless irradiance at local noon $E^*_m=E^0_m/E_k$
E_o	Quantum scalar irradiance
$E_d(\lambda)$	Downwelled spectral irradiance
$E_{dd}(\lambda)$	Spectral direct downwelling irradiance
$E_{ds}(\lambda)$	Spectral direct downwelling irradiance
E_k	Adaptation parameter of the P-I curve $E_k=P^B_m/\alpha^B$
$E_{od}(\lambda)$	Spectral downwelling scalar irradiance

$E_u(\lambda)$	Upwelled spectral irradiance
f	Proportionality factor
f_b	Zaneveld shape parameter
f_l	Zaneveld shape parameter
F_o	Mean extraterrestrial solar flux
$F_{qs}(\lambda)$	Fluorescence of Quinine Sulphate
$F_s(\lambda)$	Fluorescence of the sample
Fs_ia_d	ith factor score for the absorption of detritus
FS_ia_{ys}	ith factor score for the absorption of yellow substance
H	Depth to the bottom
I_a	Diffuse component of irradiance arising from aerosol scattering after molecular absorption
I_r	Diffuse component of irradiance arising from Rayleigh scattering after molecular absorption
γ	Junge exponent of PSD
k_1	Slope of exponential fit for marine fulvic acid
k_2	Slope of exponential fit for marine humic acid
$K_d(\lambda)$	Spectral diffuse attenuation coefficient
$L_u(\lambda)$	Upwelled spectral radiance
$L_w(\lambda)$	Water leaving radiance
m	complex index of refraction
OD	Optical density
P(z)	Instantaneous Primary Production
P'	Coefficient related to particle absorption (Prieur and Sathyendranath 1981)
$P^B{}_m$	Saturation rate of carbon fixation
p_l	Polynomial representation of the large particle mass specific VSF
p_s	Polynomial representation of the large particle mass specific VSF

Pz,t	Depth and time integrated primary production
Q	Q factor defined as E_u/L_u
Q_{ie}	Q factor for inelastic processes
$R(\lambda)$	Spectral diffuse irradiance reflectance
$R_{bot}(\lambda)$	Reflectance due to bottom contribution
$R_{fchl}(\lambda)$	Reflectance due to the fluorescence of chlorophyll
$R_{fphyc}(\lambda)$	Reflectance due to the fluorescence of phycoerythrin
$R_{fys}(\lambda)$	Reflectance due to the fluorescence of yellow substance
$R_{ram}(\lambda)$	Reflectance due to Raman Scattering
$R_{rs}(\lambda)$	Remote Sensing Reflectance (after Carder and Steward 1985) L_w/E_d
$RSR(\lambda)$	Remote Sensing Reflectance (after Zaneveld 1982) L_u/E_{od}
$s(\lambda)$	Shape factor for the VSF from Sathyendranath and Platt 1991 (b_u/b_b)
S_d	Slope of detritus exponential fit
θ	Solar Zenith Angle
S_{ys}	Slope of yellow substance exponential fit
T_{ie}	Intensity of the inelastically scattered light
$U_i a_d$	ith eigenvector for the absorption of detritus
$U_i a_{ys}$	ith eigenvector for the absorption of yellow substance
v_l	Volume of large particles (after Kopelevich 1983)
v_s	Volume of small particles (after Kopelevich 1983)
X	Concentration of the individual OAC for PDF
Y'	Coefficient related to yellow substance absorption (Prieur and Sathyendranath 1981)
z	Depth in the water column positive from surface down
α	Angstrom exponent
α^B	Initial slope of the P-I curve

$\beta(\psi,\lambda)$	Volume Scattering Function
$\beta^*_l(\psi)$	mass specific VSF for large particles
$\beta^*_s(\psi)$	mass specific VSF for small particles
β_{ie}	VSF for inelastically scattered light
Φ_{fchl}	Quantum yield of the fluorescence by chlorophyll
Φ_{fphyc}	Quantum Yield of the fluorescence of phycoerythrin
Φ_{fys}	Quantum yield of the fluorescence by yellow substance
Φ_m	Maximum Quantum Yield
Φ_{PP}	Quantum Yield of primary production
Φ_{qs}	Fluorescence quantum yield of quinine sulphate
Φ_s	Fluorescence quantum yield of the sample
η_b	Ratio of the molecular to total backscattering coefficient
η_F	Depth Fraunhofer line
κ	Average attenuation coefficient for $dE_u(z)$
λ	Wavelength
λ_0	Reference wavelength
λ_1	Wavelength of light excitation
λ_2	Wavelength of light emission
λ_F	Wavelength position of the Fraunhofer line
λ_x	Wavelength range for excitation
μ	Shape factor for lognormal distribution
μ_0	Mean cosine
$\mu_d(\lambda)$	Spectral mean cosine for downwelling light
$\mu_u(\lambda)$	Spectral mean cosine for upwelling light
ρ	Bottom albedo
ρ_d	Frensel reflectance due to direct light
ρ_s	Frensel reflectance due to direct light
σ	Shape factor of gaussian and lognormal distribution

ω	Single scattering albedo
ω_b	Backscattering normalised albedo

Glossary

AATSR	Advanced Along Track Scanning Radiometer
AOP	Apparent Optical Properties
ARIES	Australian Resource Information and Environment Satellite
AVHRR	Advanced Very High Resolution Radiometer
CDOM	Coloured Dissolved Organic Matter
CHL	Chlorophyll "a"
COASTlOOC	COAstal SurveillanceThrough Observation of Ocean Colour
CoASTS	Coastal Atmosphere and Sea Times-Series
COLORS	COastal region LOngterm measurements for colour Remote Sensing development and validation
CSIRO	Commonwealth Scientific and Industrial Research Organization
CZCS	Coastal Zone Color Scanner
DOC	Dissolved Organic Carbon
DP	Detrital Products
HPLC	High Performance Liquid Chromatography
HTCO	High Temperature Catalytic Oxidation
ICAMS	Integrated Coastal Analysis and Monitoring System
IOP	Inherent Optical Properties
IO-PAS	Institute of Oceanology - Polish Academy of Science
JRC	Joint Research Centre
LUT	Look Up Table
ME	Marine Environment

MERIS	Medium Resolution Imaging Spectrometer
MFA	Marine Fulvic Acid
MHA	Marine Humic Acid
MOS	Modular Optoelectronic Scanner
NASA	National Aeronautics and Space Administration
NCP	Non Chlorophyllous Particulates
OAC	Optically Active Components
OC	Ocean Colour
OCTS	Ocean Colour and Temperature Sensor
PAR	Photosynthetically Available Radiation
PCA	Principal Component Analysis
PDF	Probability Distribution Function
PEB	phycoerythrobilin
PSD	Particle Size Distribution
PUB	phycourobilin
QY	Quantum Yield
SAI	Space Applications Institute
SEABAM	SeaWiFS Bio-optical Algorithm Mini-Workshop
SEABASS	SeaWiFS Bio-optical Archive and Storage System
SeaWiFS	Sea-viewing Wide Field-of-view Sensor
SNR	Signal to Noise Ratio
SSF	Sun Simulated Fluorescence
TFA	Target Factor Analysis
TSM	Total Suspended Matter
ULISSE	Underwater Light Seatruth Satellite Experiment
VSF	Volume Scattering Phase Function
WMO	World Meteorological Organisation
YS	YellowSubstance

Chapter 1

Introduction

Chapter 1 Table of Content

1.1. Bio-optical Oceanography
1.2. Case I *vs.* Case II waters
1.3. Statement of the Problem
1.4. Comparative role of satellite and in-situ measurements
1.5. View point and objectives
1.6. Summary of the content of the main chapters

1.1. Introduction to Bio-optical Oceanography

Optical remote sensing of the water surface is a cost effective way to obtain colour data for remote or extended spatial areas of the marine environment. After processing and interpretation, the colour data can be converted into temporal and spatial distribution patterns of parameters of water quality such as biomass and sediment concentration. Interaction between waterbodies, such as inflow of terrigenous water through a river and the associated mixing processes, can be visualised and quantified.

From satellite, water leaving radiance (L_w), is measured in absolute units, representing the light which, having penetrated the water column, has been scattered back up through the water surface. In turn, the water leaving radiance is linked to the upwelling radiance (L_u): an apparent optical property (AOP) of the water which varies both with the angular distribution of incident light as well as with the optical properties of the water column. The use of reflectance (R), defined as the ratio of upward to downward irradiance (E_u/E_d), has the advantage of eliminating most of the dependency of the incident illumination on absolute intensities. Furthermore, R has the added advantage that it provides the relation with the Inherent Optical Properties (IOP) as shown through the radiative transfer equation (Preisendorfer 1976). IOPs are those properties which depend only upon the medium, and which therefore are independent of the ambient light field within the medium (Preisendorfer 1976). Therefore, they are not dependent on the angular radiance, as are AOPs.

The basic IOPs adopted in marine optics are defined as follows:

1: Absorption coefficient a

2: Volume scattering function $\beta(\theta,\phi)$

The volume scattering function describes the angular distribution of the light scattered out of the direction of an incident ray, with, θ the angle of light scattered away from this direction and ϕ the azimuth angle. The volume scattering function becomes independent of the azimuth angle ϕ for spherical particles without internal structure and for randomly oriented particles of arbitrary shape.

For convenience other IOPs can be derived from the absorption coefficient and the volume scattering function. The scattering coefficient b is defined by:

$$b = 2\pi \int_0^{\pi} \beta(\theta) \sin\theta d\theta \qquad (1.1)$$

the beam attenuation coefficient c is the sum of the absorption coefficient and the scattering coefficient.

$$c = a + b \qquad (1.2)$$

The scattering coefficient b to be used in models of the light field can be separated into two partial integrals so that:

$$b = b_f + b_b \qquad (1.3)$$

where the forward scattering coefficient b_f is given by;

$$b_f = 2\pi \int_0^{\pi/2} \beta(\theta) \sin\theta d\theta \qquad (1.4)$$

and the backscattering coefficient, b_b, is given by:

$$b_b = 2\pi \int_{\pi/2}^{\pi} \beta(\theta) \sin\theta d\theta \qquad (1.5)$$

Absorption diminishes light intensities and scattering changes its angular distribution. In other words, the intensity of reflected light increases with the amount of scattering and decreases with that of absorption. Therefore light, which originates from below the water surface, conveys characteristic information from each of the individual optically active components of the water column. The sub-components of the IOPs will be discussed in detail in the future chapters. In order to motivate the subsequent model of the absorption and scattering properties for marine waters, we need to have knowledge of the substances influencing the optical characteristics of these waters.

The individual elements will be termed the Optically Active Components (OACs) and may be approximated by chlorophyll ([Chl], Total Suspended Matter ([TSM]), Coloured Dissolved Organic Matter (CDOM) or yellow substance (YS) and water itself. Although in reality natural waters consist of particles ranging from water molecules of a size ~0.1nm to viruses ~100nm, ...to whales ~10m (Mobley 1994), traditionally they are divided into dissolved and particulate fractions thus justifying the subdivision presented above. In marine waters, the contribution of these OACs varies from one environment to another to determine the bulk IOP, affecting both the absorption and the scattering coefficients.

The aim of the current study is to undertake the development of the tools and know-how for the retrieval of geophysical parameters from remotely measured water-leaving radiance in waters termed as Case II.

1.2. Case I vs. Case II waters

Morel and Prieur (1977) give an original classification for marine water in the context of optical remote sensing. In their work, Case I waters are defined as:

> "waters in which the concentration of phytoplankton is high compared to that of other particles . The pigments (chlorophylls, carotenoid) play a major role in the actual absorption."

as opposed to Case II waters

> "in which inorganic particles dominate, and pigment absorption is of minor importance."

This definition whilst still holding as the standard optical classification of marine water has now been slightly refined (McClain 1995) as follows:

> "Case I waters are those in which marine phytoplankton (or marine organic matter in general) are responsible for all the OACs in the water column i.e. the non-chlorophyllous particles are purely detrital matter resulting from the phytoplankton and the CDOM is only that due to algal exudates.
>
> Case II waters are those in which the presence of non chlorophyllous components is not strictly related to the phytoplankton itself but are present through other sources in general from terrigenous inputs i.e. river runoff."

Accordingly Case II waters can generally be divided into two main types: Case IIS where sediments are the dominant component and CaseIIY where CDOM or yellow substance is the dominant one. Situations occur, such as in large river deltas (e.g. the Po river), where both of these components are abundant.

This type of classification means that an area in a large upwelling system with chlorophyll concentrations of the order of 2 mgm^{-3} may still be considered as Case I. Not all coastal waters can be termed as Case II. However, it is generally true that

coastal waters adjacent to point source inputs (i.e. river mouths) and other coastal areas typical of European waters are Case II.

1.3. Statement of the problem

In the last decade several authors have successfully found many valid approximations for the radiative transfer in oceanic waters (e.g. Morel 1991). These approximations have permitted the development of simple empirical and semi-analytical ocean colour algorithms which have been shown to be able to reproduce chlorophyll concentrations in oceanic waters at the same order of accuracy as in-situ methods (Aiken 1995).

In Case II waters no general solution seems to have been found. Various preliminary studies have been made, which include inverse radiative transfer modelling based on numerical methods (Doerffer and Fischer 1994) and neural networks (Doerffer 1997), as well as mathematical solutions based on non-linear equation solving (Roesler et. al. 1995, Lee et. al. 1994), and multivariate statistical techniques (Sathyendranath et. al. 1989). Each of these techniques has illustrated their own validity but none are globally accepted for a variety of reasons including the fact that some of the techniques require large amounts of computer time to solve the presented model at the level of a satellite image. None of the methods really contain a robust reflectance model adequately representing the spectral variability of the IOPs to be anticipated in Case II waters.

Another solution often proposed for the retrieval of geophysical parameters in Case II is the simple use of empirical algorithms based on local datasets, which may in some cases give very promising results for the datasets considered. However these algorithms tend to be rather unstable and when applied to satellite data often give erroneous results even in the area for which the algorithm was developed.

Thus there is a need for the development of reflectance models and algorithms adequately formulated to represent the natural variability of the OACs and IOPs present in Case II waters. For this, however, there is a requirement for quality datasets of IOPs for many different coastal water types in order to have an extended picture of the variability to be expected. There is also a need for large validation datasets (again

in many different water types) in order to be able to make thorough verification of the satellite derived products obtained using the new methodologies developed. These thorough validations will also give a greater credibility for end users of the derived products.

1.4. Comparative role of satellite and in-situ measurements

The interpretation of satellite observations relies on in-situ data for both the development of algorithms and product validation. In-situ data will always be inadequate if compared to the spatial resolution of a satellite image. There is in fact a requirement for a strategy to optimise the incorporation of in-situ data in the procedure for retrieving the eventual products.

Our present lack of a detailed understanding of coastal waters is due to the difficulty in making effective physical and biological field measurements. Weaknesses in observational data lie in the lack of repeated sampling (repeated sections, anchor stations etc.) for coastal evolution information, and lack of along-front synoptic information. Moreover, it is not possible to rely on a single set of experiments in these regions since multiple scales and temporal evolution are involved. In these dynamic coastal regions, where productivity is much higher, the spatial extent and temporal character of the biomass affecting the optical properties are poorly known. For example, within 30km off the Peru coast, the surface chlorophyll estimate of phytoplankton biomass ranges from 0.4 to 40 mg chl m^{-3} and the integrated primary production from <1 to >10 g C m^{-2} day^{-1} (Walsh *et. al.* 1980). Classical shipboard campaigns, which are limited to the usual 10-12 knot speed of the research vessel, are aliased within the above gradients. Another motivation for high spatial and temporal requirement is that phytoplankton species in coastal waters divide every 0.5 to 2 days. Without significant losses, an algal population during the spring bloom could increase at the same rate. To resolve the temporal and spatial consequences of this resulting growth process, a Nyquist sampling frequency of at least 0.25 day^{-1} is required (Blackman and Tukey 1957). If one sampled every 4 hours in a typical longshore

upwelling flow regime of 30 cm sec^{-1} to resolve this process, at least 5 ships would be required every 20 km^2 for the necessary biomass measurements (Kelly 1976).

We thus arrive at a major reason for the use of satellite derived ocean colour data; the need to analyse distributions of biological and bio-optical properties equivalent to or similar to the frequencies which can resolve causally the sources of their variance. This underlying motivation is highlighted in Figure 1.1 (after Dickey 1990), which shows physical and biological ocean processes and their respective time scales. The dotted line, in Figure 1.1, highlights those processes which are typical of coastal region and which could be studied by polar orbiting satellite sensors (this scale of features is generally termed mesoscale-synoptic).

The historical ocean colour sensor CZCS (Coastal Zone Color Scanner) showed its capability in monitoring coastal frontal regions, for the first time oceanographers had a complete synoptic picture of the biology and the biophysical forcing in these areas. However, although at this stage remote sensing had an obvious spatial and temporal advantage over *in-situ* measurements, it could only be considered a qualitative tool. The estimation of any quantitative products (e.g. chlorophyll, TSM etc.) was not possible in these waters (i.e. Case II waters) due to the highly complicated bio-optics. With the advent of the second generation of ocean colour sensors (i.e. SeaWiFS, OCTS, MOS) and their improved spectral resolution, it should be now possible to distinguish YS from CHL, using the appropriate methodologies, also possibly identifying ancillary pigments and retrieving sediment concentration. These quantitative products now undoubtedly promote satellite optical sensor as a well-suited tool for studying the biophysical processes associated with coastal regions and are a principal driving force of the presented research. However, the link with the in-situ observations will surely remain and it should not be inferred that remote sensing will eventually replace field observation particularly in coastal zones. On the contrary, it is in these areas that remote sensing has a fundamental need of the in-situ data both for algorithm parameterisation and for product validation. The derived products would then fuel a positive feedback

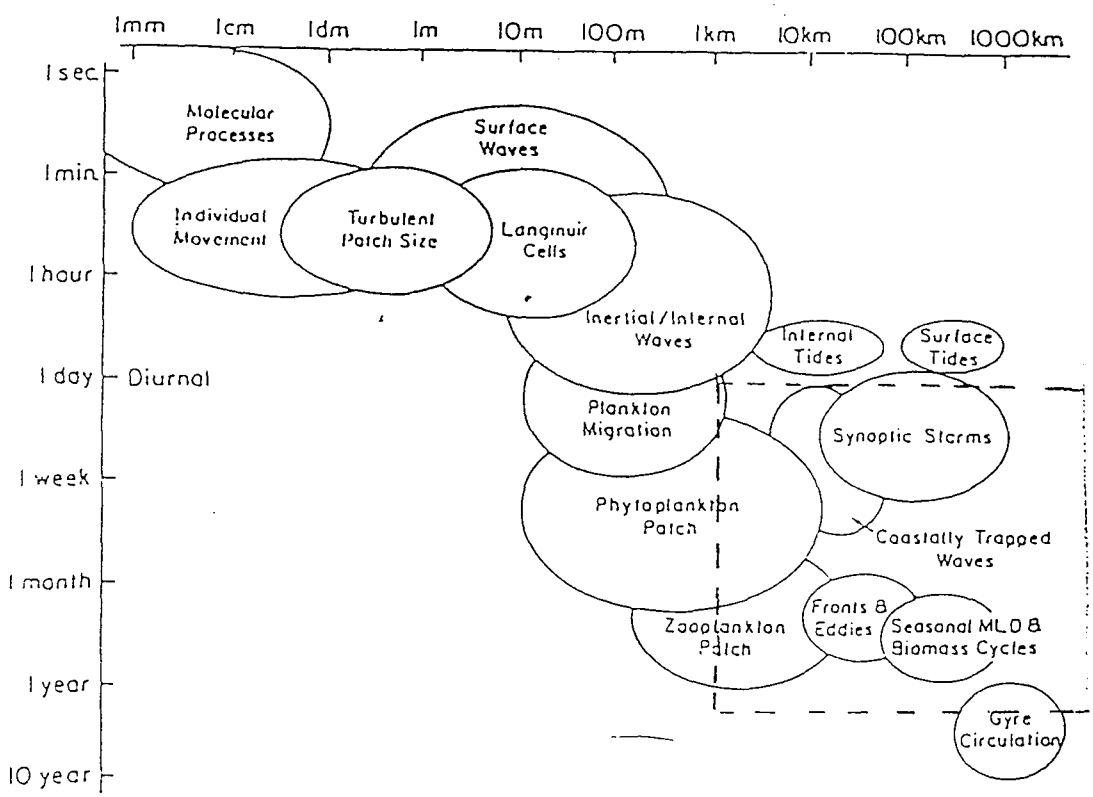

Figure 1.1: A schematic diagram illustrating the relevant time and space scales of several physical and biological processes important to the physics and ecosystem of the upper ocean (after Dickey, 1990).

of remotely sensed data providing a synoptic picture of the feature or phenomenon studied in assistance to the traditional oceanographic method available.

1.5. Objectives and Applications

The present study will address several key topics in the field of coastal bio-optical oceanography. The research will in general terms focus on the development of tools for the quantitative retrieval of geophysical products in coastal waters. This will be done by paying particular attention in these coastal waters to the significance of the non-chlorophyllous components in bio-optical models. This general aim is achieved by undertaking several specific tasks, which follow.

In marine optics and in particular in ocean colour remote sensing there is often an acknowledged payoff between limiting the number of unknowns (required for the purpose of numerical calculations) and adequately describing the complexity of the system. A first objective of this study is an attempt to identify a minimum number of components and to show the possible methodologies available to gain detailed information on the spectral variability and the budget of the natural occurrence of these individual contributions.

It has long been known that the simple models and algorithms available for Case I waters are not applicable to Case II waters. The independent variability of each of the components either requires more complex inverse numerical approaches for retrieving the OACs, or a regional method which will allow the retrieval of geophysical quantities for limited geographical area. The present study will also provide a tool which allows the systematic development of algorithms for retrieving quantitative geophysical products, whilst keeping the parameterisation relatively simple. The method should also account for or be immune to omitted processes such as bottom reflectance or fluorescence.

Land based optical remote sensing has for a long time invested in techniques based on the absolute magnitude of surface reflectance. The identification of end-members associated with a particular mineral or cereal, for example, through methods such as spectral unmixing, are established tools available to anyone approaching the field. An

objective of the current study is to take advantage of the current generation of Ocean Colour (OC) sensors and the atmospheric correction scheme which now claims to be able to achieve better than 5% error in retrieving water leaving radiances (L_w). This will allow the development of new methodologies to retrieve geophysical parameters based on absolute reflectance.

Several important applications for the tools and products proposed in the current study are conceivable. The results could be used as input for hydrodynamic and ecosystem models of the region in question. The quantitative results retrieved from the maps of the individual optically active components along with any proven correlated parameters (e.g. CDOM vs. Dissolved Organic Carbon (DOC)) could also be used as inputs for analyses of fluxes in the region. The prime application conceivable with the techniques, and know how developed in this investigation, is in coastal management, and more specifically in studies of water quality, coastal productivity and on how these relate to the complicated dynamics of the coastal environment. It has been recognised for over two decades that the use of remotely sensed data in monitoring dynamic coastal phenomena (Horstmann 1980) offers a greater synopticity than can be achieved by standard in-situ measurements. However, the investigations to date which have used ocean colour remote sensing for monitoring specific hydrodynamic features in coastal (Case II) waters, have been qualitative (for example Barale et. al. 1984 and Boxall and Robinson 1987). Moreover, it is well known that coastal frontal regions have significant biological consequences. They are areas of high productivity for all the food chain from phytoplankton through fish and marine mammals, and have always been exploited by fishermen. Fisheries management strategies must take into account the distribution and productivity in coastal regions. A clear understanding of the role of biological fronts in coastal waters is needed in the construction of biological models of ocean productivity. Also of concern are phytoplankton blooms forming in restabilising water masses in coastal zones which under favourable conditions can develop into toxic algal blooms or red tides. The ability of surface fronts in coastal waters to concentrate ocean pollutants has

important and hitherto neglected implications for the uptake into the food chain of hazardous substances such as heavy metals.

1.6. Summary of the content of the main chapters

In chapter 2 an investigation is presented which considers various Case II water in-situ datasets, and their significance in considering the variability of bio-optical characteristics in these waters. In order to encompass a broad range of environmental situations (within coastal Case II waters), datasets from very diverse water types are used. These include data from the southern Baltic, the northern Adriatic, and Tokyo Bay. The main information considered is that of the absorption properties of each of the components. The datasets illustrate the variability at different scales in both space and time, combining a series of seasonal oceanographic campaigns in the Baltic with a complete annual timeseries of monthly measurements at a fixed point in the Adriatic. The study investigates the variability of the absorption budget in these Case II waters with particular attention to the variability of the non-chlorophyllous contributions. The work then continues and examines, for substantial datasets, the variability of the spectral absorption of the individual components in the context of their current models. Also the study specifically considers the co-variability of yellow substance and detritus. In this particular investigation the validity of the currently proposed modelling of the absorption of these two components as a single variable, is analysed in Case II waters.

In chapter 3 the parameterisation of a three component reflectance model is presented. Again the emphasis here is on describing the maximum amount of variability of the non-chlorophyllous components. In the developed model the absorption is represented by four independent components and the backscattering by three. Also the proportionality factor (f) is parameterised on the basis of the sun zenith angle and the volume scattering phase function. In the model the regional characteristics of the algorithms are defined through the input datasets for the optically active components representative of the area in question. Finally, to develop algorithms an inversion

scheme based on factor analysis is used, and different wavelength combinations representing different multi-spectral sensors are compared.

In chapter 4 an investigation is made on the potential contribution of inelastic processes and bottom reflectance on the elastic signal modelled in the regional model presented in the previous chapter. The influence of these contributions is considered with respect to the elastic signal from two main points of view. The first is its spectral contribution as a proportion of the elastic signal both individually and cumulatively. Secondly and perhaps more important its influence is considered through the effect of the addition of the inelastic contribution to the elastic signal and the variability in the characteristic vectors (computed through the factor analysis). The processes both individually and cumulatively are the following: fluorescence due to chlorophyll, yellow substance and phycoerythrin, Raman scattering, and bottom reflectance.

In the final chapter (chapter 5) a novel approach is presented to retrieving both the optically active components, individual pigment concentrations and the spectral magnitudes of the Inherent Optical Properties. The algorithm presented is based on the rationale that with the advent of second generation ocean colour sensors, improved signal to noise ratios, and atmospheric correction possibilities, it is possible to derive water leaving radiances within 5% error margins. Therefore the algorithms presented here can be formulated based on absolute values of reflectance, through the direct inversion of the measured reflectance. Using such a new methodology different products can be obtained including spectral values of the absorption coefficients of the individual component as well as concentrations of the individual pigments.

Chapter 2

Bio-optical characterisation of Case II waters: the significance and variability of the Non-Chlorophyllous components

Chapter 2 Table of Content

2.1. Introduction and background on Region of Interest
2.2. Datasets Used
2.2.1. Baltic dataset (ULISSE)
2.2.2. Adriatic dataset (CoASTS)
2.2.3. Tokyo Bay dataset
2.3. Measurements made
2.3.1. Geophysical measurements: Chlorophyll "a", TSM, DOC
2.3.2. Physical measurements-Conductivity, Temperature, Density, Beam attenuation
2.3.3. Measurement of AOPs (i.e. L_u E_d and calculation of R)
2.3.4. CDOM measurements (absorption, fluorescence, Quantum Yield)
2.3.5. In-vivo pigment measurements (a_{ph} and a_d)
2.3.6. Meteorological Measurements
2.4. Theory and Results
2.4.1. The co-variability of the non-chlorophyllous contributions to absorption
2.4.2. The spectral variability absorption in Case II waters
2.4.3. The budget of absorption in Case II waters
2.5. Discussion
2.5.1. Absorption modelling and sources of variability
2.5.2. Spectral variability of pigment absorption, significance in forward modelling
2.5.3. An IOP classification and its significance in algorithm development
2.6. Conclusions

2.1. Introduction and Background on Region of Interest

Case II coastal waters are socio-economically extremely important regions of the planet. Furthermore, although coastal and continental shelf areas comprise only 10% of the total ocean area, they provide roughly half of the oceanic new production most of the sequesterable DOC (Walsh et. al. 1981) and 95% of the worlds fisheries yield. These areas are typically higher in phytoplankton pigment concentration, and also contain coloured terrigenous constituents such as CDOM and suspended sediments. In these Case II waters, the global colour ratio algorithms break down because two or more substances are present with different optical properties and which do not co-vary with chlorophyll "a" concentration. These may also be waters with exceptional/anomalous plankton blooms (such as red tides), and areas discoloured by dust transported by wind from deserts into the sea (Carder et. al. 1986). Moreover, these regions are usually influenced by river discharge of mineral and organic suspended matter, and/or CDOM. In addition, Case II waters, are characterised by small scale patchiness and dynamic variability and therefore any *in-situ* investigation in these regions must aim to cover the maximum gradients of observed parameters and obtain good statistical distribution functions which are representative of the studied areas.

In dynamic Case II waters it is shown that the spatial and temporal perspective offered by in-situ datasets is insufficient to give a complete picture of the studied phenomena. It would therefore seem that there is a good potential for the use of synoptic satellite ocean colour data provided that the methodologies exist to convert the measured radiances into viable geophysical products in these regions. The in-situ datasets will provide knowledge on existing correlations between absorption and scattering properties and geophysical variables important in models of primary production or carbon budget.

To obtain the information required for the characterisation of the reflectance models, as well as the correlations necessary for further application studies, a detailed knowledge of the budget, spectral variance and co-variability of the various components of the Inherent Optical Properties must be made in particular for the

absorption segment. The objective of this chapter is to present a series of quality datasets for different geographic regions in predominantly Case II waters (although the Adriatic platform is considered as being in certain seasons Case I). The data are continuous measurements of spectral absorption in the range 400 to 700nm for phytoplankton pigments (ph), detritus (d) and yellow substance (ys). These datasets will therefore allow the following analyses. The best exponential fits for all a_{ys} and a_d spectra are determined and a study, of both the slope and specific values of absorption for the two types of spectra through analyses of correlation and covariance for the two locations, is undertaken. This analysis will determine the minimum number of components required describing absorption in these environments. Subsequently, an investigation and description of the variability of spectral shape and amplitude for the three sites selected (Baltic, Adriatic and Tokyo Bay) of the three components (ph, d and ys) is made. Finally, considerations will be made on the contribution of each of the components to the total $a_{tot}(\lambda)$ budget, considering site and seasonal variations, and an attempt to introduce a classification scheme identifying the different optical characteristics of varying regions.

The present chapter will consider substantial in-situ datasets and in particular will present the results from a high quality dataset taken over an inter-annual period in the Southern Baltic. Many of the other datasets presented will be used in following chapters of this thesis.

2.2. Datasets Used

2.2.1. Baltic dataset (ULISSE)

The semi-enclosed basin of the Baltic Sea embodies a perfect natural laboratory for the type of studies approached in this thesis. The Baltic is an environment which can be defined either as a lake, an estuary or a sea. It has been occasionally classified as a brackish sea (Nehring 1990) and as such is the largest in the world covering an area of 415 000 km². It is bordered by 10 different countries which have an obvious impact on the enclosed basin, each contributing to large quantities of terrestrial inputs of both riverine and atmospheric origin. Both the natural (Dowell and Kriebel 1995) and

anthropogenic (Victorov 1996) land-derived inputs have been shown to influence the coastal bio-optics in a significant way.

The Gulf of Gdansk and the Polish coastal zone was the specific region chosen because of its unique properties caused by the high inputs from the river Vistula (mean discharge: 954 m^3 s^{-1}). Furthermore this river system was of interest due to its large drainage basin (approx.: 193,910 km^2 with mean annual runoff: 4.92 dm^3 s^{-1} km^2) consisting mainly of arable land and industrialised areas (e.g. power plants etc.). Hydrographically the seasonal state of the water column is very diverse. For example, April is clearly characterised by vertical water mixing and extended coastal blooms in the Gulf of Gdansk, produced mainly by diatoms (Witex, 1993). In August and September the marine conditions are affected by greater solar irradiation generating a stratified water column. During this period the influence of river inflows are less important whilst the local precipitation reaches its maximum levels (Ehlin, 1981).

The dataset presented here for the Southern Baltic is the result of a collaborative agreement between the Institute of Oceanology of the Polish Academy of Science (IO-PAS) and the Space Applications Institute (SAI) of the Joint Research Centre (JRC) in Ispra. Four cruises were carried out on-board *r/v Oceania;* one in September 1993 and three in 1994 (April, August and September). Station positions (as in figure 2.1) were not fixed before the campaigns, and a principal aim was to collect data representing the largest possible gradients in the measured parameters in order to adequately characterise the notable contribution by terrestrial inputs as well as the marine autochonous contribution. The area of investigation includes the Gulf of Gdansk, the Polish Coast as far West as the Pomeranian Bay, and part of the open sea of the so-called Baltic Proper from 15 to 60 km off the shoreline. The sampling area was defined in order to assess the full influence on the hydrobiological conditions of the basin considered by inputs from the main rivers the Vistula and Oder (situated in the Gulf of Gdansk and in the Pomeranian Bay respectively). Sampling was performed during three different seasons: April, during well-mixed water column conditions and with the maximum of fresh water inflow, August and September

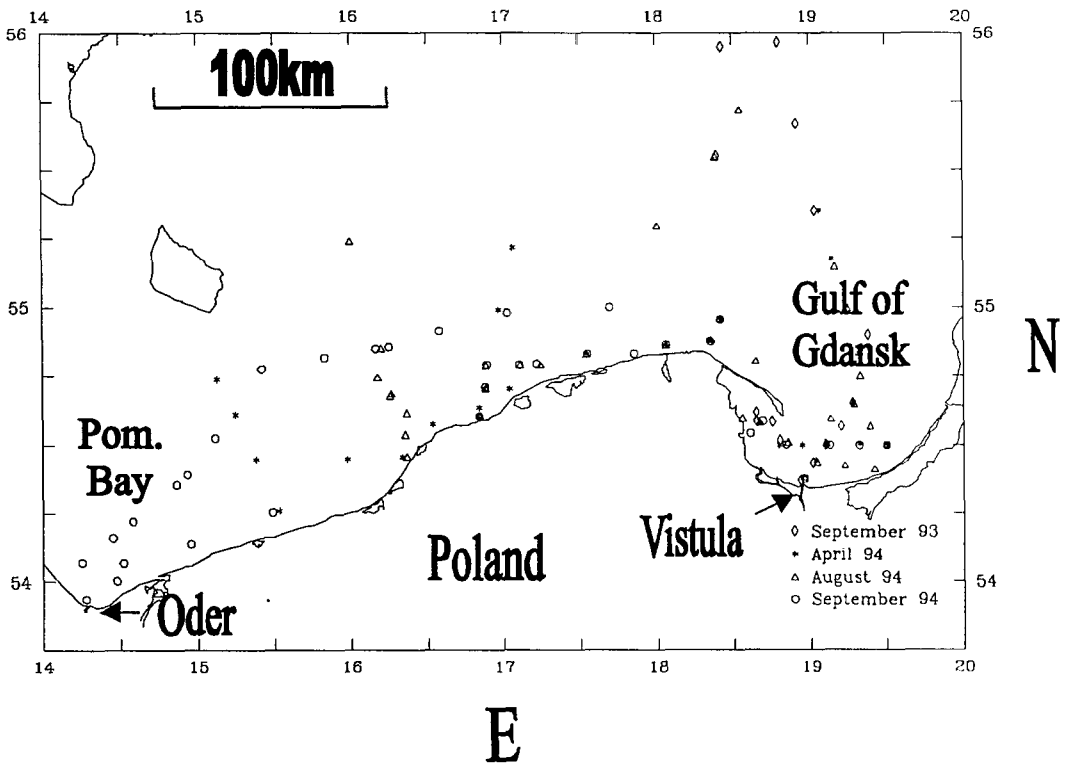

Figure 2.1: A map showing the showing the station positions for all of the ULISSE cruises. As can be seen the station positions were made in order to cover the largest gradients possible.

during stratified summer water characterised by a sharp thermocline and minimum river inflow. The survey consisted of 121 stations in total, some of which were repetitions of the same location during the three periods. The samples were collected at three depths within the euphotic depth as indicated by CTD and fluorescence profiles. Figure 2.2 illustrates typical salinity and temperature profiles showing the water mass structures in the three seasons (April, August and September) for the Gulf of Gdansk, the coastal zone and the open sea and Pomeranian Bay.

2.2.2. Adriatic dataset (CoASTS)

The datasets presented for the Northern Adriatic were taken at the fixed platform *"Acqua Alta"* belonging to the Italian National Research Council. The project (Zibordi *et. al.* 1995) under which the measurements were made is the CoASTS (Coastal Atmosphere and Sea Time-Series) project between SAI JRC and the Institute for the Study of Large Masses, of the Italian National Research Council in Venice. The CoASTS project started in September 1995 (pilot campaign in July 1995) and continued until September 1997. Monthly campaigns were made involving high quality atmospheric and oceanographic (bio-optic) measurements to support calibration/validation activities for SeaWiFS, OCTS and MOS ocean colour sensors. The site itself is at the geographic position lat. 45°19' long. 12°30' at about 30km offshore from the Venice Lagoon. The region is, depending on the prevailing currents, characterised by CaseI or CaseII waters. The site is considered to be well representative of the entire Adriatic Sea. Some typical values for the location include temperature in the range 4-26°C, salinity: 32-36 psu., chlorophyll concentrations in the range 0.1-2 mg/m^3, sediment concentrations in the range 1-5 g/m^3 and CDOM absorption coefficients at 400nm of 0.07-0.45m^{-1}.

2.2.3. Tokyo Bay dataset

The dataset presented here for Tokyo Bay was taken from the SeaWiFS Bio-Optical Archive and Storing System (SEABASS) database. The dataset (Kishino et. al. (1984)) was introduced into the current investigation as it offered diverse bio-optical

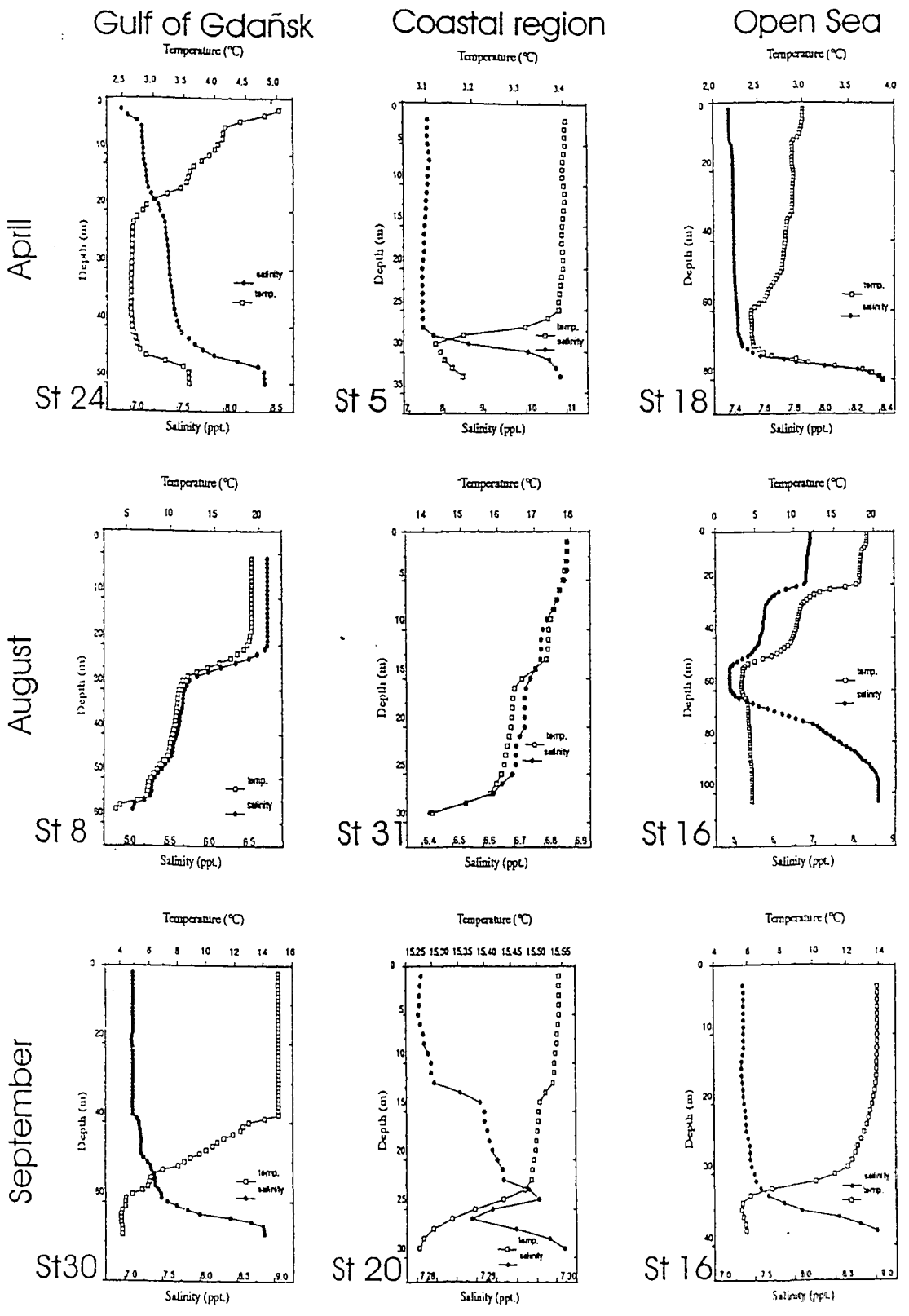

Figure 2.2: Plots representing example stations of CTD data covering the three main oceanographic province and covering three month in which the ULISSE campaign were undertaken.

characteristics compared to the previous two datasets as will be discussed later. The data from Shimoda Nabeta Bay, where typical total absorption coefficients were of the order of $0.25m^{-1}$ in the blue (400nm) and Secchi disk depth was 11m. The chlorophyll concentrations were relatively low with values of 0.5-0.9 mg/m^3 and Diffuse attenuation coefficient (K_d) values at 490nm were between 0.3 and 0.5.

2.3. Measurements made

2.3.1. Geophysical measurements Chlorophyll "a", TSM, DOC

The chlorophyll *"a"* measurements were carried out according to Strickland and Parsons (1972) using the updated equations as given in the 1984 edition. The absorption spectra were taken for the wavelength range 350-750nm with the spectrometer SPECORD M40. The filtrations for TSM (Total Suspended Matter) measurement were carried out on preweighed filters. These filters were weighed before each campaign after having been washed with distilled water and left in an oven at 60°C for 24 hours. The filtrations were then carried out on the cruise, the volumes filtered were typically between 1000 and 2000 ml. The filters were then stored in a freezer at -20°C. On return to the laboratory the samples were once again heated in the oven at 60°C for 24 hours, left for 4 hours at room temperature and then reweighed to obtain the dry temperature weight. Triplicates or duplicates and a blank were made for both [Chl] and [TSM]. Error was considered acceptable in the 10% range, and in this case the mean was taken. If this was not achieved the mean of the nearest two was taken.

For DOC measurements seawater samples collected with a 10 l Nansen bottle were stored in a 15 l seawater preconditioned PVC container in order to reduce contamination. The filtration was performed under gentle depression (100 mb) on a precombusted GFF filter rinsed with filtered seawater to eliminate the main part of particulate matter. This first filtrate was passed on a Millipore 0.22 µm membrane prerinsed with Milli-Q water. In each filtration the initial aliquots (≅ 200 ml) were discarded to prevent any possible source of contamination by the filters. The final filtrate was transferred to a 250 ml glass ambered bottle prerinsed with the same

filtered seawater. During the August 1994 campaign, the DOC samples were made in duplicate. After the addition of sodium azide the sample was stored at 4°C. The DOC analyses were performed at the JRC, Environment Institute (using the High Temperature Catalytic Oxidation (HTCO) method).

A Carlo Erba-Fisons TMC 480 analyser was used that involves a high temperature oxidation reactor thermoregulated at 1020 C. the method is described in detail by Sugimura and Suzuki (1988). The resulting methane was measured with a Flame Ionisation Detector (FID) whose signal is fed to a potentiometric chart recorder and it is directly proportional to the amount of organic carbon present in the original sample. Detailed results of the DOC analysis on the Baltic samples and the relationships identified between DOC and CDOM absorption can be found in the manuscript included as Appendix 2.A (Ferrari et. al. 1996).

2.3.2. Physical measurements-Conductivity, Temperature, Density, Beam attenuation

Scientific staff of the Oceanographic Data Centre IO-PAS carried out CTD measurements. The sensors used were either the Guildline 87104 or the Sea-Bird SBE depending on the cruise. The dataset containing values of temperature, conductivity and salinity were integrated over an interval of 1m. The light beam attenuation coefficient at λ=655nm was measured using a transmissometer built in IO-PAS. The light path length in water was 1 m and these datasets were integrated over 1m intervals

2.3.3. Measurement of AOPs (i.e. L_u E_d and calculation of R)

The profiles of downwelling irradiance and upwelling radiance, obtained from MER 2040 were used for the calculation of the reflectance at certain wavelengths (corresponding to the SeaWiFS channels) λ_i, $R(\lambda_i)$, has been computed as:

$$R(\lambda_i) = \pi \times \frac{L_u(\lambda_i, 0^-)}{E_d(\lambda_i, 0^+)} \qquad (2.1)$$

where L_u $(\lambda_i, 0^-)$ is the upwelling radiance in the nadir direction (W $m^{-2}sr^{-1}$) just under the surface and $E_d(\lambda_i, 0^+)$ is the downwelling irradiance (W m^{-2}) impinging on the

water surface. $E_d(\lambda_i,0^+)$ was obtained from measurements when the instrument was just above the surface. As it is not possible to place the instrument at the theoretical "0^-" depth, $L_u(\lambda_i,0^-)$ was estimated as follows. For each wavelength λ_i the diffuse attenuation coefficient for upwelling radiance K_{Lu} was computed by linear regression between logarithm of L_u and depth z (within the surface layer for which the slope of $\ln(L_u)$ versus z was constant, usually between 0.5 and 4.0 m). A value for $L_u(\lambda_i)$ at 0^- m was then obtained by extrapolation using K_{Lu}.

The upwelling radiance data (L_u) was also checked for the self shading effects of the instrument. Gordon and Ding (1992) modelled the errors introduced by the instrument's own shadow in the measurement of L_u. The authors showed that for the source of error to be less than 5%, without the requirement for modelled corrections, the instrument radius r must satisfy $r \leq [100\ a(\lambda)]^{-1}$ for $L_u(\lambda)$. With the MER 2040 having a radius of 10cm it is obvious that at absorption coefficients typical of those found in the Baltic the above rule cannot be satisfied. Gordon and Ding (1992) also presented a simple model correcting $Lu(\lambda)$ for the self-shadowing effect and this was therefore applied to the ULISSE dataset. They write

$$\hat{L}_u(\lambda) = \frac{\tilde{L}_u(\lambda)}{1-\varepsilon(\lambda)}$$

and

$$\varepsilon(\lambda) = 1 - e^{-k'a(\lambda)r},$$

where ^ is the true value and ~ is the measured value, $k'=y/\tan\theta_0$, θ_0 is the refracted solar zenith angle and y is an empirical factor determined though modeled calculations (y=2). This correction was applied to all spectra in the ULISSE dataset and it is the corrected dataset that is used in the rest of this thesis.

2.3.4. CDOM measurements (absorption, fluorescence, Quantum Yield)

The sample used for the CDOM measurement were in all cases filtrates from a filtration through 0.22µm Millipore filters. The filtrate was then stored in amber bottles, an inhibitor of anaerobic growth was added (sodium azide Na_2N_3) and kept at

4°C . Measurements of fluorescence were carried out on board the vessel and absorption was made as soon as the samples were returned to the laboratory (within two weeks of the cruise). To test the portability of the sample, some fluorescence spectra were made again on return to the lab. In all cases, the change in the fluorescence spectra and (therefore the absorption) was negligible i.e. <2%. More precise descriptions of the individual measurements are included below.

The CDOM samples were transported refrigerated to the laboratory and absorbance was measured with a Perkin Elmer Lambda19 dual beam spectrophotometer using fused quartz cuvettes of 10cm and Milli-Q water as a blank. The instruments were used in the range 300 to 750 nm with a spectral resolution of 1 nm. The absorbance acquired was converted in absorption coefficient (m^{-1}) using the

$a_{ys}(\lambda)=2.3\ OD(\lambda)/L$ where $OD(\lambda)$ is the optical density and L the pathlength of the cell in metres.

The instrument used for the fluorescence investigations was a Perkin Elmer LS 50 B spectrofluorimeter. The analyses were made with a 1cm cuvette, with quinine sulphate used as a standard. Two different fluorescence techniques are used to analyse CDOM. Emission spectra were obtained by exciting at 355nm (which is the same wavelength as those used for laser fluorescence from airborne sensors (Vodacek et. al. 1995)) and measuring the fluorescence emission in the range 375nm to 650nm. At this excitation the peak of the Raman is at 408nm and this can be used as well as the quinine sulphate to standardise the CDOM fluorescence. Information on the fluorescence standardisation and the dataset are given in the attached manuscript in Appendix 2.B (Ferrari and Dowell 1998). The emission spectra are most useful as an alternative way to quantify CDOM absorption (Ferrari and Tassan 1991). Synchronous spectra were also made, these spectra have not been used as much as emission spectra in CDOM experiments but they contain more diverse qualitative information than the above (Ferrari & Mingazzini 1995). These spectra basically consist of a diagonal cut across the emission excitation matrix. Excitation is performed at a certain wavelength and the emission is then measured at a wavelength, which is at a fixed interval (25 nm). Excitation is then moved on and the same

measurement is made at 1 nm increments. Fluorescence quantum yield (QY) an ancillary derived parameter that can provide support for understanding the source of CDOM was also calculated. It expresses the quantum efficiency of the fluorescence with respect to the absorption. QY is computed using the relationship (Green and Blough, 1994):

$$\Phi_s(\lambda) = \frac{F_s(\lambda) \times a_{qs} \times \Phi_{qs}}{a_s(\lambda) \times F_{qs}} \tag{2.2}$$

in which subscripts s and qs refer to the sample and quinine sulphate reference (0.5 nm/l in 0.1 NH_2SO_4 which gives an a =1.5m^{-1} at 355nm) respectively and a(λ) is the absorption coefficient of each sample and where λ in this case is 355 nm. The integration of the fluorescence emission F(355nm) is performed instrumentally between 420 to 460 nm. Φ_{qs} is typically 0.51.

2.3.5. In-vivo pigment measurements (a_{ph} and a_d)

Absorption measurements by phytoplankton pigments were performed using an alternative approach to the conventional method of particles retained on a glass fibre filter (Tassan and Ferrari 1995). This method consists in a combination of light transmission and light reflection measurements using a Perkin-Elmer Lambda 19 dual beam spectrophotometer. This spectrophotometer is equipped with a 60 mm integrating sphere, so as to remove the spurious contribution to the measured absorption caused by the sample backscattering that is particularly important is these types of waters. The phytoplankton absorption was obtained by bleaching the sample with a NaClO solution inducing a depigmentation of the organic particles. The resulting mineral absorption was then subtracted from the total particle absorption. The absorption spectra of particles retained on a filter are converted in equivalent particles-suspension absorption, using an empirical expression as described in Tassan and Ferrari (1995).

2.3.6. Meteorological Measurements

Meteorological observations were made during all campaigns. Standard measurements were performed, including: visibility, coded in accordance with the *International Meteorological* Codes of WMO; cloud cover; wind direction and velocity; dry and wet air temperature and atmospheric pressure.

2.4. Theory and Results

A general formulation relating irradiance Reflectance (R) to the Inherent Optical Properties: absorption (a) and backscattering (b_b), if the wavelength dependency is omitted, is given by:

$$R = f\frac{b_b}{a+b_b} \tag{2.3}$$

The absorption segment of the above relationship is the most significant in its contribution to the shape of the reflectance spectra-, as the spectral contribution from backscattering is fairly monotonic apart from in exceptional bloom conditions Roesler and McLeroy-Etheridge 1998). In fact for coastal waters it has recently been shown that remote sensing reflectance (R_{rs}) is proportional to 1/a for wavelengths less than 650nm (Sydor and Arnone 1997). Absorption has its own budget, comprising of *n* components which are linearly related so that:

$$a_{tot}(\lambda) = \sum_{i=1}^{n} a_i(\lambda) \tag{2.4}$$

where the overall budget has been shown to be adequately described by the following components in different investigations (e.g. Sathyendranath et. al. 1989):

$$a_{tot}(\lambda) = a_{ph}(\lambda) + a_d(\lambda) + a_{ys}(\lambda) + a_w(\lambda) \tag{2.5}$$

The subscripts *tot*, *ph*, *d*, *ys* and *w* refer to different sections of the absorption segment namely total, Chlorophyll like Pigments, detritus, Coloured Dissolved Organic Matter and water respectively. Some authors have tried to refine this differentiation even further such as Bukata (1981) who proposed a four component model excluding water in which he also differentiated the Non Chlorophyllous Particle (NCP) fraction into organic and inorganic particulates.

2.4.1. The co-variability of the non-chlorophyllous contributions to absorption

Recently several authors have proposed two component models (e.g. Carder et. al. 1989) in which the model of the absorption of the above relationship is defined by two components aph and DP (Detrital Products), where DP are a combination of detritus and yellow substance. These models of absorption were principally defined for Case I (oceanic) waters. However, their validity must also be tested in Case II (coastal) waters. The principal rational behind the grouping together of these two components in the above-mentioned model, is that these two components are very similar spectrally in their absorption properties. More specifically, both of these components can be adequately (or have been shown to be to date) described by an exponential decay fit (e.g. Roesler 1995)

Figure 2.3 and table 2.1 show the tables and graphs illustrating the results from the statistical analysis carried out on the a_{ys} and a_d absorption spectra. The data analysed involve the slope of the exponent and a specific value of absorption retrieved from the fit on the measured absorption spectra. This provided a substantial data set of 88 samples for the Baltic and 64 for the Adriatic. The datasets included distinct values of $a_{ys}(400)$, $a_d(400)$, $S_{ys}(400\text{-}600)$ and $S_d(400\text{-}600)$. Values for $a_{ys}(350)$ and $S_{ys}(350\text{-}400)$ were also included to test for any large variations in the slope of the CDOM spectra. The exponential fit used for the measured datasets was the following:

$$a_{ys}(\lambda) = a_{ys}(\lambda_o)e^{(-S(\lambda-\lambda_0))} + C \qquad (2.6)$$

for CDOM, and:

$$a_d(\lambda) = a_d(\lambda_0)e^{(-S(\lambda-\lambda_0))} \qquad (2.7)$$

for ad. Here λ_0 and S refer to the values of the specific absorption coefficient and the slope respectively. The value C in the fit for CDOM absorption represents a constant included to improve the fit, and which is proportional to the baseline occurring in the red part of the spectra. This feature is not included in the subsequent analysis as it is interpreted as being an artifactual contribution resulting from instrumental noise or very fine particles (in fact this feature is further minimised by refiltration through

	Baltic							Adriatic					
	A350(CDOM)	S350(CDOM)	A400(CDOM)	S400(CDOM)	A400(NCP)	S400(NCP)		A350(CDOM)	S350(CDOM)	A400(CDOM)	S400(CDOM)	A400(NCP)	S400(NCP)
Mean	3.2763	0.0212	1.1668	0.0188	0.1528	0.0116		0.3498	0.0186	0.1406	0.0176	0.0478	0.0135
Std. Dev.	3.9888	0.0017	1.5682	0.0029	0.2178	0.0026		0.1683	0.0029	0.0583	0.0044	0.0252	0.0026
Variance	15.9107	0.0000	2.4594	0.0000	0.0474	0.0000		0.0283	0.0000	0.0034	0.0000	0.0006	0.0000
Minimum	1.3871	0.0183	0.4781	0.0081	0.0353	0.0049		0.1372	0.0106	0.0520	0.0101	0.0070	0.0088
Maximum	30.2913	0.0280	12.1913	0.0254	1.7977	0.0168		1.0282	0.0281	0.3746	0.0258	0.1267	0.0191
Coeff. of Variation	1.2175	0.0806	1.3441	0.1548	1.4251	0.2288		0.4810	0.1585	0.4145	0.2487	0.5271	0.1898

Adriatic

	400NCP	*400CDOM*	*400TOT*		*412NCP*	*412CDOM*	*412TOT*		*443NCP*	*443CDOM*	*443TOT*
400NCP	0.00068			412NCP	0.00054			443NCP	0.00027		
400CDOM	0.00025	0.00686		412CDOM	0.00019	0.00544		443CDOM	0.00011	0.00367	
400TOT	0.00139	0.00754	0.01104	412TOT	0.00118	0.00595	0.00936	443TOT	0.00066	0.00380	0.00640

Baltic

	400NCP	*400CDOM*	*400TOT*		*412NCP*	*412CDOM*	*412TOT*		*443NCP*	*443CDOM*	*443TOT*
400NCP	0.05339			412NCP	0.04112			443NCP	0.01909		
400CDOM	0.31027	2.37852		412CDOM	0.21801	1.55378		443CDOM	0.07857	0.45182	
400TOT	0.37691	2.76798	3.24278	412TOT	0.27144	1.83908	2.19642	443TOT	0.10493	0.56145	0.71009

	Baltic			Adriatic	
	aCDOM(400) vs. aNCP(400)	SCDOM(400-600) vs. SNCP(400-600)		aCDOM(400) vs. aNCP(400)	SCDOM(400-600) vs. SNCP(400-600)
No. Obs.	88	88		64	64
F	51.85	3.21		5.35	2.89
Fcrit	1.42	1.42		1.52	1.52

Table 2.1: Correlation and covariance results from comparing the variability in the magnitudes and spectral shapes of these substances. The results of the covariance test clearly reject the null hypothesis that $var\_a_{ys}=var\_a_{d}$.

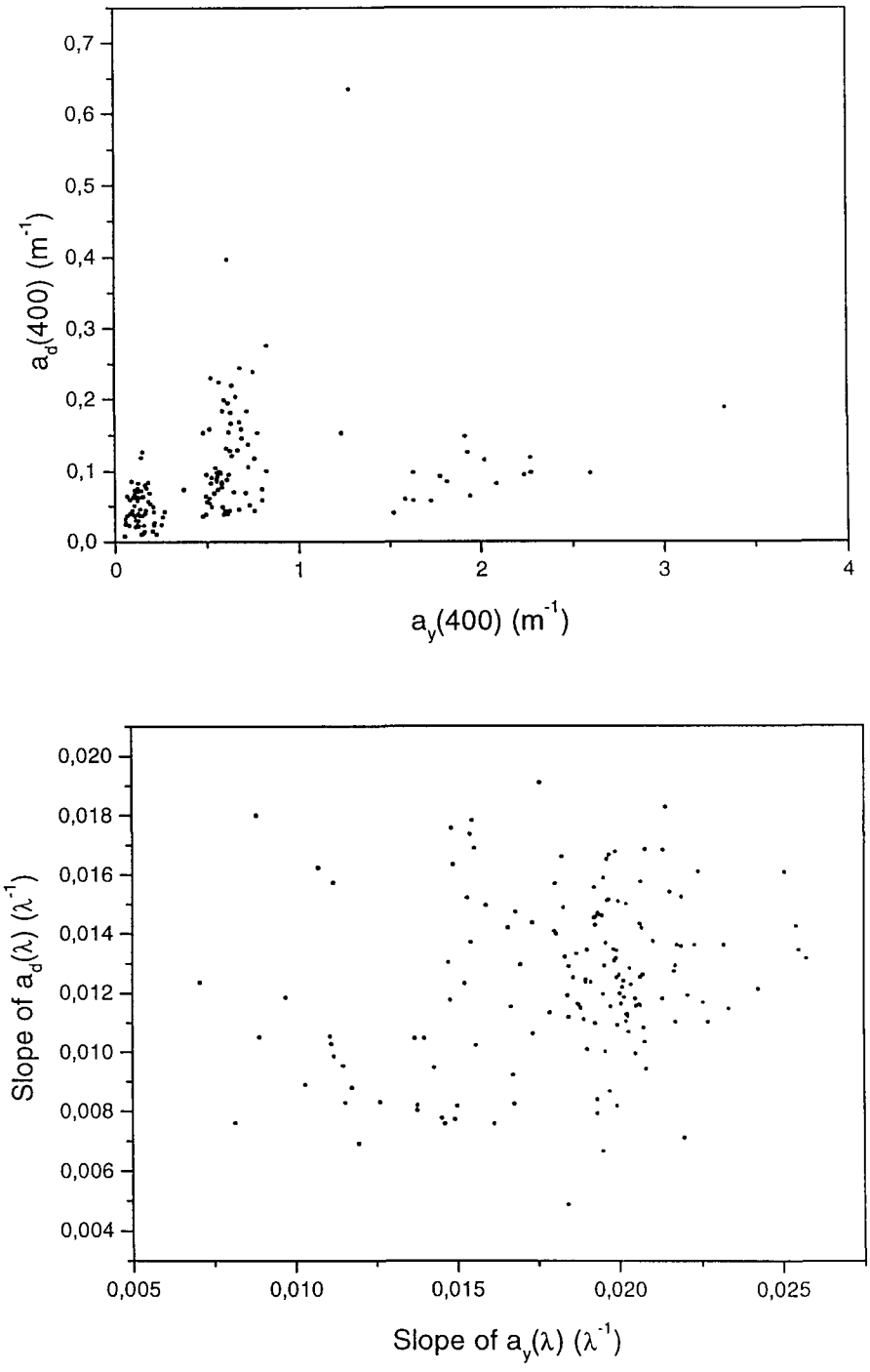

Figure 2.3: Plots examining possible relationships between $a_d(400)$ and $a_{ys}(400)$ top graph, and the slope of $a_d(\lambda)$ and the slope of $a_{ys}(\lambda)$. As can be seen no identifiable relationship is present in the datasets considered.

0.1mm nucleopore filter). The results from the statistical analysis indicate some very clear findings, namely that there is no common relationship in variability between both the specific value of absorption and the slopes of the two datasets (a_d and a_{ys}). This is shown in many ways, principally by the large scatter in the correlation plots. The absence of co-variability between the two components is also shown by the results given in table 2.1 in which it can be seen from the F-test that the calculated values of F are consistently higher than F_{crit}, thus, rejecting the null hypothesis that $\mathrm{var}a_y = \mathrm{var}a_d$.

2.4.2. The spectral variability of absorption in Case II waters

In order to be able to improve current models of absorption (and thus ultimately reflectance) it is necessary to understand and quantify the sources of variance. Absorption spectra themselves are characterised by two main sources of variance in magnitude and spectral shape. In the current study these two aspects of variability over a large dataset of absorption spectra presented in section 2.2. will be considered. Figure 2.4 a-c represents absorption spectra for the three components, phytoplankton, detritus and yellow substance. As can be seen for the three sites considered, these show a reasonable degree of variability in magnitude both at each individual site and when the sites are considered with respect to each other. To be able to understand the site to site variability and more importantly accurately model the total absorption budget, it is essential to have knowledge of the spectral variability of each of the absorption coefficients. To be able to both visually and statistically analyse the spectral variability of each of the components, it is necessary to perform some kind of normalisation of the spectra. This has been traditionally undertaken either by dividing the spectra throughout by a specific concentration (i.e. chlorophyll, sediment, and dissolved carbon) or by normalising the spectra at a specific wavelength (e.g. 440nm). Both of these methods have their disadvantages. With the first method it is often incorrect to assume that the spectral variability will be represented by the chosen normalisation concentration. The second normalisation technique on the other hand tends to distort the true spectral variability in the vicinity of the normalisation

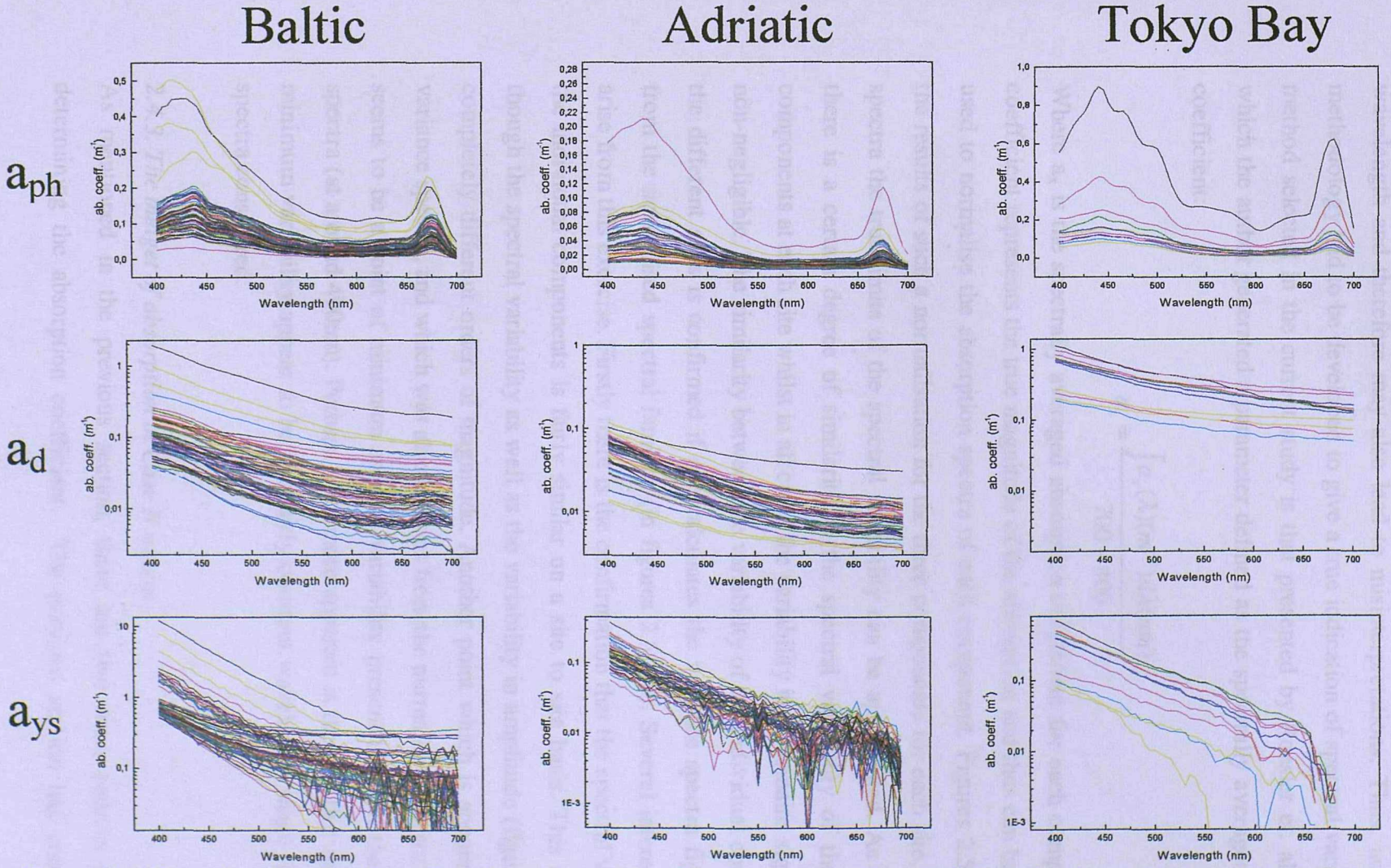

Figure 2.4: Plots showing the absorption datasets considered in the investigation. Including the three sites considered (Baltic, Adriatic and Tokyo Bay from left to right) and the three absorbing components (phytoplankton pigments, detritus, and yellow substance). It is important to note that the scales are not the same and that large ranges of absorption coefficient are covered by the datasets considered.

wavelength and therefore may also lead to misinterpretations. Thus, an alternative methodology had to be developed to give a true indication of spectral variability. The method selected in the current study is that presented by Roesler et. al. (1989), in which the author generated a parameter defined as the spectrally averaged absorption coefficient:

$$a_x = \frac{\int a_x(\lambda)(m^{-1})d\lambda(nm)}{700-400} \tag{2.8}$$

Where a_x is the spectrally averaged absorption coefficient for each component. This coefficient represents the true magnitude of the absorption and thus can be effectively used to normalise the absorption spectra of each component. Figures 2.5 a,b,c show the results of such a normalisation for the three components for each site. From these spectra the true limits of the spectral variability can be appreciated. As can be seen there is a certain degree of similarity in the spectral variability of the individual components at each site whilst in all cases the variability itself remains significant and non-negligible. The similarity between the variability of the individual components at the different sites is confirmed if one calculates the variance spectra figure 2.6 a-c from the normalised spectral families (in figures 2.5 a-c). Several interesting points arise from this exercise. Firstly there is the confirmation that the spectral variability of the individual components is fairly similar on a site to site basis. This is true even though the spectral variability as well as the variability in amplitude (figure 2.4) is of completely different orders of magnitude. Another point which is apparent from the variance spectra, and which was also obvious from the normalised spectra is that there seems to be a point of minimum spectral variability present in all of the families of spectra (at around 490nm). Perhaps even more apparent is the fact that these areas of minimum variability appear to be in a fairly constant wavelength range for all of the spectra considered.

2.4.3. The budget of absorption in Case II waters

As mentioned in the previous section, there are two main sources of variance determining the absorption coefficient. The previous section has considered the

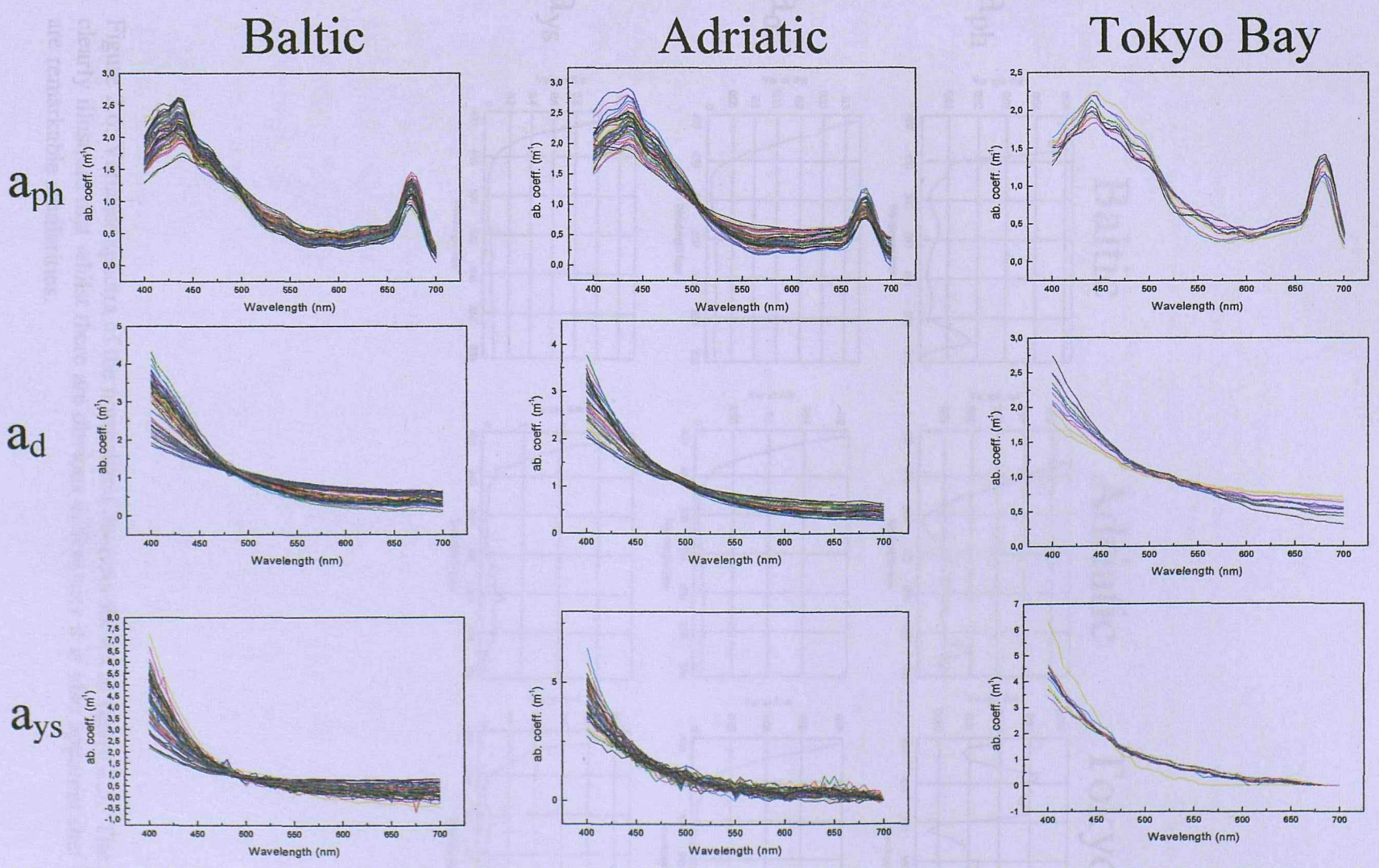

Figure 2.5: Plot showing the spectra from figure 2.4 normalized to the spectrally averaged absorption coefficient. The spectral variance variability observed underlines the need for spectrally variable models for absorption.

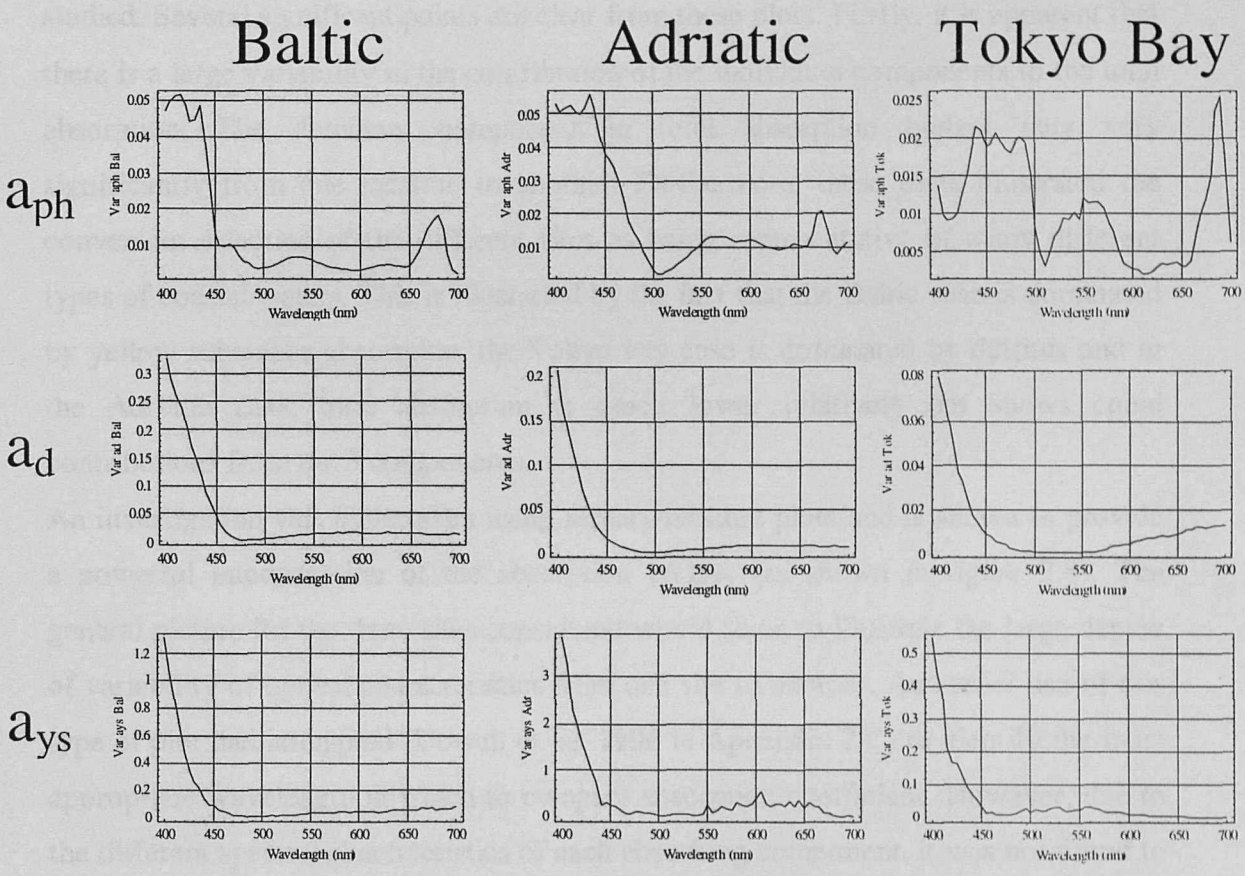

Figure 2.6: Variance spectra of the normalized datasets shown in figure 2.5. The plots clearly illustrate that whilst there are obvious differences it is also apparent that there are remarkable similarities.

spectral variability, although the magnitude variability is also obviously of significant interest and is often found to be closely related to the concentration of the OACs found in the water column (i.e. Chlorophyll, TSM etc). Figure 2.7 shows plots illustrating the contribution of the three components to the total absorption. The plots in figure 2.7 represent the average contribution from each component at each location studied. Several significant points are clear from these plots. Firstly, it is apparent that there is a large variability in the contribution of the individual components to the total absorption. The dominant component in total absorption budget may vary significantly from one location to another. Furthermore, these plots illustrated the convenient selection of the different sites as being representative of many different types of coastal waters. This is illustrated by the fact that the Baltic case is dominated by yellow substance absorption, the Tokyo bay case is dominated by detritus and in the Adriatic case, total absorption is much lower relatively but shows equal contributions from the 3 components.

An investigation was undertaken using ternary/mixture plots and is shown to provide a powerful interpretation of the absorption budget (as shown in figure 2.8). The general picture for the three sites considered would seem to illustrate the large degree of variability of optical characteristics from one site to another. An earlier use of this type of plot had attempted (Dowell et. al. 1996 in Appendix 2.C) to identify the most appropriate wavelength at which to compare absorption coefficient. However, due to the different spectral characteristics of each absorbing component, it was not found to be a straightforward task and a wavelength in the red was used as a best solution. In the present study the use of the spectrally averaged absorption coefficients, as defined in section 2.4.2, was found to be a more appropriate solution as it clearly allows to differentiate between the different optical characteristics of different waters. Following the use of mixture plots in this investigation, it is suggested that their use may be useful for classification purposes. This approach is in reality a modification of a technique originally proposed by Prieur and Sathyendranath 1981 and the merits of such a method in classifying marine waters are presented in detail later.

Baltic

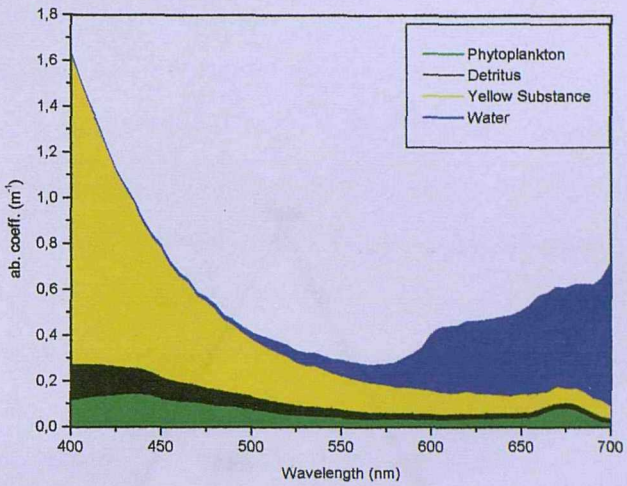

Adriatic

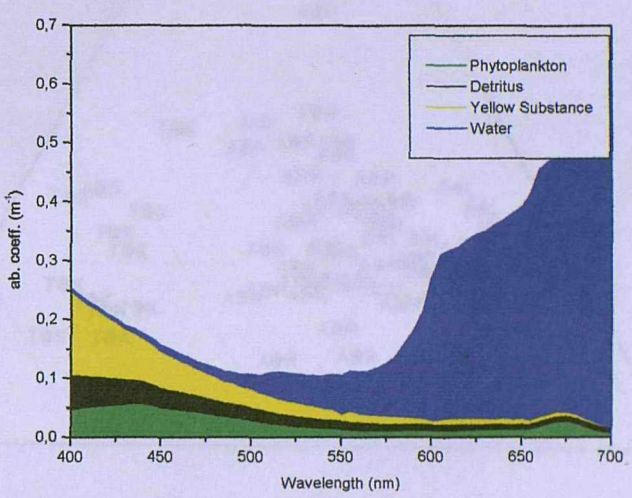

Tokyo Bay

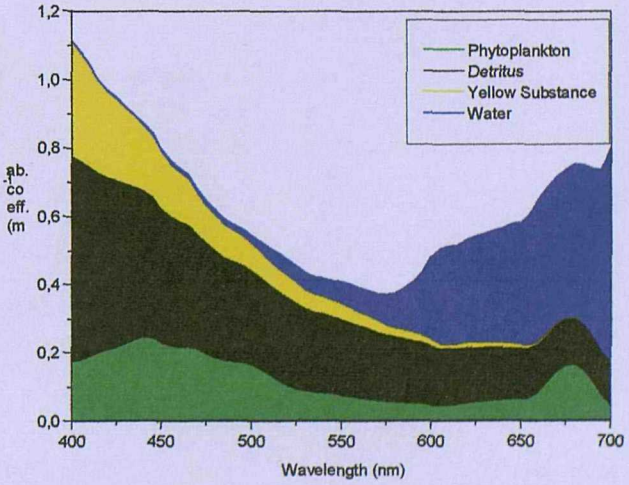

Figure 2.7: Graphs illustrating the total absorption budget for each of the sites considered as an average over all stations. The importance of different components at each site is clearly seen.

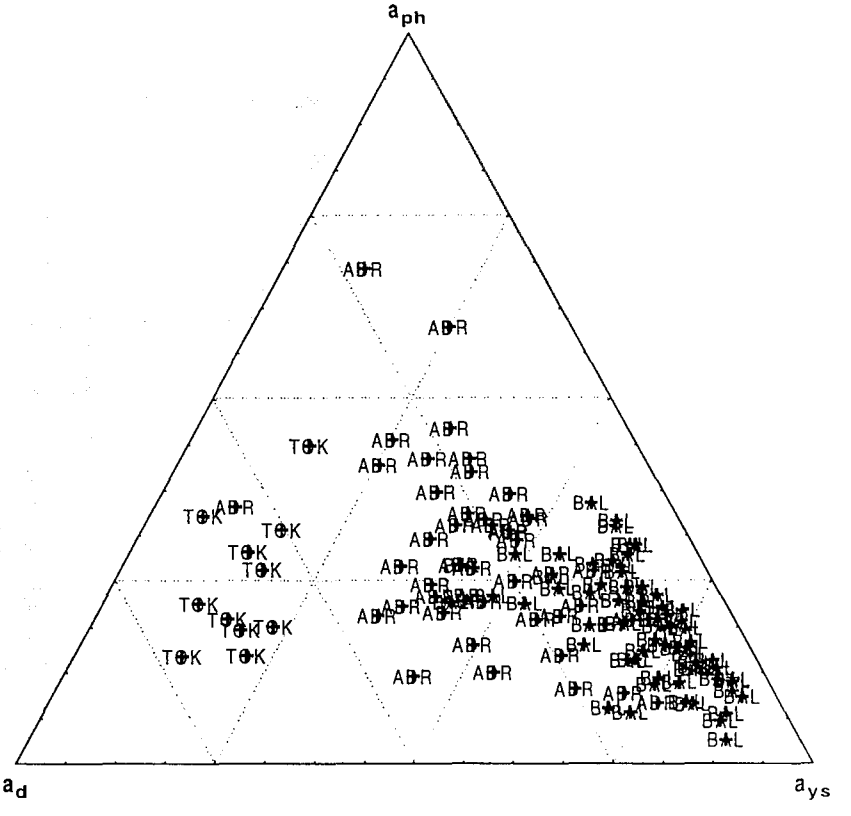

Figure 2.8: A ternary plot of the wavelength average absorption coefficient is used to illustrate the relative composition proportion of the different datasets considered. As can be seen the datasets adopted cover many different water types.

2.5. Discussion

2.5.1. Absorption modelling and sources of variability

In the context of reflectance and primary production modelling, an accurate knowledge of the spectral shape and magnitude of both the individual contributions to absorption and the total absorption coefficient itself is of paramount importance. This is for a number of reasons. Firstly, in the model of surface reflectance a main source of the variability is in spectral shape of reflectance results from the spectral shape of the total absorption coefficient. Secondly, in the model of primary productivity (as will be discussed in further detail in Chapter 5) an important determinant particularly in coastal waters is in the combined effect of the absorption of pigments and the total downwelling diffuse attenuation coefficient. Their importance is determined by the fact that, in coastal waters, a large amount of the light available at the water surface for use by photosynthetic pigments is removed by these other light absorbing constituents in the water column, i.e. particulate detritus and yellow substance. Also in coastal waters the pigment absorption spectra can often be characterised by the contribution of accessory pigments which are important in order to adequately quantify the amount of light used by pigments in photosynthesis.

The need to adequately model the absorption budget is self-evident. Many pieces of work have either instrumentally (e.g. Kishino et. al. 1985), statistically/ mathematically (e.g. Bricaud and Stramski 1990) or on the basis of specific absorption coefficient (e.g. Hoepffner and Sathyendranath 1991) attempted to subdivide and model the various contributions to absorption. Of these a further category aimed at developing a model to describe the in-situ absorption of each component (water, phytoplankton, detritus and yellow substance) based on *a priori* knowledge. These types of work originated with the paper of Prieur and Sathyendranath (1981) and continued with a manuscript by Roesler et. al. (1989). It is believed these papers have contributed significantly to the understanding of absorption characteristics, and it is to the knowledge developed in these studies that the current study would aim to contribute. In general the detrital curve has a lower exponential slope than the CDOM, although in both cases the slope has been shown to

vary over a considerable range (e.g. Bricaud and Stramski (1990) for detritus, and Roesler et. al. 1995 for CDOM).

Krijsmann (1994) proposed an alternative model of the spectral dependence of absorption spectra of humic substances from Dutch lakes, based on Target Factor Analysis (TFA). Krijsmann (1995) showed, through a detailed residual analysis, that the TFA model for humic substance absorption performed much better than any of the exponential models and even better than the two component model suggested by Carder et. al.(1985). Therefore it was decided to analyse the same datasets using the TFA to evaluate the improvement in the spectral models for both a_d and a_{ys}.

For each dataset considered, the first two eigenvectors were calculated and are shown in figure 2.9. (figure 2.9a shows yellow susbtance and figure 2.9b detritus). As can be seen there is very little variability and therefore the eigenvector taken from a cumulative dataset can be considered as being global and can be used in the subsequent analysis. To determine the accuracy of the calculated eigenvectors in evaluating the spectral absorption a residual analysis was performed on both the cumulative a_{ys} and the cumulative a_d datasets (Figure 2.10). This was done using the eigenvector algorithm and comparing with the fit of a 0.014 exponential model and a 0.018 exponential model and finally a model where the slope was also allowed to vary. As can be seen the eigenvector performed better than the traditional exponential models in both the case of a_{ys} absorption and a_d absorption, therefore justifying the use of these models in any further description of absorption.

Furthermore it would seem that the eigenvectors retrieved and used in the model were universal (or at least over the datasets investigated) to the extent that these vectors did not significantly change when either the whole dataset was considered or only subsets of the dataset. These analyses were carried out on both the a_d and a_{ys} spectra giving positive results in both cases and therefore ensuring a more accurate deconvolution of the total absorption coefficient. However, none of the factor scores from the two different absorption coefficients were found to be correlated with each other between detritus and yellow substance, therefore confirming the conclusions made in section 2.4.1 on the co-variability of detritus and yellow substance absorption coefficients.

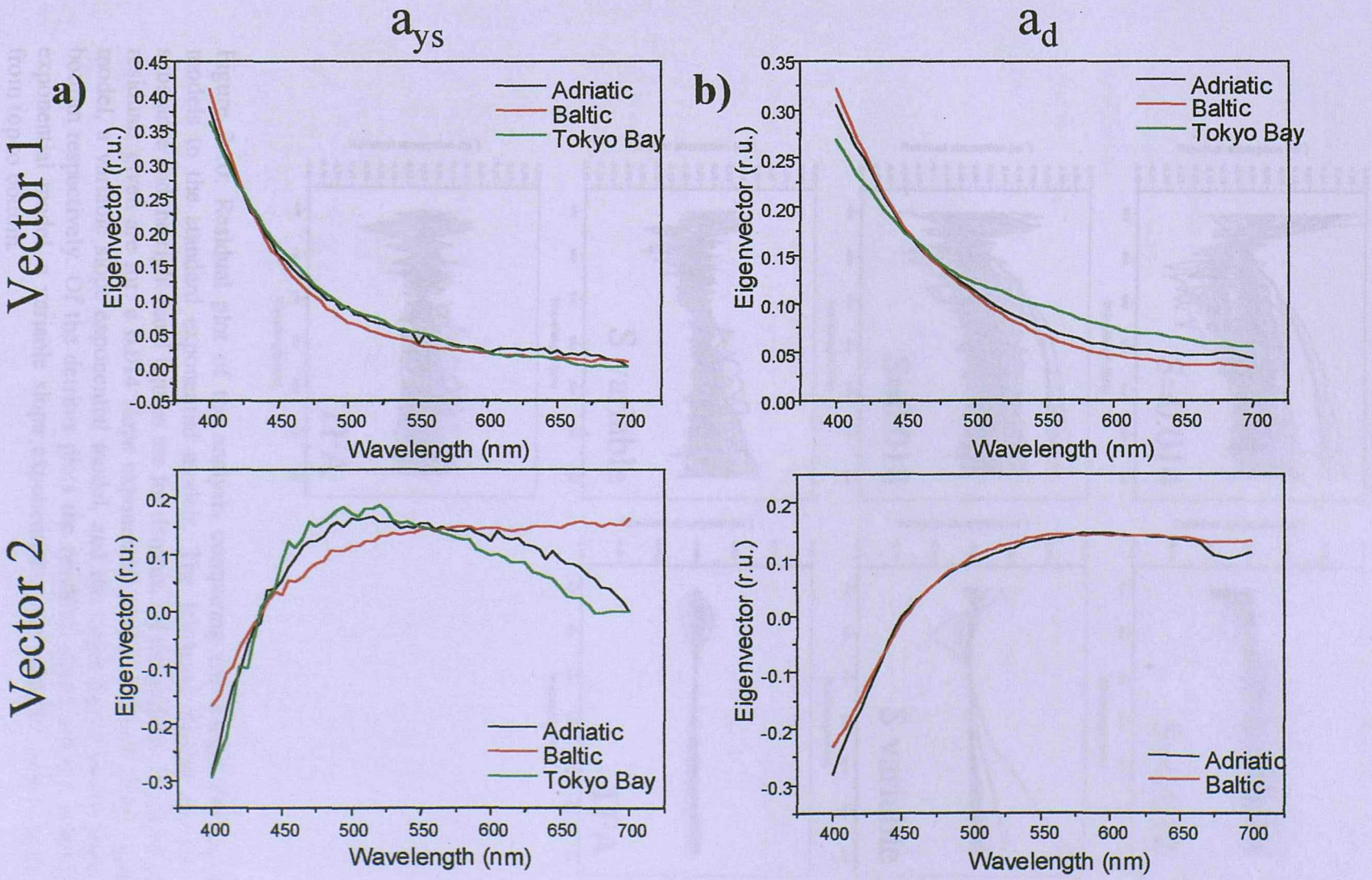

Figure 2.9: Plot showing the first (top) and second (second) eigenvectors for the three datasets. On the left (figure 2.9a) the plots for yellow substance and on the right (figure 2.9b) the plots for detritus.

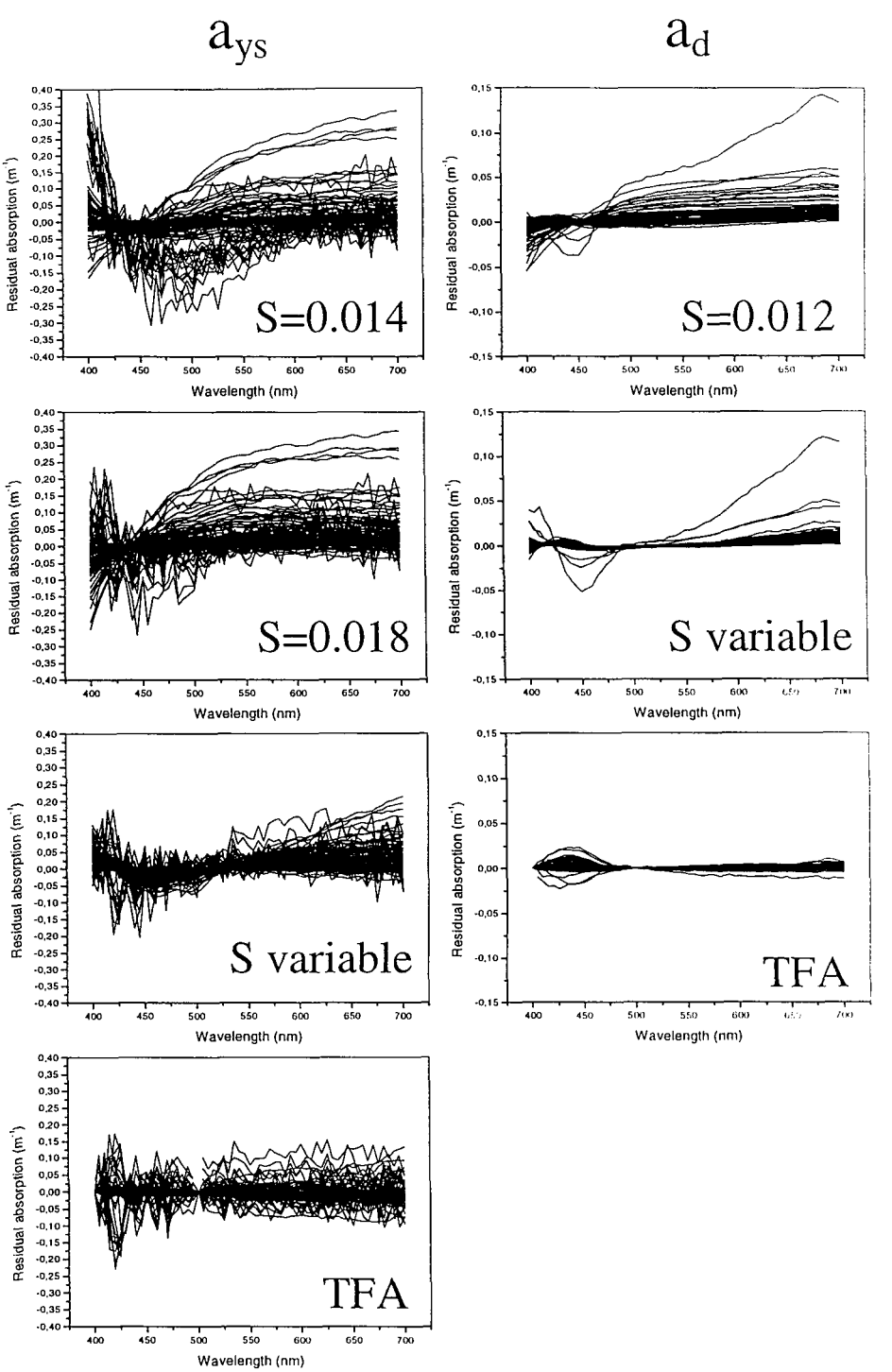

Figure 2.10: Residual plot of the analysis comparing the Target Factor Analysis models to the standard exponential models. The left-hand figures are for yellow substance and the right-hand figures are for detritus. Of the yellow substance plots the residuals given are for: a 0.014 slope exponential model, a 0.018 slope exponential model, a variable slope exponential model, and the target factor model from top to bottom respectively. Of the detritus plots the residuals given are for: a 0.012 slope exponential model, a variable slope exponential model and the target factor model from top to bottom.

the datasets investigated) to the extent that these vectors did not significantly change when either the whole dataset was considered or only subsets of the dataset. These analyses were carried out on both the a_d and a_{ys} spectra giving positive results in both cases and therefore ensuring a more accurate deconvolution of the total absorption coefficient. However, none of the factor scores from the two different absorption coefficients were found to be correlated with each other between detritus and yellow substance, therefore confirming the conclusions made in section 2.4.1 on the co-variability of detritus and yellow substance absorption coefficients. A standard formulation for retrieving the absorption coefficient of yellow substance is given by:

$$a_{ys}(\lambda) = (a_{ys}U_1(\lambda)a_{ys}FS_1) + (a_{ys}U_2(\lambda)a_{ys}FS_2). \quad (2.9)$$

The equivalent formulation by detritus is given by

$$a_d(\lambda) = (a_dU_1(\lambda)a_dFS_1) + (a_dU_2(\lambda)a_dFS_2). \quad (2.10)$$

In both of the above equations U_1a_{ys}, U_2a_{ys}, U_1a_d and U_2a_d are the first and second eigenvectors for yellow substance and detritus respectively and FS_1a_{ys}, FS_2a_{ys}, FS_1a_d and FS_2a_d are the respective factor scores which are calculated through the best fit to equations 2.9 and 2.10. The first two eigenvectors for yellow substance and detritus are shown in table 2.2 here below for SeaWiFS/OCTS wavelengths.

	412	443	490	510	555	670
a_{ys} Vector 1	0.831	0.472	0.218	0.164	0.096	0.045
a_{ys} Vector 2	-0.356	0.125	0.426	0.459	0.499	0.465
a_d Vector 1	0.727	0.508	0.320	0.263	0.176	0.107
a_d Vector 2	-0.506	0.022	0.342	0.426	0.495	0.447

Table 2.2: First and second mean Eigenvectors for a_{ys} and a_d.

The applicability of this type of formulation is well accepted in that it explains several aspects of the absorption of these two components that were known but not accounted for. For example it is well known that detrital matter has a baseline of absorption at

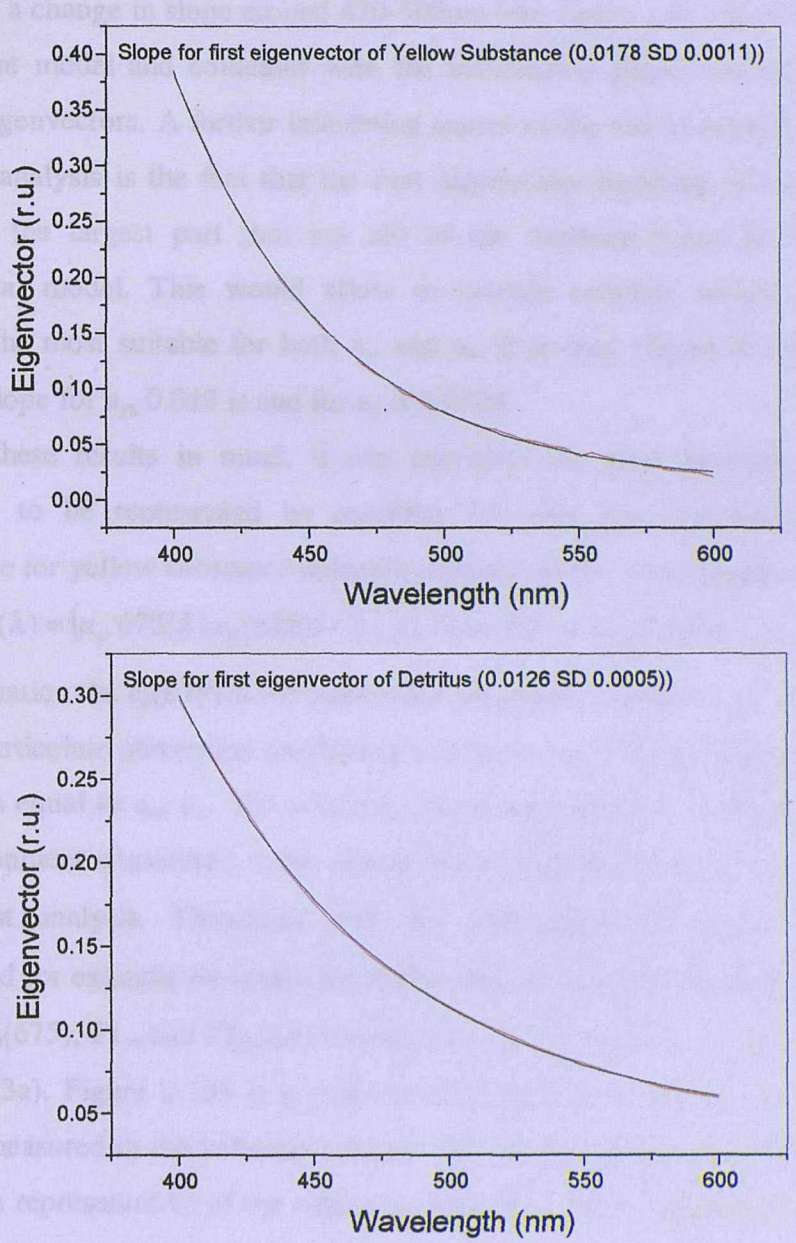

Figure 2.11: Plots showing the averages of the first eigenvectors for the datasets considered and their best exponential fits, for yellow substance (top) with a best fit of ~0.018 and detritus (bottom) with a best fit of ~0.0125.

700nm and is the main contributor to absorption in this range apart from the constant and known absorption of water itself and this new formulation of the absorption coefficient is able to account for this. Also in the a_{ys} spectra it was often observed that there was a change in slope around 470-500nm (see figure 2.4) and this is reflected in the current model and coincides with the intersection points between the first and second eigenvectors. A further interesting aspect of the use of vectors resulting from the TFA analysis is the fact that the first eigenvector resulting in both cases which describes the largest part (but not all) of the variance could be fitted using an exponential model. This would allow to crudely estimate which slope value is globally the most suitable for both a_{ys} and a_d. It is seen (figure 2.11) that the most suitable slope for a_{ys} 0.018 is and for a_d is 0.0125.

Bearing these results in mind, if one considers the total absorption by in-water substance to be represented by equation 2.5, one can rearrange this with the knowledge for yellow substance absorption gained in the above analysis so that:

$$a_{sub}(\lambda) = \left(a_p'675(\lambda)a_p(675)\right) + \left((a_y U_1(\lambda)a_y FS_1) + (a_y U_2(\lambda)a_y FS_2)\right) \qquad (2.11)$$

in this equation the $a_p(675)$ is the particulate absorption coefficient at 675nm and $a_{p'}$ is a mean particulate absorption coefficient normalised at 675nm (shown in figure 2.12) and a_{sub} is equal to a_{tot}-a_w. The accuracy of the normalised a_p spectra in representing the environment considered is not of significant importance as it will not be used in subsequent analysis. Therefore, with the knowledge on $a_{sub}(\lambda)$ which can be determined for example by in-situ measurements of $a_{tot}(\lambda)$ (as with the AC-9) one can retrieve $a_p(675)$, $F1_{ys}$ and $F2_{ys}$ and therefore a_{ys} for the satellite wavelengths (shown in figure 2.13a). Figure 2.13b is a plot showing the correlation between $a_{ys}(412)$ and $a_{ys}(412)$ measured in the validation dataset. As can be seen the high levels of CDOM absorption representative of the validation dataset are well represented by the model. We can now retrieve the *real* $a_p(\lambda)$ as follows:

$$a_p(\lambda) = a_{sub}(\lambda) - a_{ys}(\lambda) \qquad (2.12)$$

With $a_p(\lambda)$ calculated a similar procedure as previously carried out to retrieve $a_{ys}(\lambda)$ can now be carried out to retrieve $a_d(\lambda)$ using:

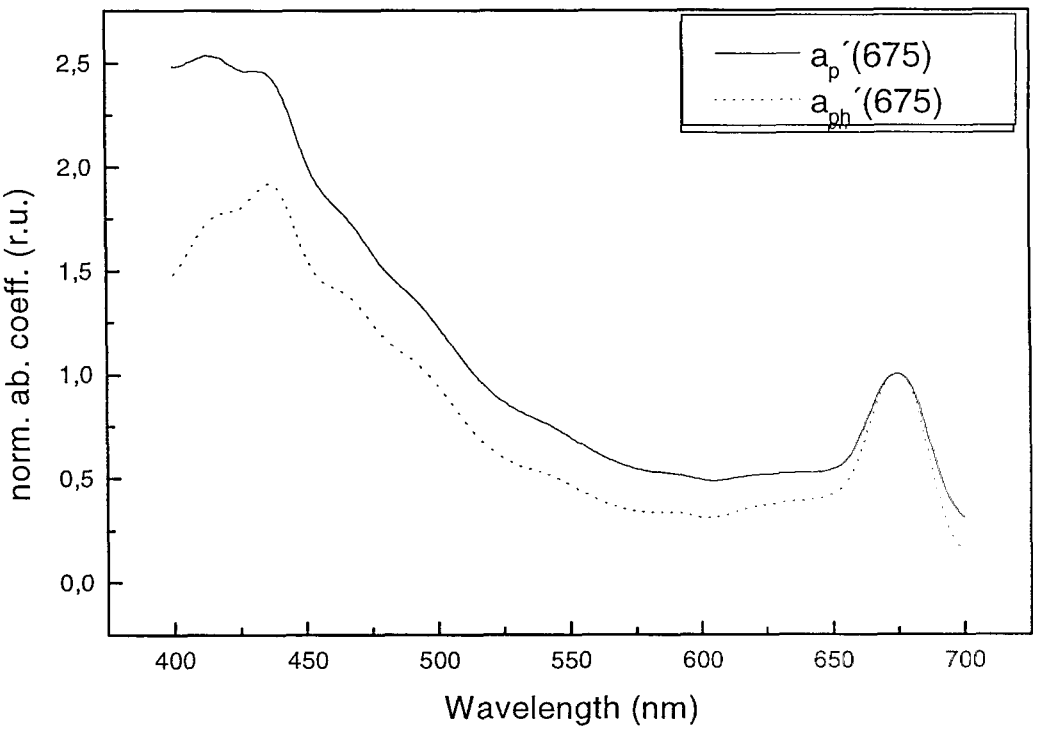

Figure 2.12: Plot showing the average normalised spectra used for phytoplankton pigment and particle absorption in the deconvolution process.

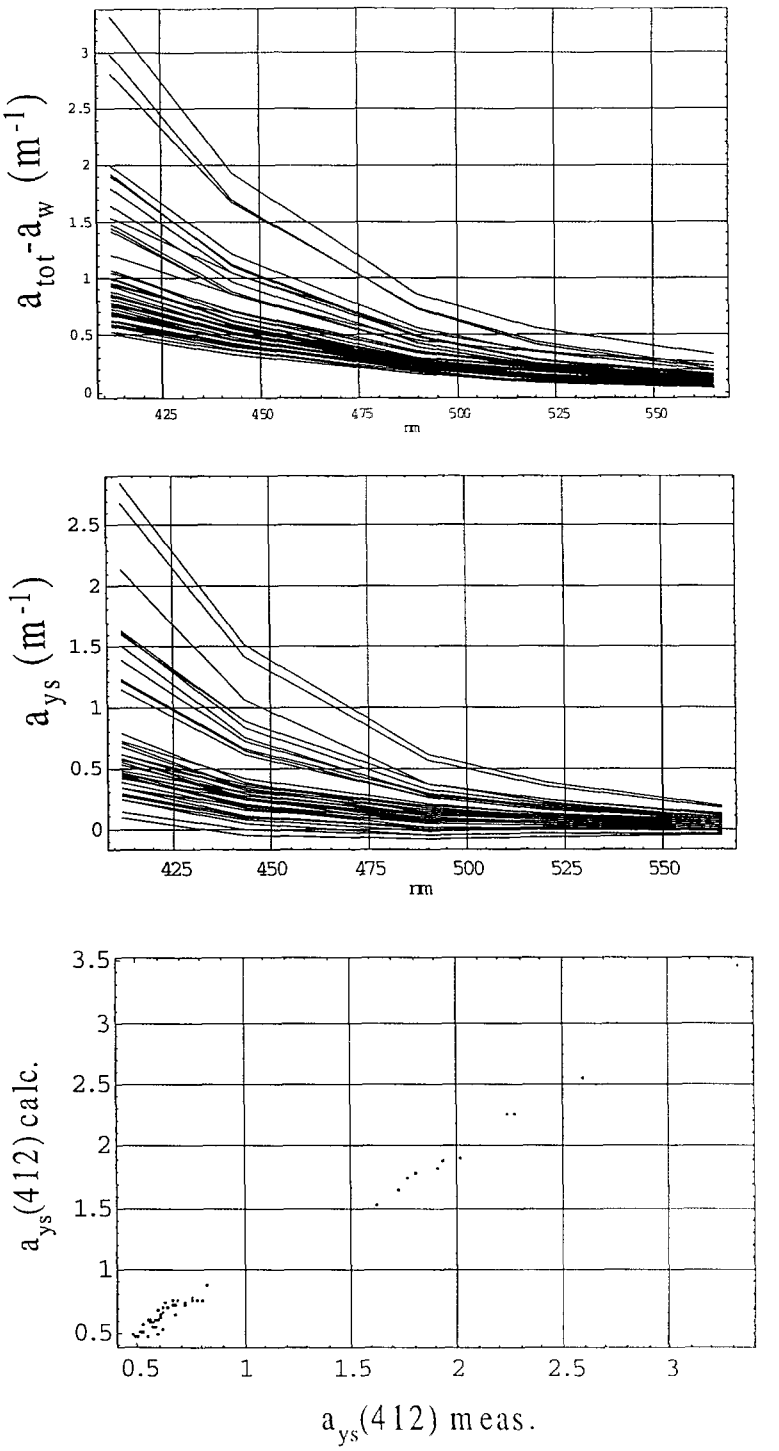

Figure 2.13: Graph showing phases of the deconvolution process. The top figure is the total substance absorption, the middle figure the calculated $a_{ys}(\lambda)$ absorption, and the bottom figure is a graph illustrating the retrieved against measured $a_{ys}(412)$ values.

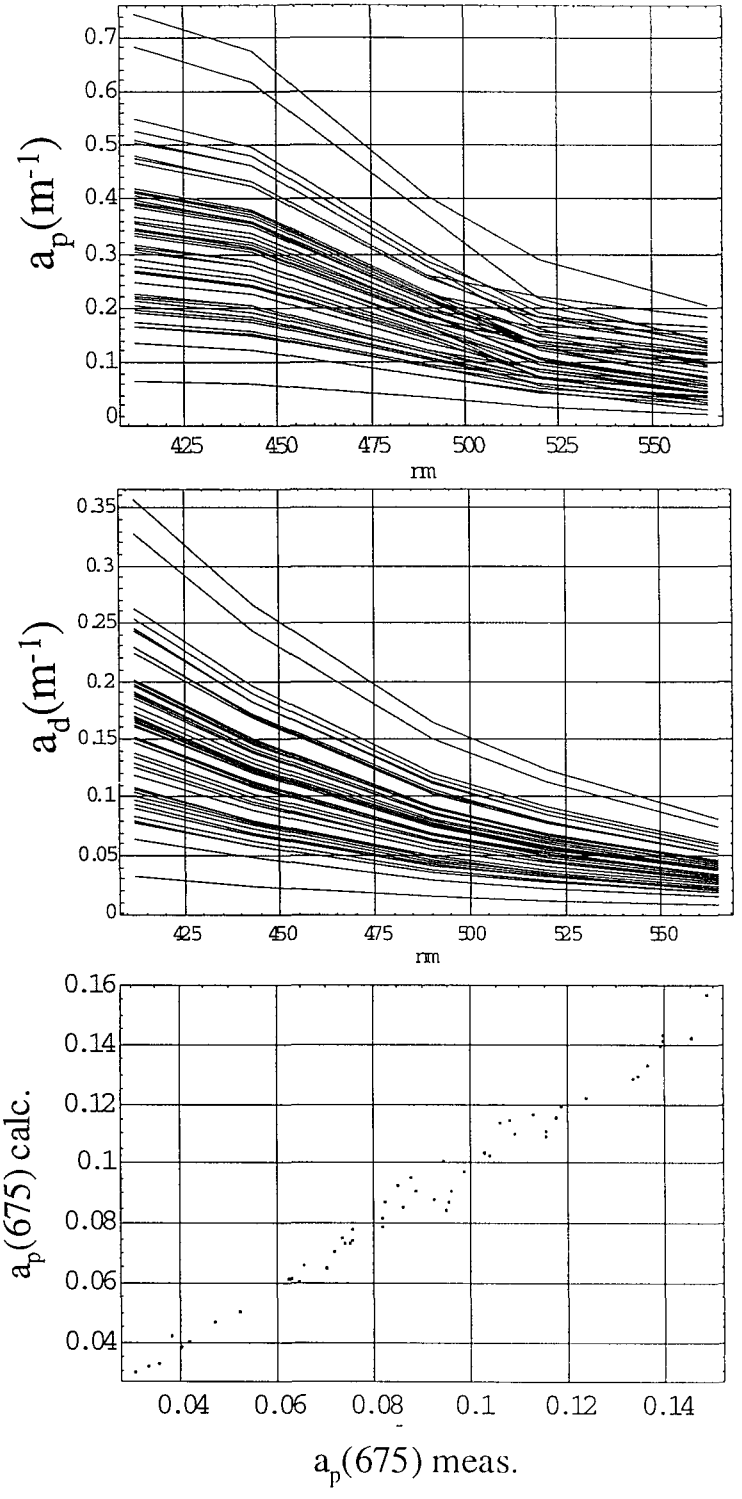

Figure 2.14: Graph showing further phases of the deconvolution process. The top figure is the total particle absorption the middle figure is the computed detritus absorption and the bottom figure is a graph illustrating the retrieved against measured $a_p(675)$.

$$a_p(\lambda) = \left(a_{ph}'675(\lambda)a_{ph}(675)\right) + \left((a_d U_1(\lambda)a_d FS_2) + (a_d U_2(\lambda)a_d FS_2)\right) \quad (2.13)$$

Here $a_{ph}(675)$ is the pigment absorption at 675nm and a_{ph}' is the mean absorption coefficient for phytoplankton like pigments (also shown in figure 2.12). Again the U1, U2 and FS_1, FS_2 refer to the first and second eigenvectors and the first and second factor scores for detritus respectively. Using the information on $a_p(\lambda)$ from equation 2.12 Equation 2.13 can be solved and $a_{ph}(675)$, $F1_d$ and $F2_d$ retrieved. With the factor scores $a_d(\lambda)$ can be calculated (shown in figure 2.14a) from the eigenvectors, figure 2.14 also shows a correlation between the $a_p(675)$ calculated and that measured in the validation dataset. Thus finally the real absorption due to phytoplankton pigments can be calculated from this expression:

$$a_{ph}(\lambda) = a_p(\lambda) - a_d(\lambda) \quad (2.14)$$

The pigment absorption spectra calculated ($a_{ph}(\lambda)$) are shown in figure 2.15.

Thus, use of the alternative model of the spectral distribution of absorption of detritus and CDOM has allowed the development of a more flexible method for deconvolving the total absorption coefficient. However, in order to verify whether this model of the two non-chlorophyllous components truly represents the spectral variability of these two components in the natural environment a further investigation can be made. This investigation involves taking the datasets presented in the current study and shown in figure 2.4 for a_{ys} and a_d using the above eigenvector fits to retrieve the factor scores for each sample and then reconstructing the absorption spectra based on this best fit. Once this has been done then a spectral analysis can be performed on the spectra as undertaken on the original spectra in section 2.4.2 to retrieve the variance spectra for a_d and a_{ys}. This analysis was undertaken and the results are shown in figure 2.16. As can be seen the TFA model is able to reproduce a similar spectral variance spectra for a_y and ad as found in the original field spectra, thus justifying its use in an absorption model as presented above and underlining its improved accuracy over the traditional exponential approximation.

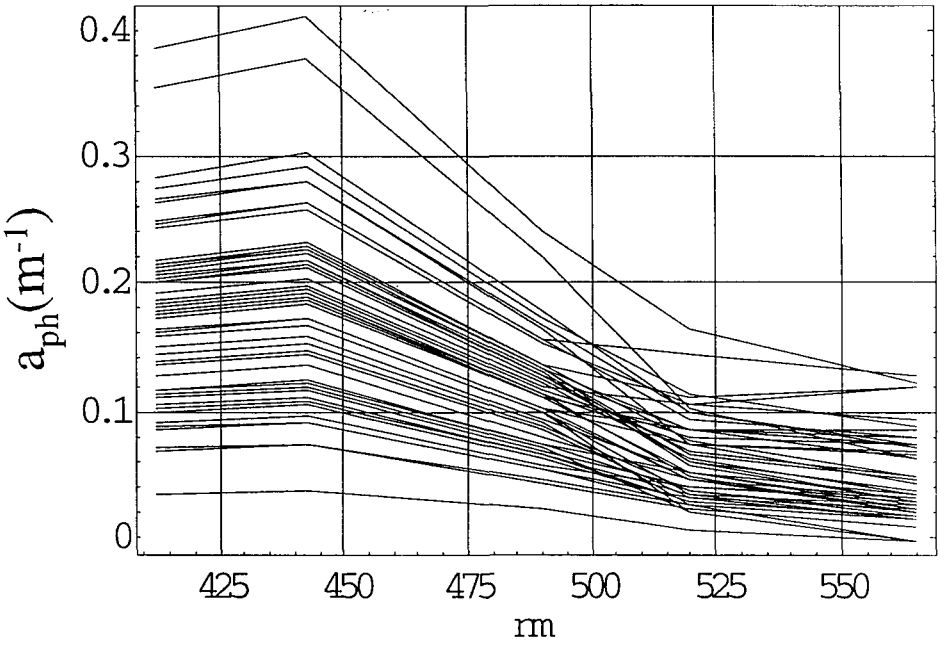

Figure 2.15: Graph of the phytoplankton pigment absorption resulting from the deconvolution process.

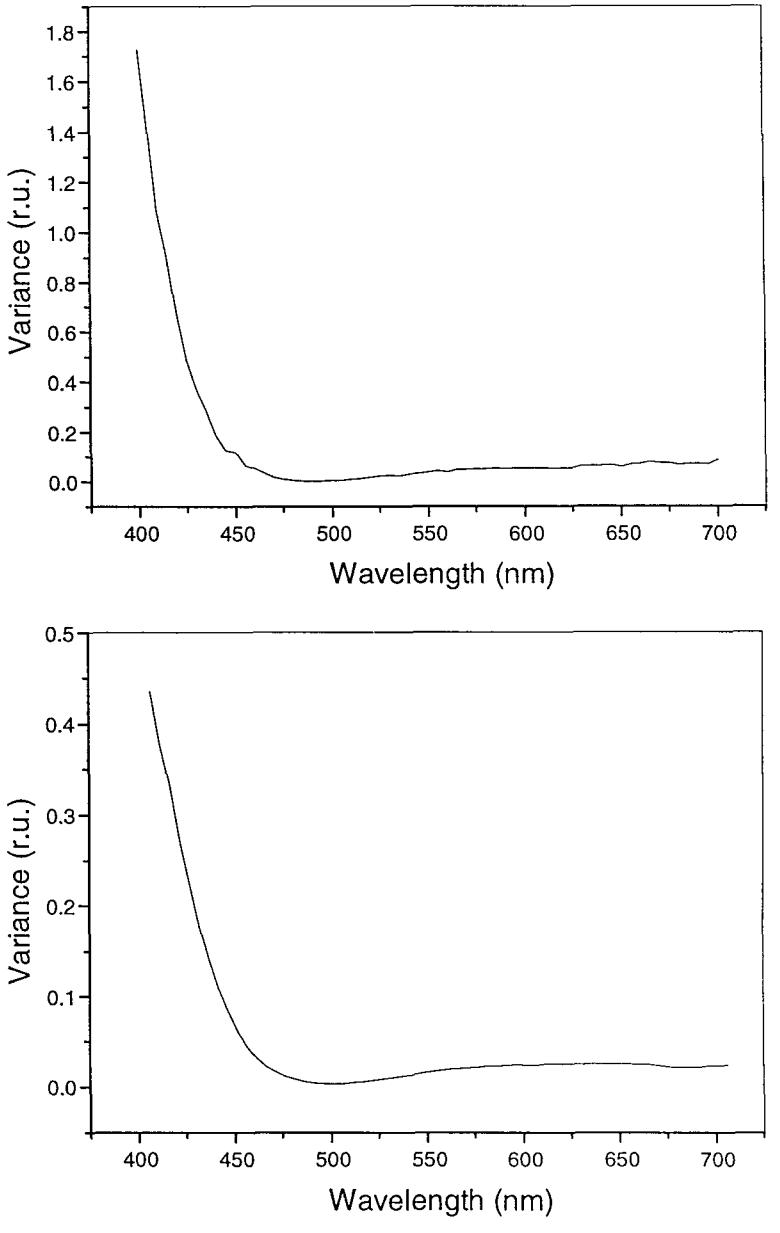

Figure 2.16: Plots of the spectral variance spectra reproduced using the Target factor model, for yellow substance (top) and detritus (bottom). It is seen that the shape of the calculated spectra compares very well with those of the field spectra given in figure 2.6.

2.5.3. Spectral variability of pigment absorption, significance in forward modelling

The variance spectra presented in figure 2.6a for in-vivo pigment absorption show a fairly recurrent shape, particularly above 500nm where they are almost identical. Furthermore these spectra are seen to be very similar (particularly for the Adriatic and the Baltic cases) to that shown by Roesler et. al. 1989 for a dataset from San Juan Island.

The spectral variability in spectral variance is known to be principally dependent on pigment composition (Hoepffner and Sathyendranath 1992, Bidigare et. al. 1989) and pigment packaging (Kirk 1975). In an ideal model for absorption an objective would be to reproduce the spectral variance in the model that has been observed in the field data. Standard approaches, such as identifying specific absorption spectra for the spectral distribution of pigment absorption for a particular region, are obviously inadequate as they do not allow for variability in spectral shape whatsoever (e.g. Prieur and Sathyendranath 1981, Hoepffner and Sathyendranath 1992). A recent model proposed by Bricaud et. al. (1995) offers an alternative solution in that it varies the specific absorption coefficient as a function of chlorophyll concentration as well as the absorption coefficient itself. In their formulation (Bricaud et. al. 1995) represent the absorption coefficient of phytoplankton pigments as,

$$a_{ph}(\lambda) = a^{*}_{ph}(\lambda)\langle Chl \rangle \tag{2.15}$$

where,

$$a^{*}_{ph}(\lambda) = A(\lambda)\langle Chl \rangle^{-B(\lambda)}. \tag{2.16}$$

Here a^{*}_{ph} is the specific absorption coefficient and $A(\lambda)$ and $B(\lambda)$ are spectral coefficients retrieved by the authors through a best fit analysis of 815 spectra with equivalent chlorophyll a concentrations. The values of $A(\lambda)$ and $B(\lambda)$ are tabulated at 2nm intervals in the above mentioned paper. Since this model allows a certain degree of spectral variability in the derived absorption it was thought that this would be a good model for which to test the spectral variance compared to those obtained from the field spectra. Therefore, a dataset of pigment absorption spectra were simulated using the Bricaud model within the empirical limits of the data presented in the above

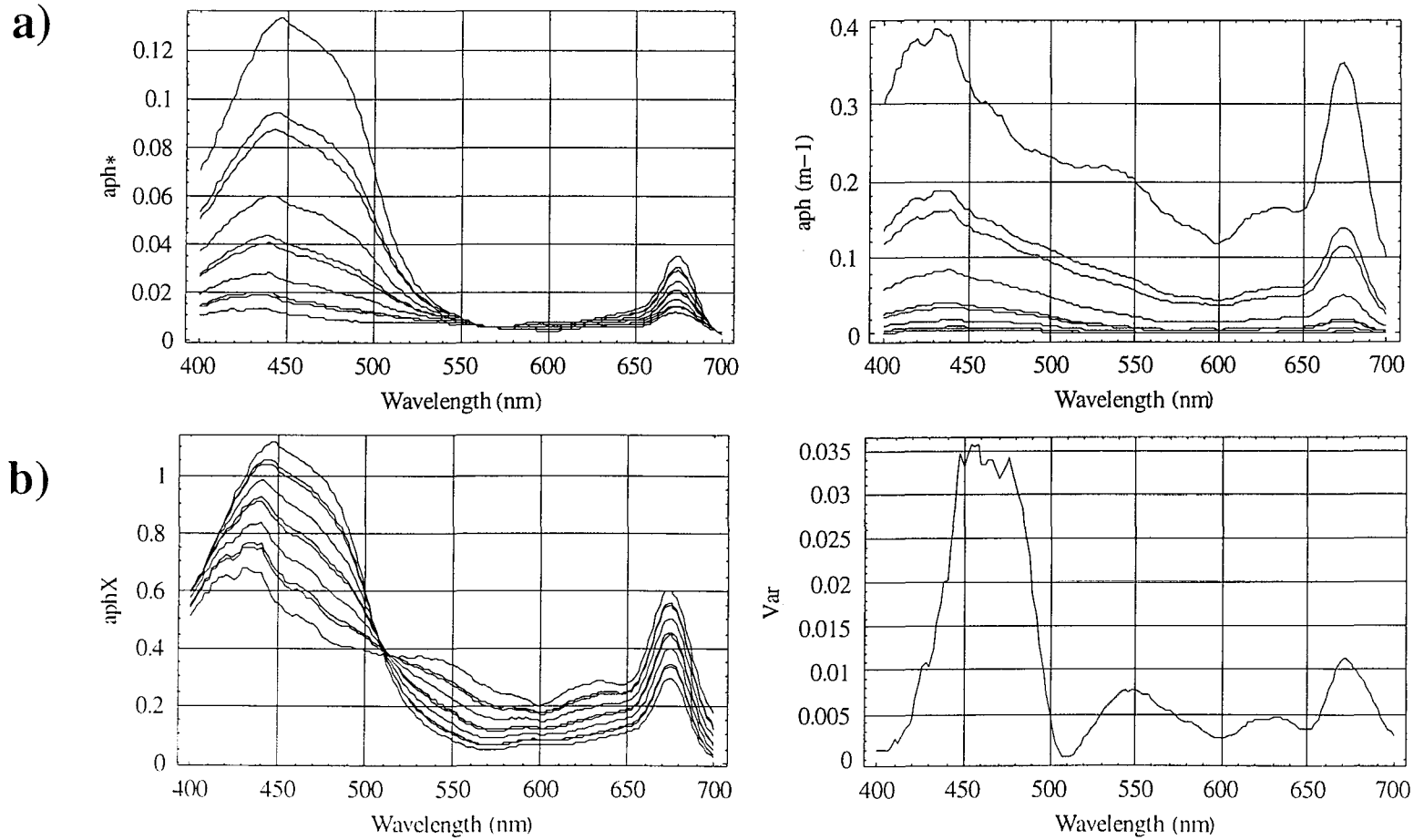

Figure 2.17: Plots showing the calculation of spectral variance spectra for phytoplankton pigment absorption using the Bricaud et. al. (1995) model. From top left to bottom right the following plot are given: The specific absorption spectra, the absorption coefficient, the normalised absorption spectra and the spectral variance spectra.

paper (the resulting spectra are shown in figure 2.17a). Then an analysis identical to that previously applied on the field data (section 2.4.2.) was carried out, to calculate the spectral variance spectra. This was performed normalising the spectra to their own *spectrally averaged absorption coefficients* and the results are shown in figure 2.17b. As can be seen the variance spectrum from the model has many similarities with the field spectra. Differences in the blue for some of the field spectra are due to the presence or absence of pheophytin *a* in the individual datasets. These characteristics, i.e. a first peak shifted further into the blue are also reproduced in some of the in-situ datasets i.e. Tokyo Bay.

The implications of these model results reach beyond the application in the general absorption model. Such a model would have a notable impact on the integration of absorption in reflectance modelling particularly because of the fact that the parameterisation of the model is kept simple. Further investigations could only consolidate the appropriateness of such a technique, in that it may for example be interesting to regenerate such a dataset of As and Bs as those presented by Bricaud et. al. (1995) for coastal waters with higher chlorophyll concentrations i.e. above 0.5 mg/m^3. This will allow the reproduction of spectral variance similar to that shown in the Baltic and Adriatic and by Roesler (1989) for the San Juan Islands.

2.5.4. An IOP classification and its significance in algorithm development

Historically, optical classification of waters had received much attention beginning with Jerlov (1951) then improved in Jerlov (1976) who pioneered this subject with a classification based on the spectral diffuse attenuation coefficient. Jerlov's classification, whilst representing a significant initial contribution, only represented a restricted number of water types. In fact as shown by Prieur and Sathyendranath (1981) the nomenclature adopted by Jerlov was primarily relevant to yellow substance dominated waters (their inverse J type) and therefore not generally applicable. Smith and Baker (1978) presented an improvement on the Jerlov model. Their technique separates the influence of phytoplankton pigment and the covarying substances on the diffuse attenuation coefficient. This technique however is shown to be inapplicable in

areas of high sediment concentration (Prieur and Sathyendranath 1981). All of the above mentioned methods were based on the diffuse attenuation coefficient. This variable in itself is not an IOP but an AOP i.e. it is not only dependent on the absorption and scattering properties of the water mass but also on the angular distribution of the radiance field and the sun earth geometry. This implies that an equivalent, from the point of view of the water constituents, water mass may be classified differently from one area to another exclusively on the basis of illumination characteristics. It was for this reason that Prieur and Sathyendranath (1981) proposed the use of Ternary plots with their coefficients P′, C′ and Y′ to classify optically the water types from region to region. In the present study it is intended to proceed with a similar idea. However, instead of using values of absorption at a specific wavelength (in their case $P'+C'+Y'=a_{tot}(440)$), which may be subject to the spectral characteristics of the individual absorbing component in that range, it is proposed that the spectrally averaged absorption coefficients be used instead. These coefficients represent a true indicator of the variability in magnitude of each absorbing component (as defined in equation 2.8). The Ternary plot shown in figure 2.8 can be used to subdivide water types when a classification nomenclature such as that shown in figure 2.18 is adopted. This type of representation illustrates the true diversity of the datasets used in the present investigation and underlines the potential of a classification based on the absolute magnitude of the IOPs. In fact there is a possible use of such a classification scheme in order to delimit areas where specific remotely sensed algorithms could be applied. For example if one considers the factor analysis type of algorithms (e.g. Sathyendranath et. al. 1989, Fisher et. al. 1986, chapter 3 of the current thesis) it may be more accurate to determine the specific characteristic vectors typical of each sub area in a ternary plot (i.e. YS, CHL, DET, YS-CHL, YS-DET etc.). This would permit

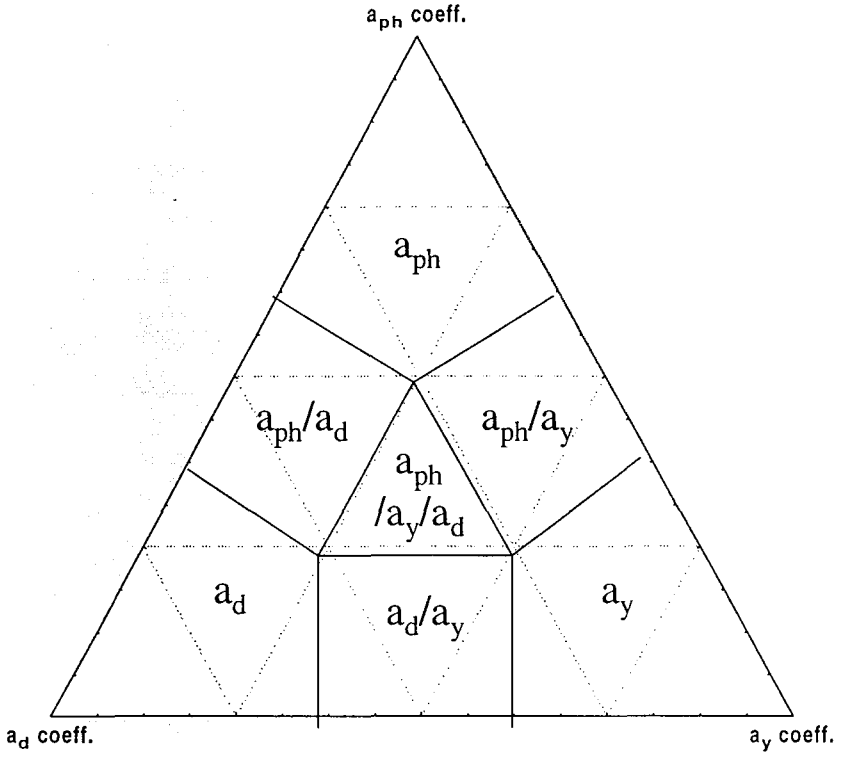

Figure 2.18: A schematic of a possible classification method, based on the use of ternary/mixture plots and the use of spectrally averaged absorption coefficients.

the development of individual algorithms for each of these water types that could be subsequently chosen on the basis of an advanced flagging system.

2.6. Conclusions

The presented study has shown the need to independently describe the contributions to the total absorption budget of surface Case II waters by a_d and a_{ys}. The ranges, means and standard deviations found are in some cases substantially different to those presented in literature, indicating that allocating a mean slope in the model of the absorption of these parameters may represent a considerable source of error. The results have further shown the importance of these two components in the composition of Case II waters, where either of these constituents can prove to be dominant in the budget of the total absorption. The analyses of the variance coefficients has shown that it is incorrect to assume co-variability of the two components or that there is a seasonal variability, as there are strong gradients in the variables considered for the two datasets showing no relationship (within 95% confidence levels). The detailed investigation in the source of variance of the individual components both in magnitude and in spectral shape has shown that the traditional models used for each of the components are inadequate in describing a large amount of the spectral variability. The use of TFA is proposed for a more accurate representation of the yellow substance and detritus components and a model deconvolving absorption to retrieve in-vivo absorption from total absorption coefficient is presented and shown to reproduce absorption at satellite wavelengths to within 20% error. A model published by Bricaud et. al. (1995) was considered in its capacity to reproduce the type of spectra variance found in the field datasets considered. The analysis applied on a simulated dataset using the model showed similar results. Differences between several of the spectral variance spectra in the wavelength range 400-450nm were attributed to the presence or absence of pheophytin a in the dataset considered. The variance spectra resulting from Bricaud et. al. (1995) suggested an absence of pheophytin a, it is therefore suggested that an alternative dataset of As and Bs required for the Bricaud et. al. (1995) model could be

generated (this would be typical of certain coastal waters and could be implemented in models with a flagging system i.e. > or < 0.5 mg/m^3). Alternatively if the model for a_{ph} is for use in, for example, primary production modelling where pheophytin a is not a photosynthetically active pigment, then some way should be found to incorporate this pigment in the detrital term.

The results from the ternary plots have indicated the potential of the spectrally averaged absorption coefficients, in describing and differentiating the different components. It also illustrated the adequacy of the datasets considered in the present study in covering many different water types. It is suggested that the proposed classification scheme be of considerable importance in the formulation of models and algorithms for basins exhibiting a large degree of variability of the three components.

A recent study (Garver et. al. 1997) made use of Empirical Orthogonal Function analysis to investigate the sources of variability of a large database of particulate absorption spectra. Their study concluded that the only sources of variability detectable from ocean colour are the absolute magnitude and the spectral variability due to phytoplankton and detritus.

It is the author's opinion that these conclusions are a result of the methodologies and datasets adopted. In particular with the nature of the study made one may have imagined that a more diverse dataset should have been used representing different extreme examples of particulate absorption coefficient to truly assess the possible sources of spectral variability to the signal measured from satellite. The present study has evidenced the large degree of spectral variability in each of the components. This is shown not only through the change in accessory pigment concentrations apparent in the aph spectra (see figures 2.5 and 2.6) but also through the changes in slopes and hinge points of the ay and ad spectra. Furthermore it is the author's firm belief that if future fundamental research in ocean colour remote sensing is to fulfil the applications it claims to be capable of (e.g. coastal water quality studies), it will have to concentrate on methods to study the noise remaining after three main components are removed (Garver et. al. (1997)). It is here that much of the interesting information which could be available from multispectral or hyperspectral optical data lies.

Chapter 3

A three component Reflectance model for developing regional algorithms in Case II waters

Chapter 3 Table of Content

3.1. Introduction
3.2. Reflectance Theory
3.3. Statistical Distributions of the OACs
3.4. Forward Model
3.4.1. Relationship between OACs and the IOPs
3.4.2. Inherent Optical Property parameterisation
3.4.2.1. Parameterisation of absorption
3.4.2.2. Parameterisation of the backscattering
3.4.3. *Calculation of the proportionality factor (r)*
3.4.4. Determination of the Q-factor
3.5. Inversion procedure
3.6. Discussion
3.6.1. Parameterisation of CDOM absorption
3.6.2. The two component model for scattering
3.6.3. Determination of r is the remote sensing context
3.6.4. Reproduced shape of reflectance
3.6.5. Adequacy of the spectral information from RS wavelengths for Case II waters
3.6.6. PCA inversion scheme and the geophysical algorithms
3.7. Conclusions

3.1 Introduction

A significant proportion of European waters can be either continuously or sporadically considered as being turbid, or optically defined as Case II waters (Morel and Prieur 1977). The development of accurate algorithms to systematically retrieve quantitative information on water constituents from remote platforms in these areas is not straightforward due to the large spatial and temporal variability of the in-water components from region to region as well as within a region itself. There is still a need therefore to define a standard methodology for the development of regional algorithms in Case II waters.

A reflectance model can be formulated if the necessary information exists on the spectral scattering and absorption, and on how these determine water leaving radiances and reflectance. The mathematical description relating these parameters constitutes the "forward reflectance model".

All algorithms have to use, in some form, a forward reflectance model. What mainly differentiates one algorithm from another is the subsequent inversion procedure. These inversion procedures can be categorised under three main *schools*:

Statistical: in this case the "forward" model is systematically applied to a wide range of its initial variables in order to generate a set of simulated reflectance spectra. On this simulated dataset statistical analyses are applied (e.g. Principal Component Analysis) with the aim of building algorithms relating reflectance to the OACs (e.g. Sathyendranath et. al. 1989, Gower et al 1986).

Semi-analytical: in this case mathematical methods are used to solve a system of equations based on the relationship between reflectance and the IOPs (for the wavelengths of interest) defined within the forward model (e.g. Carder 1989, Roesler et. al. 1995, Siegel and Garver 1997).

"Inverse modelling" or analytical: complete radiance spectra at the sensor level are generated for given OACs as well as for atmospheric content in aerosol using a

radiative transfer model for both atmosphere and ocean. Mathematical models are then used to retrieve the right set of components that produces the set of radiances corresponding to the one actually measured by the sensor (e.g. Doerffer and Fisher 1995).

The *statistical* model presented here is intended to offer a framework applicable to many different geographic regions where each region would be parameterised by specific distribution function characterising the natural variability of the Optically Active Components (OAC). The optically active components considered in the current study include Chlorophyll concentration (CHL), Total Suspended Matter concentration (TSM) and Yellow Substance concentration (YS, also referred by many authors as Coloured Dissolved Organic Matter (CDOM)). The model also addresses the specific requirements of Case II water optics, including an emphasis on accounting for the variability needed to describe the non-chlorophyllous components in the absorption and scattering segments of the forward model.

The development of the model is conducted following three major steps:

1) At first, the distribution functions of the individual OAC are defined for the region in question for all periods of the year. These functions are represented as log-normal distributions which have been recently identified as the most suited function to describe the bio-optical variability in marine environments (Campbell, 1995).
2) The second step includes the development of a forward reflectance model itself, relating the OACs to the IOPs and the latter to the Apparent Optical Properties (AOP) represented in this case by the spectral irradiance reflectance just beneath the sea surface ($R^{0-}(\lambda)$).
3) Finally, an inversion technique of the simulated reflectance spectra is developed using statistical multivariate techniques, i.e. Principal Component Analysis (PCA), to retrieve the OACs from remotely sensed ocean colour data.

3.2 Reflectance Theory

As established in *chapter 1* the irradiance reflectance R is defined as:

$$R = \frac{E_u}{E_d} \tag{3.1}$$

where E_u is the upwelling irradiance and E_d is the downwelling irradiance. As already mentioned in *chapter 1* the wavelength (λ) dependence is always present but omitted and all mathematical relationships are considering surface waters only unless indicated to be depth dependent by z.

Many approximations of radiative transfer models for the sea have established relationships between R and the IOPs (a and b_b), starting with the quasi-single scattering approximation of Gordon (1973, 1975) which was derived for homogeneous waters with a flat air-water surface. The expression for R was obtained through a regression analysis performed on results acquired by Monte Carlo simulations, and is given by:

$$R = \sum_0^3 r_n x^n \tag{3.2}$$

where,

$$x = \frac{b_b}{(a + b_b)} \tag{3.3}$$

In this polynomials fit, r is the fitting term from the regression analysis and the first order term is predominant. In fact Gordon found r_1 to vary from 0.32 in the case of parallel illumination from the zenith, to 0.37 for totally diffuse illumination.

Since then it has been general practice to adopt this type of relationship of the general form

$$R = f\frac{b_b}{a + b_b} \qquad \text{or} \qquad R = f\frac{b_b}{a} \tag{3.4}$$

with the assumption in the second case of equation 3.4 that $b_b << a$ (Morel and Prieur 1977). In these expressions, f is a proportionality factor relating R to the IOPs (a and b_b). This f factor has been shown to be dependent on the zenith angle (e.g. Kirk 1981,1984). However it has recently been shown that its angular dependence changes also with the total volume scattering function (Morel and Gentili 1991) and shown to

vary (Morel and Gentili 1993) in the range 0.25 to 0.54. In all the above cases the parameterisation of the f factor has been determined by regression. In each study, for a given set of initial conditions (zenith angle and volume scattering phase function), Monte Carlo simulations are carried out for a given range of b_b/a (or $b_b/(a+b_b)$). On this simulated dataset the computed values of R are regressed against the latter to obtain f. However the use of results from this type of approach in the operational remote sensing context required the use of extremely large Look Up Tables (LUT), with no analytical definition of f explaining the physical basis of the relationship.

A recent analytical solution presented by Sathyendranath and Platt (1997) follows the quasi-single scattering approximation of Gordon (1975) assuming that reflectance should be proportional to $b_b/(a+b_b)$. However it deviates from this approach in that it deals directly with irradiance rather than radiance. They achieved the solution by considering the upward flux that is generated at an arbitrary depth z owing to elastic scattering, then considered the transmission of that flux to the surface (figure 3.1a) and finally integrated the contributions from all depths to obtain the total upwelling irradiance.

As commented above, their investigation aimed at a solution in terms of irradiance, and arrived at a solution for upwelling irradiance at the sea surface $E_u(0)$ of the form:

$$E_u(0) = \frac{sb_b}{\mu_d} \times \frac{E_d(0)}{(K+\kappa)} \tag{3.5}$$

This would imply that the irradiance reflectance is given by:

$$R(0) = \frac{E_u(0)}{E_d(0)} = \frac{sb_b}{\mu_d (K_d + \kappa)} \tag{3.6}$$

where s is the shape factor defined as b_u/b_b (b_u is the upward-scattering coefficient, as defined by Sathyendranath and Platt 1991 see figure 3.1b), μ_d is the mean cosine for downwelling irradiance, K_d is the attenuation coefficient for downwelling irradiance and κ is the quasi-diffuse attenuation coefficient for upwelling irradiance. So as to express the equation in the same form as equation 3.4 the authors give K and κ in terms of a and b_b:

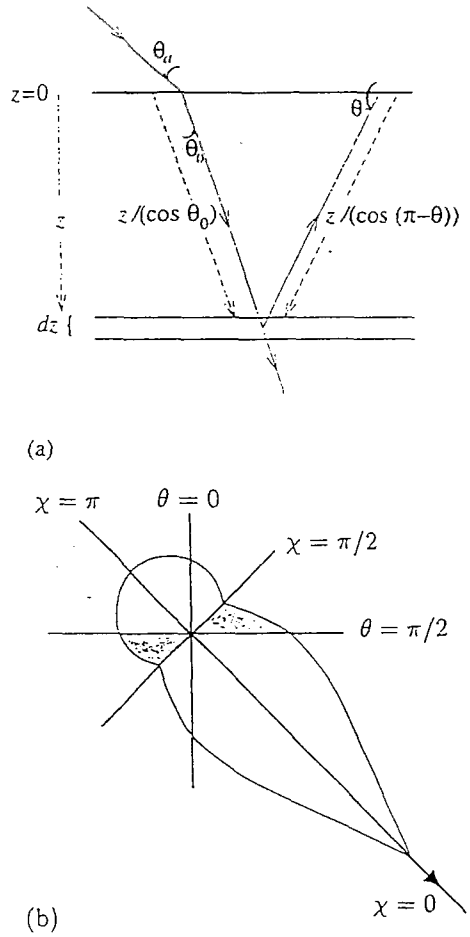

Fig. 1. Geometry of the optical processes: (a) Path length of light per unit vertical excursion is a function of the zenith angle of the light beam. Light is incident at the sea surface ($z = 0$) at an angle θ_a. After refraction this light is transmitted through the water column at an angle θ_0. Scattering takes place over the depth interval dz at depth z, and scattered light is transmitted back to the sea surface at angle θ. (b) The geometry of scattering: The direction of the incident light is shown by an arrow. The closed curve is a schematic representation of the volume-scattering function. Note that the backscattering coefficient is computed with reference to the scattering angle χ whereas the upward-scattering coefficient is computed with reference to the zenith angle of the scattered light θ. The back-scattering coefficient differs from the upward-scattering coefficient when the two shaded areas are not equal to each other.

Figure 3.1: Geometry of the optical processes considered after Sathyendranath and Platt (1997).

$$K_d = \frac{a + b_b}{\mu_d(z)} \tag{3.7}$$

and,

$$\kappa = \frac{a + b_b}{\mu_u(z)} \tag{3.8}$$

where μ_u is the mean cosine of upwelling irradiance. Finally, assuming that μ_d and μ_u are invariant with depth and substituting for K and κ in Equation 3.6, the solution for R(0) is:

$$R(0) = \frac{\mu_u s}{(\mu_u + \mu_d)} \times \frac{b_b}{(a + b_b)} \tag{3.9}$$

The first term on the right hand side of the equation must be equivalent to the proportionality factor *f* in equation 3.4, thus offering an analytical solution for this parameter. The implementation of this model for the case discussed in this manuscript, and more generally in the remote sensing context, requires information on μ_u, μ_d, and s in addition to a and b_b. An in depth analysis of the parameterisation of the proportionality factor through the determination of μ_u and s will be given at the end of section 3.5.

3.3 Statistical Distributions of the OACs

Now a mathematical structure exists on which to base the forward model, one needs to start parameterising the inputs and relationships of the model. A fundamental part of the presented model involves the parameterisation of the input data sets used to simulate the reflectance spectra and inverted to produce the bio-optical algorithms for the region in question. Much of the criticism of the use of the inversion procedure presented later in this chapter has concentrated on the *blindness* of the methodology relating to the natural environment. With this in mind it was decided to use concentration distribution functions representative of the environment studied and to define the increment of the concentration of each of the OACs used as input in the simulation of reflectance.

A recently reviewed (Campbell 1995) mathematical function that has been extensively used to describe biological and bio-optical variability in the sea is the lognormal distribution. It was shown to be representative of numerous parameters over a wide range of scales in both space and time, including Chlorophyll both from satellite and in-situ, water leaving radiances (L_w), Photosynthetically Active Radiation (PAR), fluorescence, and primary production. Furthermore the lognormal distribution has also been extensively used in representing particle size distributions (e.g. Jonasz & Fournier 1996).

The use of the lognormal distribution in the current investigation has provided a representative distribution of input increments for the forward reflectance model through an absolute number of intervals for each OAC, and was conducted using the described method.

First, in-situ data were used to characterise lognormal function by fitting a lognormal Probability Distribution Function (PDF) of the form:

$$f(X) = \frac{1}{X\sigma(2\pi)^{1/2}} \exp\left[-\frac{(\ln X - \mu)^2}{2\sigma^2}\right] \tag{3.10}$$

where X represents the individual OAC concentration and μ and σ^2 are the shape factors of the lognormal curve i.e. the mean (μ) and the variance (σ^2) of $\ln X$. The parameters μ and σ^2 of the fit are therefore used to define the PDF used in the subsequent analysis. The PDFs for each of the OACs are shown in Figure 3.2a, b and c. The in-situ data used to define the fits were the following: For [CHL] a data set of 1500 datapoints contributed by Dr. Lepannen (Finnish Institute for Marine Research) were also compared with data from the ULISSE campaigns and showed to be very representative. The [TSM] population used was that of the ULISSE cruises (100 samples) as were those for YS (120 samples). The equations representing the best fit for the components are as follows:

for CHL:

$$f([CHL]) = \frac{0.87e^{-2.40(-1.06+\ln[CHL])^2}}{[CHL]} \tag{3.11a}$$

for TSM:

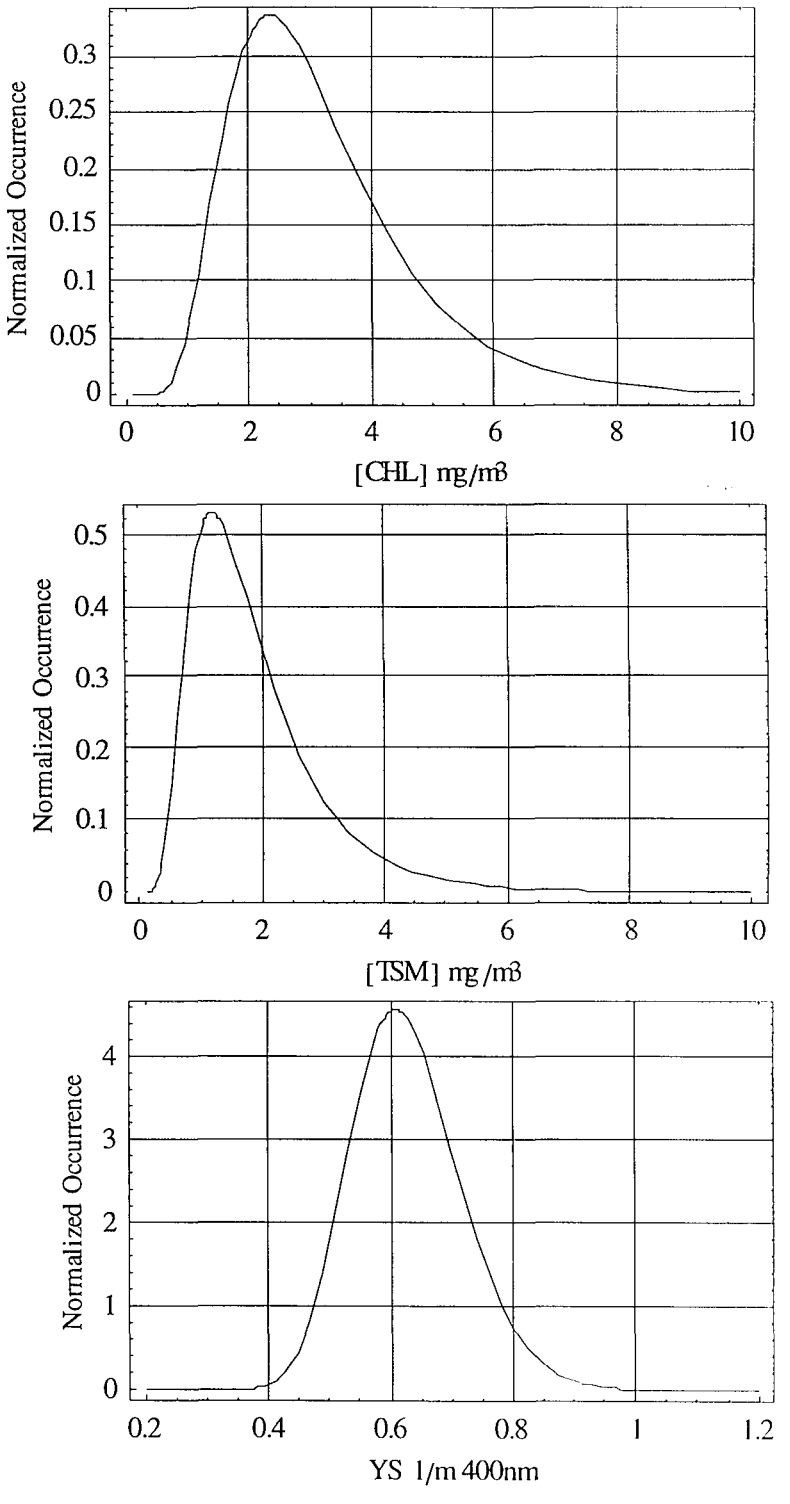

Figure 3.2: Plots of the probability distribution functions for chlorophyll (top), TSM (middle) and yellow substance (bottom) for the Southern Baltic to be used for the initiation of the forward model.

$$f([TSM]) = \frac{0.73e^{-1.69(-47+\ln[TSM])^2}}{[TSM]} \quad (3.11b)$$

and for YS:

$$f([YS]) = \frac{2.80e^{-24.69(0.48+\ln[YS])^2}}{[YS]} \quad (3.11c)$$

Once the PDFs have been defined then the subsequent procedure is as follows. The indefinite integral is found for each of the PDFs. Then a definite integral is performed for each of the PDFs, over a range that is known to cover each of the OACs. The numeric value of the definite integral of each of the OAC PDFs is then divided by the number of intervals (n) determined to be used for each OACs; in the present study a value of 20 intervals was chosen. Finally an equation is solved for each cumulative interval in the indefinite integral therefore retrieving the list of concentrations equivalent to the density of observations in each PDF. The retrieved values, 20 for each OACs, were then used to generate a permutation table of 8000 combinations to be used in simulation of the reflectance. The table is thus representative of the natural variability of the OACs in a specific region (here the Baltic). Values external to the range were also added to test the sensitivity of the model. Note that the YS distribution function represents only the background YS concentration (i.e. open waters) and does not include the fraction of YS observed in the immediate vicinity of the river mouths. This fraction is added in the simulation at linear intervals ranging between 1.2 and 12 m^{-1} at 400nm.

3.4 Forward Model

3.4.1 Relationship between OACs and the IOPs

The initialisation of a forward model for water reflectance requires one to define the relationships between the OACs and their optical properties (i.e. the IOPs). Table 3.1 shows the general formulation used for such relationships. It includes:

- a^*_{ph} (the specific absorption of phytoplankton pigments),

- $a_{ys}(400)$ and $a_d(400)$ (the absorptions of coloured dissolved organic matter and non-chlorophyllous particulates respectively at 400nm),
- and v_s and v_l (the concentrations of small and large particles respectively and will be used as inputs for the backscattering model).

Relationships between OACs and IOPs
$a^*_{ph}=A[CHL]^B$
$a_{ys}(400)=[YS]$
$a_d(440)=f$ ([CHL] and [TSM])
$v_s=f([TSM])$
$v_l= f([CHL])$

Table 3.1: relationship between OACs and the IOPs

As seen in the above table a listing of general relationships are given for each relationship between the OAC and its related IOP, apart from YS which by definition is described in its concentration by the absorption coefficient at 400nm (i.e. $a_{ys}(400)$) which is generally accepted by the bio-optics community. The parameterisations used for each of these cases were initially based upon relationships identified for the Baltic ULISSE dataset but which have additionally been verified with other coastal datasets (e.g. Adriatic) or from values taken from literature. For example an invaluable source of information is the data catalogue given by Gohs et. al. (1978) which had almost identical PDFs for the OACs as taken from the ULISSE set and is invaluable because it has both Particle Size Distribution (PSD) and Volume Scattering Phase Functions (VSF) which allow it to characterise the b_b model.

For the chlorophyll specific absorption coefficient (a^*_{ph}) the tabulated values from Bricaud et. al. (1995) were taken as this model has been shown (chapter 2) to well represent the spectral variability of in-vivo pigment absorption in coastal waters. The relationship between YS and $a_y(400)$ is intrinsically the same. In the case of $a_d(400)$ the following approach was taken. It is obvious that to represent the true variability in

magnitude that can be associated with a_d in Case II water it would be interesting to find a formulation for $a_d(400)$ that is dependent both on [CHL] and [TSM]. Prieur and Sathyendranath (1981) showed that a parameter X was directly related to the absorption coefficient $a_d(440)$, where $X=b-b_{min}$ and $b_{min}=0.3CHL^{0.62}$. In their study the value of b was in reality the scattering coefficient at 550nm (i.e. b550). In the present study it was decided to assume TSM to be roughly equal to b(550). The resulting regression of X with $a_d(440)$ for the ULISSE data is shown in figure 3.3. Therefore the expression used is:

$$a_d(440) = 0.051\left([TSM] - 0.3[CHL]^{0.62}\right) \tag{3.12}$$

Finally the relationships for the volume of small particles (v_s) and the volume of large particles (v_l) which constitute the basis of the backscattering segment, were investigated. The data from the Gohs et. al. (1978) data catalogue were used providing the information required on the volume scattering phase function. Also relationships previously identified by Haltrin and Kattawar (1991) were taken into consideration. The computation of the values for v_s and v_l were performed using two angles taken from the VSF, namely 1° and 45°, and applying two algorithms given by Kopelevich (1983):

$$v_s = 10.2\beta(45^\circ) - 1.4\times10^{-4}\beta(1^\circ) - 0.002 \tag{3.13a}$$

and:

$$v_l = 2.2\times10^{-2}\beta(1^\circ) - 1.2\beta(45^\circ). \tag{3.13b}$$

These relationships along with the VSF therefore gave tabulated values of v_s and v_l which could be regressed against [TSM] and [CHL] as shown in figure 3.4a and 3.4b where the best fit equations are given on the graphs.

3.4.2. Inherent Optical Property parameterisation

The IOPs presented in right hand side of equation 3.9 refer to the total coefficients for absorption (a) and backscattering (b_b). These two segments which determine the optical properties of the water column are adequately represented by the linear subdivision into a limited number of sub-components (i),

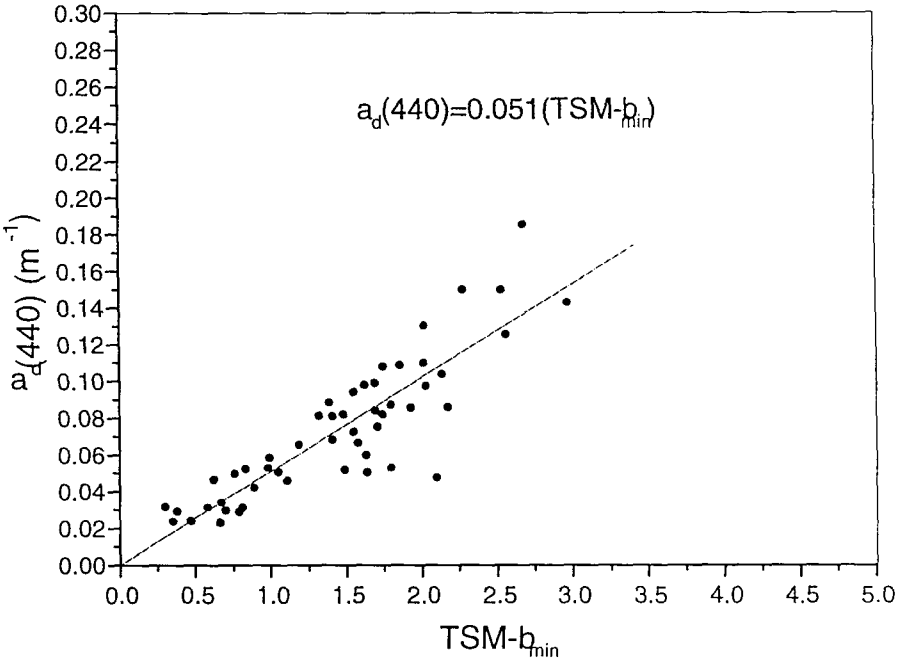

Figure 3.3: Plot showing the relationship between $a_d(440)$ and the term TSM-b_{min}. The slope between these two variable shows that $a_d(440)=0.051(TSM-b_{min})$ which is similar but not identical to the $a_d(440)=0.041(b550-b_{min})$ relationship identified by Prieur and Sathyendranath (1981).

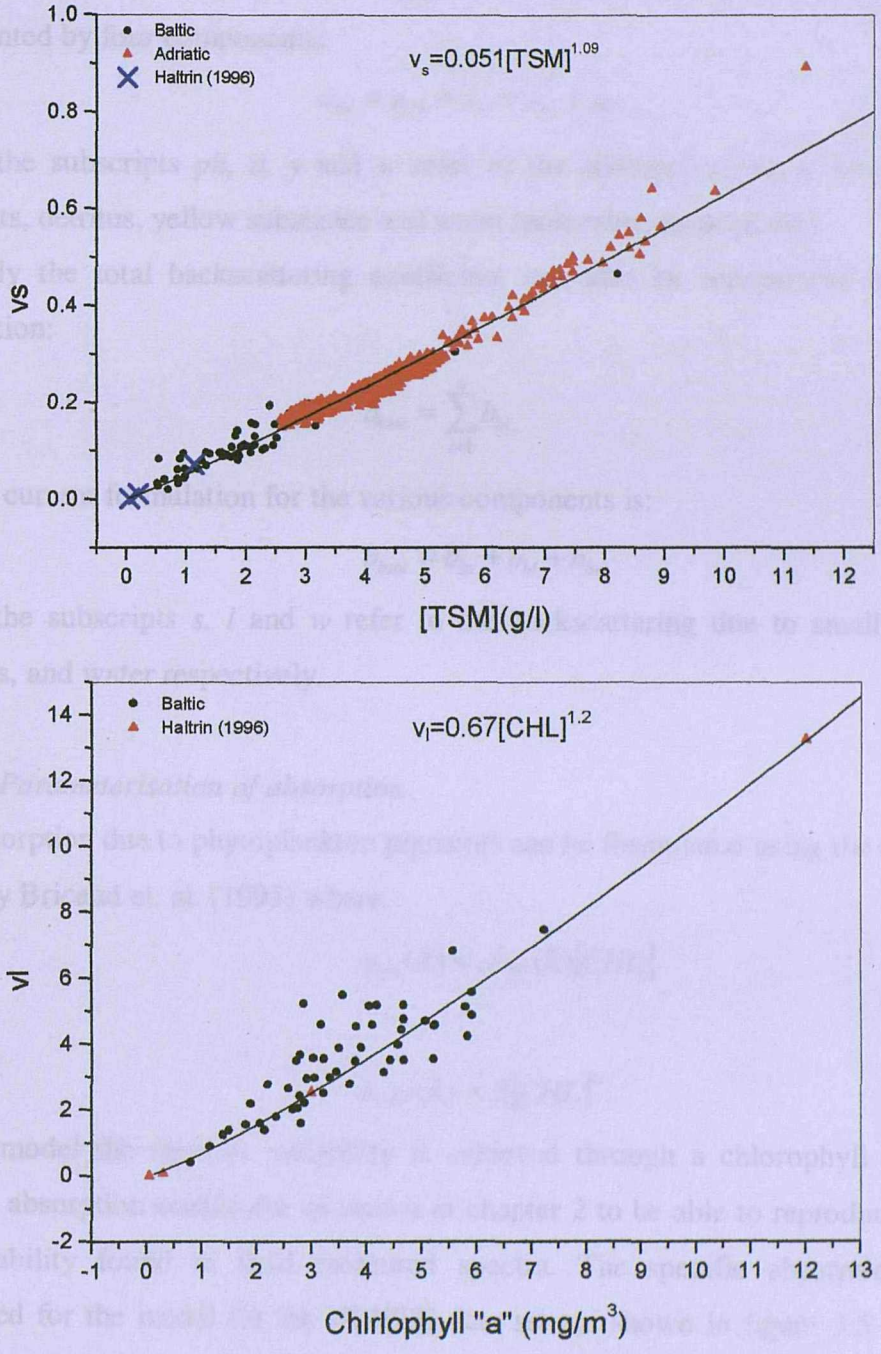

Figure 3.4: Plots showing the relationships between a) v_s and TSM and b) v_l and CHL. Plot 3.4b showing the v_l, CHL relationship also shows (represented as crosses) the equivalent relationship used by Haltrin (1997).

$$a_{tot} = \sum_{i=1}^{n} a_i \tag{3.14}$$

where n is the total number of components. In coastal waters, a_{tot} is usually represented by four components:

$$a_{tot} = a_{ph} + a_d + a_{ys} + a_w \tag{3.15}$$

where the subscripts *ph, d, y* and *w* refer to the absorption due to phytoplankton pigments, detritus, yellow substance and water molecules, respectively.

Similarly the total backscattering coefficient can also be represented by a linear summation:

$$b_{btot} = \sum_{i=1}^{n} b_{bi} \tag{3.16}$$

and the current formulation for the various components is:

$$b_{btot} = b_{bs} + b_{bl} + b_{bw} \tag{3.17}$$

where the subscripts *s, l* and *w* refer to the backscattering due to small and large particles, and water respectively.

3.4.2.1 Parameterisation of absorption

The absorption due to phytoplankton pigments can be formulated using the expression given by Bricaud et. al. (1995) where.

$$a_{ph}(\lambda) = a^*_{ph}(\lambda)[CHL] \tag{3.18}$$

and,

$$a^*_{ph}(\lambda) = A[CHL]^B \tag{3.19}$$

In this model the spectral variability is achieved through a chlorophyll dependent specific absorption coefficient as shown in chapter 2 to be able to reproduce the type of variability found in field measured spectra. The specific absorption spectra computed for the model for the ULISSE data set are shown in figure 3.5 as well as the computed absorption spectra for the phytoplankton like pigments.

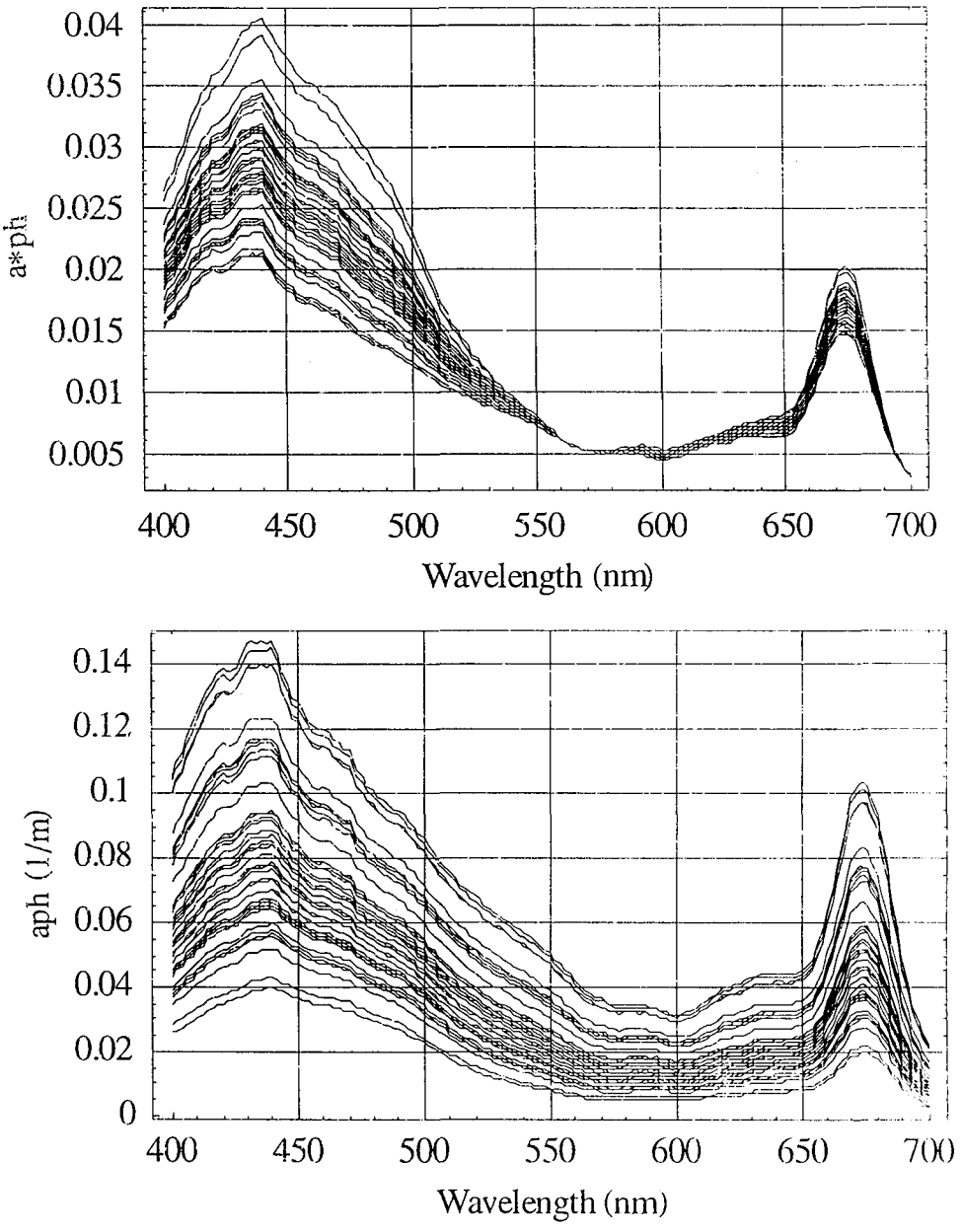

Figure 3.5: Two plots showing for the ULISSE stations the spectra for $a_{ph}(\lambda)$, and $a_{ph}(\lambda)$ calculated using the model after Bricaud et. al. (1995).

The absorption component representing the non-chlorophyllous particulates or detritus, varies exponentially within the spectral range as shown by,

$$a_d(\lambda) = a_d(440)e^{-Sd(\lambda-440)} \tag{3.20}$$

where the slope of the exponent (S) has been set constant with a mean value of 0.0116 (SD ± 0.002). This value, determined in the studied area from a population of 98 datapoints, is in good agreement with that given by Roesler *et. al.* (1995) of 0.011 in other oceanic provinces. It would be optimal to allow variability in slope of the exponent of the function. However, due to the complexity of the sources of these substances and the limited investigations on its variability made so far (e.g. Nelson 1993, Bricaud and Stramski 1990, Dowell et. al. 1996) the above formulation will be used. The modelled spectra are shown in figure 3.6.

Light absorption by YS is of extreme importance in the coastal region where it can contribute up to 70% of the total absorption of the water in the blue/green spectral range (Dowell *et. al.* 1996). As for the detritus, the YS absorption spectra can be formulated as an exponential curve,

$$a_{ys}(\lambda) = a_{ys}(400)e^{-Sys(\lambda-400)} \tag{3.21}$$

in which the slope of the exponent (S) is allowed to vary as a function of the magnitude of the YS absorption coefficient at 400nm, through the following expressions:

$$\text{For } a_{ys}(400)\leq 1.2 \qquad S_{ys}=0.032-0.021a_{ys}(400) \tag{3.22}$$

$$\text{For } a_{ys}(400)>1.2 \qquad S_{ys}=0.018+0.012e^{-(ays(400)/1.2)}$$

which were derived from a dataset of 100 points as shown in figure 3.7a. These expressions can also be derived from a dataset presented by Green (1992), where both the cut off point of the two relationships and the asymptote of the exponential relationship are almost identical to those found in the present study. This observation, suggests that these two distinct relationships between the absorption coefficient and the slope may be indicative of different sources of YS (i.e. marine autochnous or terrigenous). The value of the slope of YS can therefore be calculated over a large

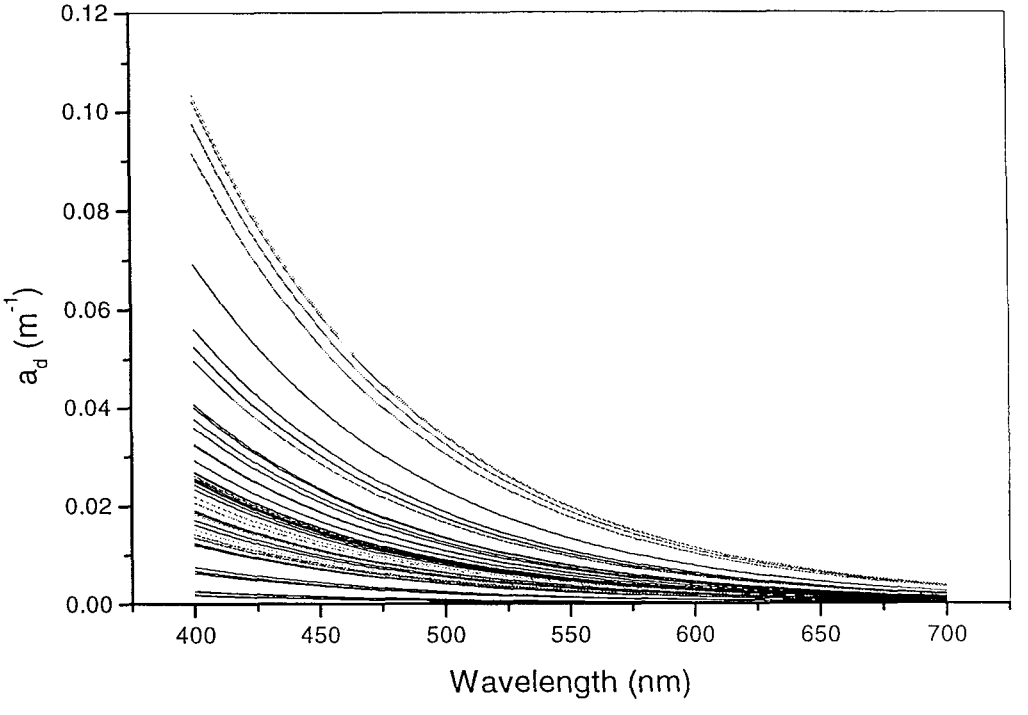

Figure 3.6: A plot of the modeled spectra calculated for $a_d(\lambda)$ for the ULISSE stations, using the $a_d(440)$ calculated from the relationship given in figure 3.3, and using a fixed slope of 0.012.

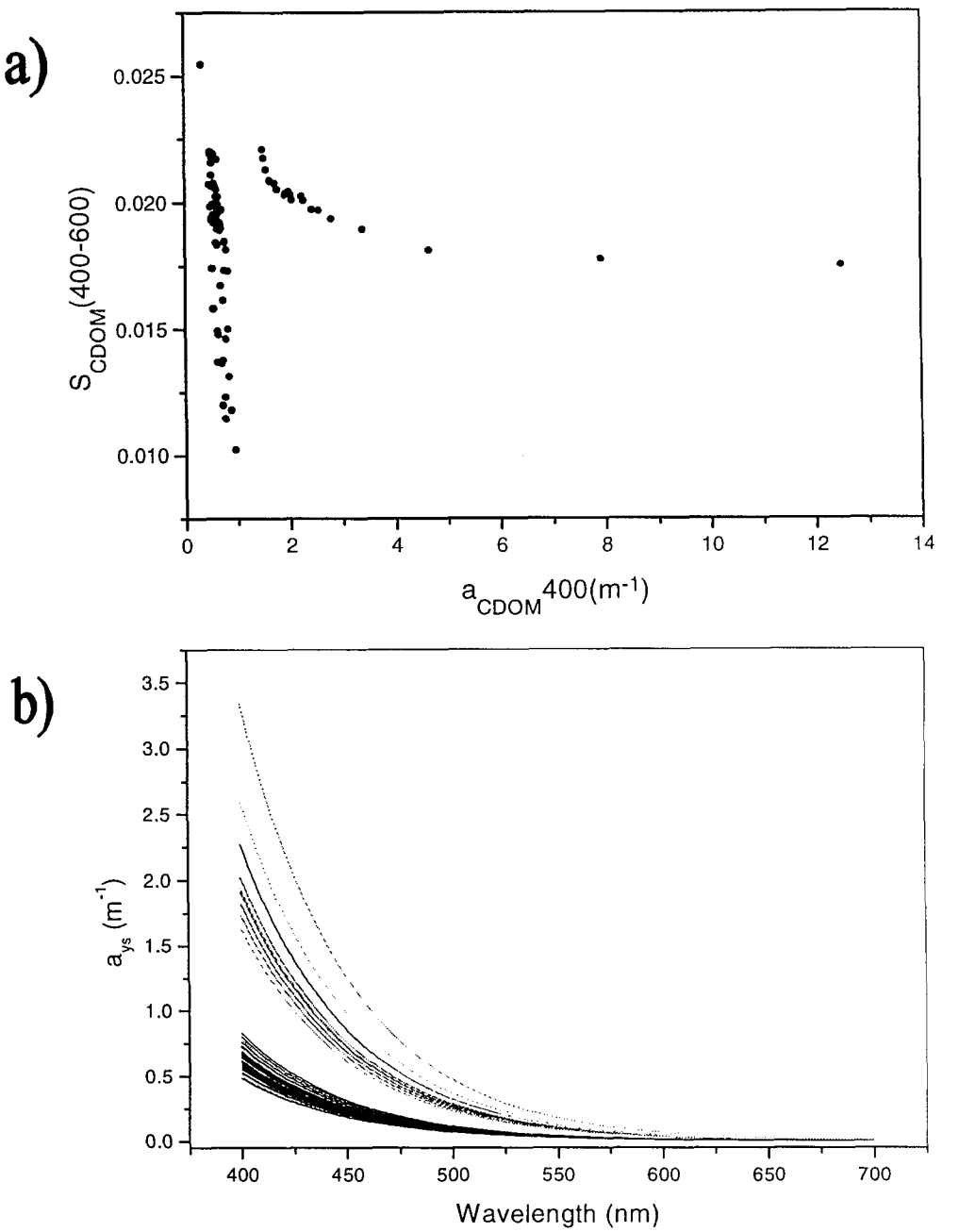

Figure 3.7: Plot illustrating the model adopted for yellow substance spectral absorption. Figure 3.7a shows the relationship between the $a_{ys}(400)$ and $S_{ys}(400\text{-}600)$ and graph 3.7b shows the modeled spectra for the ULISSE stations. The relationships for the relationship in 3.7a are given in equation 3.22

range from 0.008 to 0.030. The modelled YS absorption spectra coincident with the ULISSE stations are shown in figure 3.7b.

The absorption spectrum for seawater (a_w) is taken from literature (Pope and Fry 1997), a plot of which is shown in figure 3.8a.

3.4.2.2. Parameterisation of the backscattering

The backscattering property of water molecules (b_{bw}) will be considered as known, and valuesare taken from the following expression given by Morel (1974), as illustrated in figure 3.8b

$$b_{bw} = \frac{1}{2}\left(0.00288\left(\frac{500}{\lambda}\right)^{4.3}\right). \tag{3.23}$$

The backscattering segment due to particles has been split up into two sub-components representing the contributions due to small and large particles. Kopelevich (1983) proposed the following model to describe the VSF for marine particles:

$$\beta_{part}(\psi,\lambda) = v_s\beta_s^*(\psi)\left(\frac{550}{\lambda}\right)^{1.7} + v_l\beta_l^*(\psi)\left(\frac{550}{\lambda}\right)^{0.3} \tag{3.24}$$

Where β_s^* and β_l^* are the concentration specific VSFs for small and large particles respectively. Plots of these two functions are shown in figure 3.9. The coefficients v_s and v_l represent the concentrations of small and large particles in ppm. The following characteristics can be considered for the two fractions as defined by Kopelevich (1983): a small inorganic fraction with a complex index of refraction of 1.15, a maximum diameter of 2μm and a power law slope of 1.7; and a large organic fraction with a complex index of refraction of 1.03, a minimum diameter of 2μm and a power law slope of 0.3.

The above expression can therefore be transformed into an expression for scattering (b) by integrating β^* over the full range of the phase function 0 to π, giving the expressions:

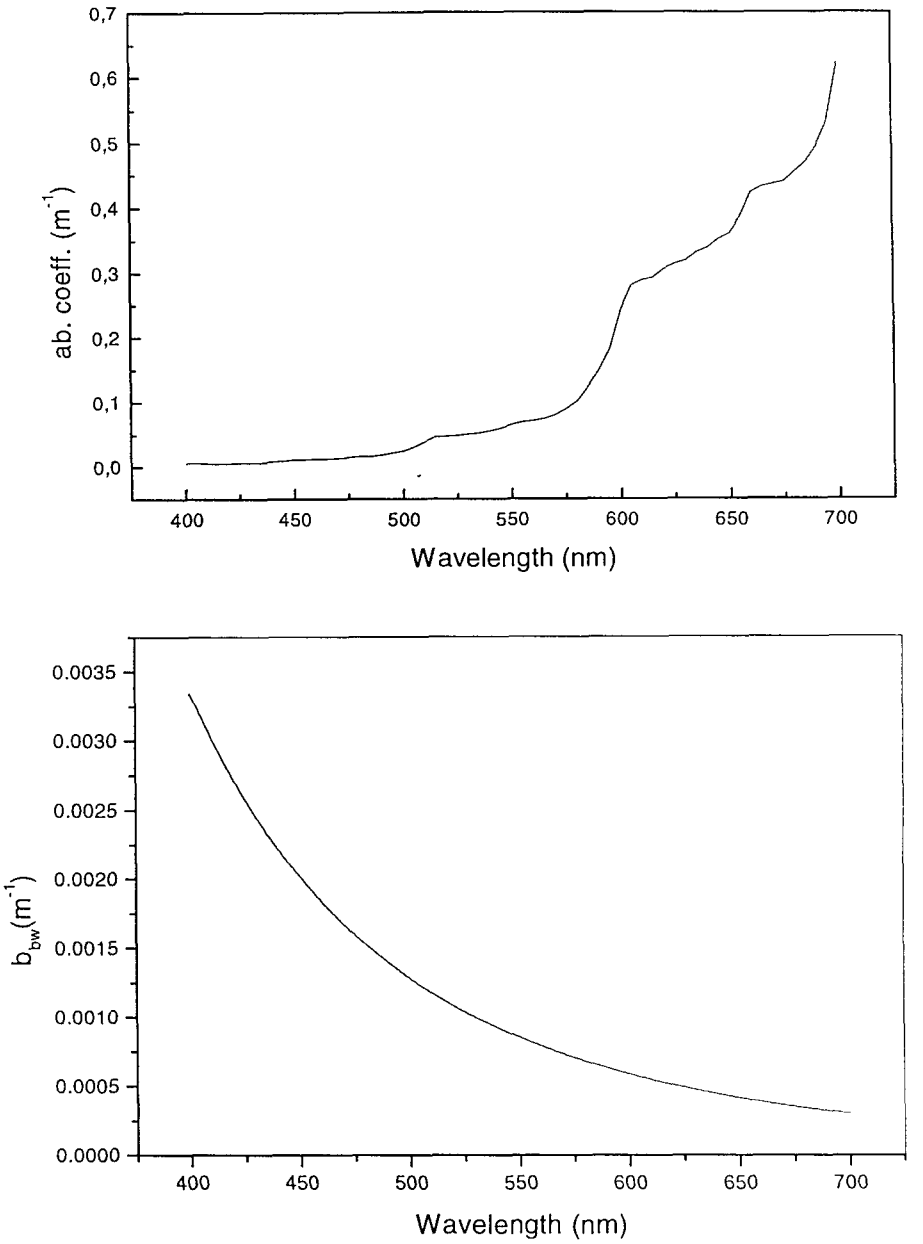

Figure 3.8: Figure 3.8a give the water absorption used in the current model (after Pope and Fry 1997), and figure 3.8b gives the water backscatter spectra used (after Morel 1974).

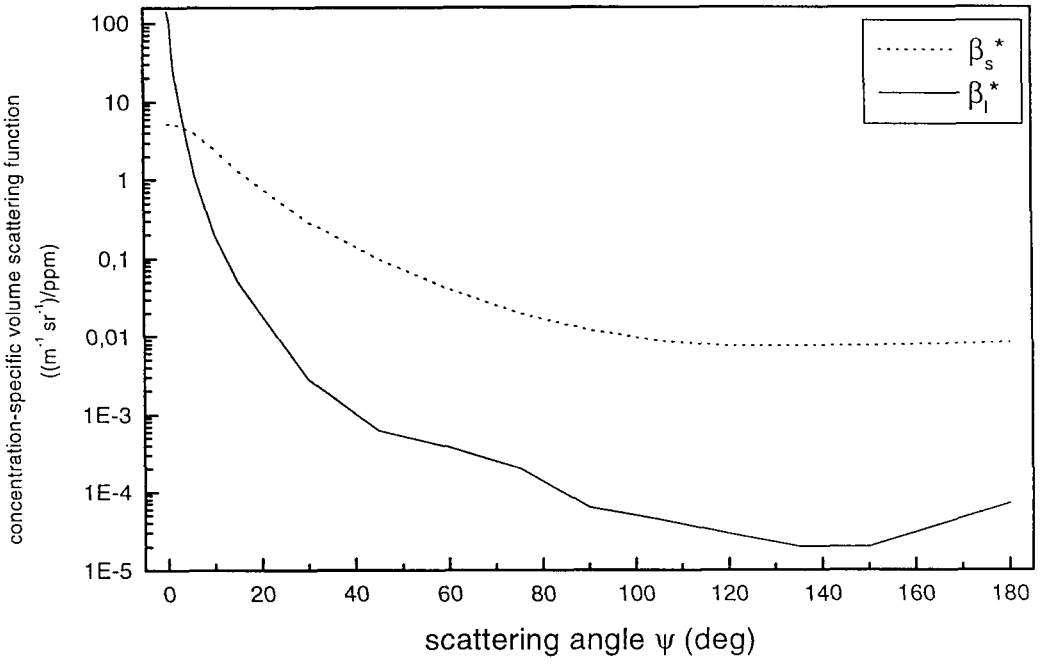

Figure 3.9: A plot illustrating the angular distribution of the mass specific Volume Scattering Functions for small inorganic particles (dotted line) and large organic particles (solid line) (after Kopelevich 1983).

$$b_s(\lambda) = 1.34 v_s \times \left(\frac{550}{\lambda}\right)^{1.7} \qquad \& \qquad b_l(\lambda) = 0.312 v_l \times \left(\frac{550}{\lambda}\right)^{0.3} \tag{3.25}$$

Finally this formulation can be presented in terms of backscattering (b_b) which is of interest here in the context of reflectance modelling. By calculating the backscattering probability (b_b/b or $\tilde{b}_b$) for both small and large particles through integration of β^* for small and large particles in the range $\pi/2$ to π; this integration leads to the following expression.

$$b_{bpart}(\lambda) = \tilde{b}_{bs} \times b_s(\lambda) + \tilde{b}_{bl} \times b_l(\lambda) \tag{3.26}$$

The values of $\tilde{b}_{bs}$ and $\tilde{b}_{bl}$ computed for the wavelength 550nm were 0.039 and 0.00073 respectively.

Kopelevich's (1983) model for particulate scattering was chosen as it is best suited for applications in coastal Case II waters. This is demonstrated by the dynamic range covered by various related variables. The cumulative ratio of $\tilde{b}_b$ can range between 0.1 to 3.5%, the slope of the power law function may have values from 0.3 to 1.6, whereas the complex index of refraction m which is intrinsically contained in the Mie calculations, which determined the mass specific VSFs, may vary from 1.03-1.15. These values will cover most values found in the marine environment as stated in literature (for an overview see Mobley 1994).

The following equations were then used to evaluate the relative contributions due to small and large particles to the total backscattering coefficient of the water for the dataset considered:

$$b_{bs} = 0.039\left[1.34\left(\frac{550}{\lambda}\right)^{1.7} v_s\right]$$

$$b_{bl} = 0.00073\left[0.312\left(\frac{550}{\lambda}\right)^{0.3} v_l\right] \tag{3.26}$$

The resulting spectra are shown in figure 3.10 where the contribution due to small particles is shown in figure 3.10a and that due to large particles is shown in figure

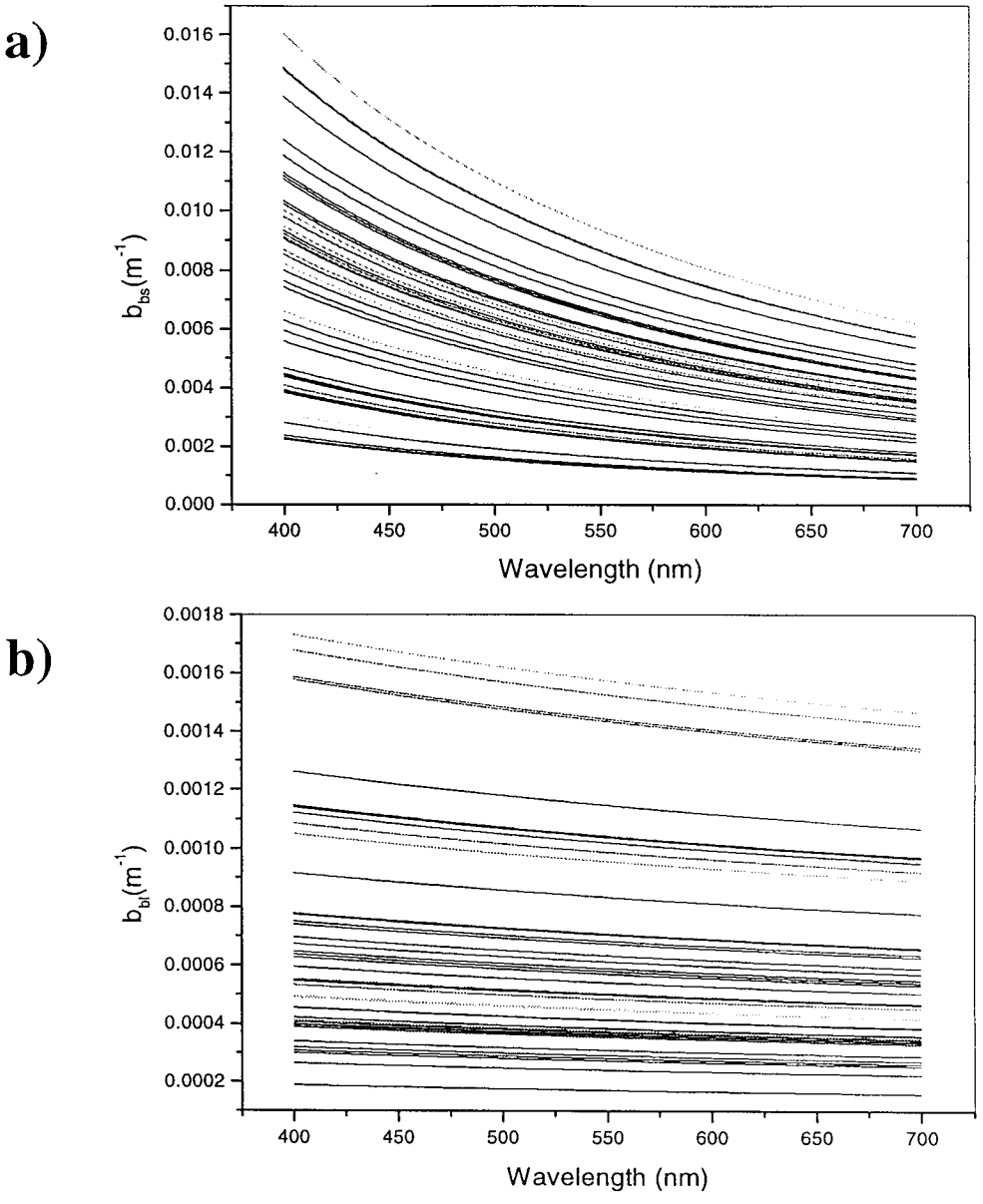

Figure 3.10: Two plot showing the modeled spectral distribution of backscattering for the ULISSE test dataset for a) the small particle fraction and b) the large particle fraction. As can be seen in coastal waters such as those considered the small inorganic fraction contributes a much greater amplitude in backscattering than the large fraction.

3.10b. As can be seen the contribution due to small non-organic particles is significantly higher in magnitude than that due to larger organisms.

It is therefore now possible to simulate the right hand term in equation 3.4. This term will be defined as the backscatter normalised albedo:

$$\omega_b = \frac{b_b}{a + b_b} \tag{3.27}$$

Figure 3.11 shows the simulations for a_{tot}, b_{btot} and ω_b respectively using the formulations presented in this section and the parameterisation of the optical properties inherent to each of the OACs described in section 3.4.1.

3.4.3. *Calculation of the proportionality factor (f)*

It is known that *f* the proportionality factor is not systematically constant and has been shown to be satisfactorily evaluated through the analytical solution given in equation 3.4 (Sathyendranath and Platt 1997). A further aim is to formulate a reflectance model which adequately accounts for the large variability of the proportionality factor through changes in the particulate VSF in the region considered. The parameterisation of the *f* factor will be carried out using equation 3.4. Firstly, μ_d just beneath the surface can be easily calculated as $\mathrm{Cos}[\theta_o]$, as given by Gordon (1989), where θ_o is subsurface solar zenith angle in radians. For the calculation of μ_u and *s* Sathyendranath and Platt (1997) considered two possibilities, one in which the upward scattering is dominated by molecular scattering and a second in which the influence of particulate scattering is dominant. However, it is seen that, with chlorophyll concentrations ≥ 0.01 mg/m^3 in Case I waters, the particle scattering becomes more significant than molecular scattering (Sturm 1986). Therefore, since the present model is intended to be applied to Case II water studies, only calculations relating to the case of particulate scattering were performed. Thus, μ_u (the upwelling mean cosine) and s (the shape factor of the VSF (b_u/b_b)) can both be expressed in terms of parameters describing the VSF (in this the parameters of the Kopelevich model) and the sun zenith angle.

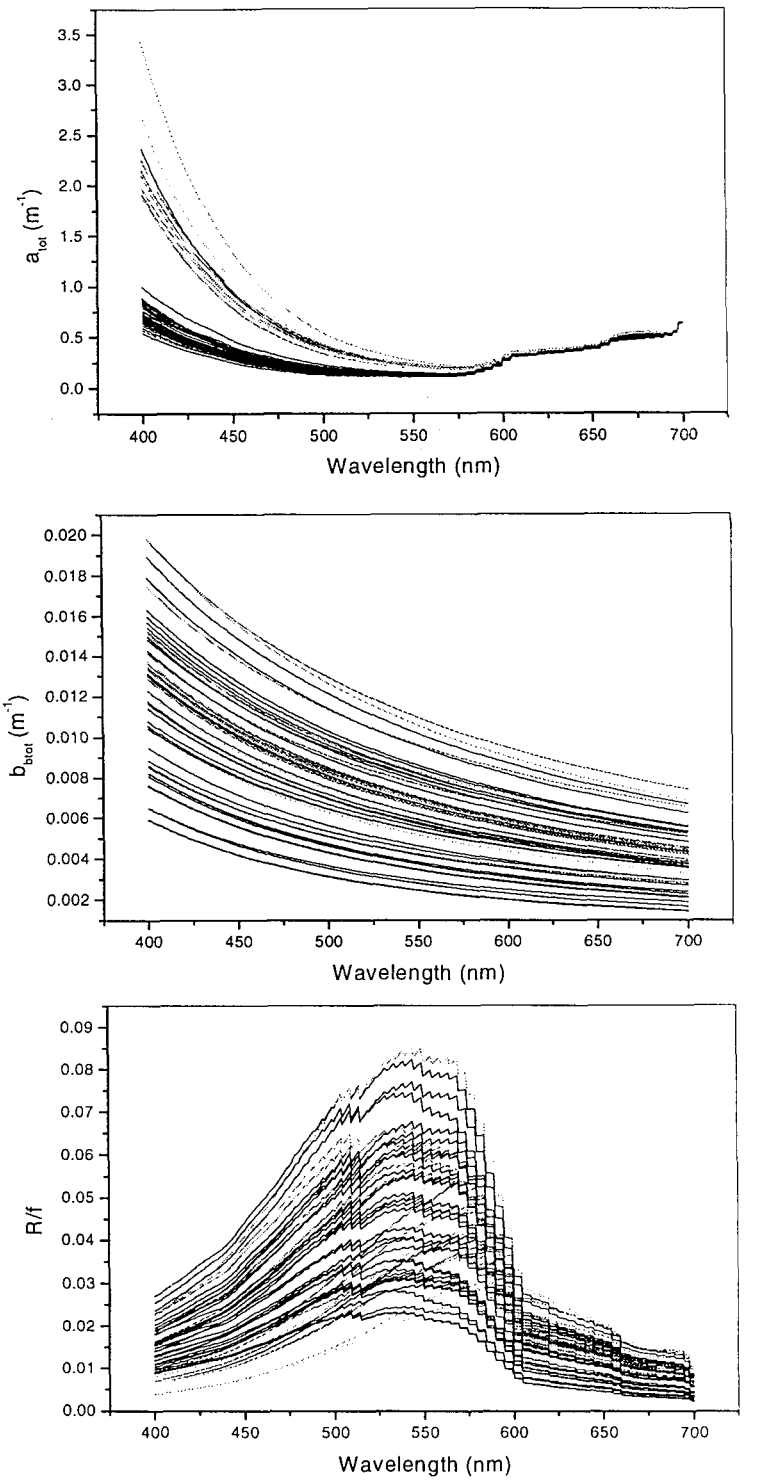

Figure 3.11: Graphs showing the total coefficients for absorption (top plot) backscattering (middle plot) and the normalised backscattering albedo (bottom plot). The latter is directly related to the irradiance reflectance through the proportionality factor *f*.

If one considers the situation for collimated incident light then the expression for μ_u is:

$$\mu_u = \frac{\int_{\phi=0}^{2\pi}\int_{\theta=\pi/2}^{\pi} L(\theta,\phi,0)\cos\theta\sin\theta\, d\theta\, d\phi}{\int_{\phi=0}^{2\pi}\int_{\theta=\pi/2}^{\pi} L(\theta,\phi,0)\sin\theta\, d\theta\, d\phi} \tag{3.28}$$

where,

$$L(\theta,\phi,0) = \frac{E_d(0)}{(a+b_b)}\frac{(\sec\theta\sec\theta_0)}{(\sec\theta-\sec\theta_0)}bP(\psi) \tag{3.29}$$

here θ is the zenith angle ϕ is the azimuth angle θ_0 is the incident angle just beneath the surface, $P(\psi)$ is the phase function at scattering angle ψ $P(\psi)=\beta(\psi)/b$, where $\beta(\psi)$ is the volume scattering phase function at angle ψ, and ψ is determined by θ, θ_0 and ϕ according to:

$$\cos\psi = \cos\theta_0\cos\theta + \sin\theta\sin\theta_0\cos(\pi-\phi) \tag{3.30}$$

if the azimuth angle is measured counter-clockwise from the direction of the incident ray.

The parameter s is defined as b_u/b_b, where b_u is parameterised as follows:

$$b_u(\theta) = 2\int_{\frac{1}{2}\pi-\theta}^{\frac{1}{2}\pi+\theta}\left[\pi - \arccos\left(\frac{-\cos\theta\cos\psi}{\sin\theta\sin\psi}\right)\right]\beta(\chi)\sin\psi\, d\psi + 2\pi\int_{\frac{1}{2}\pi+\theta}^{\pi}\beta(\psi)\sin\psi\, d\psi \tag{3.31}$$

As has been shown, the VSF play an important role in the parameterisation of both of the above terms (i.e. μ_u and s). Since the VSF is modelled in the present study using the formulation of Kopelevich (1983) as described in section 3.5 it was decided to use a recently derived regression (Haltrin 1997) to describe the Kopelevich's VSFs for small and large particles. This was mainly done because it considerably decreased processing time which is critical when the model is applied to satellite imagery. The two component VSFs of Kopelevich can be expressed by the following regressions:

$$p_s(\mu) = \exp\left(\sum_{n=0}^{5} s_n\psi^{\frac{3n}{4}}\right) \quad \text{and} \quad p_l(\mu) = \exp\left(\sum_{n=0}^{5} l_n\psi^{\frac{3n}{4}}\right) \tag{3.32}$$

and $\psi=\cos^{-1}(\mu)$, where ψ is the scattering angle in radians and s_n and l_n are given below in table 3.2.

n	0	1	2	3	4	5	r2
s_n	1.725880	-2.957089E-2	-2.782943E-2	1.255406E-3	-2.155880E-5	1.356632E-7	0.999
l_n	5.238466	-1.604327	8.157686E-2	-2.150389E-3	2.419323E-5	-6.578550E-8	0.999

Table 3.2: Haltrin's coefficients for P_s and P_l

So with the above formulations f can be calculated for the ULISSE stations with corresponding ω_b spectra (figure 3.11c). The results for f are shown in figure 3.12a with respect to station number. As can be seen the constant value of 0.33 often used as a constant (e.g. Morel and Prieur 1977) for simulating reflectance is far from the truth in the case of the calculations made here.

3.4.4. Determination of the Q-factor

In order to realistically compare the computed reflectance with the reflectance measured in-situ one has to re-compute the in-situ measured reflectance described in chapter 2 using a variable value instead of the value of π used originally. This is due to the fact that the measured ratio L_u/E_d is related to irradiance reflectance in reality not through π but through the ratio of E_u/L_u, also called the Q-factor (Austin 1979), and has often been given a mean value of 4.5. However given the availability of the parameters affecting the variability of Q it was decided to formulate a relationship for Q to be able to resolve this parameter analytically. Therefore the following approach was adopted which is based on both the information already presented of the relationships between irradiance reflectance and the IOPs, and a formulation for remote sensing reflectance as defined by Zaneveld (1982, 1989, 1995). These are developed through the following steps. Knowing the relationship given in equation 3.2 and through the definition of the Q factor as given above

$$\frac{L_u}{E_d} = \frac{f}{Q}\frac{b_b}{a} \tag{3.33}$$

Remote Sensing Reflectance (RSR) as given by Zaneveld (1982) is equivalent to:

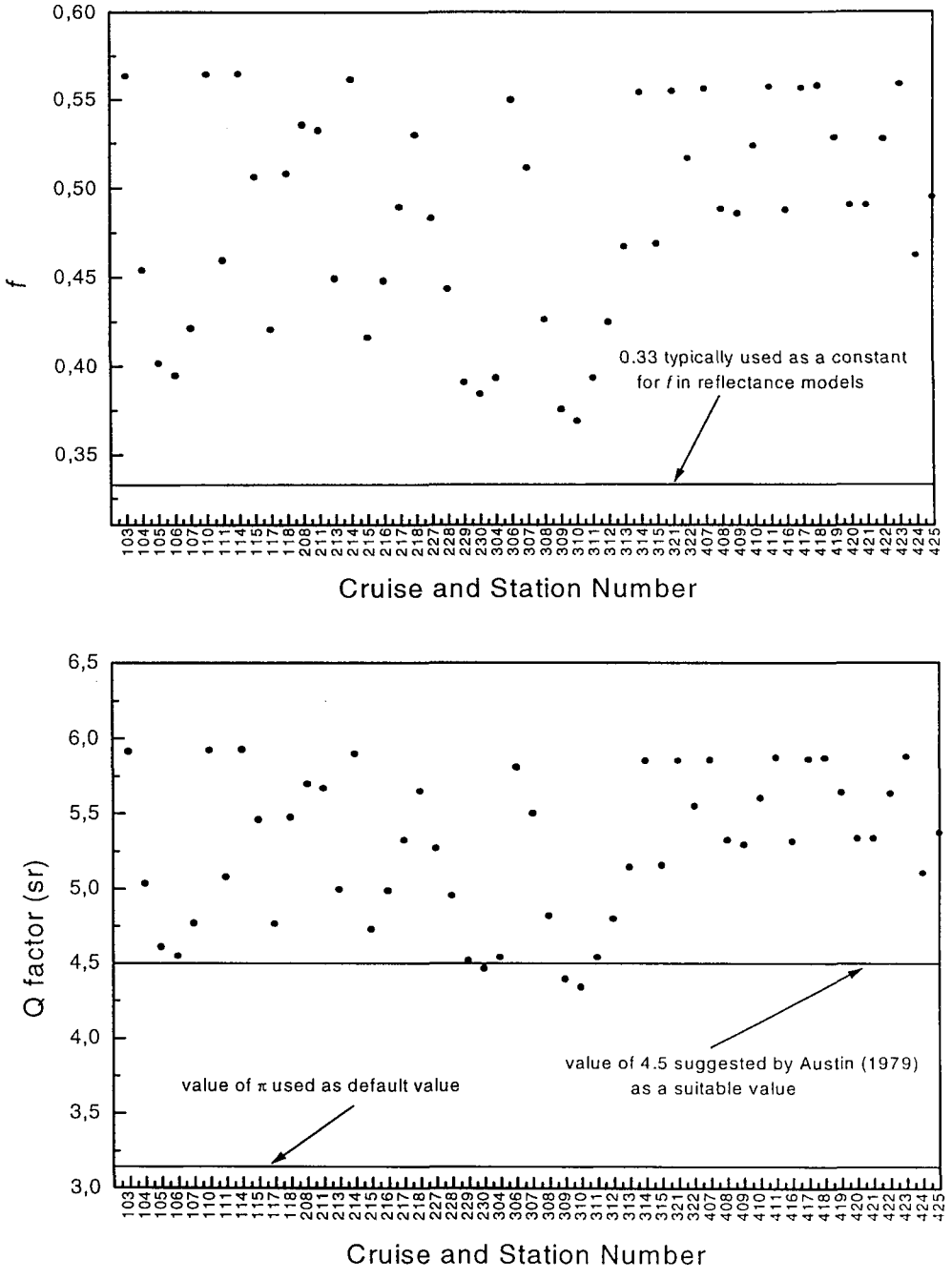

Figure 3.12: a) Plot of f, the proportionality factor calculated using the analytical solution given by Sathyendranath and Platt (1997) for the ULISSE stations. The line at 0.33 illustrates a typical value used to represent f (e.g. Morel and Prieur 1977). b) Plot of Q factor values for the ULISSE stations. Typical values used π and 4.5 are shown by horizontal lines.

$$RSR = \frac{L_u}{E_{od}} \tag{3.34}$$

where

$$E_d = \overline{\mu}_d E_{od} \tag{3.35}$$

E_{od} is the downwelling scalar irradiance. Therefore

$$RSR = \overline{\mu}_d \frac{f}{Q} \frac{b_b}{a}$$

If we now substitute Zaneveld's (1995 eqn. 11) expression for RSR

$$RSR(\pi) = \frac{L(\pi)}{E_{od}} = \frac{f_b(\pi)\frac{b_b}{2\pi}}{k(\pi) + c - f_l(\pi)b_f}$$

and rearrange in terms of Q we obtain (Zaneveld 1982),

$$Q = 2\pi\overline{\mu}_d \frac{f}{f_b}\left[\frac{\kappa(\pi) + b_b}{a} + 1 + (1 - f_l)\frac{b_f}{a}\right] \tag{3.36}$$

where f_b and f_l are shape factors of the VSF, which can be approximated to 1. In reality f_l varies from 1 to 1.1 and f_b between 0.9 and 1.4 (Weidemann et. al. 1995) but it has been shown that for chlorophyll concentrations > 1mgm^{-3} the values tend towards unity, and therefore:

$$Q = 2\pi\overline{\mu}_d f\left[\frac{\kappa(\pi) + b_b}{a} + 1\right] \tag{3.37}$$

Thus, with the values of f calculated from Sathyendranath and Platt (1997), Q can be evaluated. It is however immediately obvious that the wavelength dependency of the equation would not produce results which would be equivalent to those reported in the past both through Monte Carlo simulations (Morel and Gentili 1993) and through in-situ measurements (Zibordi et. al.1997). In these cases the general trend is a positive slope from the blue to the red part of the spectrum. It was therefore suggested to compute the values of Q at 550nm so as to have values comparable with those given in literature. In fact the computed values of Q_{550} were in the range 4-6, shown in figure 3.12b, which are comparable with values given in literature.

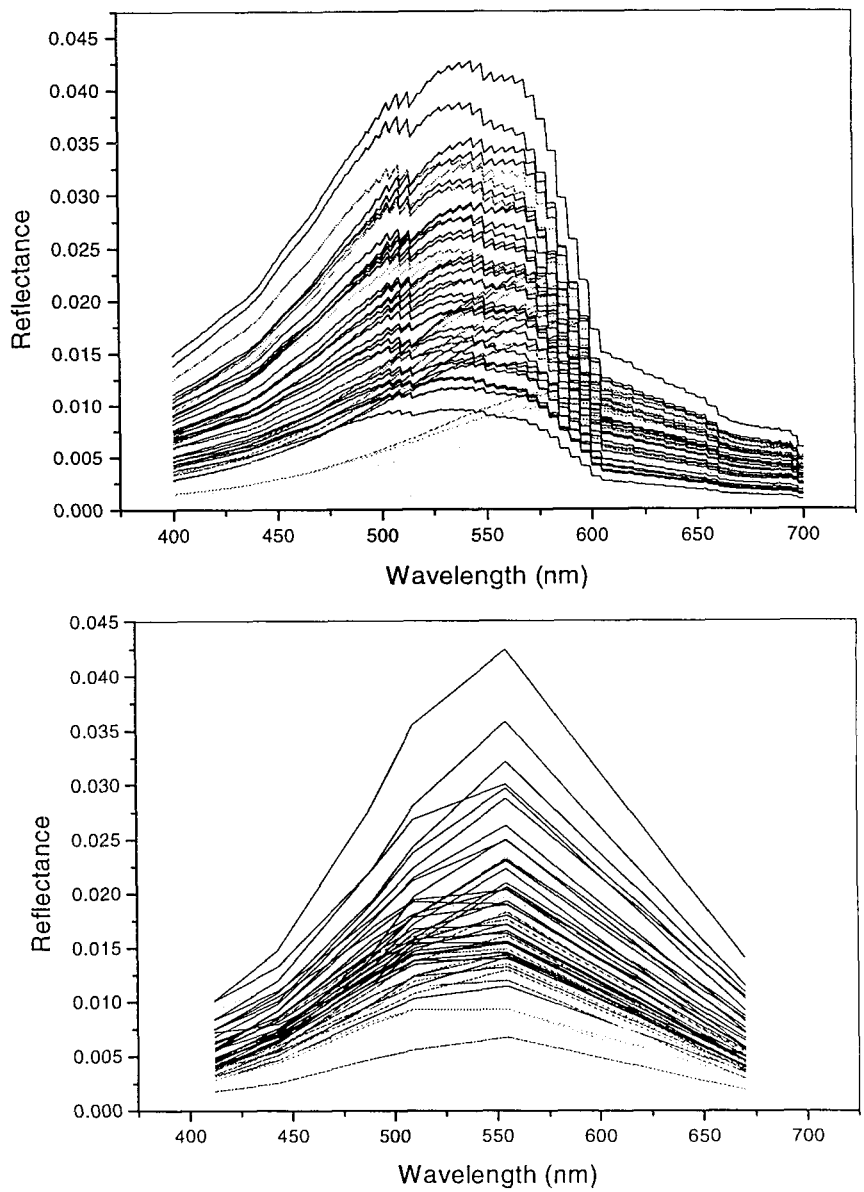

Figure 3.13: a) Plots showing the simulated reflectance at 1nm resolution using the *f* values taken from figure 3.12, and the in-situ measured reflectance using the Q factors also given in figure 3.12.

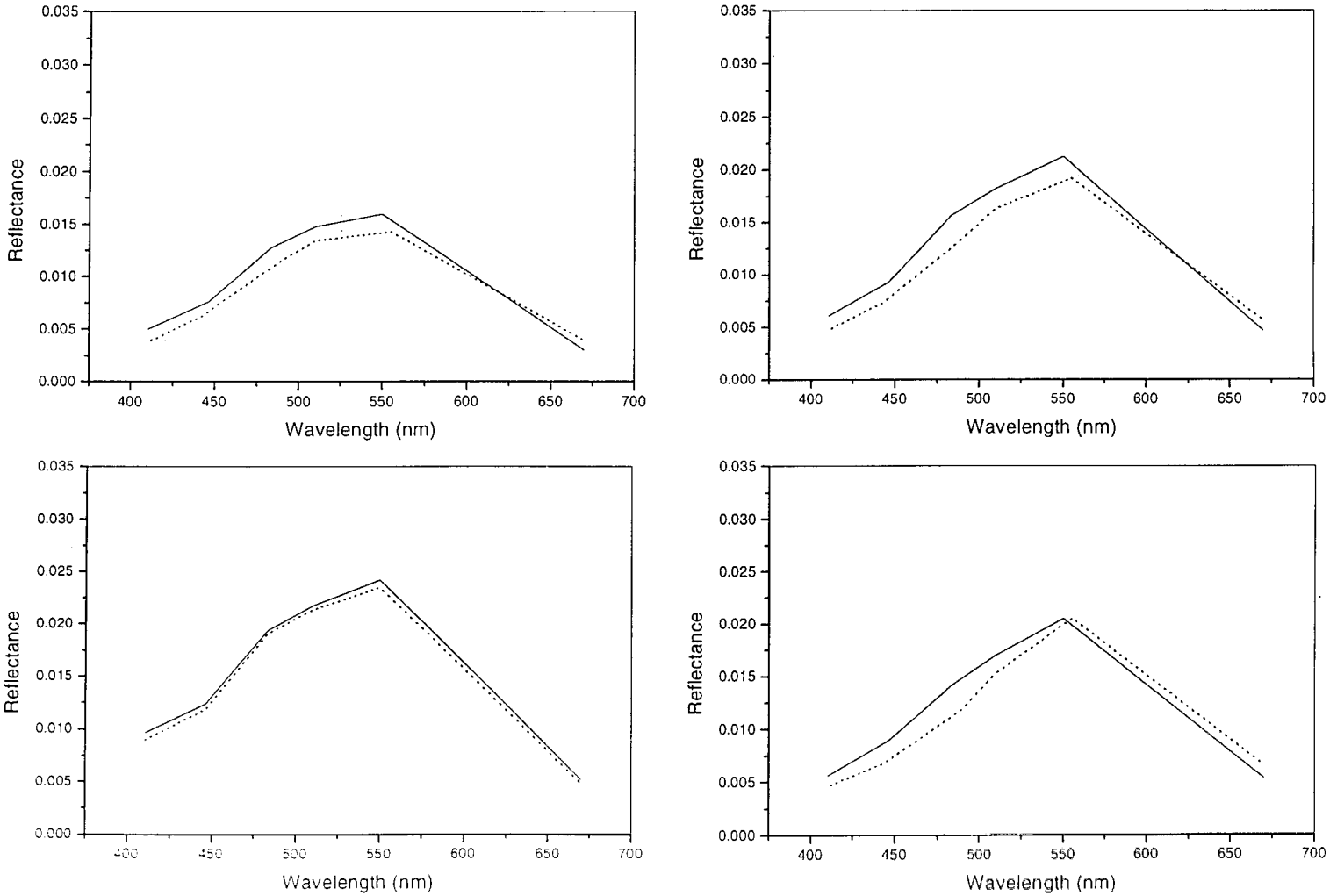

Figure 3.13: b) Four graphs are shown illustrating the performance of the forward model through a comparison of modeled spectra (solid line) and measured spectra (dotted line).

So it is now possible to view the relationships between the modelled reflectance and the in-situ measured reflectance.

The spectra of simulated reflectance are shown at 1nm resolution in figure 3.13a. The figure also shows the spectra of the in-situ measured reflectance. Furthermore figure 3.13b shows 4 examples of modelled reflectance compared with the measured reflectance (using the calculated Q factors given above ($Q\ L_u/E_d$)). As can be seen the modelled spectra compare very well with the measured spectra in both spectral shape and magnitude.

As is apparent from the previous discussion the values of both Q and f hold a certain amount of uncertainty associated with their determination, and furthermore they depend not only on the inherent optical properties but also on the sun earth geometry. For this reason it was decided to carry out the inversion procedure not on the simulated reflectance but simply on the ω_b i.e. purely on the IOPs and therefore the f factor will be subtracted from the satellite reflectances before the algorithm is applied. The datasets were simulated for ω_b at the wavelengths of all of the satellite sensors for which algorithms were developed as shown in table 3.3

Channel	CZCS	OCTS	SeaWiFS	MOS	MERIS	Domain
1		412	412	410	412.5	CDOM
2	443	443	443	446	442.5	Chlorophyll
3		490	490	487	490	High Chlorophyll
4	510	520	510	517	510	Turbidity
5	550	565	550	567	560	Chlorophyll
6				618	620	Sediment
7	670	670	665	$654^{N/A}$	665	Chlorophyll/Pigs
8				683	681.25	Fluorescence

Table 3.3: Sensors and wavelengths considered in the inversion procedure

Channel 8 (shown in table 3.3.) has not be used in the present study as it is highly influenced by the Chlorophyll "a" fluorescence band which is not included in the forward model, therefore it is not justified to include it in the inversion procedure. Figure 3.14 shows a plot of the simulated reflectance datasets for the six sensors used

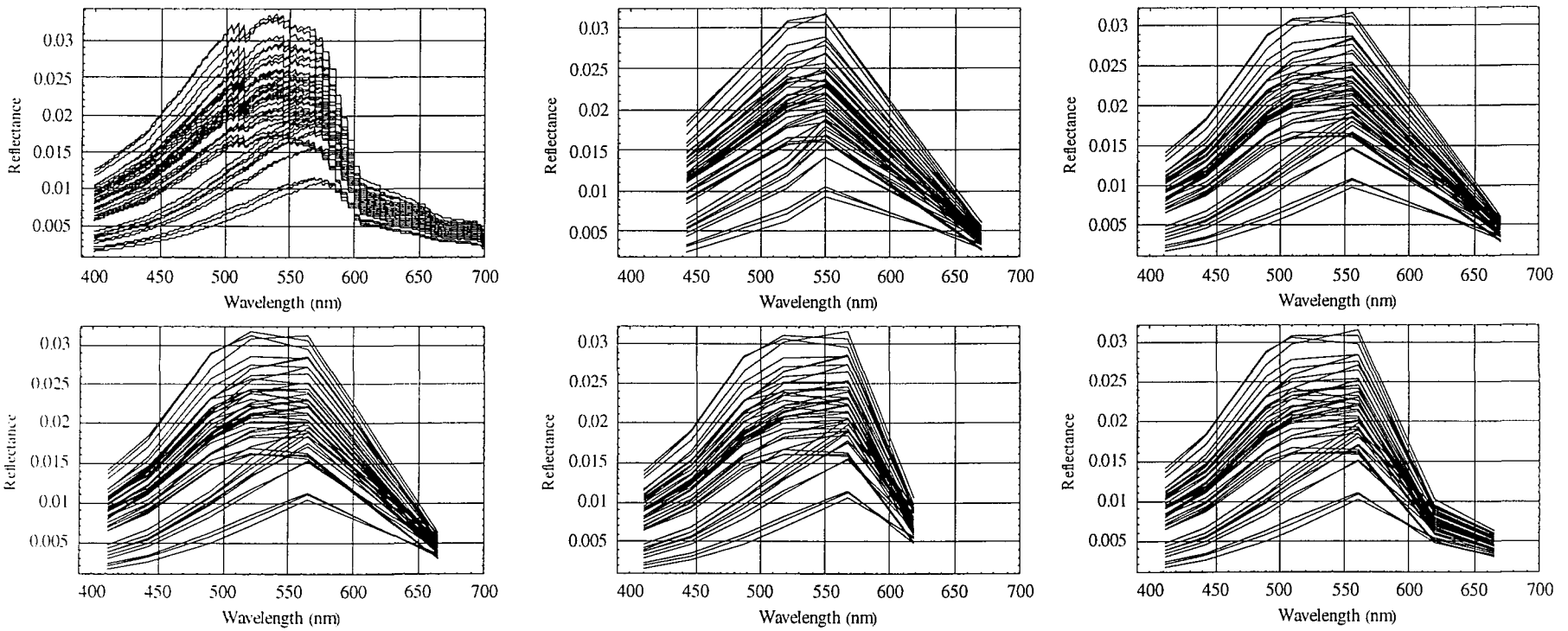

Figure 3.14: Figure showing the output of the forward model for different bandsets. These include 1nm resolution, CZCS, OCTS, MOS, MERIS, SeaWiFS and the in-situ dataset (from top left to bottom right). These plots enable one to appreciate the amount of spectral variability described by each bandset when compared to the 1nm resolution data.

(i.e. CZCS, SeaWiFS, OCTS, MOS, and MERIS). The simulated spectra shown here are those taken from the OACs of the ULISSE cruises, whilst those used in the actual inversion procedure are the 8000 spectra simulated from the OAC distribution functions.

3.5. Inversion procedure

In order to define the algorithms for the region in question, relating the OACs to reflectance, we now need to define an inversion procedure. The approach adopted in this study is to invert the simulated reflectance for each of the satellite sensors considered using a multivariate statistical approach, namely Principal Component Analysis. This technique has been used before by many authors to analyse large datasets of reflectance spectra; notably Sathyendranath et. al. 1989 but also Mueller 1976, Gower et. al. 1986 and Hinton 1990.

Principal Component Analysis (PCA) (also called Characteristic Vector Analysis) is a statistical procedure, which reduces a set of spectra or responses to an intrinsic minimum. The technique is a method of examining a large multivariate dataset (here represented by multispectral reflectance measurements) and determining linear transformations of the data to a smaller number of parameters essentially reproducing all of the information of the original data.

A recent manuscript (Neumann 1995) has presented a novel use of PCA by applying the analysis directly to satellite measured radiance. His method has been shown to perform fairly well, although it is apparent that performing a PCA at the top of the atmosphere may not necessarily satisfy the underlying assumption that linear estimates are used. Also the algorithm proposed by Neumann (1995) is to be indiscriminately applied to whole satellite scenes even though an underlying assumption made in the use of PCA is that the distinct output vectors must be mutually uncorrelated. Therefore the use of this type of method for Case I water pixels may be misleading.

An advantage of the use of PCA for the analysis of multispectral remote sensing data compared to band ratios or other more traditional methods is that it always makes full

use of the available spectral information in the derivation of the physical quantities, whilst separating the signal from the noise. The procedure adopted in the current investigation is described below where the notation is that used by Gower et. al. (1984) (taken from Simmonds 1963).

From the matrix of reflectance spectra $R_{n,\lambda}$, where n is the number of samples (measured or modelled), a mean spectra is calculated. This spectrum is then subtracted from the original matrix so as to obtain a matrix of residual spectra, $P_{n,\lambda}$. This operation is carried out to eliminate the possible influence of the difference in absolute magnitude of the subsequently retrieved eigenvectors, i.e. small differences occurring about a constant mean or base line. The residual matrix is transposed P′ and a matrix multiplication (P·P′) is made between the original and the transposed matrix. The resulting square variance-covariance matrix is used in the PCA and thus the eigenvectors and eigenvalues of this matrix are calculated. The *intrinsic dimensionality* (Neumann 1995) of the calculated eigenvectors is established indicating the number of significant vectors giving information on the shape of the spectra above the level of the noise. For the current datasets there were four vectors identified as significant in describing the shape of reflectance. Figure 3.15a shows the eigenvectors identified for the six satellite sensors selected for the inversion procedure. As can be seen they are all equivalent to each other and to the vectors identified from the 1nm resolution simulated reflectance and are also equivalent to the in situ measured reflectance shown in figure 3.15b. Once significant vectors have been identified the factor scores can be calculated:

$$FSi_1^n = \sum_{\lambda\min}^{\lambda\max} R_{n\lambda} Ui_{n\lambda} \tag{3.39}$$

where i is the eigenvector number and n is the number of samples.

Finally a multiple regression is made between the factor scores and each of the OACs to retrieve the geophysical algorithms of the form:

$$[CHL] = FS1 \times c1 + FS2 \times c2 + FS3 + c3 + FS4 + c4 + const1$$

$$[TSM] = FS1 \times t1 + FS2 \times t2 + FS3 + t3 + FS4 + t4 + const2$$

$$[YS] = FS1 \times y1 + FS2 \times y2 + FS3 + y3 + FS4 + y4 + const3$$

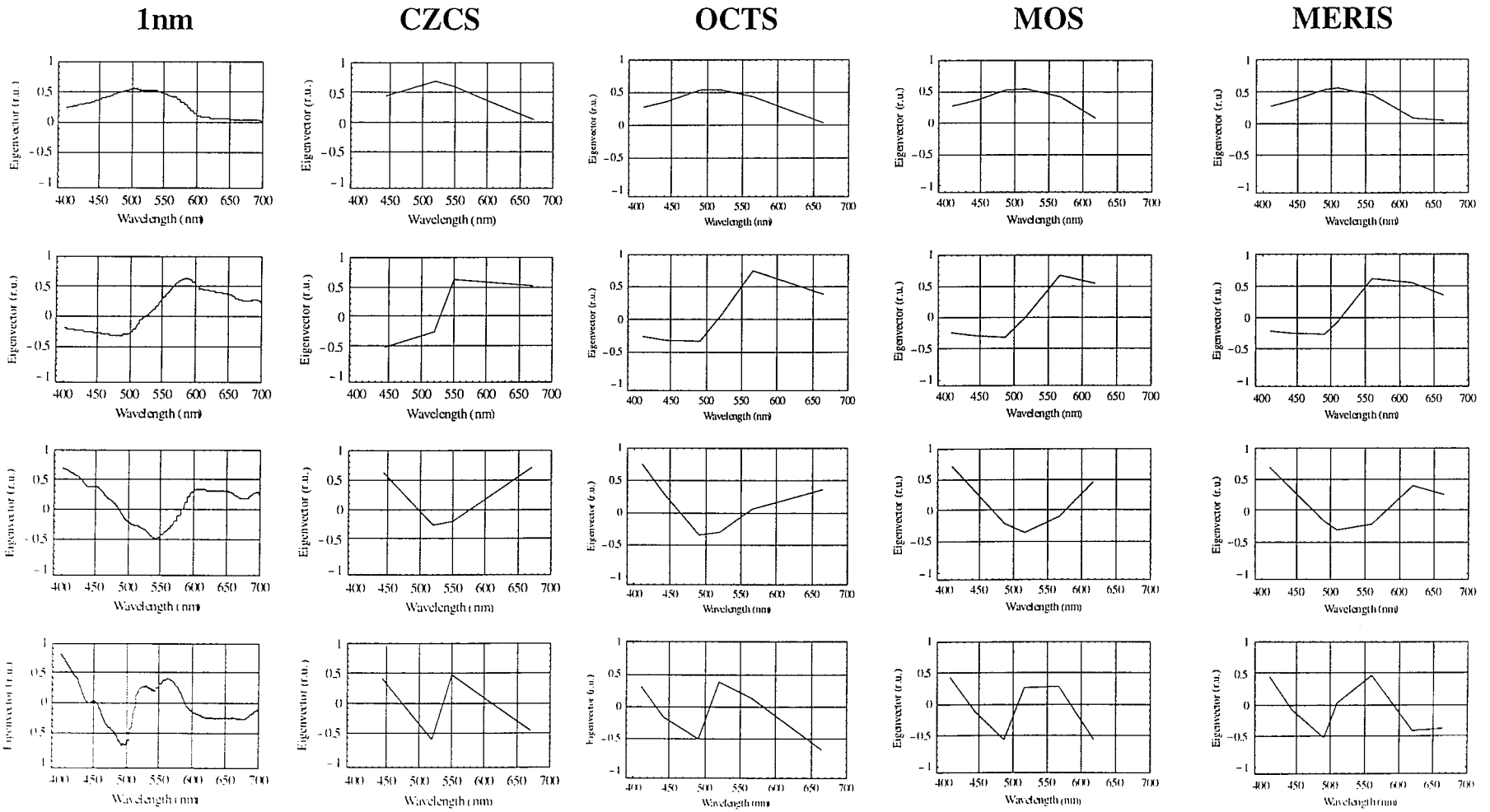

Figure 3.15: a) Plots showing the first four eigenvector for the individual bandsets and illustrating the capacity of typical satellite wavelength configuration in reproducing the information content of the 1nm resolution data.

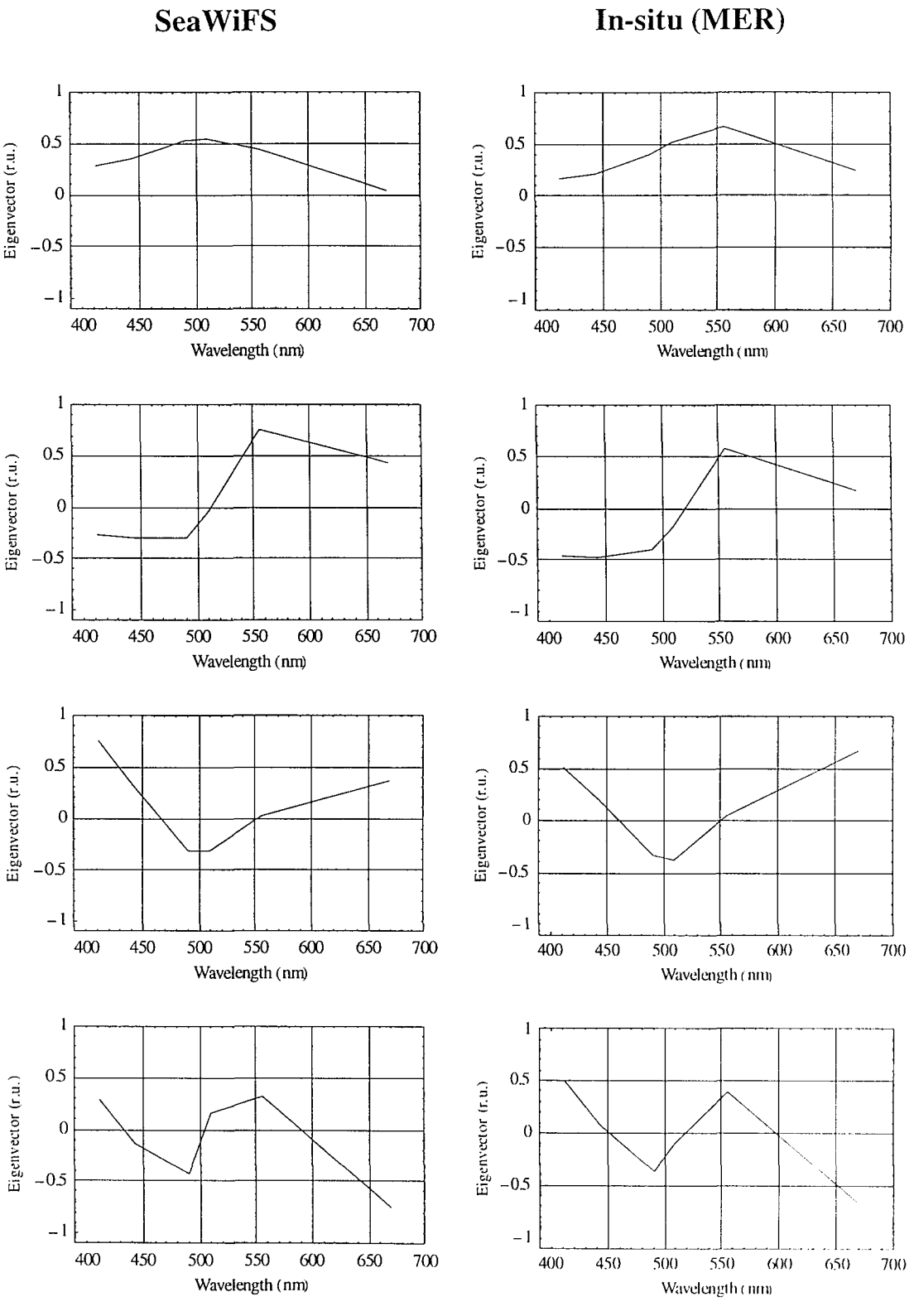

Figure 3.15: b) Plots of the first four eigenvectors for SeaWiFS and the in-situ dataset.

Here the coefficients *c1..c4, t1..t4* and *y1..y4* and *const 1..4* are the coefficients determined by the regression. Therefore these algorithms will allow one to calculate the geophysical parameters for regions in which the computed eigenvectors are valid. The coefficients from the regression analysis as well as the correlation coefficients are given in Table 3.4 for each of the satellite sensors for the three OACs.

	OAC	1	2	3	4	*const.*	r^2
CZCS	**[CHL]**	**3.26**	**224.67**	**1269.23**	**-3569.79**	**3.11**	**0.71**
	[TSM]	**-22.03**	**112.48**	**116.94**	**324.91**	**1.67**	**0.98**
	[YS]	**13.33**	**126.76**	**118.31**	**1115.02**	**0.95**	**0.86**
SeaWiFS	**[CHL]**	**4.26**	**-171.08**	**-1252.23**	**-680.33**	**3.12**	**0.76**
	[TSM]	**-17.67**	**-92.42**	**-41.24**	**232.72**	**1.67**	**0.99**
	[YS]	**12.06**	**-94.88**	**42.70**	**565.08**	**0.95**	**0.86**
OCTS	**[CHL]**	**3.09**	**-156.62**	**1243.37**	**-766.96**	**3.12**	**0.76**
	[TSM]	**-18.20**	**-80.25**	**32.83**	**224.57**	**1.67**	**0.99**
	[YS]	**11.53**	**-87.12**	**-43.76**	**550.98**	**0.95**	**0.86**
MOS	**[CHL]**	**2.68**	**-141.96**	**1029.71**	**-900.50**	**3.11**	**0.76**
	[TSM]	**-18.34**	**-70.19**	**23.94**	**176.27**	**1.67**	**0.99**
	[YS]	**11.33**	**-77.44**	**-29.62**	**447.26**	**0.95**	**0.84**
MERIS	**[CHL]**	**3.30**	**143.47**	**-927.69**	**-938.38**	**3.12**	**0.76**
	[TSM]	**-17.98**	**71.59**	**-18.13**	**152.17**	**1.67**	**0.99**
	[YS]	**11.52**	**76.75**	**28.49**	**422.07**	**0.95**	**0.87**

Table 3.4: Table showing coefficients resulting for each algorithms

To give the developed algorithms some validation the algorithm developed for SeaWiFS channels is applied to the in-situ reflectance data from the ULISSE cruises, the results are plotted against in-situ measured OACs (figure 3.16). These relationships show positive results of the developed algorithms on an independent dataset with correlation coefficients (r^2) for Chlorophyll, TSM and YS retrieval of 0.79, 0.89 and 0.80 respectively.

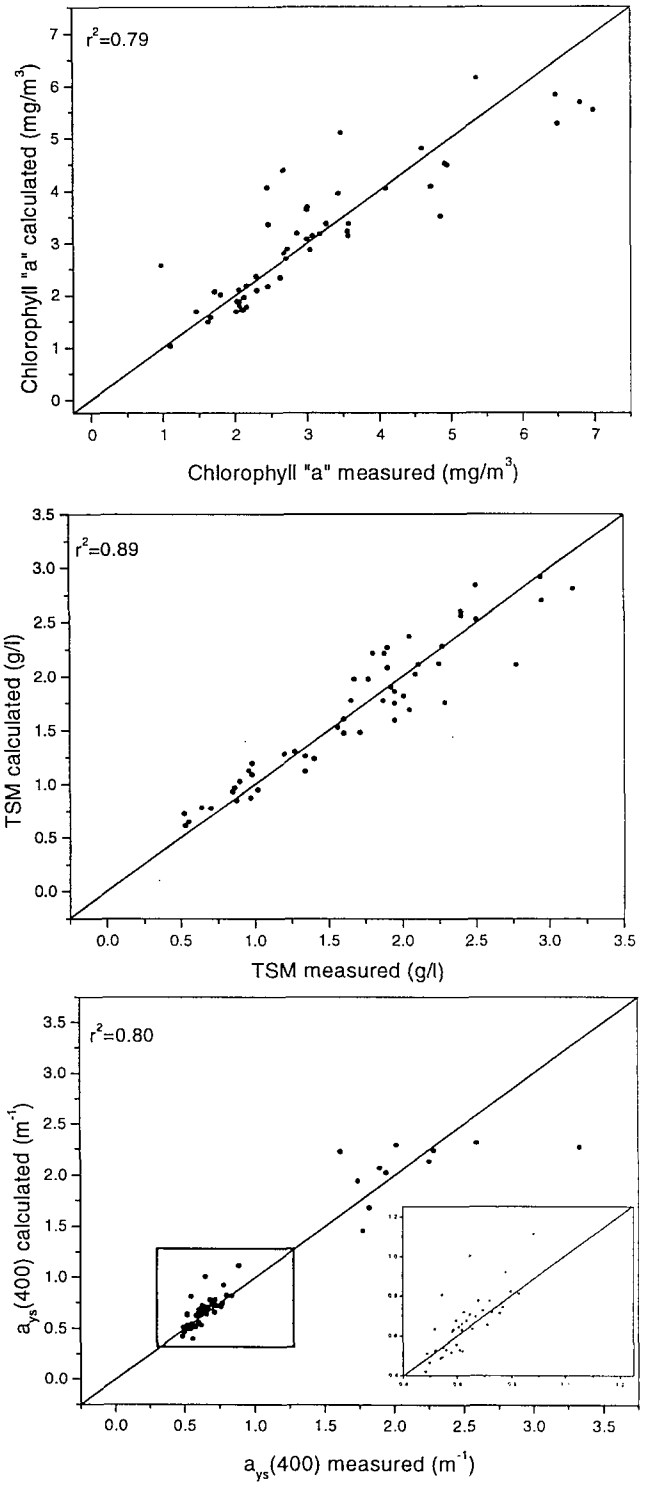

Figure 3.16: Plot showing relationships between measured and modeled values of the OACS (CHL, TSM, and YS) for the ULISSE stations. The correlation coefficients obtained are 0.79 for chlorophyll, 0.89 for TSM and 0.80 for yellow substance.

3.6. Discussion

3.6.1. Parameterisation of CDOM absorption

Since early work on the absorption budget the CDOM spectral absorption coefficient has been modelled as an exponentially decaying curve with a fixed slope of around 0.014 (Bricaud 1981). This representation was shown to be adequate in various marine environments and was confirmed by numerous authors throughout the 1980's (e.g. Ferrari and Tassan 1991). However, recently in a number of publications (Roesler 1989, Vodacek 1997, Dowell et. al. 1996) the range of the variability of the slope of a_{ys} has been shown to vary over a very large scale from 0.008 to 0.03 (Vodacek 1996). This evidence underlines the requirement to allow variability of slope in the modelling of CDOM absorption. Evidence that CDOM was composed of many different sources has been long acknowledged by the scientific community (e.g. Harvey et. al. 1983). Initial attempts to reflect the complexity of the composition of CDOM in bio-optical models for absorption were made by Carder et. al. (1986), in which the authors divided the total absorption coefficient of CDOM in terms of the mass specific absorption curves and their relative concentrations for two components of CDOM - namely Marine Humic Acid (MHA) and Marine Fulvic Acid (MFA) - so that:

$$a_g(\lambda) = C_f a^*_f \, e^{(k1)} + C_h a^*_h \, e^{(k2)}$$

where $k1=S_f(450-\lambda)$ and $k_2=S_h(450-\lambda)$. C_f and C_h are the MFA and MHA concentrations (gm^{-3}), the parameters a^*_f, a^*_h, S_f and S_h are 0.00728 m^2g^{-1}, 0.1304 m^2g^{-1}, 0.01890 nm^{-1} and 0.01105nm^{-1} respectively (note a_g is equivalent to a_{ys}). This two component model will obviously give more variability to the shape of the absorption curve. However, it is also apparent that the maximum slope that such a model could represent would be ~0.018nm^{-1} which corresponds only to a mean and not a maximum value for the studied dataset. Another approach to characterise the absorption spectra of CDOM has been made by Krijsmann (1994). In this study the author considered the use of Target Factor Analysis (TFA) (Malinowski et. al. 1980) to model $a_{ys}(\lambda)$ with positive results. Krijsmann (1994) used a population of absorption spectra taken from different locations in the Netherlands, and investigated

the spectral residuals resulting from the application of traditional models of a_y as well as from the models formulated from his TFA. The results showed that applying an exponential model with a fixed slope (both 0.014 and 0.016) led to considerable errors. It was also shown that the MFA+MHA model of Carder et. al. (1986) presented above was not very representative. However, the results from the first few vectors of the TFA produced spectral residuals that were a significant improvement on the more traditional methods in which the first three vectors reproduced the absorption spectra within the instrumental error of a spectrophotometer and the first two vectors reproduced the spectra within levels typical of the measurement error for absorption. A TFA analysis was also applied on the spectra for a_{ys} used in the present study (i.e. from the ULISSE dataset). The results of the residuals had the same levels of error as those given by Krijsmann, but significantly the eigenvectors retrieved from the dataset were almost identical to those given by Krijsmann (1993) from a contrasting environment. These similarities would seem to suggest that standard components could be identified to reproduce the absorption spectra of a_{ys}. This is of considerable value but it is also apparent that it needs to be the subject of further research to enable its integration in reflectance modelling.

The relationship presented here to describe the wavelength dependency of a_{ys} (given in equation 3.22) considers the slope of the exponent used in the range of the model to be dependent on the absorption coefficient of CDOM at a specific wavelength (here 400nm is used). It has been demonstrated that this model is valid for the entirety of the studied dataset, covering a range of values of the slope from 0.010 to 0.025. Furthermore, although not commented by the respective authors several other datasets in literature have been observed in which the identified relationship would seem to be applicable. The first of these is that in Green (1992) where the asymptote of the exponent of the relationship between the two a_{ys} *vs.* S_{ys} models is the same value, 0.018, found in the Baltic. This value can also be verified in a very large dataset presented by Vodacek (1996) in which, although the scattering is higher, both the asymptote and the cut off point of the two relationships are apparent. If the presented data and cited references can be considered as representative then this would imply

that the relationship identified here could given an indication of a general formulation for deriving the slope of the a_{ys} exponential curve over a very large range, i.e. 0.02-20m^{-1}, at 400nm.

One aspect of proposed formulation for determining S_{ys}, which has not been possible to analyse using the current dataset, is the behaviour of the relationship at lower levels. Although the graphs shown in the cited literature (e.g. Vodacek 1996) would seem to suggest that the cut off point i.e. the highest value of S_{ys} is about 0.04 (corresponding to the lowest value of a_{ys}), this would need to be established with further *oceanic* datasets. The relationship identified (equation 3.22) separates the measured a_{ys} into two main groupings and since these two groupings are linked to the intensity of absorption one obvious conclusion is that the two relationships could indicate two different sources of YS; namely terrigenous and allochtonous (marine algal exudates). As a plausible way of qualitatively differentiating these two types of YS one can use synchronous fluorescence spectroscopy, a measurement which was made also during the ULISSE campaigns (section 2.3.4). Synchronous fluorescence spectra make a diagonal transect across the Emission Excitation Matrix and have been used to differentiate higher weight from lower weight molecular compounds. The original application of this technique was to differentiate hydrocarbons with a different number of aromatic rings (Gordon 1976). However, they have since been used in marine science (Cabaniss 1987, Ferrari and Mingazzini 1995) to differentiate dissolved organic molecules of different weight and therefore differentiate YS of terrestrial origin and larger molecular weight from that of direct marine origin and lower molecular weight. It would seem that as a first order differentiation between these two sources one could use a value of ~3 for the ratio between the first and second peaks of the synchronous fluorescence spectra (hA:hB) (see Ferrari and Mingazzini 1995 figure10), to distinguish between waters with YS predominantly of terrestrial origin (below 3) and of marine allochtonous origin (above 3). This notion was therefore applied to a subset of 6 spectra from figure 3.7a, including 3 spectra from the linear relationship and 3 spectra from the exponential relationship. As can be

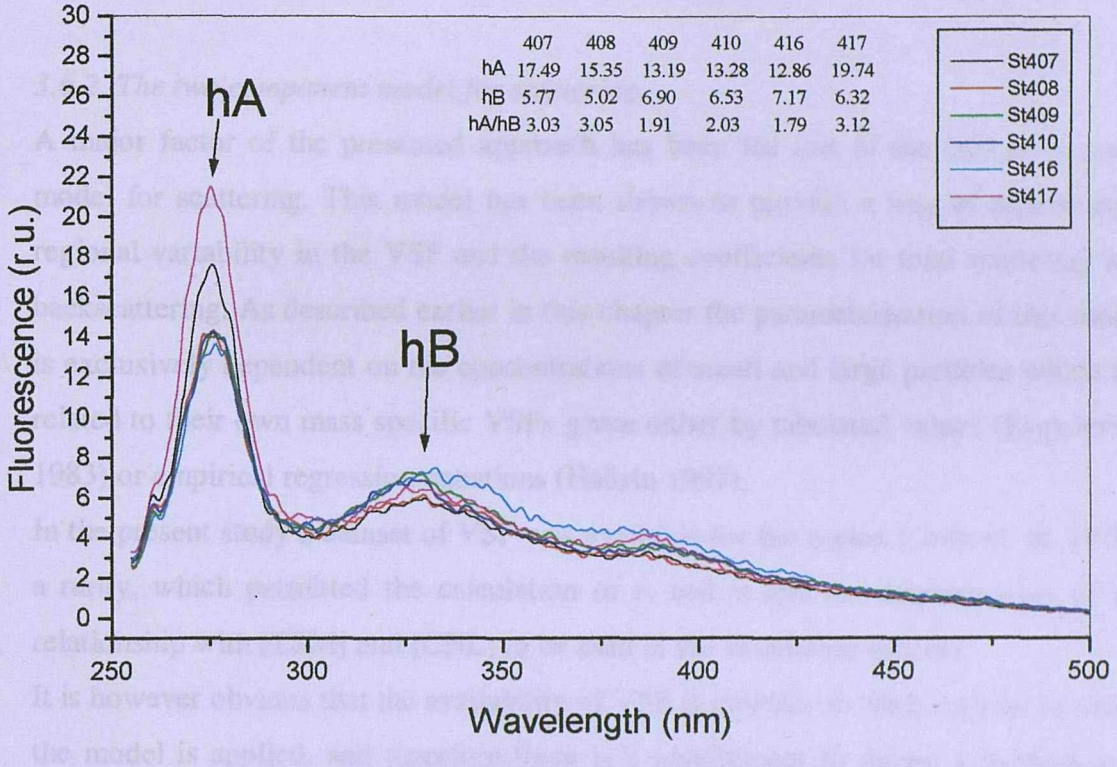

	407	408	409	410	416	417
hA	17.49	15.35	13.19	13.28	12.86	19.74
hB	5.77	5.02	6.90	6.53	7.17	6.32
hA/hB	3.03	3.05	1.91	2.03	1.79	3.12

Figure 3.17: Plot showing example synchronous fluorescence spectra. These spectra clearly allow to differentiate between yellow substance of terrestrial and autochthonous origin, and show the distinction in the $S_{ys}(400\text{-}600)$, $a_{ys}(400)$ relationship used in the present model.

seen in figure 3.17 the spectra show some quite distinct differences and when the hA:hB ratio are calculated (also shown in figure 3.17) these results show that the cut off point of 3 is a good approximation for distinguishing between the two sources of YS as deduced from the earlier work. This implies that the two different S_{ys} a_{ys} relationships divides the coastal and marine dominated YS.

3.6.2. The two component model for scattering

A major factor of the presented approach has been the use of the two component model for scattering. This model has been shown to provide a way of representing regional variability in the VSF and the resulting coefficients for total scattering and backscattering. As described earlier in this chapter the parameterisation of this model is exclusively dependent on the concentrations of small and large particles which are related to their own mass specific VSFs given either by tabulated values (Kopelevich 1983) or empirical regression equations (Haltrin 1997).

In the present study a dataset of VSF was available for the region (Gohs et. al. 1978), a rarity, which permitted the calculation of v_s and v_l and the determination of the relationship with [TSM] and [CHL] to be used in the simulation process.

It is however obvious that the availability of VSF is unlikely in other regions to which the model is applied, and therefore there is a requirement to devise a methodology which determines the concentrations of v_s and v_l from traditional measurements. A preliminary suggestion is given here, although it is obvious that this needs to be a topic of further investigation.

As defined by Kopelevich (1983) the presented model describes two distinct particle groupings contributing in different ways to the total VSF. In short the two fractions consist of a small inorganic fraction and a larger organic fraction. Similarly a recent publication by Jonasz and Fournier (1995) has presented a model for the Particle Size Distribution (PSD) based on a multiple lognormal distribution. If one considers the proportion of the PSD making any significant contribution to the backscattering, which is the main coefficient of interest in the context of reflectance modelling, then this limits the number of lognormal components (Jonasz and Fournier 1995) required

to describe the PSD in this range. Furthermore, if one considers their results then clearly for the very large dataset analysed by the authors (412 PSD), a series of common recurrent components was found. In particular the first two components represented ~60% of a total 853 components; the first of these has a mean diameter of 0.64μm and the second 10.5μm. These two components should cover the range of interest in calculations of b_{b_p}. It is therefore suggested that an investigation be made into the amplitude and shape coefficients of these in the context of a Kopelevich type two parameter scattering model through measured PSD and Mie calculations. The eventual objective is to parameterise v_s and v_l for the region under consideration using the variables of the in-situ measured PSDs.

3.6.4. Determination of f in the remote sensing context

It was shown earlier in this chapter that it is feasible, using a published model (Sathyendranath and Platt 1997), to analytically calculate the proportionality factor *f*, with the necessary information on the VSF and the sun earth geometry. The results from these calculations (see figure 3.12) illustrated the gross error which could be incurred by systematically applying a constant value (i.e. 0.33) to simulated reflectance. This therefore justifies the decision made to carry out the final inversion scheme and algorithm development not on simulated R(λ), but more simply on a simulated matrix of ω_b and that *f* would therefore be determined *a posteriori* for each satellite pixel. This approach would seem to be logical as the resulting algorithm would in theory be applied to the variability due to the IOP. However, the evaluation of *f* for each pixel using the model given in Sathyendranath and Platt (1997) would prove impractical on the scale of a thematic image, and therefore a more simple relationship is required. Thus, the relationship shown in Figure 3.18 was defined between the calculated *f* and the sun zenith angle in air. This may be expected to be a simple relationship having been previously proposed (i.e. Kirk 1984), but the use of the Sathyendranath and Platt (1997) model allowed this relationship to be made specific to the region of study based on the regional model for the VSF. Such an approach would therefore allow this type of relationship to be identified for any

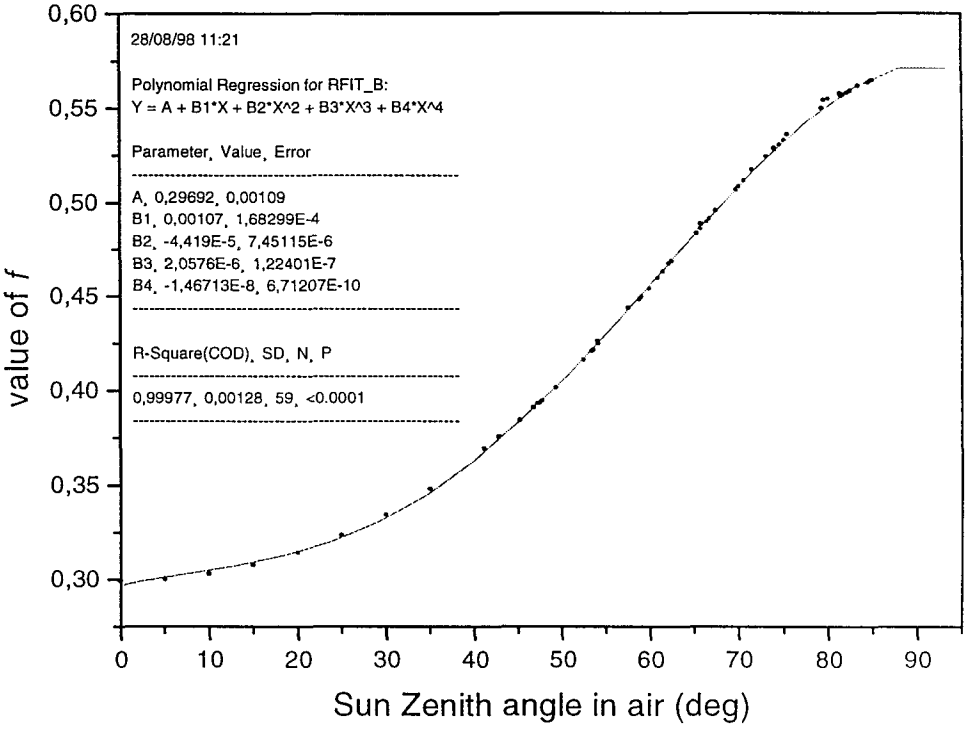

Figure 3.18: Graph showing a plot of f against the sun zenith angle in air. The polynomial fit shows a very good relationship between these two variables over the full ranges expected.

region studied and ultimately look up tables of regional relationships could be formulated (i.e. for European basins). The relationship obtained from fitting the calculated data resulted in a four-term polynomial. However, if one considers the range of values which could be expected in the situation of a polar orbiting satellite with a near local noon overpass, even at the highest latitude, values higher than 70-75° would not be possible and the polynomial fit would be of a lower order.

3.6.5. Reproduced shape of reflectance

The simulated ω_b and $R(\lambda)$ has shown to reproduce the measured $R(\lambda)$ in shape and magnitude. Slight differences in the shape and magnitude particularly in the red part of the spectra may be partly explained by the inaccuracy of determining the Q factor particularly in its spectral shape. Thus, if model results are to be validated with in-situ measured reflectance, it is strongly urged that the $Q(\lambda)$ factor (E_u/L_u) be made a standard measurement during bio-optical field work. Some recent results of Q measured in-situ (Zibordi et. al. 1997) have shown that the spectral differences between the blue and red parts of the spectra can be quite large (in the order of 1:2 blue:red). Therefore either analytical models need to be developed for Q which reflect the wavelength dependency of this variable, or in-situ measurements must be systematically made. This point will become of considerable importance as Ocean Colour sensors become more sophisticated with higher signal to noise ratios allowing for the formulation of bio-optical models based not only on the shape but also on the magnitude of radiances in defining geophysical algorithms. Another important aspect of the reproduction of reflectance or ω_b using the presented model, is that discrepancies may be due to some form of transpectral (in-elastic) process or bottom effect but these factors and their context are discussed in much more detail in chapter 4.

Having commented on differences, it is also of considerable importance that the shape reproduced by the model is the same as those measured. This is underlined by the fact that the reflectance model reproduces even certain anomalous spectra observed in the in-situ spectra. A good example of a case in which the model reproduces an

anomalous situation is in a series of about 5-10 spectra showing a flat or negative slope between 510 and 550 (where the slope is normally positive), both in the measured and modelled spectra (figure 3.13). A possible explanation for this is in the slope of the backscattering spectra. As the slope of the backscattering spectra approaches 0 (i.e. in highly turbid water of biological origin) the reflectance or ω_b spectra in this region, where the absorption is low, will become flat. In some cases the slope of the measured reflectance is negative in the same region, therefore implying that the slope of backscattering would be positive. This has been suggested by several authors (Berthon et. al. 1996). However, in the present case this may also be the result of contributions from CDOM fluorescence.

3.6.6. Adequacy of the spectral information from RS wavelengths for Case II waters

If one sets off with the fundamental assumption that the 1nm resolution spectral ω_b simulation is a true representation of the IOPs in the environment studied then a major benefit of using PCA for the inversion of the simulated data is that it should in theory preserve the information content of the original data; but eliminates the noise. This notion is not new, but a test was made in this study to verify whether the information content obtained for a series of historical, current and future ocean colour sensors at distinct channels is equivalent to that produced by the 1nm data. The results presented in figure 3.15, show that all of the eigenvectors have the same shape including the in-situ measured reflectance. The one exception is the CZCS with only with 4 channels (443, 510, 550, 670) which are not capable of reproducing the whole information content of the simulated reflectance. These results however do imply that the channels available to the 6 channel sensors (SeaWiFS, OCTS) or higher are sufficient to describe the full information content contained in the original data. A slight aside is the observation that the sensors with a 620nm channel i.e. MOS/ MERIS represent the reflectance spectra much better in this part of the spectrum (see Figure 3.13 and Figure 3.16). This seems to have no major impact on the calculation of the eigenvectors but may be of significant importance in Case II waters in particular when channels in the red are effected by in-elastic processes (see in chapter 4).

3.6.7. PCA inversion scheme and the geophysical algorithms

A main criticism of the use of inversion techniques, such as Principal Component Analysis, in the analysis of large sets of reflectance data is that these types of multivariate statistical analysis are linear approaches to account for a non-linear process. This is because the interaction between the IOPs involved and responsible for the variability of reflectance are not necessarily linearly related with each other. Having said that both in this study and in many previous a certain level of validity has been shown in the application of the PCA to invert simulated reflectance. It is possible that in the present study the use of this technique is valid because such restricted area and therefore restricted distribution functions were adopted. The non-linearity of the system may become more apparent when such techniques are applied to datasets for much wider concentrations ranges. One possibility in such a case may be to look into higher level statistical techniques such as source separation and Independent Component Analysis (Comon 1994) which are specifically intended for non-linear systems and are in themselves a direct extension of the PCA. Additionally one typical way of implementing such a technique is through neural networks which are being explored as a potential means of inverting reflectance data. These however are topics of further consideration and should not overshadow the success and potential of PCA in the development of regional algorithms.

The algorithms derived from the inversion procedure and shown in Table 3.4 have proven to perform well. In all cases the best OAC retrieved is TSM followed by YS and lastly CHL. This is different to previous models (e.g. Sathyendranath 1989) which found that CHL was better retrieved than YS, though in the present case this is due to the large contribution by YS. Another advance in the algorithms is an improvement in the algorithm retrieval accuracy (Table 3.4.) the higher spectral resolution of sensors has improved the retrieval of CDOM from an r^2 of ~0.8 to r^2 of ~0.9 (due to the addition of the channel in the blue). The addition of the 620nm channel (i.e. MOS and MERIS) does not seem to have any major effect; this channel may become more important with the consideration of the effect of inelastic processes (*see chapter 4*).

The test of the validity of the derived SeaWiFS algorithm against the in-situ measured reflectance (see figure 3.16) proved to be quite acceptable with a CHL retrieval of r^2 0.79, TSM of 0.89 and YS of 0.80, giving an initial confirmation of the proposed modelling system.

3.7. Conclusions

We have seen that with a limited amount of in-situ knowledge for a specific region, it is possible to define a reflectance model which is able successfully to reproduce the varying spectral shape of the in-situ measured reflectance. The reflectance model presented, although used in the current study with the aim of producing algorithms for a specific region, could also prove to be a useful oceanographic tool in many other circumstances e.g. in the study of the budgets of absorption and scattering. The simulated reflectance spectra show a similar occurrence to the in-situ measured spectra in that a small number of spectra i.e. 10-15% show a negative slope between the blue-green and the green, explained with the model.

The forward reflectance model as presented here is most efficient in simulating the shape of the reflectance spectra in the Case II waters of the Southern Baltic. Differences in the absolute magnitude when compared to in-situ measured spectra have little effect in the inversion procedure, suggesting that the technique developed is adequate to retrieve the optical characteristics of coastal turbid waters from satellite.

It is worth comment that the shape of the simulated reflectance in the red part of the spectra is better represented with the wavebands available on the MOS sensor when compared with those of SeaWiFS and OCTS. The higher spectral resolution of this sensor may thus be best suited to retrieving multiple components in Case II waters, particularly in the presence of Chlorophyll "a" fluorescence.

A scheme was presented which successfully inverted the simulated reflectance using the PCA technique. Also the technique highlighted that the information content offered by the spectral bands of the new ocean colour sensors is no less representative than the full 1nm resolution, and that the first four eigenvectors represent 99% of the

total variability. The algorithms resulting from the inversion scheme that allow the retrieval of the OACs from reflectance have shown that a major improvement in the availability of a new generation of more spectrally resolved sensors allows for a more accurate distinction between YS and CHL. Thus it is feasible that all OACs can be estimated for the region chosen within an error of 25% as verified through an independent dataset of in-situ measured reflectance.

Chapter 4

Contamination of the elastic signal by transpectral processes and bottom reflectance

Chapter 4 Table of Content

4.1. Introduction
4.2. Methodology and Theory
4.2.1. Determination of the surface light field
4.2.2. Modelisation of in-elastic processes and bottom reflectance
4.2.2.1. Modelisation of CDOM fluorescence
4.2.2.2. Modelisation of Chlorophyll "a" fluorescence
4.2.2.3. Modelisation of Phycoerythrin fluorescence
4.2.2.4. Modelisation of Raman Scattering
4.2.2.5. Modelisation of bottom reflectance
4.3. Results
4.3.1. Proportional contribution of inelastic processes to modelled reflectance
4.3.2. Influence of in-elastic processes on calculated eigenvectors
4.4. Discussion
4.4.1. The contribution of inelastic processes to absolute reflectance
4.4.2. The importance of the in-elastic processes in the PCA inversion procedure
4.4.3. Partition of the visible spectral range by elastic and inelastic processes
4.5. Conclusions

4.1. Introduction

The reflectance model for Case II waters presented so far exclusively accounts for elastic processes which contribute to the diffuse reflectance without modifying the wavelength of incident (λ_1) and emitted (λ_2) light. On the contrary, in-elastic or transpectral processes are associated with a specific redistribution function of light so that $\lambda_1 \neq \lambda_2$. In general this wavelength shift is to higher wavelengths.

The inelastic processes can be divided into Raman Scattering and those consisting of Solar Stimulated Fluorescence (SSF). In coastal marine waters, SSF is caused by CDOM (yellow substance), and cells containing Chlorophyll "a" and Phycoerythrin. Chlorophyll "a" fluorescence, has been studied extensively and even proposed as a technique for deriving Chlorophyll "a" concentration (e.g. Gower and Borstad 1985). Phycoerythrin SSF has been previously observed in radiometric data (Culver 1995). However, its contribution to reflectance has never been modelled. The importance of incorporating in-elastic processes into reflectance models has been addressed in two major investigations by Lee et. al. (1994) and Haltrin and Kattawar (1993). More recently, Haltrin et. al. (1997) suggested that the visible part of the electromagnetic spectrum could be split into two parts: a first blue region in which reflectance is dominated by elastic processes and a red region dominated by inelastic processes. The cut off point occurs at a wavelength not lower than 550nm and is itself a function of the in-water optical properties. Also according to Haltrin (1997), Raman scattering has a dominant contribution over chlorophyll and CDOM fluorescence successively. Such individual contributions to the total in-elastic reflectance may change in Case II water for which one would expect Raman scattering to be less significant. In this chapter, the effect of inelastic processes on reflectance is investigated together with the effect of bottom reflectance which is not in itself an inelastic process but which may contribute to the diffuse reflectance.

As an aside some recent calculations by Ge et. al. (1993) have shown that the high spectral resolution measurements of Fraunhofer lines can be used to estimate the contribution of inelastically scattered light to the total underwater light field. The basic idea involved in this approach is very simple. In the case of no inelastic

scattering processes the line depth (η_F) at wavelength λ_F (wavelength of a Fraunhofer line will remain unchanged with the geometric depth of the water (z). However, if there are broad band (with respect to the width of the Fraunhofer line) inelastic contributions to the light field near λ_F, then the line depth η will decrease in the water with depth as the solar contribution decreases. Thus, the total light field becomes dominated by inelastically scattered light, which is nearly constant over the wavelength intervals of a few nanometers. Using the measured values of η at the surface (z=0) and at depth one can separate the total irradiance into its elastic and inelastic parts. This type of method is however only applicable for CDOM fluorescence and Raman scattering (Ge et. al. 1995) as there is no Fraunhofer line associated with the Chlorophyll "a" fluorescence peak.

The objectives of this study are two-fold: i) establishing the inelastic contribution (total and individual processes) to the diffuse reflectance calculated through the elastic model; ii) evaluating the contribution of these in-elastic processes to the eigenvectors computed in the inversion procedure of the regional model (Chapter 3).

This type of investigation therefore requires a complete assessment of in-elastic contributions, both spectrally and in magnitude, but it is less vital that the overall accuracy of the individual calculation is precise.

The modelling of in-elastic scattering requires information on the spectral distribution of downwelling irradiance that is computed according to an existing model (Gregg and Carder 1990).

4.2. Methodology and Theory

4.2.1. Determination of the surface light field

In the last ten years the importance of accurate knowledge of spectral information on the spectral distribution of downwelling irradiance ($E_d(\lambda)$) has become much appreciated. It has been shown to be particularly relevant to studies of primary productivity (i.e. Bidigare et. al. 1987, Sathyendranath and Platt 1988).

In the present study the Gregg and Carder (1990) model is applied to the evaluation of $E_d(\lambda)$ for the excitation and emission wavelength ranges of the transpectral processes

considered. Some brief details of the layout of the model is given below although the reader is referred to the original manuscript (Gregg and Carder 1990) and references therein for further detail.

The total solar irradiance at the sea surface is spectrally computed and partitioned into two components, so that:

$$E_d(\lambda,\mathbf{0}^-) = E_{dd}(\lambda,\mathbf{0}^-) + E_{ds}(\lambda,\mathbf{0}^-) \tag{4.1}$$

where E_{dd} is the contribution from direct irradiance and E_{ds} is the contribution from diffuse irradiance, just beneath the sea surface. The two components can be described by the two following functions (omitting the wavelength dependency for sake of simplicity):

$$E_{dd} = F_o \cos\theta\, T_r T_a T_{oz} T_o T_w (1-\rho_d) \tag{4.2}$$

and,

$$E_{ds} = [I_r + I_a](\mathbf{1}-\rho_s) \tag{4.3}$$

Where the variables are described in the following table:

Symbol	Definition
F_o	mean extraterrestrial irradiance corrected for earth-sun distance and orbital eccentricity
θ	solar zenith angle
T_i	Absorption or scattering by the *i*th component, *i* corresponds to r=Rayleigh scattering, a=Aerosol scattering, oz, o, w=ozone, oxygen and water absorption
I_r	the diffuse component arising from Rayleigh scattering
I_a	Diffuse component arising from aerosol scattering
ρ_d	direct sea surface reflectance
ρ_s	Diffuse sea surface reflectance

The aerosol scattering component is critical in the computation of the downwelling irradiance in coastal waters. Gregg and Carder (1990) have adopted a method proposed by Gathman (1983) which is based on the analysis of more than 800 aerosol

size distributions. As a result of his study the aerosol size distribution could be adequately represented by the summation of three lognormal components:

$$dN/dr = \sum_{i=1}^{3} A_i \exp\left\{-\left[\ln\left(r/fr_{oi}\right)\right]^2\right\} / f \qquad (4.4)$$

Each of the identified components is associated with a particular type of aerosol and parameterised as such.

The first component describes the continental derived aerosol (present as a background even in remote marine areas) and is parameterised by the Air Mass type (AM). The second component represents the equilibrium sea-spray particles in the atmosphere and is related to the mean 24 hour windspeed (WM). The third is a large, ephemeral component resulting from the instantaneous windspeed. The f factor given in the equation above relates the particle size to the relative humidity. Therefore the particle size distribution for aerosols can be determined with varying contributions from both maritime and terrestrial aerosols and being parameterised on the basis of basic meteorological observations. However, as equation 4.4. requires Mie calculations to retrieve the efficiency factors Q_{ext} , thus over extending computing time Gregg and Carder (1990) approximated the aerosol size distribution by the following Junge distribution.

$$\sum_{i=1}^{3} A_i \exp\left\{-\left[\ln\left(r/fr_{oi}\right)\right]^2\right\} / f = dN/dr = Cr^{\gamma} \qquad (4.5)$$

Where C is the amplitude function. From this one can retrieve the Junge γ exponent and thus calculate the Angstrom exponent (α), through:

$$\alpha = -(\gamma + 3) \qquad (4.6)$$

and thus the aerosol transmittance can be calculated. Figure 4.1a shows the spectral distribution of the aerosol transmittance for the stations of the ULISSE cruises (see chapter 2). The downwelling irradiances $E_d(\lambda)$ beneath the sea surface at these stations (4.1b) are retrieved using the equations 4.1 to 4.3 and the necessary meteorological data, including surface pressure (mb), air mass type, relative humidity

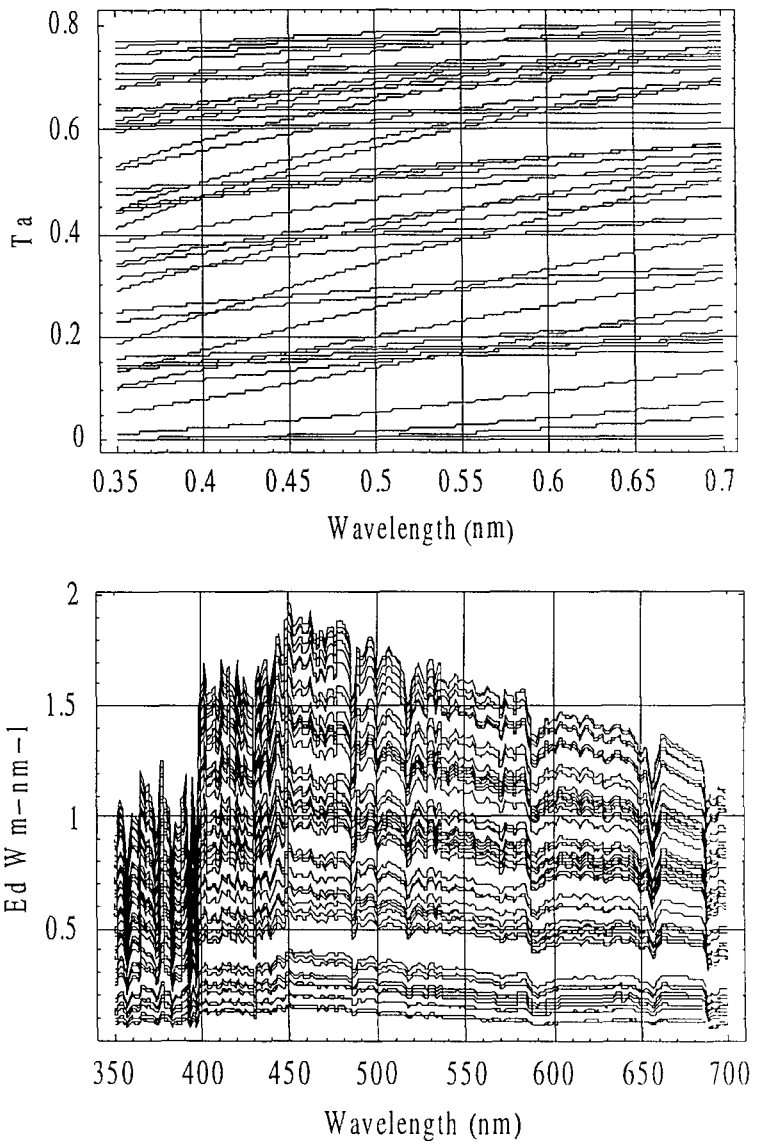

Figure 4.1: Plots showing the spectral resolution of the aerosol transmittance (top) and the total downwelling irradiance (bottom). These spectra were calculated using the Gregg and Carder (1990) clear sky model, which has a very high spectral resolution of 1nm.

(%), precipitable water (cm), mean windspeed (m/s), instantaneous windspeed (m/s) and visibility (km).

4.2.2. Modelling of in-elastic processes and bottom reflectance

Because of clear differences in the quantity and spectral quality of the redistributed light field, the parameterisation of inelastic scattering is conducted by initially looking at each responsible process individually.

4.2.2.1. Modelling of CDOM fluorescence

As mentioned CDOM fluorescence was the first inelastic process considered in the present investigation as it was apparent that in the region considered, i.e. where CDOM absorption is so high, this process could be a major contributor to the surface light field.

According to Lee et. al. (1994) the volume scattering phase function for inelastic scattering is defined as follows:

$$\beta_{ie}(\alpha,\lambda_x,\lambda)=\frac{T_{ie}(\alpha,\lambda)}{E(\lambda_x)dV} \tag{4.7}$$

where $T_{ie}(\alpha, \lambda)$ is the intensity of the inelastically scattered light at scattering angle α, dV is the scattering volume, $E(\lambda_x)$ is the irradiance of the excitation beam and α is the angle between the excitation beam and the output photon directions. As β_{ie} is considered to be isotropic, the reflectance resulting from SSF of CDOM can be expressed as (Lee et. al. 1994):

$$R_{fys}=\frac{1}{2}\int_{\lambda x}\Phi_{fys}(\lambda_x)\frac{\lambda_x}{\lambda}\frac{a_{ys}(\lambda_x)E_d(0^-,\lambda_x)}{[2a_{tot}(\lambda)+a_{tot}(\lambda_x)]E_d(0^-,\lambda)}\frac{\exp\left[-s\left(\ln\frac{\lambda-\lambda_0}{\sigma}\right)^2\right]}{A}\,d\lambda_x \tag{4.8}$$

The term Φ_{fys} is the quantum yield for the fluorescence of CDOM at the excitation wavelength (λ_x). In the ULISSE dataset, $\Phi_{fys}(\lambda_x)$ varied between 0.9 and 1.3% with a mean of 1.1% (NB the higher values occur in spring and seem to be associated with an increased chlorophyll concentration (Ferrari and Dowell 1997). The term on the right hand side of equation 4.8. describes the light emission curve. In the case of

CDOM, the emission curve is represented by a lognormal distribution, which is parameterised by the value of λ_0 and the shape factors s and σ . These parameters were determined from the emission curves made on the ULISSE samples, shown in figure 4.2a. The reference wavelength λ_0 is determined according to Lee et. al. 1994 ($0.95\lambda_x$-45) which was also verified with the ULISSE dataset. The integral of equation 4.8. is thus derived over the excitation wavelengths for CDOM fluorescence (i.e. 350-450nm), knowing Ed from section 4.2.1. and both the total (a_{TOT}) and CDOM (a_{CDOM}) absorption spectra, respectively shown in figure 4.2.b and 4.2.c.

The calculated values of R_{FCDOM} are expressed in terms of irradiance reflectance (i.e. $R_w=E_u/E_d$) and not remote sensing reflectance (i.e. $R_{rs}=L_w/E_d$) as presented by Lee et. al. (1994). These two parameters are related to each other as follows:

$$R_{rs} = \frac{I}{Q} R_w \tag{4.9}$$

where I is a factor describing the influence of the air sea interface on the water leaving radiance and given a constant value by Lee et. al. of 0.533, Q is the Q factor (see chapter 3) i.e. Eu/Lu, which in the case of inelastic processes (Q_{ie}) can be given a constant value of 3.7 (Gordon 1979 and Lee et. al.).

A further difference between the present work and Lee et. al.'s (1994) study is that they only considered, as far as fluorescence processes go, the CDOM fluorescence, whereas in the current work both Chlorophyll "a" and Phycoerythrin fluorescence are considered.

4.2.2.2. Modelling of Chlorophyll "a" fluorescence

The calculation of the reflectance due to the SSF of chlorophyll requires basically the same additional information as that for CDOM. Thus, in a similar formulation to the CDOM fluorescence, the reflectance due to the SSF of chlorophyll can be computed as follows:

$$R_{fCHL} = \frac{1}{2}\int_{\lambda x} \Phi_{fchl}(\lambda_x)\frac{\lambda_x}{\lambda}\frac{a_{ph}(\lambda_x)E_d(0^-,\lambda_x)}{[2a_{tot}(\lambda)+a_{tot}(\lambda_x)]E_d(0^-,\lambda)}\frac{\exp\left[-\left(\frac{\lambda-\lambda_0}{2\sigma^2}\right)^2\right]}{A}d\lambda_x \tag{4.10}$$

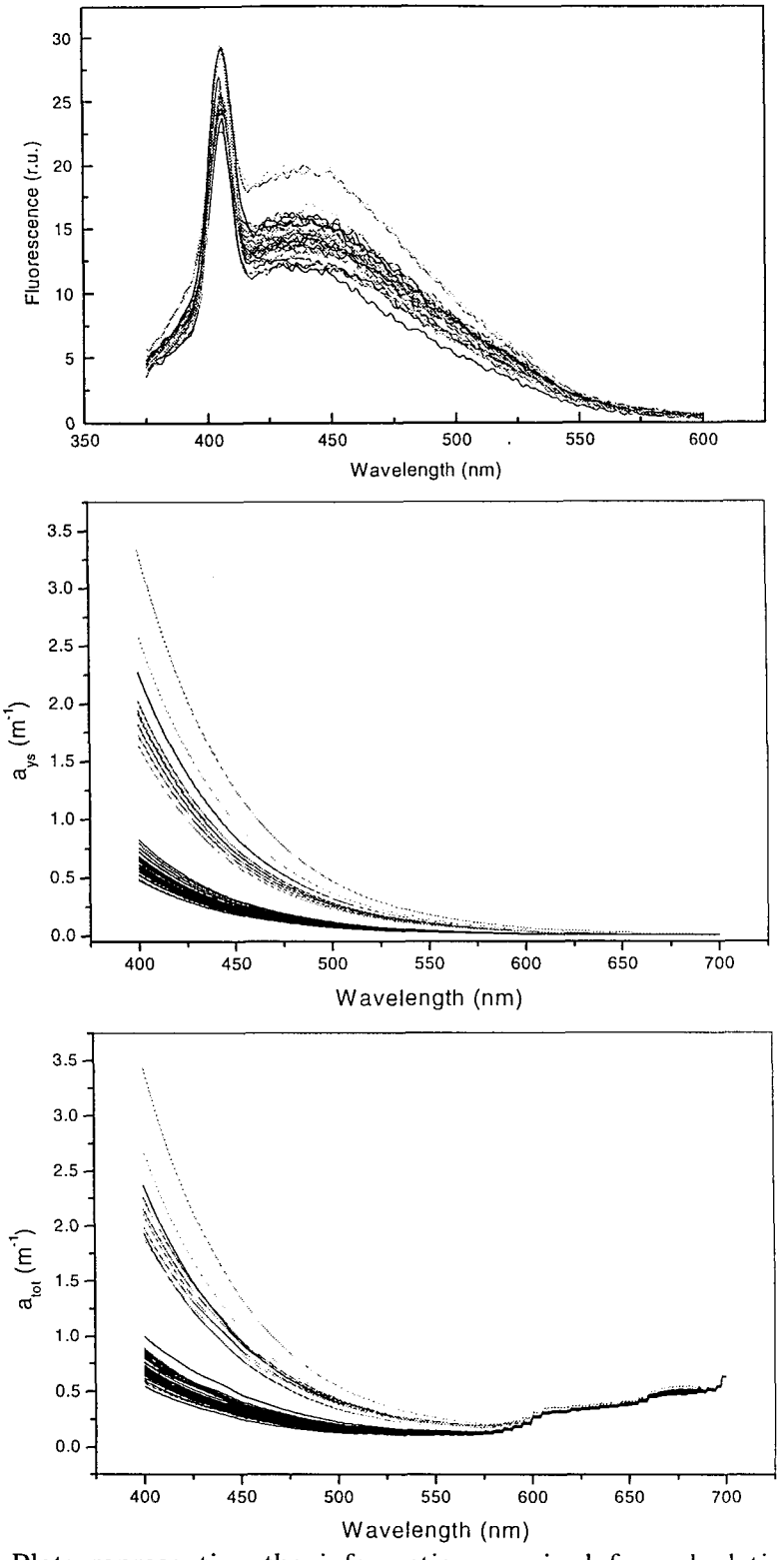

Figure 4.2: Plots representing the information required for calculating the SSF of yellow substance. The emission spectra (top) which gives the information required on the gaussian emission curve, and the yellow substance (middle) and total absorption (bottom) for calculations of the absorbed energy budgets in the excitation and emission ranges.

The lognormal emission curve used for the CDOM fluorescence is replaced by a Gaussian emission curve where λ_0 is 685nm, σ is 10.6 (as given by Gordon 1979). The excitation wavelengths over which the integration is made is between 370 and 690nm, using phytoplankton pigment spectra (a_{ph}) as shown in figure 2.4. The quantum yield of fluorescence for chlorophyll is the most critical aspect of the model parameterisation because of its large variability in the field. Carder and Steward (1986) observed values ranging from 1 to 10%. For the purpose of this study a value of 5% (0.05) was chosen assuming that it would be more representative of eutrophic water bodies.

4.2.2.3. Modelling of Phycoerythrin fluorescence

The SSF of Phycoerythrin pigment has recently been the focus of several studies showing a clear signal in their upwelling radiometric spectra in the 580nm region (eg. Culver and Perry 1994). Also, discrepancies at this wavelength between bio-optical models and observations could be attributed to phycoerythrin fluorescence (eg. Lee et. al. 1994). Therefore, the modelling of this process, particularly in a region where this pigment is quite abundant, would be a useful contribution to increase the accuracy of bio-optical models.

The SSF of phycoerythrin is modelled following a similar formulation for the determination of the reflectance as that for the other two fluorescent components previously described:

$$R_{fphyc} = \frac{1}{2}\int_{\lambda x} \Phi_{fphyc}(\lambda_x)\frac{\lambda_x}{\lambda}\frac{a_{phyc}(\lambda_x)E_d(0^-,\lambda_x)}{[2a_{tot}(\lambda)+a_{tot}(\lambda_x)]E_d(0^-,\lambda)}\frac{\exp\left[-\left(\frac{\lambda-\lambda_0}{2\sigma^2}\right)^2\right]}{A}d\lambda_x \quad (4.11)$$

As with chlorophyll, the emission curve for the fluorescence is represented by a Gaussian curve with a centre wavelength λ_0 at 585nm and shape factor σ of 16 as retrieved by fitting to published spectra (Lazzara et. al. 1996). The equation is integrated over the wavelength of phycoerythrin excitation, i.e. 450-550nm according

to Itturiaga (1990). Additional information on the absorption coefficient of phycoerythrin was not available in the ULISSE dataset.

Therefore, such a coefficient was approximated through a pigment deconvolution method of in-vivo absorption spectra (Hoepffner and Sathyendranath 1991), using pigment specific absorption spectra of chlorophyll "a", chlorophyll "b", chlorophyll "c" and carotenoids from Hoepffner and Sathyendranath (1994) and phycobiliproteins from Bidigare et. al. (1990), together with the in-vivo absorption spectra for phytoplankton shown in figure 2.4. The specific absorption spectra are shown in figure 4.3a. Only Phycoerythrobilin (PEB) was used in the present investigations as it is known to be typical of eutrophic water bodies. However, if the same investigation were to be carried out in oligotrophic oceanic waters then PUB would be used. The five wavelengths corresponding to the peaks of the specific absorption spectra of the five pigments were selected and a set of simultaneous equations such as those shown below were evaluated to obtain the concentrations of each of the pigments considered:

$$
\begin{aligned}
a_{ph}(412) &= C_a a_a^*(412) + C_b a_b^*(412) + C_c a_c^*(412) + C_{car} a_{car}^*(412) + C_{phyc} a_{phyc}^*(412) \\
a_{ph}(443) &= C_a a_a^*(443) + C_b a_b^*(443) + C_c a_c^*(443) + C_{car} a_{car}^*(443) + C_{phyc} a_{phyc}^*(443) \\
a_{ph}(490) &= C_a a_a^*(490) + C_b a_b^*(490) + C_c a_c^*(490) + C_{car} a_{car}^*(490) + C_{phyc} a_{phyc}^*(490) \quad (4.12) \\
a_{ph}(520) &= C_a a_a^*(520) + C_b a_b^*(520) + C_c a_c^*(520) + C_{car} a_{car}^*(520) + C_{phyc} a_{phyc}^*(520) \\
a_{ph}(565) &= C_a a_a^*(565) + C_b a_b^*(565) + C_c a_c^*(565) + C_{car} a_{car}^*(565) + C_{phyc} a_{phyc}^*(565)
\end{aligned}
$$

where the values C_i correspond to the concentration of each of the pigments and a^*_i are the specific absorption values of the equivalent pigments. Although the retrieved concentrations of phycoerythrin can not be compared to in-situ values, the accuracy of the technique can be evaluated by comparing the retrieved chlorophyll "a" concentration against that measured, as shown in figure 4.3b. Once the phycoerythrin concentrations have been estimated, which incidentally are rather high for marine waters (ranging form 0.2 to 4mg/m^3) but more similar to values found in lakes (underlining the Baltic's special character), the specific absorption spectra for phycoerythrin can be used to compute the phycoerythrin absorption coefficients, shown in figure 4.3c.

a)

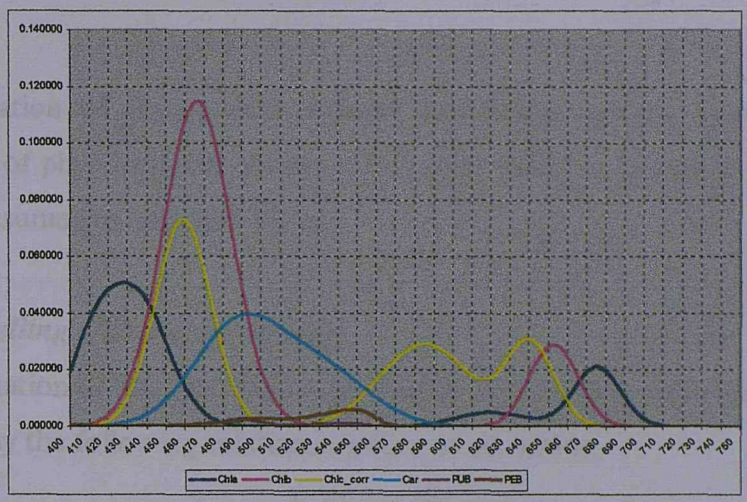

b)

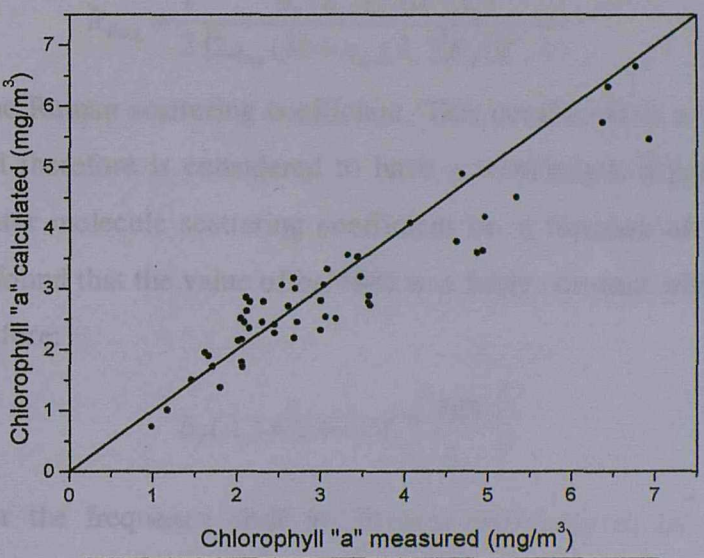

c)

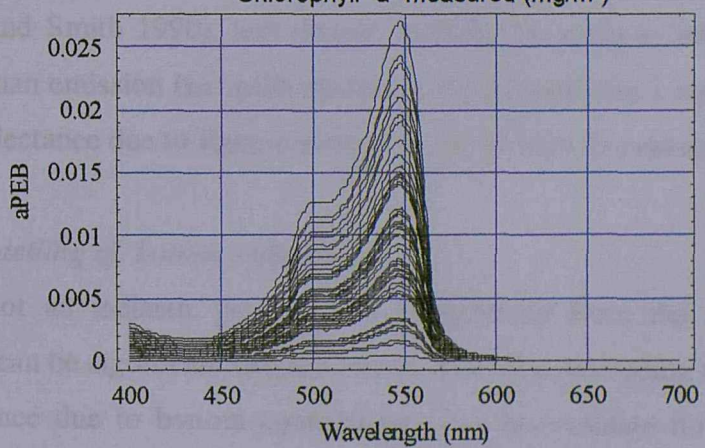

Figure 4.3: These plots show the specific absorption spectra used to solve the simultaneous equations (figure 4.3a), the relationship between measured and calculated chlorophyll "a" concentration (figure 4.3b) and the reconstruct phycoerythrin pigment absorption (figure 4.3c).

The computation of R_{fPHYC} still requires knowledge on the quantum yield for fluorescence of phycoerythrin. As no values were found in literature, an initial value of 1% was assumed to calculate R_{fPHYC}.

4.2.2.4. Modelling of Raman Scattering

The determination of the contribution by Raman Scattering is relatively simple and is represented by the following relationship (Lee et. al. 1994):

$$R_{Ram} = \frac{1}{2} \frac{b_R(\lambda_x) E_d(0^-, \lambda_x)}{[2a_{tot}(\lambda) + a_{tot}(\lambda_x)] E_d(0^-, \lambda)} \tag{4.13}$$

where b_R is the Raman scattering coefficient. This coefficient is a type of molecular scattering, and therefore is considered to have a wavelength dependency similar to that of the water molecule scattering coefficient i.e. a function of λ^{-4}. Marshall and Smith (1990) found that the value of $b_R(488)$ was fairly constant with a value of 2.6E-4m^{-1} and therefore:

$$b_R(\lambda_x) = 2.6 \times 10^{-4} \left(\frac{488}{\lambda_x} \right)^4 \tag{4.14}$$

If we consider the frequency shift for Raman Scattering to be fixed at 3350m^{-1} (Marshall and Smith 1990), and do not consider the narrow bandwidth but assume narrow Raman emission (i.e. each excitation wavelength has 1 emission wavelength), then the reflectance due to Raman scattering can be simply evaluated.

4.2.2.5. Modelling of bottom reflectance

Although not an inelastic process, the contribution from the sea-bottom to total reflectance can be significant (Maritorena et. al.1994). According to Lee et. al. (1994), the reflectance due to bottom contributions can be evaluate through the following relationship.

$$R_{bot} = \rho \exp[-(K_d + \kappa)H] \tag{4.15}$$

This expression is very similar to that proposed by Philpot (1989) and Maritorena et. al. (1994), all broadly dependent on ρ the bottom albedo and H the water depth in m. The downwelling diffuse attenuation coefficient (K_d) and the radiance attenuation coefficient (κ) have to be determined. K_d is determined by the equation given by Kirk (1984) as follows

$$Kd = \frac{1}{\mu_0}\left[a^2 + (g_1\mu_0 - g_2)ab\right]^{\frac{1}{2}} \tag{4.16}$$

Here μ_0 is the cosine of the solar zenith angle refracted at the air water interface and g_1, g_2 are coefficients determining the relative contribution of scattering to vertical attenuation and Kirk gives as average values over the surface layer g_1=0.425 and g_2=0.190. κ is given by $a+b_b$ (as in Lee et. al. 1994). Values for H, the depth to the bottom, were given for each station in the ULISSE dataset. Note that the bottom depth ranged from more than 100m to less than 10m, therefore including values above and below the SeaWiFS bathymetric flag for possible contamination by bottom reflectance (i.e. 30m, McClain 1995). The values of ρ were taken from a sedimentological map for the Southern Baltic (Ignatius 1982) and the station positions were plotted on top of this. The albedos were considered to be spectrally constant for three categories, which were defined on the basis of the map (Ignatius 1982) whereas each corresponding albedo value was taken from literature. The categories defined were as follows *sand soft bottom* with a value of 0.3 (Spitzer and Dirks 1987) *sand and hard bottom* with a value of 0.2 (Jaquet et. al. 1997) and *muddy bottom* with a value of 0.06 (Spitzer and Dirks 1987).

4.3. Results

4.3.1. Proportional contribution of inelastic processes to modelled reflectance

The spectral distributions of in-elastic processes are evaluated for all of the stations of the ULISSE campaigns as described in chapter 3 to support the formulation of the reflectance model. The resulting spectra are shown in figure 4.4 with the top figure showing the spectral distribution of the elastically modelled reflectance (produced by the reflectance model presented in chapter 3). As apparent from the other five plots,

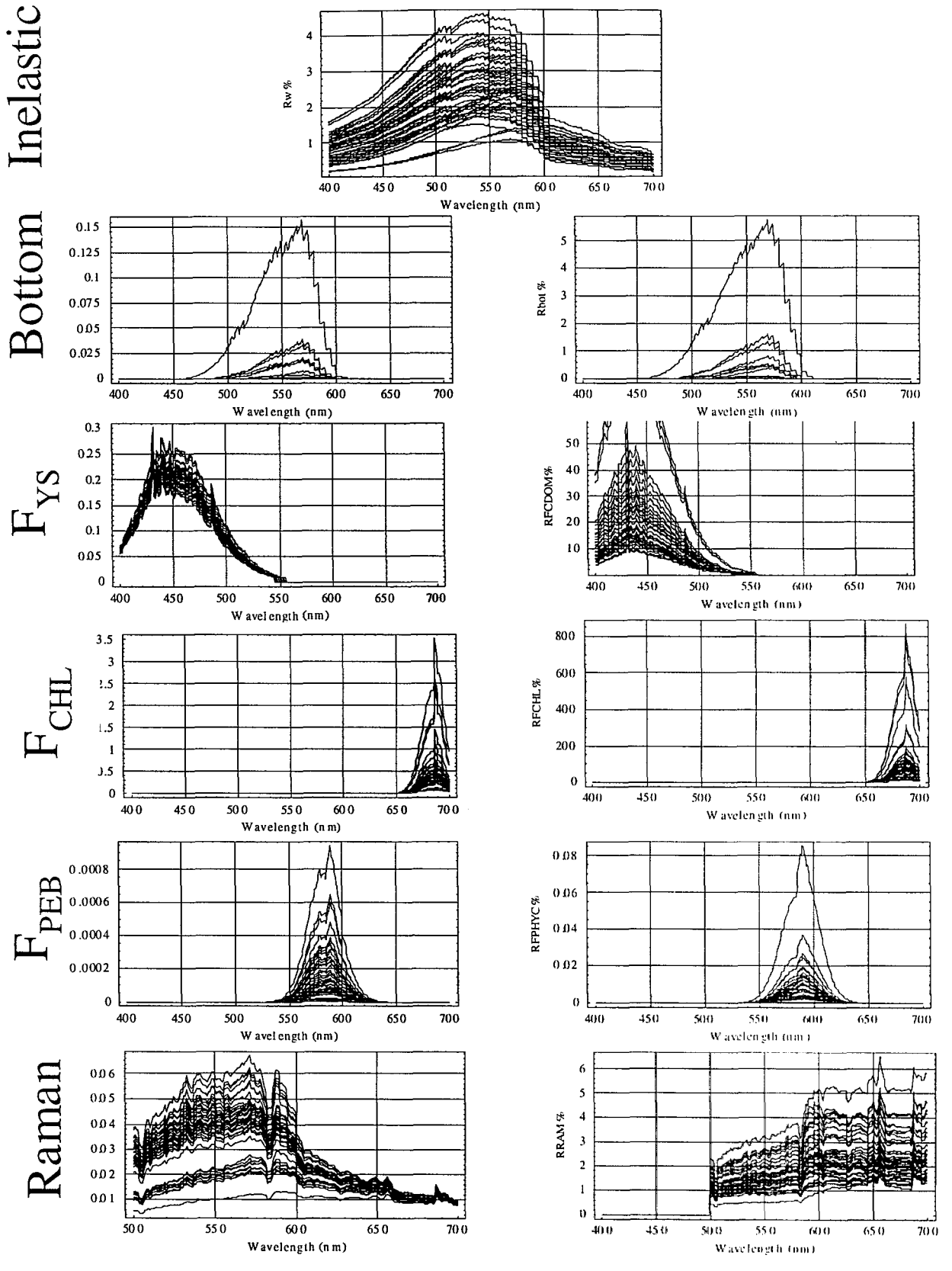

Figure 4.4: Plot illustrating the results from all of the calculations of the in-elastic processes. The elastic model reflectance is given at the top, of the two lower columns the left hand column represents the modeled reflectance and the right hand column represents the latter as a proportion of the elastic signal.

the spectral distribution of each in-elastic component is quite diverse, in terms of position within the spectrum and span over different ranges of wavelengths. It is clear that these additional in-elastic processes affect the full spectrum. Only a limited number of the evaluated spectra show a significant signal due to bottom reflectance (<10 spectra in figure 4.4). The spectral region influenced by sea-bottom signal is between 500 to 600nm with a peak at 570nm, coinciding with the lowest values of total absorption coefficient. The contribution by CDOM fluorescence to the irradiance reflectance is shown in figure 4.4. Most of the CDOM influence is in the range 400 to 550nm with a peak around 450-460nm. Comparatively, chlorophyll "a" fluorescence exhibits a much narrower area of influence than R_{FCDOM}, between 650 and 700nm with a peak at 685nm. The contribution to reflectance from phycoerythrin fluorescence occurs in the range 540 to 630nm with a peak at 585nm and is shown to affect an area of about 80nm. Finally the reflectance spectra resulting from Raman scattering is shown in figure 4.4. This contribution was considered in the present study in the range 500 to 700nm as literature commonly quotes this as the range in which it is of major influence to the AOP of the water column (e.g. Mobley 1994, McClain 1994). The influence due to Raman scattering spans a broad band in the range 500 to 700nm with a peak at around 580nm, (close to that of bottom reflectance).

To be able to put the individual contributions by each of the processes in the context of their potential contamination of the elastic signal, they were each plotted as a proportion of the modelled reflectance (due to elastic processes) shown in figure 4.4a. The resulting spectra are plotted in the right hand column of figure 4.4 and are each represented as the spectral distribution of the percentage proportion of the elastic reflectance. The first spectra, in figure 4.4, shows the percentage proportion of bottom reflectance with respect to the elastic reflectance. It can be seen that of the spectra that show any signal whatsoever the highest contributor consists of around 5% of the elastic signal at the peak wavelength i.e. 570nm whereas the other spectra showing a signal are all inferior to 1.5% at the peak wavelength. The contribution from R_{FCDOM} to the total reflectance is shown in figure 4.6. It is seen that in the range 400 to

550nm, the effects of this component can be quite considerable; the contributions go from 10% to as high as 50% (for $a_{ys}(400)$ values of $1m^{-1}$) at the peak wavelength (440nm) and between 5 and 20% and 5 and 10% at 400 and 500nm respectively. The second fluorescent component chlorophyll shows an extremely large contribution as a proportion of the total processes in the red where reflectance is in general quite low. This is evidenced by several spectra showing more than 150% contribution at 685nm. The average range of values covered in the red part of the spectra varies from 20 to 100% at the peak wavelength 685nm and between 0 and 70% at 670nm.The last fluorescent contribution is that due to phycoerythrin. This process seems to have little influence as a proportion of the elastic signal as its main influence is at 585nm where the reflectance due to elastic processes is at its highest and therefore its influence at this wavelength is much less than 1%. The last process considered, Raman scattering, is shown in figure 4.4 as a product of its contribution to the reflectance, illustrating a non-negligible influence even in eutrophic waters such as those considered in the presented study, and varies between 0 2% at 500nm, and ~1.5 to 5% at 700nm with a constant increase between these two extremes.

4.3.2. Influence of in-elastic processes on calculated eigenvectors

In a second phase of the analysis, the effects of in-elastic processes on calculated characteristic vectors of diffuse reflectance and, thus, on satellite algorithms are investigated. This analysis is undertaken by looking at the new eigenvectors resulting from a Principal Component Analysis (PCA) applied to the reflectance datasets including both elastic and in-elastic processes and comparing them with the original vectors calculated exclusively from the elastic datasets (as in chapter 3). The results shown in figure 4.5 clearly indicate little change among the calculated eigenvectors. An exception to this is the case of chlorophyll "a" fluorescence, where the first vector remains unchanged, while the second and third vector are significantly different. This point underlines the importance of chlorophyll "a" fluorescence in the magnitude and information content of the reflectance in the red bands. Note that, even though YS fluorescence contributes up to 50% of the total signal in the blue part of the spectra, it

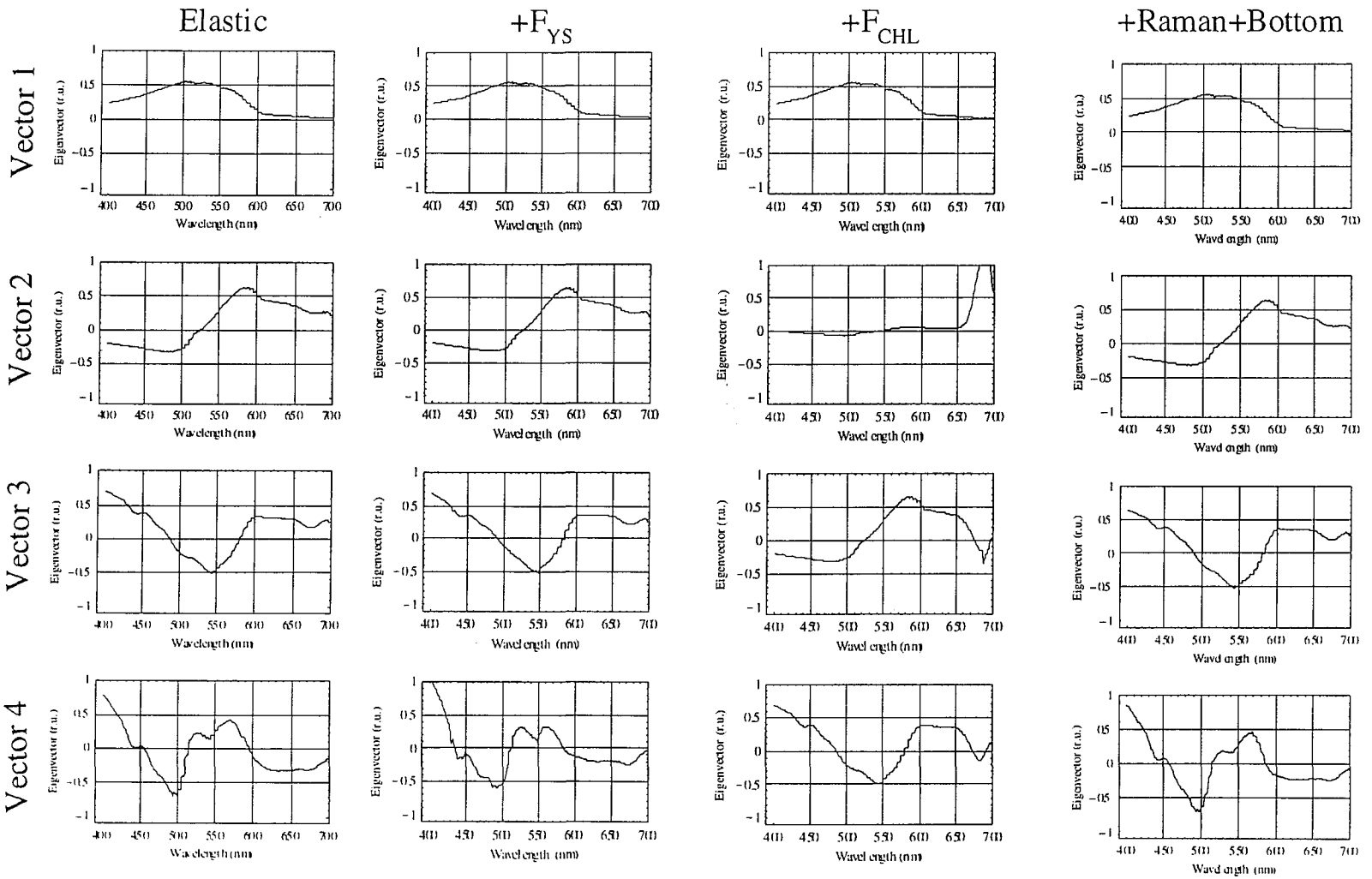

Figure 4.5: Plot showing the first four eigenvector of the datasets resulting from the elastic reflectance plus each of the inelastic processes having a significant contribution. From left to right there is elastic processes alone, then elastic+YS SSF, then elastic+ chlorophyll SSF and finally elastic+PEB SSF+Raman+Bottom reflectance. As can be seen only the chlorophyll fluorescence instance shows any significant impact on the shape of the resulting eigenvectors.

does not have significant impact on the eigenvectors, justifying the use of the algorithms developed in regions dominated by YS.

4.4. Discussion

4.4.1. The contribution of inelastic processes to absolute reflectance

The results presented in the current study have highlighted the importance of inelastic processes and bottom reflectance as additional processes adding to the reflectance caused by elastic processes i.e. absorption and scattering in the measured spectra. These results obviously have several significant implications in the context of various bio-optical topics. Firstly, these processes and in particular the fluorescence contributions may be found in in-situ measured reflectance, e.g. Culver and Perry 1994 observed the phycoerythrin fluorescence peak in reflectance spectra over a lake. If such reflectance spectra are used, as groundtruth to validate bio-optical models, then these processes should at least be acknowledged if not accounted for when the modelled and measured data are compared. Additionally these processes, and in particular the fluorescence emission, are well evident in the hyperspectral radiometric measurements (i.e. 1nm resolution) but are not always so apparent in submersible radiometers which typically measure in specific bands (normally coinciding with those of a satellite sensor). In these cases the contribution may still be significant, even if not so apparent, to the measured reflectance and therefore good knowledge of the full spectral range of influence of each of the inelastic components is needed when processing the radiometric data.

Apart from their influence on in-situ radiometry inelastic processes also have a significant impact on satellite measured reflectances. For example, if we consider the traditional blue:green reflectance ratio then an influence from YS fluorescence in the blue would anomalously raise the value at 443 thus giving an erroneously low value of chlorophyll which is sometimes the case in the Southern Baltic. This same contamination still occurs, if not so strongly, for the choice of the new ratio for chlorophyll estimation i.e. 490:550 (SeaWiFS tech Note Aiken, SEABAM dataset) which is still well within the CDOM fluorescence emission curve. The wavelengths

associated with chlorophyll "a" fluorescence are not used so often in band ratio algorithms and therefore should not be less significant. The spectral region potentially effected by phycoerythrin fluorescence fortunately does not coincide with any of the wavelengths sampled by current ocean colour sensors (except on the very tails of the emission curve), so that the only indication of phycoerythrin to the ocean colour signal will come through its influence on the absorption.

It should also be considered that in the future, as atmospheric correction schemes become more advanced, a new generation of algorithms and models will be developed dealing not with ratios but with absolute reflectance. In this context it will obviously be imperative to have a confident estimate of possible contamination of the elastic signal by the inelastic processes, perhaps through a sophisticated system of flags set up to alert the processing chain when there is a possibility of contamination.

Finally a few words should also be spent on the contribution from bottom reflectance as mentioned in section 4.3. Only a few of the spectra gave any signal whatsoever and these were minimal contributions themselves, due to the very high attenuation. However those stations which showed a signal all had a water depth shallower than 30m metres defined by NASA (McClain 1995) as the flag for possible contribution by bottom reflectance. Therefore the results obtained in the present study confirm the adequacy of this flag in highlighting water potentially affected by some bottom effect, even in a high attenuation Case II water with minimal bottom contribution as those studied here.

4.4.2. The importance of the in-elastic processes in the PCA inversion procedure

A fundamental reason for undertaking the presented work was to evaluate the possible sources of unconsidered contribution to the elastic reflectance using the model presented in chapter 3. The end would be to analyse in particular the effect of adding products of these processes to the modelled reflectance to see how these additional processes affect the inversion procedure through the modification of the eigenvectors. The results from this analysis have demonstrated that many of the in-elastic processes have little absolute contribution and therefore show no or little contribution to the

eigenvectors either. The main reason for this is the very high attenuation present in Case II waters through high coefficients of absorption. Within such conditions, therefore, processes such as Raman scattering or bottom reflectance show no significant influence to the information content of the spectra.

The phycoerytherin SSF also show no significant impact on the computed eigenvector and represents a very small contribution. On the other hand, the levels of CDOM present in the Baltic waters considered are very high with optical properties closer to those found in lakes by Spitzer and Dirks (1985) than to the marine environment (Hawes et. al. 1992, Vodacek 1995). Yet YS SSF shows little or no variation in the computed eigenvectors. This result was not expected, when considering that the contribution to the elastic reflectance by adding YS SSF was in some cases as high as 50% at 450nm. The only possible explanation for this is that the emission curve is so broad that it eliminates any major change in the eigenvectors which are sensitive to more abrupt changes. However, looking at the following relationship:

$$FSi_1^n = \sum_{\lambda\min}^{\lambda\max} R_{n\lambda} Ui_{n\lambda} \tag{4.17}$$

it is clear that a change in R, due to YS SSF in the blue region, would possibly affect the value of the FS as well. To verify this a test was made with the ULISSE dataset. The FS values were calculated from the elastic reflectance model, and the eigenvectors were then compared with those from a dataset derived from the same model with the addition of YS SSF. The first four eigenvectors considered were those used in the algorithm development procedure. The results figure 4.6 show that the YS SSF has a negligible influence on the calculated factor score, with a maximum of 7% difference for the fourth eigenvector (which only contributes 5% to the total variance).

The sensitivity of the eigenvectors to abrupt changes is well evidenced when dealing with the SSF by chlorophyll "a". For this contribution the resulting eigenvectors (apart from the first) resulting from the calculation with the addition of R_{FCHL} are shown to be significantly different from those resulting from the elastic dataset. Note however that the eigenvectors were calculated for the full 1nm spectra showing a peak

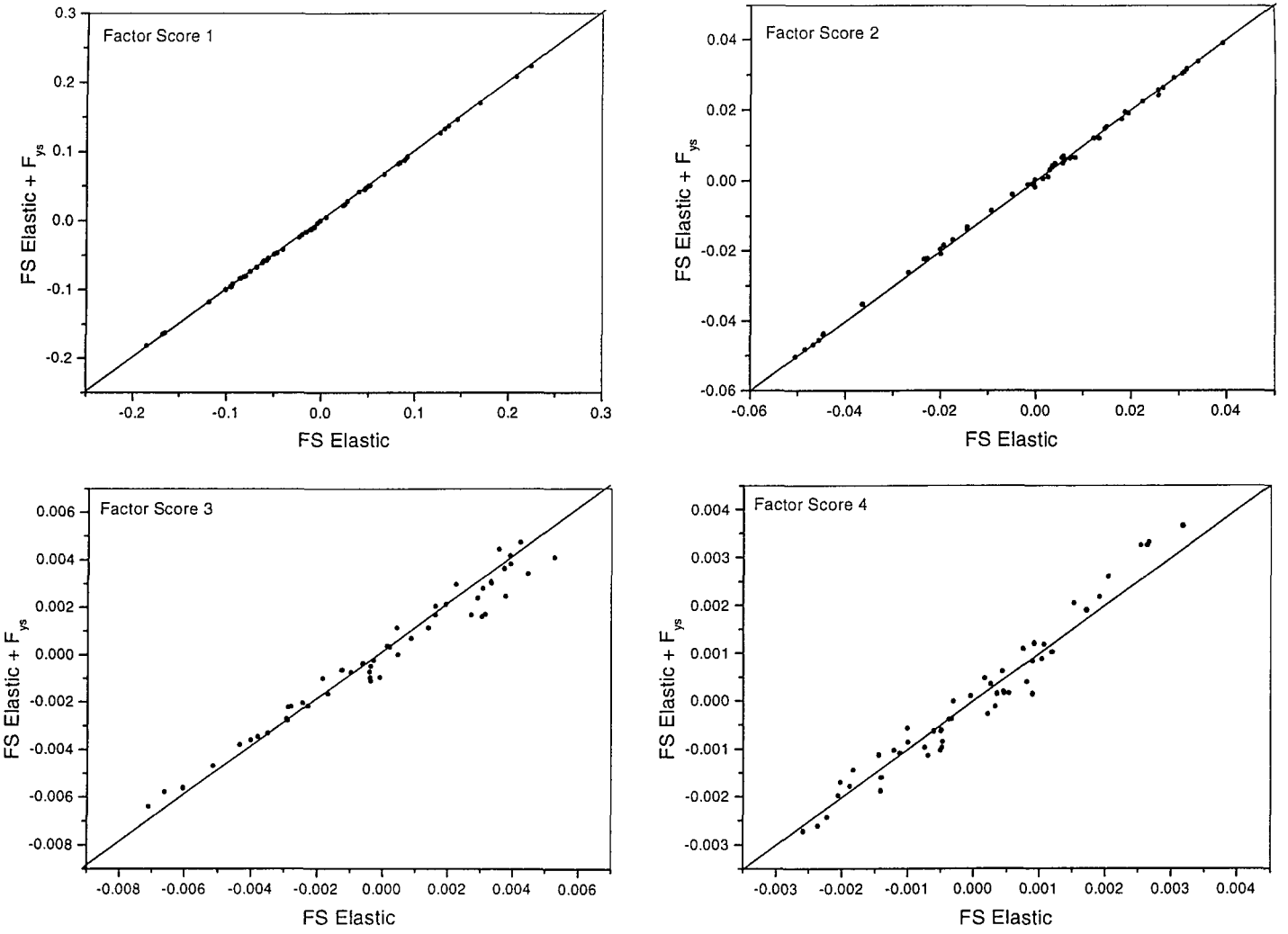

Figure 4.6: Graphs showing the relationship between the factor scores calculated for a dataset of only elastic reflectance against a dataset of elastic reflectance + fluorescence due to CDOM. Little difference is seen between the two situations for the first four eigenvectors.

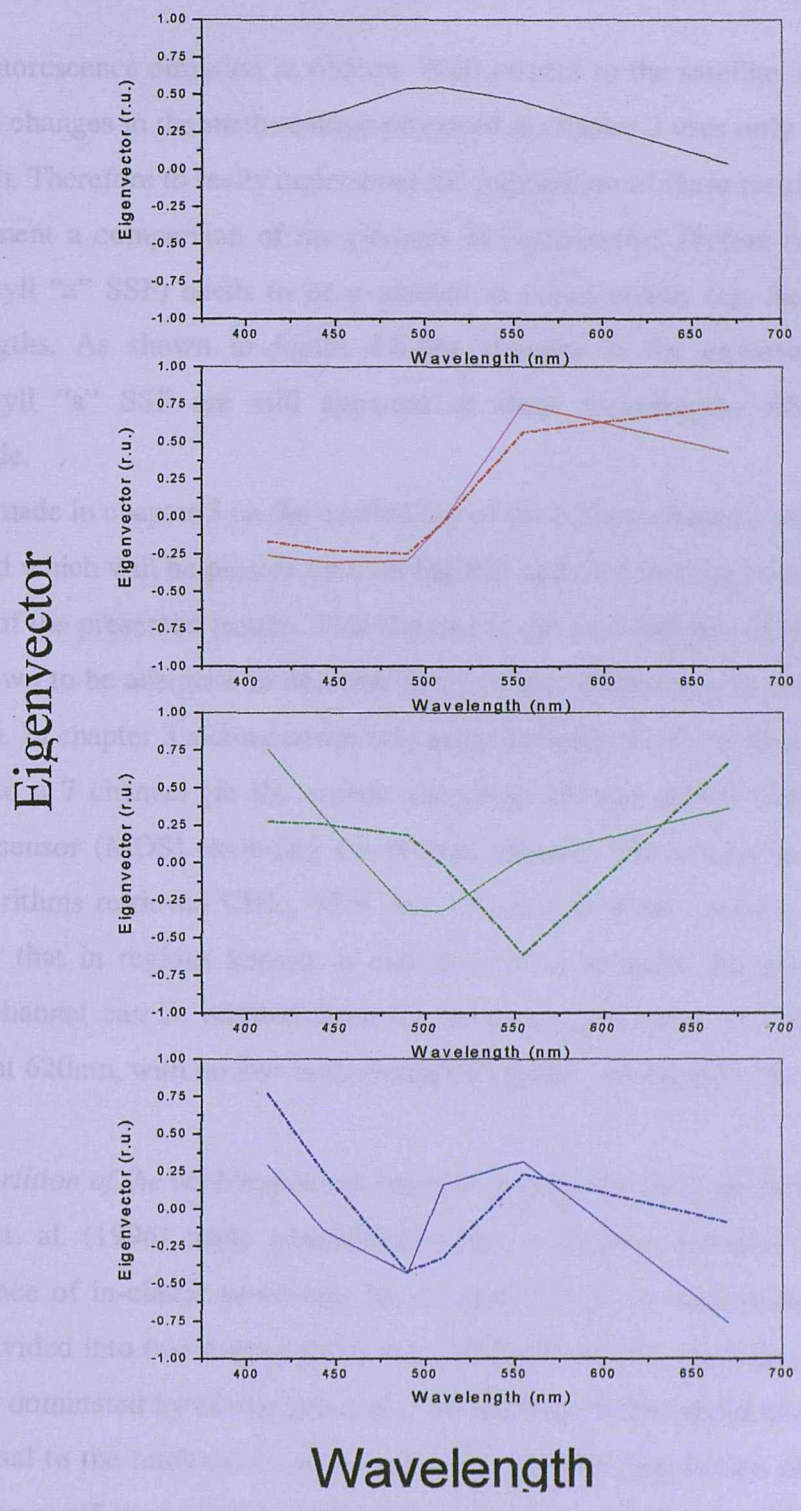

Figure 4.7: Plot showing a comparison of the first four eigenvectors resulting from the elastic reflectance dataset (full line) and those from the dataset with the addition of chlorophyll fluorescence (dotted line) at SeaWiFS wavelengths. As can be seen whilst the difference is not as significant as in the 1nm vector there exists however a difference which would have impact of PCA based retrieval algorithms.

of the fluorescence emission at 685nm. With respect to the satellite applications, the potential changes in the methodology proposed in chapter 3 uses only wavelengths up to 670nm. Therefore to really understand the implication of these results for algorithm development a comparison of the changes in eigenvectors (before and after adding chlorophyll "a" SSF) needs to be evaluated at ocean colour (eg. SeaWiFS, OCTS) wavelengths. As shown in figure 4.6 the changes in the eigenvectors from the chlorophyll "a" SSF are still apparent at these wavelengths albeit reduced in magnitude.

A point made in chapter 3 on the availability of the 620nm channel, which is found on MOS and which will be present on both MERIS and GLI becomes extremely relevant in view of the presented results. This channel in the near red part of the spectrum has been shown to be adequate to describe much of the information in the red part of the spectrum. In chapter 3 a comparison was made between the PCA inversion procedure applied to a 7 channel (in the visible excluding 685nm) sensor (MERIS) with a 6 channel sensor (MOS) excluding the 660nm channel. The results indicated that the two algorithms retrieved CHL, TSM and YS with identical correlation coefficients, implying that in regions known to exhibit high chlorophyll fluorescence the 660-670nm channel can be omitted from the inversion procedure so long as there is a channel at 620nm, with no loss in the retrieval capacity of the algorithm.

4.4.3. Partition of the visible spectral range by elastic and inelastic processes

Haltrin et. al. (1996) made several important concluding remarks on the spectral significance of in-elastic processes. He concluded that the underwater light spectra can be divided into two main parts; a red part dominated by inelastic processes and a blue part dominated by elastic processes. He defines the threshold of this division as being equal to the minimum wavelength in the spectral distribution of the irradiance attenuation coefficient plus one half of a Raman shift wavelength (~35nm) and shows (his Figure 3) that as the chlorophyll concentration increases so this divide gets pushed further into the red. Haltrin's results were based on theoretical computations over a large chlorophyll range and therefore it would be interesting to verify the

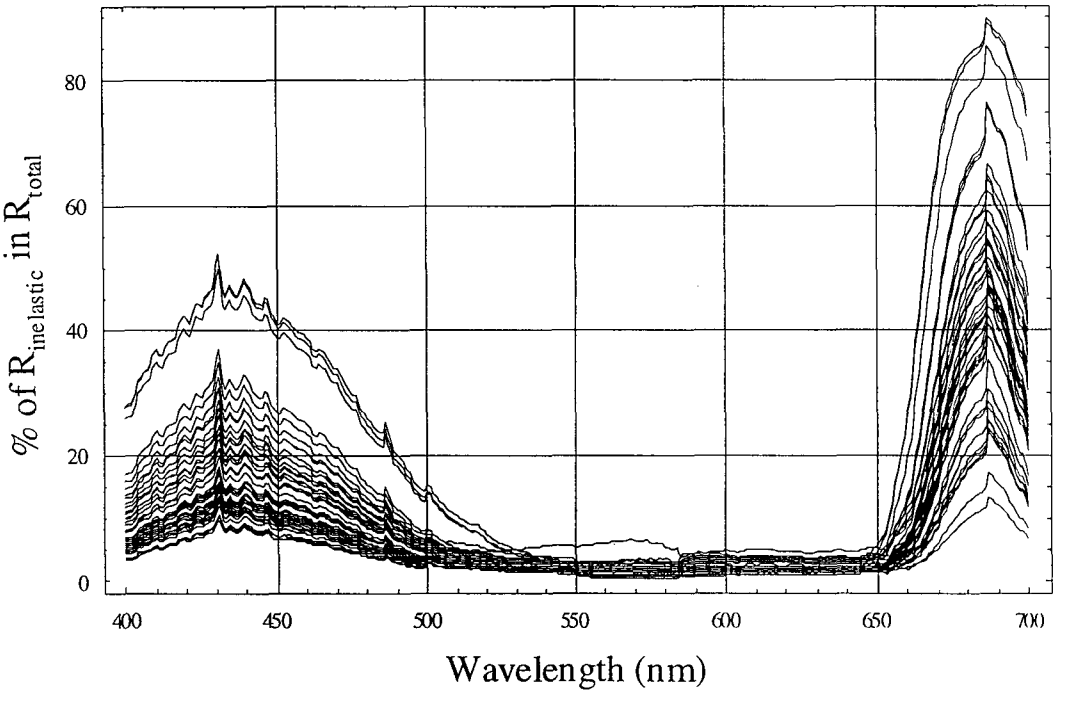

Figure 4.8: Plot showing the proportion of inelastic processes to the total signal in the visible wavelength range as a proportion the elastic signal. As can be seen the present case shows a strong signal from the yellow substance fluorescence but apart from this the in-elastic signal is restricted to wavelength higher than 650nm.

validity of these hypotheses in a pure Case II situation. To accomplish this the proportion of all of the inelastic processes (summed together) as a portion of the total (elastic+inelastic) is plotted in figure 4.7. As can be seen the divide between the elastic and inelastic processes is pushed high into the red as the attenuation coefficient for the region considered the effect of the Raman scattering is minimal and the major contributor is R_{fchl}. Figure 4.7 shows the important influence of R_{fys} in the region considered which may be the case in many other large estuaries or areas influenced by high river runoff. Whereas Haltrin (1996) concluded that the order of importance of inelastic processes was Raman scattering followed by Chlorophyll and then CDOM, if one were to make the same list for the type of Case II waters encountered in the present study then it would be Chlorophyll fluorescence followed by YS fluorescence and then Raman scattering and Phycoerythrin fluorescence. This would hold valid even in waters where the CDOM absorption coefficient was not as high as in the Southern Baltic, as the Raman scattering is eliminated with the high attenuation typical of Case II waters.

4.5. Conclusions

This study clearly demonstrates that the absolute reflectance in Case II waters is little affected by Raman scattering and bottom reflectance which have their highest emission in the green, coinciding with a minimum absorption (and therefore the highest signal from the elastic processes). The proportion of Raman scattering influencing the elastic processes increases toward the red part of the spectrum but remains beneath the 10% level.

With respect to fluorescing compounds, phycoerythrin fluorescence never contributed more than 1% in all cases considered, as its fluorescence emission peak corresponds to the reflectance maxima and therefore any effect should be dampened unless an exceptional (i.e. perhaps during a cyanobacteria bloom) event were in progress. Furthermore the fluorescent emission range does not correspond with any existing or planned ocean colour sensor channel, avoiding potential contamination of satellite derived radiances by this pigment. One could imagine a future hyperspectral sensor

with a high spatial resolution for use in lakes and estuaries specifically making use of this fluorescence signal in water quality assessments.

As for the contribution of both the SSF of YS and the SSF of chlorophyll "a" these effects are much more significant and affect the underwater light field in ranges that are particularly sensitive for remote sensing studies. The contribution of YS fluorescence in the blue was shown to be up to 50% of the elastically contributed reflectance in this range. The addition of this process could obviously be detrimental to traditional (and new 490:550) blue:green band ratios in these regions giving an erroneously low value of chlorophyll. However from the subsequent analysis with the computed eigenvectors it would seem that even at the high levels of YS fluorescence found in the area studied there is no significant impact of this processes on the computed eigenvectors. This is most probably due to the fact that the very broadband CDOM emission (150nm) caused a less represented variation in the eigenvector than much abrupter fluctuations. Furthermore a calculation of the effect of YS SSF on the calculated factor scores showed minimal influence thus confirming the use of methodologies just as those proposed in chapter 3 in YS dominated waters. Chlorophyll "a" fluorescence has by far the most significant effect on the reflectance in the red where it constitutes 150% of the elastic signal. Through the calculation of the eigenvector it is seen that chlorophyll also makes a significant impact on the eigenvectors of the reflectance spectra significantly changing all but the first vector.

It is proposed that this source of contamination should be avoided when developing algorithms based on information from the full spectrum (i.e. PCA type algorithms) by the use of satellite wavelengths only up to and including 620nm. This has been shown here to be feasible (Chapter 3) with no information loss in the produced algorithms. Alternatively a simple method should be developed through an initial estimation of the in-water constituent to estimate the contribution by chlorophyll fluorescence and thus correcting the water leaving radiances for the elastic signal.

The analysis of the cumulative contribution of the inelastic processes to the total irradiance reflectance in order to verify the conclusions made by Haltrin et. al. (1997), illustrated that in Case II waters with an extremely high attenuation coefficient the

threshold between elastic and inelastic processes still exists but is pushed right to the far red end of the spectra occurring at about 650nm (and therefore almost exclusively due to the contribution from chlorophyll fluorescence). Also in the particular waters studied (Southern Baltic) there is the obviously important contribution from the CDOM fluorescence which contradicts the assumption that the blue is dominated exclusively by elastic processes.

Finally the results presented in section 4.3 also included a first attempt at a model of the SSF of phycoerythrin. The results showed quite promising representation of the spectral distribution of the R_{FPHYC}. However, this was a qualitative approach intended to represent an indicative contribution from this process in marine waters; it may be significantly higher in lacustrine environments. Additionally there is no existing information on the quantum yield of fluorescence of this pigment in-vivo and the value used here of 1% (coinciding with the lowest quantum yields for chlorophyll) may be significantly higher than reality. However, it will be important in future studies to make more accurate estimates of this process, for example in the context of eutrophication and cyanobacteria bloom investigations. Thus further work needs to be undertaken to better define the QY of fluorescence and the redistribution function of this pigment's SSF.

Chapter 5

Retrieval of spectral absorption and multiple pigments from absolute reflectance: Direct Inversion Algorithm

Chapter 5 Table of Content

5.1. Introduction
5.2. Methodology and Results
5.2.1. Estimation of the backscattering coefficient
5.2.2. Calculation of the proportionality factor
5.2.3. Evaluation of the total absorption coefficient
5.2.4. Deconvolution of the absorption coefficient
5.2.5. Calculation of multiple pigment concentrations
5.3. Discussion
5.3.1. Parameterisation of b_{bTOT} - a generic algorithm for TSM
5.3.2. Determination of f and possibility of replacing with f/Q
5.3.3. Considerations on band position and number on pigment retrieval accuracy
5.3.4. Globalisation of the algorithm suite
5.3.5. Application of presented algorithm
5.3.5.1. Primary production
5.3.5.2. Chemotaxonomy
5.4. Conclusions

5.1. Introduction

So far, the methodology of using characteristic vector analysis in inversion algorithms of remotely sensed reflectance has concentrated on the use of the spectral information content of the individual optically active components to estimate the total reflectance. These considerations have been implemented through a reflectance model and the statistical inversion of the residuals of a very large reflectance dataset. Therefore the variance information in the algorithms accentuates the shape rather than magnitude of the spectral dataset.

In the past the scientific community has considered various algorithm development techniques as being acceptable (*cf.* Sathyendranath and Morel (1982) for a synopsis of these different approaches). These techniques encompass most of the algorithm types adopted during the research into CZCS data and include:

- ratio algorithms, both linear polynomial and of more complex nature such as three band ratios (e.g. Gordon and Morel 1983),
- Principal Component Analysis algorithms such as those presented in Chapter 3 (Gower et. al. 1986, Sathyendranath et. al. 1989)
- and curvature algorithms (Campbell and O'Reilly 1988, Hoge et. al. 1994).

The use of these algorithms in providing trustworthy basic products (i.e. Chlorophyll "a" or pigment concentration) is well accepted.

Several determining factors resulting both from theoretical developments in the field of bio-optics and the progression of the second generation of ocean colour sensors currently in orbit (SeaWiFS and MOS) and planned for the near future (MERIS and GLI) can lead to the conception of diverse algorithmic methods.

The new generation of satellite sensors have considerably improved: i) in the Signal to Noise Ratio (SNR) and ii) their spectral resolution both in the visible and near infrared. The higher number of channels in the infrared when compared to the CZCS sensor yield better atmospheric correction schemes. All of the above reasons motivated the National Aeronautical and Space Agency (NASA) to set 5% as the aim for the permitted error in retrieving water leaving radiances (L_w) for the recently launched SeaWiFS sensor. This error condition is prerequisite to the model presented

here which uses the absolute magnitudes of subsurface irradiance reflectance to evaluate the concentrations of the optically active components as well as the specific concentrations of multiple pigments including: Chlorophylls "a", "b" and "c", carotenoids and phycoerythrin.

Note that this error margin was determined in the context of Case I waters. For the purpose of methodologies developed for CaseII waters the standard atmospheric correction algorithm as developed by Gordon and Wang (1993) will be incapable of achieving the 5% accuracies required. Therefore an iteration scheme as recommended by Smith and Wilson (1981) or Bricaud and Morel (1987) to accurately separate the attenuation due to aerosol and that to hydrosol is adopted.

A fundamental aspect of the presented model is its use in retrieving multiple pigment concentrations. This result is obtained by using a modified technique based on a methodology presented by Hoepffner and Sathyendranath (1993) for de-convoluting total particulate absorption and retrieving pigment concentration. Hoepffner and Sathyendranath (1991) decomposed spectral of in-vivo phytoplankton absorption coefficients into components associated with the major photosynthetic pigments and computed *true* specific absorption coefficients of Chl a, b, c and carotenoids. Bidigare et. al. (1989) made a similar study deriving true specific absorption coefficient for the biliproteins (PUB and PEB). In both cases the authors show that these coefficients can be used to reconstruct the in-vivo absorption spectrum if the pigment concentrations are known. Hoepffner and Sathyendranath (1993) considered the inverse problem that involves using the true specific absorption coefficients to retrieve pigment concentrations from known phytoplankton absorption spectra. It is this inverse problem that is considered in this study with the sole exception that the phytoplankton absorption used to derive the concentrations is obtained by the inversion of irradiance reflectance either measured in-situ or derived from remotely sensed radiances.

A recent topic of interest in the field of pigment analysis is that of chemotaxonomy or the identification of phytoplankton classes (or better) on the basis of pigment information. If these classification techniques could therefore be ported to the scales and synopticity of a satellite sensor through the methodologies presented here then the

resulting products would imply differential biomass products covering all oceanic regions. These products would undoubtedly provide a huge source of applications, examples of which include the possibility of developing advanced productivity products subdividing into the different biomass classes, and the use of specific pigment products in studies of water quality and/or eutrophication in coastal waters.

5.2. Methodology and Results

The formulation of the system of equations used to retrieve the geophysical products presented in the introduction is based again (as is the model presented in chapter3) on the relationship between irradiance reflectance and the inherent optical properties absorption (a) and backscattering (b_b), so that:

$$R(\lambda) = f \times \frac{b_b(\lambda)}{\left(a(\lambda) + b_b(\lambda)\right)} \tag{5.1}$$

The basic objective of the model is to develop an algorithm/system of equations, which allows one to invert the measured subsurface reflectance from satellite or from in-situ sensor, to retrieve total absorption. The method then deconvolves the total absorption into the individual components: water (w), Coloured Dissolved Organic Matter (CDOM), detritus (d) and phytoplankton like pigments (ph). The final step involves the retrieval of pigment concentrations from the absorption coefficient of phytoplankton. The datasets used in parameterising the presented model are from various sources and include both Case I and Case II water types in an attempt to achieve a generic algorithm set applicable to all water types. These datasets include: the ULISSE datasets taken in the Baltic sea (Case II CDOM dominated waters), a dataset from the Northern Adriatic (CaseI/ CaseIIS water transition zone), a dataset from Tokyo Bay, and two Case I data sets from Glen Cota and the MOCE datasets. For the validation of the model the Baltic ULISSE data set was used as it is a more complete dataset for a very extreme environment and therefore a thorough test case for the model. The individual steps of the algorithm development are discussed in further detail below. The model here will be formulated for OCTS wavelengths (as it was developed in the context of the ADEOS PI project commented above). It is

however obvious that the inputs required for the initialisation of the model are reflectance in the first six channels of the OCTS sensor (i.e. 412, 443, 490, 520, 565, 670) and the sun zenith angle in air.

5.2.1. Estimation of the backscattering coefficient

The first step in the model involves the determination of the backscattering coefficient from the OCTS reflectance. The approach used for this involves the Kopelevich (1983) two component particulate backscattering model that is given by:

$$b_b(\lambda) = \tilde{b}_{bs} b_s(\lambda) + \tilde{b}_{bl} b_l(\lambda) \tag{5.2}$$

where

$$b_s(\lambda) = 1.34 v_s \left(\frac{550}{\lambda} \right)^{1.7} \tag{5.3}$$

and

$$b_l(\lambda) = 0.312 v_l \left(\frac{550}{\lambda} \right)^{0.3} \tag{5.4}$$

Further detail is given on this model in chapter 3. As can be seen the model is solely parameterised on the basis of v_s and v_l which are the volume of small particles and the volume of large particles respectively. In the original model Kopelevich (1983) defined the v_s and v_l coefficients as products of the small and large angles of the volume scattering phase function. Haltrin (1991) and Haltrin et. al. (1997) propose a empirically derived relationship between the concentrations of v_s and v_l with chlorophyll concentration based on experimental results. In chapter 3 of the current work the author presents a relationship between v_s and TSM and v_l and CHL based on both the work of Haltrin et. al.(1991, 1997) and on experimental results obtained from a dataset of VSFs for the Baltic and NE Atlantic (Gohs et. al. 1978). This relationship between v_s, v_l and TSM, CHL is the one used in the current model. For the determination of the required TSM and CHL concentration for parameterising the model, simple algorithms were used as a first estimate of chlorophyll concentration (operational SeaWiFS data processing algorithm for Case I waters).

$$CHL = 10^{0.341-3.001R+2.811R^2-2.041R^3} - 0.04 \quad (5.5)$$

where,

$$R = Log\left(\frac{Rrs490}{Rrs555}\right)$$

This is only considered as a first approximation as the contribution to b_{bTOT} of b_{bl} is fairly small compared to that due to b_{bs} in all but the most eutrophic/turbid waters. It is however much more significant that the concentration of TSM is accurately determined. There have been numerous studies presented using principal component analysis to investigate the information content of reflectance spectra (e.g. Gower et. al. 1985, Sathyendranath et. al. 1989, and chapter 3 of this thesis). These studies have always resulted in the conclusion that the easiest and most accurate component retrieved is TSM, which in general has retrieval accuracies better than 10%. Also TSM is in general very well correlated with the first eigenvector.

So as to verify the general application of a generic algorithm reflectance datasets resulting from various forward models were investigated. These models included the CaseIIY parameterised model presented in chapter 3 of this thesis, the model presented in Sathyendranath et. al. (1989) and also a CaseI model taken from Morel (1988). In each of these cases reflectance spectra were simulated using ranges suggested by each of the above authors. Figure 5.1a show the eigenvectors for each of the simulated datasets. As can be seen a prominent feature in all three cases is the decrease in the first eigenvector from the green to the red wavelengths. This may suggest therefore that a *sensitive-compensating* type algorithm as originally suggested by Tassan (1994) may be the best solution in formulating a generic algorithm for TSM. This was accomplished with the datasets mentioned above and the results are shown in figure 5.1b. The resulting algorithm shows to retrieve TSM concentration considered over the range considered with an r^2 of 0.96, the equation is given in 5.6, where it can be seen that the same band combinations as Tassan were adopted. However, as the presented algorithm is intended to be generic and therefore covers a very large range (4 orders of magnitude), a polynomial fit of the third degree was used

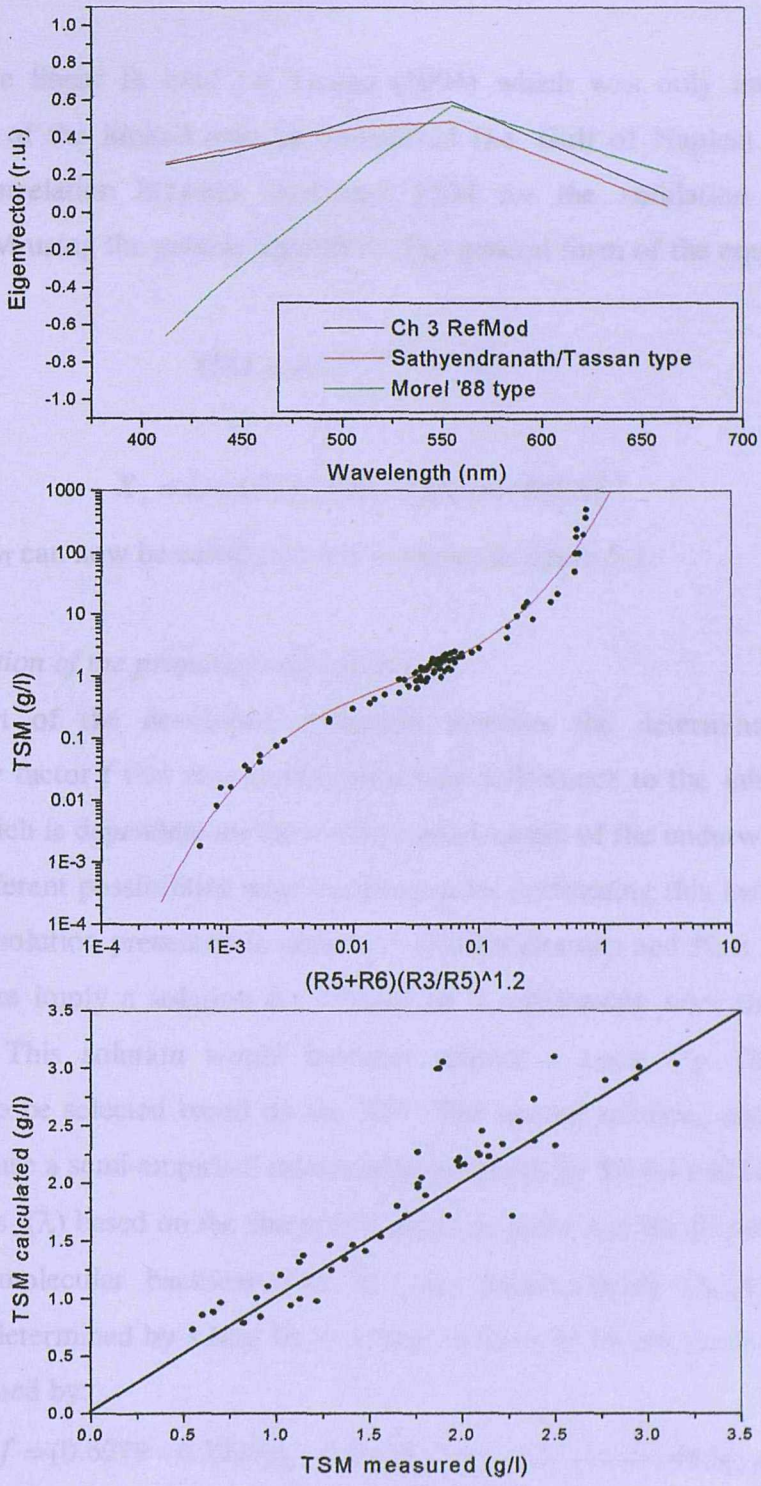

Figure 5.1: Plots showing a) the similarity between the first eigenvector for different modeled datasets particularly in the green to red wavelength range, b) the polynomial fit on a large dataset resulting from different models, the relationship between modeled and measured TSM concentration from the ULISSE datasets.

rather than the linear fit used by Tassan (1994) which was only intended to be representative of the limited area he considered (i.e. Gulf of Naples). Figure 5.1c shows the correlation between measured TSM for the validation dataset and calculated TSM using the generic algorithm. The general form of the equation used is given by,

$$TSM = 10^{2.81+3.67X_s+1.71X_s^2+0.34X_s^3} \tag{5.6}$$

where,

$$X_s = Log(R555+R670)(R490/R555)^{1.2}$$

Therefore b_{bTOT} can now be calculated and is shown in figure 5.2.

5.2.2. Calculation of the proportionality factor

The next part of the developed algorithm involves the determination of the proportionality factor f that relates the subsurface reflectance to the inherent optical properties, which is dependent on the bi-directional nature of the underwater radiance field. Two different possibilities were considered for performing this task: the first is the analytical solution presented in chapter 3 (Sathyendranath and Platt 1997) which would therefore imply a solution for f based on a relationship with the sun zenith angle in air. This solution would however require a Look Up Table of such relationships to be selected based on the VSF. The second solution, and in fact that selected, is to use a semi-empirical relationship proposed by Morel and Gentili (1991) which retrieves $f(\lambda)$ based on the sun zenith angle in water and the factor η_b which is the ratio of molecular backscattering to total backscattering (b_{bw}/b_{bTOT}). Their equation was determined by a best fit to a large number of Monte Carlo simulations, and is represented by:

$$f = (0.6279 - 0.2227\eta_b - 0.0513\eta_b^2) + (-0.3119 + 0.2465\eta_b)\mu_0 \tag{5.7}$$

In a more recent paper (Morel and Gentili 1993) the authors propose an updated expression, which also includes the single scattering albedo (ω). This improved expression was not used in the present investigation, as it would require information on the absorption coefficient that is not present at this stage of the formulation. Thus

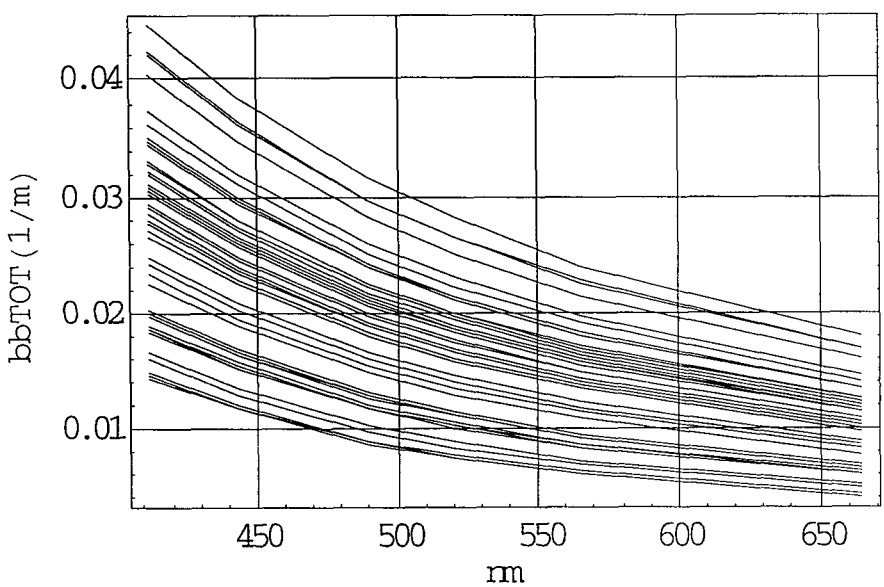

Figure 5.2: A plot showing the total backscattering coefficient derived using the Kopelevich model parameterized using satellite derived CHL (ranging from 0.3 and 7 mg/m^3) and TSM (ranging from 0.5 and 5 g/l).

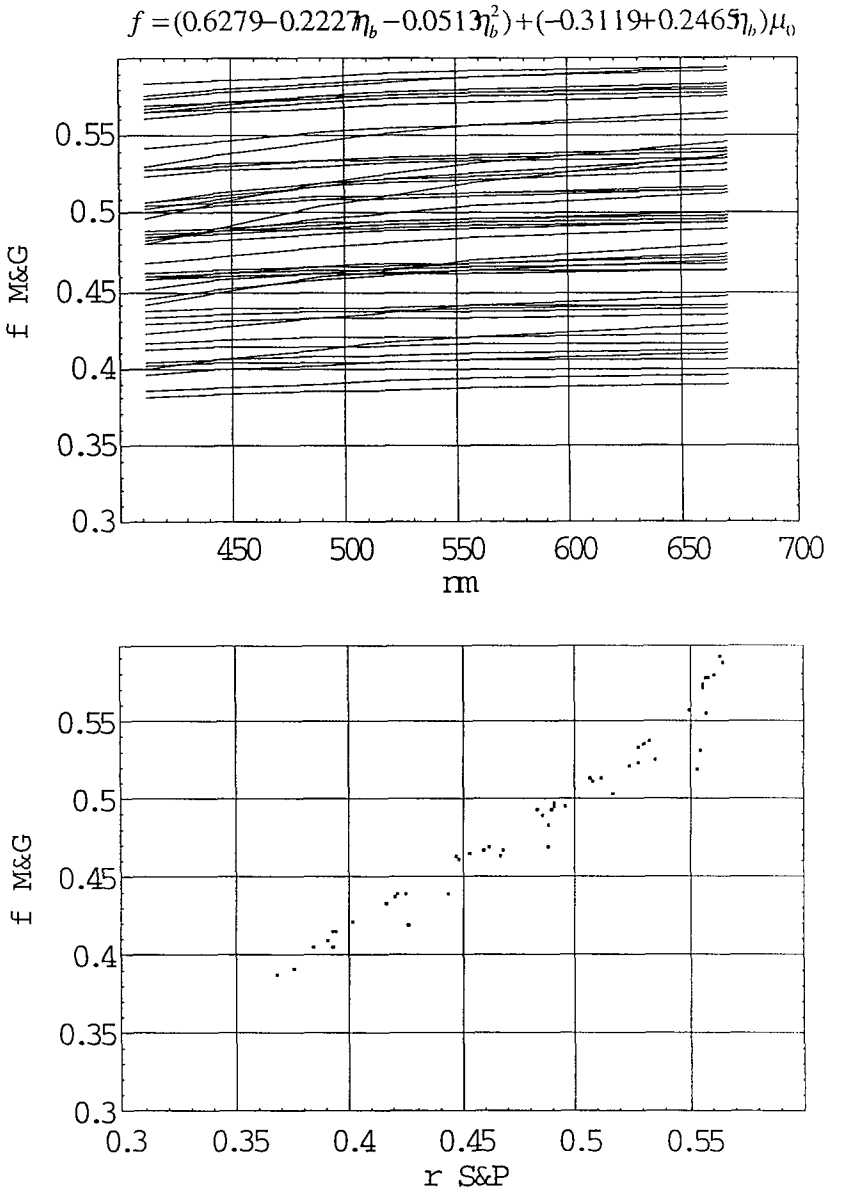

Figure 5.3: Graphs showing a) the spectral distribution of $f(\lambda)$ calculated from Morel and Gentili (1991), which shows that the proportionality factor is fairly spectrally constant. b) a plot showing the very positive relationship between f (550) calculated with Morel and Gentili (1991) (*M&G*) and the analytical solution obtained with Sathyendranath and Prieur (1997) (*S&P*).

equation 5.7 is used to evaluate *f*. Figure 5.3a shows the spectral values of *f* for the validation dataset illustrating almost no spectral signal in the *f* factor. Therefore, the value of *f* at 550nm will taken and used as a spectral constant for each reflectance spectra considered. Figure 5.3b shows the correlation between the values of *f* at 550nm evaluated using equation 5.7 against the value of *f* evaluated using the analytical solution of Sathyendranath and Platt (1997), and parameterised specifically with VSF information specific to the area in which the validation dataset was taken.

5.2.3. Evaluation of the total absorption coefficient

With the determination of b_{bTOT} and the proportionality factor *f* one can therefore rearrange equation 5.1 to retrieve the total absorption coefficient (a_{TOT}):

$$a_{tot}(\lambda) = a_{ph}(\lambda) + a_d(\lambda) + a_{ys}(\lambda) + a_w(\lambda) \qquad (5.8)$$

The calculated values of a_{TOT} for the validation dataset are given in figure 5.4 that can be seen to follow the known shape of an absorption coefficient. From this a_{TOT} spectra the constant values of the known water absorption can be simply subtracted (the values used are those taken from Pope and Fry (1997)) so that the remaining absorption is exclusively due to the in-water optically active substances a_{SUB}.

5.2.4. Deconvolution of the absorption coefficient

It is known that the spectral absorption values retrieved in 5.2.3. are due to the linear summation of the individual components contributing to the in-water absorption (see chapter 2). The individual contributions are given in equation 5.8, where a_{ph} is the absorption due to phytoplankton like pigments and a_d and a_{ys} are the absorption coefficient due to detritus and yellow substance respectively. Both of the latter absorption coefficients have been traditionally modelled spectrally as exponentially decaying absorption curves (with increasing wavelength). However as discussed in detail in chapter 2 an alternative model can be defined which better describes the spectral variance of the non-chlorophyllous contributions to absorption. The models selected in chapter 2 are based on eigenvectors resulting from factor analysis and are shown to adequately reproduce the spectral variance of various families of in-situ

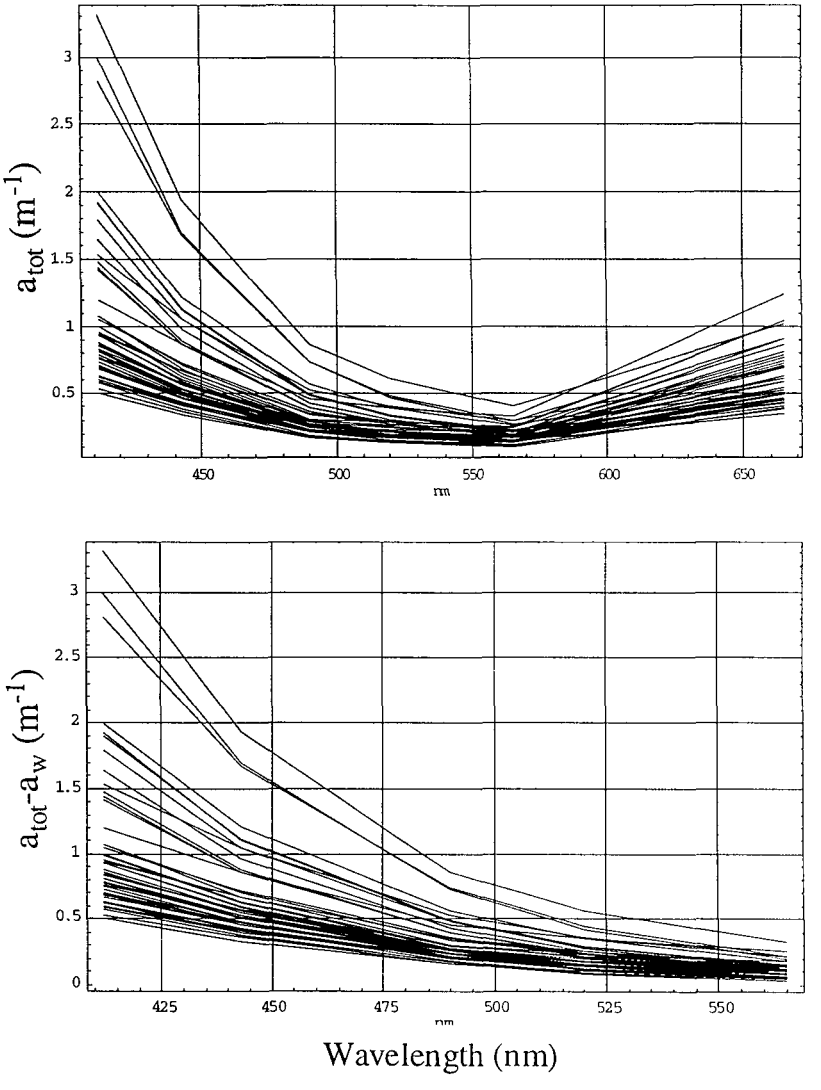

Figure 5.4: Plot showing the calculated spectra of the total absorption coefficient (top) from the knowledge of $R(\lambda)$, $b_{btot}(\lambda)$ and f, and the spectral distribution of the total substance absorption (bottom) having subtracted water for the first five wavelengths.

measured field spectra for detrital and yellow substance. Thus to satisfy the requirements of the present investigation i.e. the accurate deconvolution of the individual contributions to the total absorption, the method proposed in chapter two is adopted. Therefore the following series of equations are solved in order to retrieve pigment absorption.

$$a_s(\lambda) = \left(a_p^{*}675(\lambda)a_p(675)\right) + \left((a_y U_1(\lambda)a_y FS_2) + (a_y U_2(\lambda)a_y FS_2)\right) \quad (5.9)$$

and

$$a_p(\lambda) = \left(a_{ph}^{*}675(\lambda)a_{ph}(675)\right) + \left((a_d U_1(\lambda)a_d FS_2) + (a_d U_2(\lambda)a_d FS_2)\right) \quad (5.10)$$

By solving for the unknowns (i.e. ap675, Fsys1, Fsys2, aph675, Fsd1, Fsd2) the equations can be evaluated and the pigment can eventually be retrieved. The evaluation dataset was tested with the above procedure at various stages verifying the retrieved parameters with measured values for the same dataset. The eventual results of phytoplankton absorption coefficient at three wavelengths (443, 490,520) are shown in figures 5.5 which illustrates the measured against modelled coefficients.

5.2.5. Calculation of multiple pigment concentrations

Finally having deconvolved the absorption to the point where we now have phytoplankton pigment absorption (shown in figure 5.6a), one is at the stage where one can mathematically retrieve the pigment concentrations. This is performed quite simply by solving a set of simultaneous equations,

$$a_{ph}(\lambda) = \sum_{i=1}^{n} a_i^{*}(\lambda)C_i \quad (5.11)$$

where $a_i^{*}(\lambda)$ are the spectral values of the specific absorption coefficients at the wavelengths considered. C_i is the concentration of each of the pigments considered where i in the present study refer to the pigments: chlorophylls *a,b*, and *c*, carotenoids and phycoerytherin (represented by the symbols *a, b, c, car* and *phyc*). The specific absorptions used come principally from the work of Hoepffner and Sathyendranath

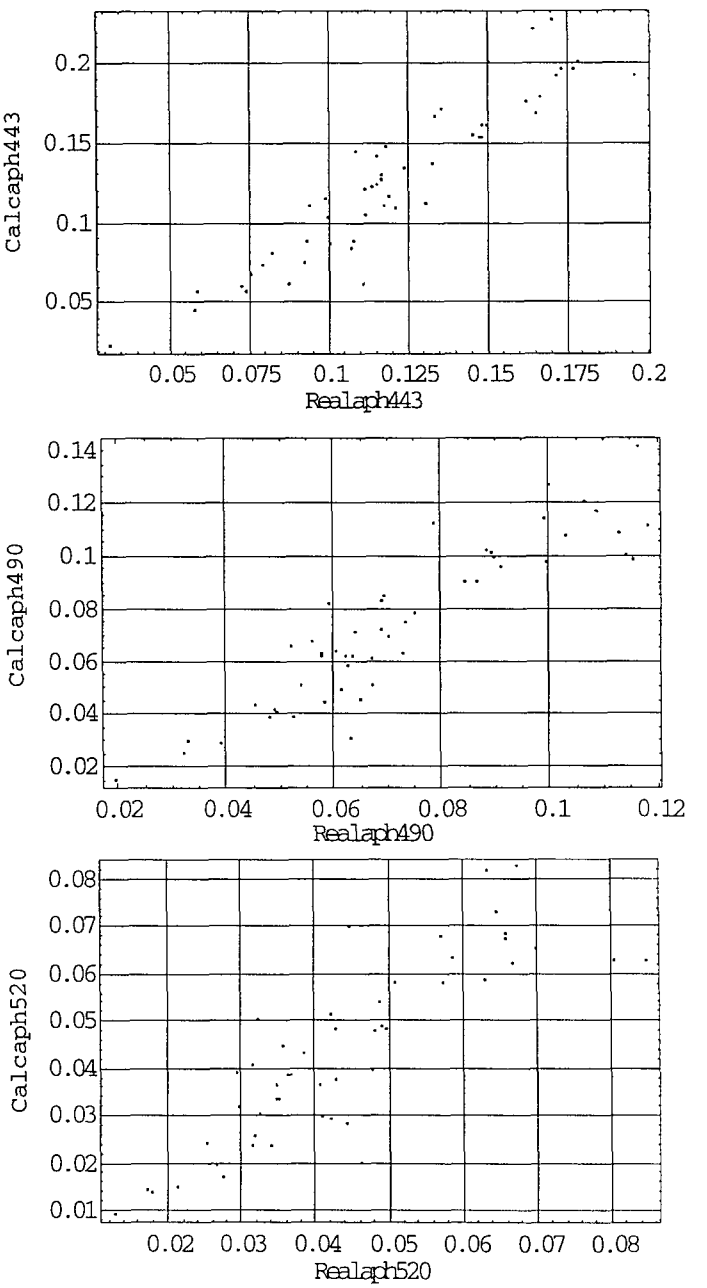

Figure 5.5: Graphs showing the calculated phytoplankton absorption coefficients resulting from the deconvolution process at three of the five wavelengths (443, 490, 520).

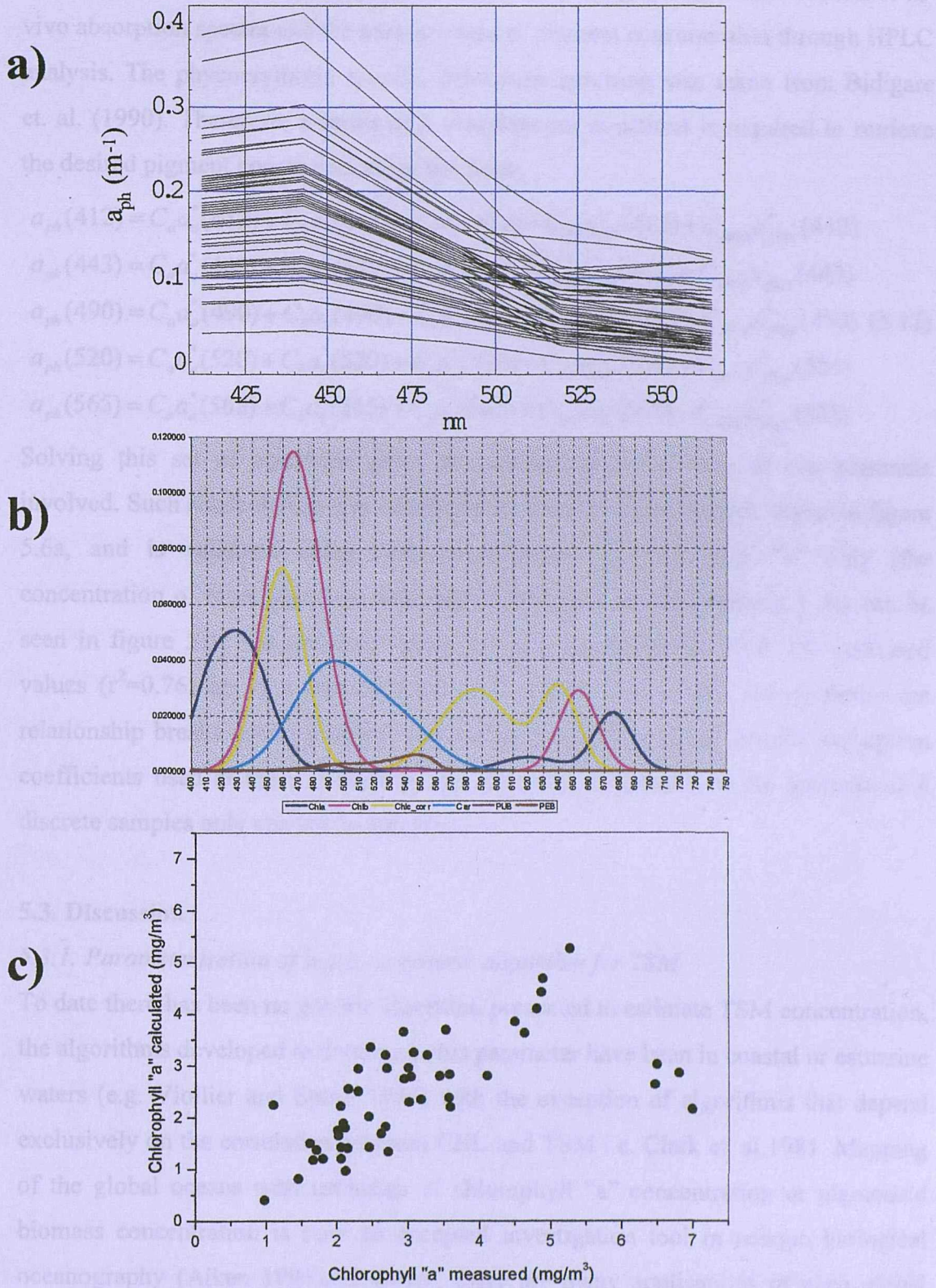

Figure 5.6: Plots showing a) modeled phytoplankton spectral absorption, b) the specific absorption coefficients of the individual pigments and c) Chlorophyll "a" calculated using the DIA.

(1993) (for *a, b, c* and *car*) and were obtained from the gaussian deconvolution of in-vivo absorption spectra and the measurement of pigment concentration through HPLC analysis. The phycoerytherin specific absorption spectrum was taken from Bidigare et. al. (1990). Therefore, a series of 5 simultaneous equations is required to retrieve the desired pigment concentrations of the form:

$$
\begin{aligned}
a_{ph}(412) &= C_a a_a^*(412) + C_b a_b^*(412) + C_c a_c^*(412) + C_{car} a_{car}^*(412) + C_{phyc} a_{phyc}^*(412) \\
a_{ph}(443) &= C_a a_a^*(443) + C_b a_b^*(443) + C_c a_c^*(443) + C_{car} a_{car}^*(443) + C_{phyc} a_{phyc}^*(443) \\
a_{ph}(490) &= C_a a_a^*(490) + C_b a_b^*(490) + C_c a_c^*(490) + C_{car} a_{car}^*(490) + C_{phyc} a_{phyc}^*(490) \quad (5.12) \\
a_{ph}(520) &= C_a a_a^*(520) + C_b a_b^*(520) + C_c a_c^*(520) + C_{car} a_{car}^*(520) + C_{phyc} a_{phyc}^*(520) \\
a_{ph}(565) &= C_a a_a^*(565) + C_b a_b^*(565) + C_c a_c^*(565) + C_{car} a_{car}^*(565) + C_{phyc} a_{phyc}^*(565)
\end{aligned}
$$

Solving this set of equations gives the concentrations of each of the pigments involved. Such a calculation was conducted on the absorption spectra shown in figure 5.6a, and is validated using field observations of chlorophyll "a" only (the concentration of other pigments were not available in the filed datasets). As can be seen in figure 5.6c the retrieved values are in good agreement with the measured values (r^2=0.76) up to a concentration of 5 mg/m^3. Above this concentration the relationship breaks down, probably due to the inadequacy of the specific absorption coefficients used at these concentrations, although an artefact in the analysis of 4 discrete samples only can not be ruled out.

5.3. Discussion

5.3.1. Parameterisation of b_{bTOT} - a generic algorithm for TSM

To date there has been no generic algorithm presented to estimate TSM concentration, the algorithms developed to determine this parameter have been in coastal or estuarine waters (e.g. Viollier and Sturm 1984) with the exception of algorithms that depend exclusively on the correlation between CHL and TSM i.e. Clark et. al.1981. Mapping of the global oceans with estimates of chlorophyll "a" concentration or pigmented biomass concentration is now an accepted investigation tool in pelagic biological oceanography (Aiken 1991). However, there are many applications of such global maps of TSM. For example it has been shown that there is a well defined relationship

between TSM and Particulate Organic Carbon in oceanic waters (Morel 1991), another use of TSM could be in estimating the offshore transport of fine sediments from the world's continental shelf regions therefore aiding in particle flux studies. As can be seen there are different requirements for global TSM concentrations, and the algorithm presented here (equation 5.6) may be able to contribute to this task. The algorithm proposed is based on the knowledge of the spectral influence of different sediment concentrations of reflectance spectra and was defined from simulated reflectance datasets from diverse models. These model are the product of many years of experience by different authors and may be considered representative of many different water types. The product of the Case I model (Morel 1988) through its scattering contribution (*b*) (converted into TSM using published empirical relationships) was shown to be correlated with the presented band combination. The use of the derived [TSM] has been successfully shown here in its use to partly parameterise component b_{bTOT} contributing to the total reflectance. In the model used (Kopelevich (1983)) the component parameterised by [TSM] is that due to small particles which make the major contribution to backscattering in most marine waters. Also the relationship used to relate [TSM] to v_s , the parameter characterising the small particle model, is shown to be very linear. This, and the fact that the relationship holds well over a large concentration range in both Case I and Case II, is probably because at particle sizes less than 1-2μm the refractive index of the particles becomes almost irrelevant (Spinrad 1986) and the backscattering intensity is dominated exclusively by the large particle numbers. On the other hand the large fraction characterised by the chlorophyll is largely dependent on the type of particle (i.e. refractive index) and in fact the CHL shows a less linear relationship with vl (the variable characterising the large fraction of the model).

5.3.2. Determination of f and possibility of replacing with f/Q

In the present study and to satisfy the requirements for precise absolute magnitudes of the inherent optical properties the determination of the proportionality factor *f* traditionally relating irradiance reflectance $R^{0-}(\lambda)$ to the IOPs *a* and b_b (Gordon 1975,

Morel and Prieur 1977) was undertaken. The determination of spectral values of this parameter in the present study over the range considered for the current generation of ocean colour sensors has shown that the wavelength dependency is fairly monotonic and that therefore the common practice of setting this as a spectral constant is justified. However as already discussed in chapter 3 the magnitude of the *f* factor can not be set as a constant value as it is shown to be highly variable, particularly at high zenith angles. Furthermore it is also shown that the equation presented by Morel and Gentili (1991) compares very well with the analytical method presented by Sathyendranath and Platt (1997) which is parameterised for a phase function for the specific region in question. This implies that the η_b ratio well represents the shape of the volume scattering phasefunction even in coastal waters such as those presented in the current study. A point, which needs to be given further study, is whether it would be more appropriate to retrieve values of *f*/Q rather than simply *f* alone. A point in favour of the former is that currently used atmospheric correction schemes compute normalised water leaving radiances $[L_w]_N$ rather than simple water laving radiances (Lw) (Gordon 1988) (this allows intercomparison between radiances from different locations and/or seasons). Therefore Gordon (1988) and Morel and Gentili (1993) have suggested that R/Q be used as the basis for models relating to the inherent optically properties as it is simply retrieved from $[L_w]_N$ through the following equation:

$$[L_w]_N = \left[\frac{(1-\rho)(1-\bar{\rho})F_0 R}{m^2 Q(1-rR)} \right] \tag{5.13}$$

All of the parameters in the above equation can be considered constant aside from R and Q and therefore R/Q can be retrieved implying that the relationship with the inherent optical properties can be expressed as follows:

$$\frac{R}{Q} = \frac{f}{Q} \frac{b_b}{a+b_b} \tag{5.14}$$

Morel and Gentili (1991, 1993, 1996) considered this approach in detail. In their work they showed that spectrally these two components compensate each other and that an iteration scheme could be developed to retrieve this ratio from $[L_w]_N$ based on a look

up table computed through Monte Carlo calculations. Therefore, in view of these developments, it may make more sense in the future in the context of the current model to derive f/Q rather than f, especially in the interest of retrieving absolute magnitudes.

5.3.3. Considerations on band position and number on pigment retrieval accuracy

The presented version of the *Direct Inversion Algorithm* has considered the waveband associated with the channels of the OCTS sensor that flew on board the belated ADEOS satellite. This sensor had its channels in the visible and near infrared centred on the wavelengths 412, 443, 490, 520, 565, 670 as have been presented on numerous occasions through the current presentation. It is however apparent that, in the retrieval of the individual pigment concentrations from the derived pigment absorption (equation 5.12), the retrieval accuracy may be significantly biased by the wavelengths available as inputs to the system of equations. Furthermore, it would also seem quite obvious that all of the calculations preceding the pigment retrieval, given the mathematical formulations used, would be completely insensitive to a change in wavelengths. With such considerations in mind it may be interesting to consider an application of the MERIS sensor of the European Space Agency on the ENVISAT satellite. This sensor will have the opportunity to select the band positions for certain time intervals and therefore could prove an excellent test bed for the model presented in the current study. As an attempt at simulating the improvement achieved from using a specific set of wavelengths selected for retrieving the individual pigment concentrations a dataset of in-vivo pigment spectra were used. From this dataset the wavelengths of the OCTS, and MOS sensors are taken out as well as the optimum set of wavelengths (6 channels) which could be used to set the MERIS sensor. The wavelengths selected for this set were chosen on the basis of the specific absorption spectra shown in figure 5.6a as well as from the discussion given in the paper by Hoepffner and Sathyendranath (1993). Thus the optimum set of six wavelengths selected corresponding to the peaks in the spectra of specific absorption of each pigment are shown in table 5.1, below.

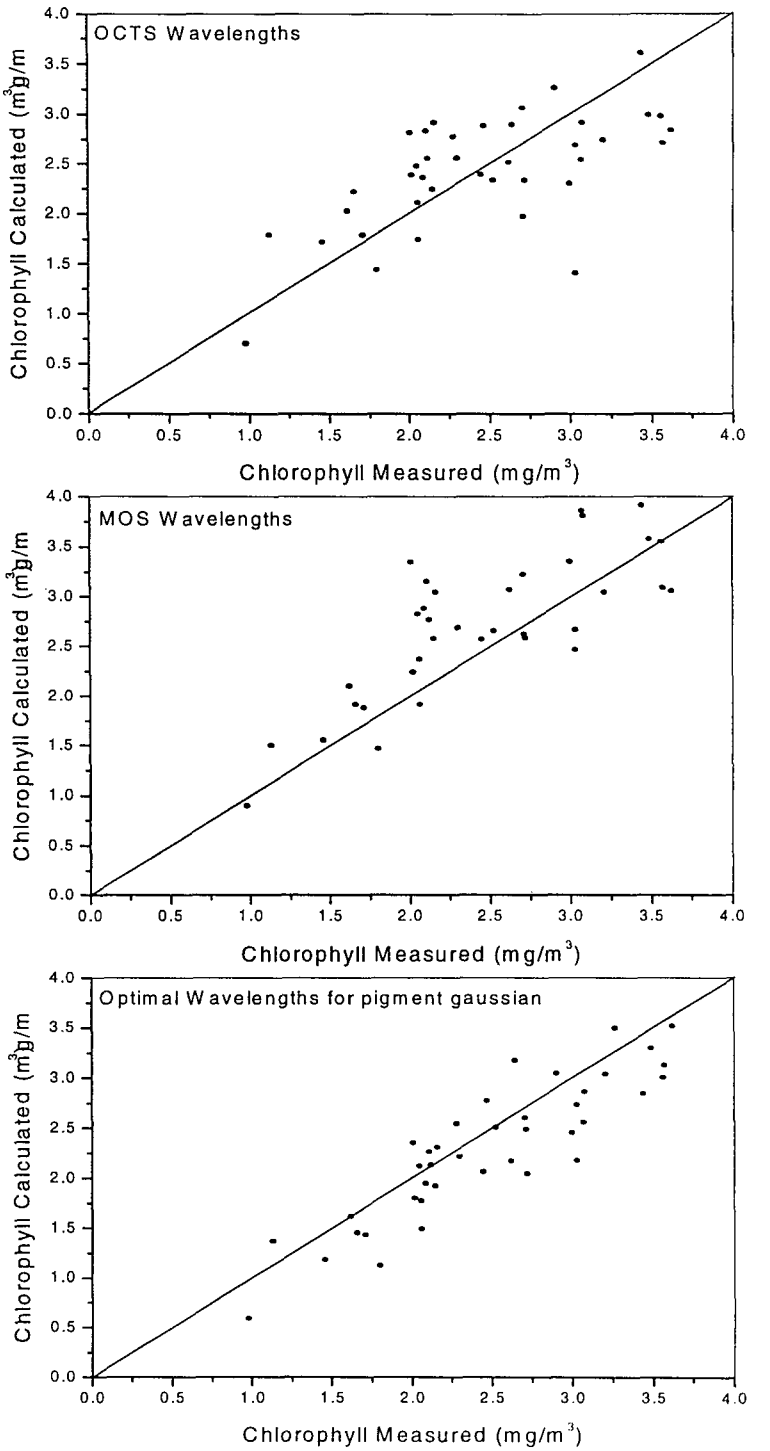

Figure 5.7: Plots showing the variations in retrieval accuracy of chlorophyll "a" using the simultaneous equations and the specific absorption spectra of the individual pigments. Comparison is made between OCTS, MOS and an optimal band set associated with the gaussian centres.

Pigment	Chl"a"	Chl"b"	Carotenoids	PEB	Chl"c"
Proposed Band Centre	434	467	494	548	641
Band Number	2	3	4	5	7
Original Band Centre	442.5	490	510	560	665

Graphs showing the retrieval accuracy of each of the datasets are shown for the chlorophyll a pigment in figure 5.7 a-c where figure 5.7c represents the retrieval for the optimal band set.

5.3.4. Globalisation of the algorithm suite

It is the intention of the presented model to provide a series of algorithms which were globally applicable, unlike the model presented in chapter 3 which was regionally parameterised. This requires the model at various stages to be validated based on datasets and/or models representing many different environments. In particular these validation procedures refer to specific stages of the computation procedure including the TSM algorithm, the representation of the normalised particulate and pigment absorption spectra, and the consistency for different water types of the eigenvectors retrieved for detritus and yellow substance. The specific absorption spectra used for the pigment retrieval from the phytoplankton absorption spectra may also be a point of discussion in the global validity of the model. However, at present the specific absorption spectra used (i.e. Hoepffner and Sathyendranath 1991 and Bidigare et. Al. 1990) are assumed to be valid. This is in part justified by their extensive use in subsequent publications to date (e.g. Aiken 1995, Lutz.1997). As far as the TSM algorithm is concerned the chosen band combination; the *sensitive-compensating;* is shown to be a good choice for the retrieval of TSM over a wide range of values, and with the polynomial fit adopted gives an excellent correlation coefficient of 0.96. This is undoubtedly due to the role of TSM as almost monotonically determining the scattering of the water type and therefore the magnitude of the reflectance. Thus the

use of the presented algorithm is considered to be generically applicable and may be systematically applied. The use of the normalised absorption spectra for the parameterisation of a_p and a_{ph} in equation 5.9 and 5.10 requires consideration. These spectra, whilst playing a fundamental part in the solving of the unknown in the equations for the deconvolution of absorption, are not themselves intended to represent accurate spectral variability of the absorption properties of a_p and a_{ph}. Therefore, the use of the normalised spectra as described in the previous section has the sole purpose of retrieving the factor scores, which allow the reconstruction of the a_{ys} and a_d spectra and therefore the retrieval of the *real* values for a_p and a_{ph}. Having said this the normalised spectra used are selected from a mean of many different regions and thus are supposed to be a good first estimate. Furthermore, there may be scope in the future to use a variety of different normalised spectra which could be selected based on, for example the chlorophyll concentration computed in the earlier stages of the computation. This type of supplementary sub-classification, which could be considered as a crude example of that, proposed by Bricaud et. al. (1995) may allow the differentiation between the spectral shape of a_p and a_{ph} spectra in very different environments (i.e. very eutrophic and very oligotrophic waters), potentially increasing the stability of the mathematical computation. Finally the validity of globally applying a single set of eigenvectors for both ay and ad needs to be considered. In chapter 2 the vectors used were obtained on the basis of the investigation of different absorption datasets from coastal water (i.e. Baltic, N. Adriatic, Tokyo Bay) as shown in figure 2.4 and relevant text. Furthermore the derived vectors were also shown to be in good agreement with those given by Krijsmann (1995) which were based on data from an inland water body, thus exhibiting completely different optical characteristics.

5.3.5. Use of presented algorithm in primary production and chemotaxonomy

The flowchart showed in figure 5.8 illustrates the functionality of the proposed model with the each of the boxes representing the computation described in 5.2 and the inputs required for the initialisation of the model. The above mentioned diagram also

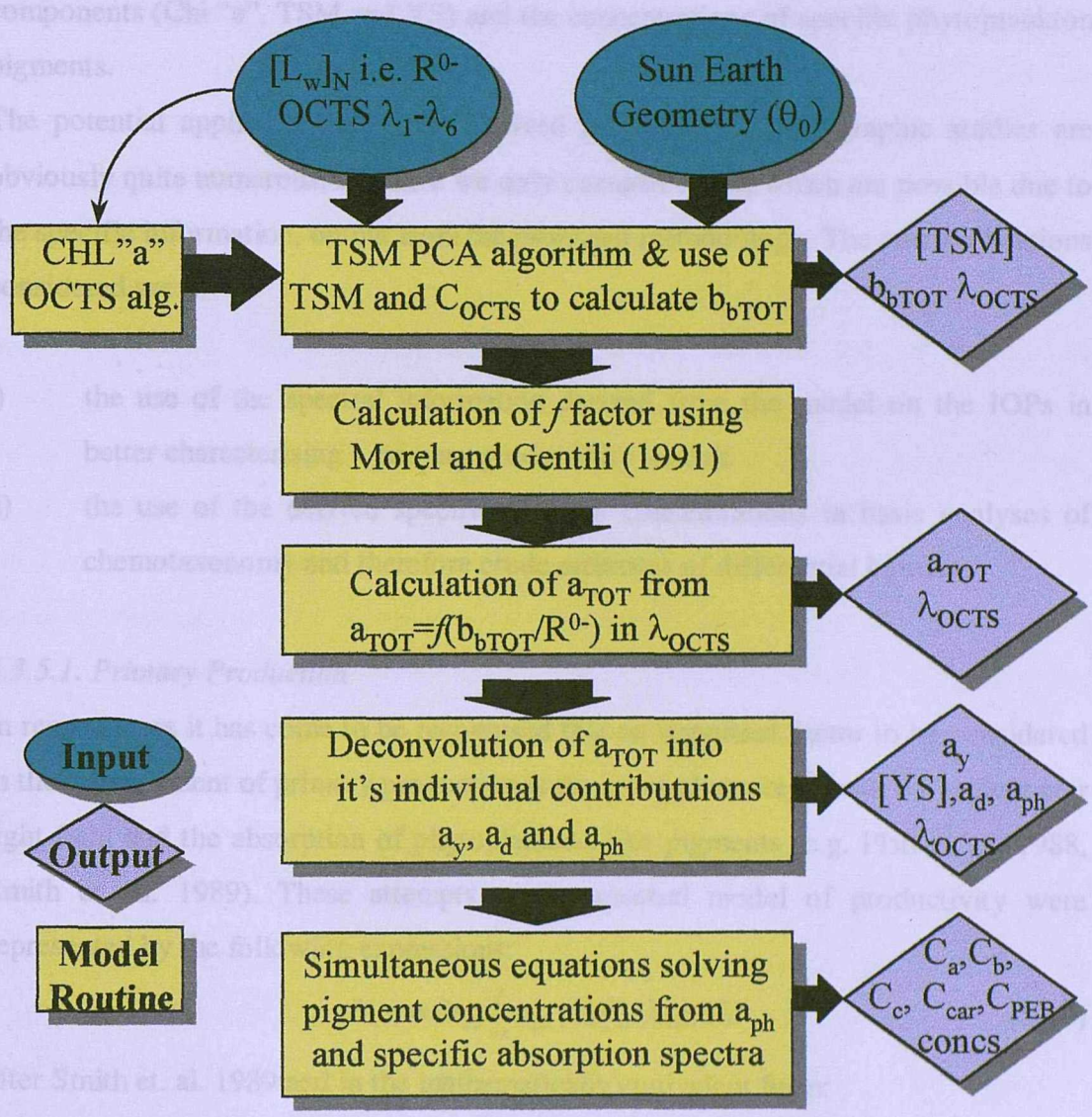

Figure 5.8: Schematic showing a flowcharts of inputs, outputs and processes involved in the *Direct Inversion Algorithm*.

illustrates the numerous outputs from the model at the various stages. As can be observed from the outputs the derived products include both spectral quantities of the Inherent Optical Properties as well as concentrations of the main optically active components (Chl "a", TSM and YS) and the concentrations of specific phytoplankton pigments.

The potential applications of these derived products in oceanographic studies are obviously quite numerous, and here we only consider those, which are possible due to the specific information, output from the proposed methodology. The two applications considered are:

i) the use of the spectral information derived from the model on the IOPs in better characterising a primary productivity model;

ii) the use of the derived specific pigment concentrations in basic analyses of chemotaxonomy and therefore crude estimates of differential biomass.

5.3.5.1. Primary Production

In recent years it has come to be recognised that an important factor to be considered in the development of primary production is the spectral nature of both the underwater light field and the absorption of phytoplankton like pigments (e.g. Platt et. al. 1988, Smith et. al. 1989). These attempts at the spectral model of productivity were represented by the following expressions:

$$P(z) = \Phi_{PP} \int_{\lambda} a_{ph}(\lambda) E_0(\lambda, z) d\lambda \tag{5.15}$$

after Smith et. al. 1989 and in the mathematically equivalent form:

$$P(z) = \int_{\lambda} \alpha^B(\lambda, z) B_{CHL} E_0(\lambda, z) d\lambda \tag{5.16}$$

where,

$$\alpha^B = \Phi_{PP} a_{ph}^* \tag{5.17}$$

after Platt et. al. 1988 (here P is the instantaneous primary production, Φ_{PP} is the quantum yield of photosynthesis, E_0 is the quantum scalar irradiance, B_{CHL} is the chlorophyll biomass concentration and α^B is the rate of photosynthesis). In both of

these cases to obtain the daily productivity over the unit surface area of the water column, which is the principle variable of interest to the community involved in large scale estimates of productivity from remote sensing data, these expressions are integrated both over a daily cycle and over depth to retrieve the daily estimate of primary production per integrated surface unit area. It was this recognition that comparisons of phytoplankton productivity in different waters are best carried out in terms of total phytoplankton production per unit area i.e. the integral, photosynthetic rate for the whole water column. Some very early formulations of this quantity showed it could be modelled through a simple product of the inherent optical properties of the water, the photosynthetic parameters and information on the irradiance field (e.g. Talling 1957). Recently Platt and Sathyendranath (1993) made the comparison of these early solutions and a more complex analytical solution (Platt et. al. 1991) but with a fairly simple parameterisation. In the above studies the authors illustrated that the analytically derived expression was just as efficient as the solution based on empirical observations (of which the best was judged to be that by Talling 1957) in computing daily water column integrated production. These techniques can also be shown to be generalised so as to adequately to cover shallow water columns. This expression offered by Platt et. al. 1991 is given by

$$P_{z,T} = \left(\frac{P_m^B BD}{K} \right) \sum_{x=1}^{5} \Omega_x (E_*^m)^x \qquad (5.18)$$

This solution represents the analytical solution through a polynomial fit to the fifth degree of the true solution which deviates from the original solution with a maximum error of 1% over the full range of known variability of the parameters involved.

It will have been noticed throughout this discussion that all of the solution proposed for daily depth integrated productivity are expressed in terms of biomass concentration with spectrally integrated values for the absorption due to pigments contained in the P_m^B term and the diffuse downwelling attenuation coefficient.

If we are to consider in the near future the formulation of models to be applicable in coastal water environment then either we have to rely on completely empirical productivity relationships (e.g. Babin et. al. 1991, Cole & Cloern 1984, 1987) which

will only be locally applicable, or the alternative is to accurately account for the variability of in-water constituent through the pigment absorption spectra as well as through the variability in the diffuse attenuation coefficient. It is therefore suggested that if we consider in coastal waters (where vertical profile will in general be fairly homogeneous and where the determining factor governing the spatial variability of productivity will be the in water spectral characteristics of the inherent optical properties) the output of the model presented in the current study could prove to be of utmost importance in the formulation of a daily production model. Accounting for both the large variability of pigment composition in coastal waters and more interestingly accurately characterising the removal of a large proportion of the light energy through the attenuation of PAR by the non-phytoplanktonic material (i.e. gelbstoff, particulate detritus and suspended minerals), the expression given by Platt et. al. (1991) and shown here in equation 5.16 could be modified to meeting the criteria of the output from the *Direct Inversion Algorithm.* If we consider that $P_m^B = a_c^* \phi_m E_k$ and $a_{ph} = B \times a_c^*$ then equation 5.16 will become:

$$P_{Z,T} = \int_{\lambda} \frac{a_{ph}(\lambda)}{K_d(\lambda)} \phi_m E_k \sum_{x=1}^{5} \Omega_x (E_*^m)^x \,. \qquad (5.19)$$

If one uses this equation where a_{ph} and K_d are retrieved from the model, ϕ_m is the maximum quantum yield considered as a constant here for eutrophic waters (0.015-0.03), E_k is the adaptation parameter (from the P-I curve) and E^*_m is equal to E_d/E_k at noon. A positive factor about this parameterisation is that all of the variable can be determined by satellite. For example the photosynthetic parameter E_k has been shown to be well correlated with temperature (see table in Kirk 1983) and therefore could be accurately derived from SST product from AVHRR or any other sensors having thermal channels (e.g. OCTS and GLI). Also the downwelling irradiance values required to quantify the downwelling light field can be acquired from satellite source either:

- through the ISCCP (Bishop and Rossow 1991) which now has a dataset with 30km resolution,

– or using a satellite based parameterisation of the Gregg and Carder (1990) model (Aiken and Moore 1997a).

Finally the parameters aph and Kd can be evaluated from the Direct Inversion Algorithm aph as a direct output and Kd as a product of other outputs and through the relationship given by Kirk 1984,1991, where the expression is:

$$Kd = \frac{1}{\mu_0}\left[a^2 + (g_1\mu_0 - g_2)ab\right]^{\frac{1}{2}} \tag{5.20}$$

Here μ_0 is the cosine of the solar zenith angle refracted at the air water interface and g_1, g_2 are coefficients determining the relative contribution of scattering to vertical attenuation Kirk gives as average values over the surface layer g_1=0.425 and g_2=0.190. This expression has shown to be applicable for all aquatic environments (Kirk 1991) and is more suitable for coastal applications than simpler formulations such as those provided by Gordon (1989). Thus it is believed that the proposed formulation may provide a basis for Primary Production modelling in coastal waters in the future and should be verified, as such, through extensive testing.

5.3.5.2. Chemotaxonomy

As commented in the introduction a fundamental application for the proposed model is in its ability to retrieve the individual pigment concentrations. This potential has its obvious implications. In short, the use of the relationship is giving an estimate of the genre of phytoplankton found and therefore estimating the differential biomass, through a crude form of chemotaxonomy. The limitation of the possibility of such a technique lies in the difficulty of separating the different carotenoids through the specific absorption spectra and therefore any relationships possible must be carried out on the basis of total carotenoid concentration. Kirk (1983) gives some broad ranges of pigment concentration ratios associated with different algal group and these are re-offered here as an initial qualitative estimate of differential biomass. It is only the intention of the present study to provide a good solid example of the application of the outputs of the presented model. Therefore, an example was selected that is simple but having an important environmental significance, namely the differentiation

between diatom and dinoflagellate populations. This simple flag could be an important environmental indicator in coastal waters where in numerous areas both past and present the balance of these two classes has represented the environmental state of the specific water body e.g. Belgium coast, N. Adriatic. In particular in most situations a large bias in the ratio dinoflagelates:diatoms is indicative of a negative situation in the particular region. A chosen relationship which could be used as a chemotaxonomic indicator is that using the carotenoid to chlorophyll a+c ratio which is in general 1:0.5 i.e greater than 1 for diatoms and 1:1.5 i.e. less than 1 for dinflagelates

5.4. Conclusions

The presented study has considerably developed a previous method published by Hoepffner and Sathyendranath (1993). The published method retrieved phytoplankton absorption and subsequently the individual pigment concentration from the total particle absorption. In the current study this technique is taken a few steps further by presenting a method originally submitted as an application study for the OCTS sensor (onboard ADEOS). The method included the separation of a_{ys} as well as the components contributing to particulate absorption. Furthermore the total absorption retrieved and used in the deconvolution process was retrieved through the direct inversion of reflectance thus implying that the presented method could eventually be adopted with satellite measured reflectances to retrieve surface maps of pigment concentration and phytoplankton absorption as well as other in water IOPs.

The formulation of the presented model has been discussed in depth and a validation dataset was used to test the model performance at various stages. The results have shown that the model has the capacity to recover products of acceptable accuracy where the chlorophyll a is retrieved with an accuracy of ~30% error. This is slightly higher than the threshold set down by NASA for the retrieval. However, it must be remembered that these limits were established for Case I waters and the validation dataset presented in the current study from the southern Baltic and is clearly not Case I water. Thus to make an in depth analysis of the validity of the proposed model for

meeting NASA criteria an oceanic CaseI dataset should be identified. Moreover discussions of the capacity of the current models to retrieve chlorophyll a concentration at acceptable levels of accuracy overshadow the technique's real potential in deriving new and interesting products. These additional products include the individual photosynthetic pigment concentration but also the spectral properties of all of the individual inherent optical properties as well as the more *traditional* products such as TSM concentration. Considerable effort was expended to justify the global nature of the proposed model. Whilst there is still some work that needs to be performed to evaluate the truly representative nature of expressions such as the algorithm for TSM, the modelled and measured datasets used to consolidate the method seem to suggest that the model selected for each component are as representative as possible in the natural environment of many different types of waters.

The model is obviously very heavily dependent on the original hypothesis that the water leaving radiances are accurate to within 5%. This is a very ambitious target. However different authors (Gordon and Wang 1995, Gentili and Morel 1998) have claimed it to be feasible in Case I water. The model holds many potential interests in its application in coastal waters through studies in water quality and coastal production. In these waters many parts of the methodology and in particular the first steps involving the calculation and subtraction of the backscattering contribution could be heavily biased by the inaccurate performance of the atmospheric correction algorithm. Therefore it is proposed in the future that some type of *bright pixel* add-on (Aiken and Moore 1997b) is used together with the standard atmospheric correction procedure. The addition of such a method together with an iteration scheme similar to that used with CZCS for the red and near-infrared channels would allow a more definite division between aerosol and hydrosol attenuation (see Bricaud and Morel 1987).

Undoubtedly a most promising aspect of the proposed methodology lies in the diversity of new applications opening its products to the wider oceanographic community. For whilst there is still work to be done in validation and consolidation of

the parameterisation of the model, the use of the technique even in a limited geographic region is likely to provide new insight on various aspects of oceanography e.g. the fine scale synoptic distributions of the individual photosynthetic pigments. Furthermore the technique also has the potential, as sensors become more spectrally resolved, to provide information on the inherent optical properties and the associated geophysical parameters and pigment over extended spatial areas.

Chapter 6

Summary and Conclusions

Chapter 5 Table of Content

6.1. Summary of the Individual Chapters
6.2. Accomplishment of the Main goal and objectives
6.3. Applications of presented work
6.4. Future work

The current study has contributed to the field of coastal oceanography and more specifically to the field of coastal bio-optics. The contribution made has involved the development of tools and know-how to make quantitative use of remote sensing in studying optically complex coastal waters. The developed tools and methodologies should prove to be of particular use in the fields of operational oceanography with particular reference to coastal zone management, water quality monitoring and impact assessment. Quantitative synoptic products for these regions will provide a useful source of data to be used in global studies of continental sources of POC, DOC and CO_2.

6.1. Summary of the Individual Chapters

The core chapters of the thesis have set out to address the above-mentioned aim. In chapter 2 the investigation of field data was used to quantify the spectral variance and magnitude contribution to the absorption budget, which is the principle determinant of the spectral shape of reflectance in Case II waters. The study demonstrates that a minimum of four components (including water) is required to reproduce total absorption to an acceptable degree of accuracy in Case II waters. It was also shown that whilst the individual families of spectra are significantly different from one area to another the overall spectral variance show some clear recurrent characteristics. Once these sources of variance can be reproduced then more accurate models of absorption (e.g. to retrieve phytoplankton absorption) can be developed. A classification methodology is presented which will classify waters for the subsequent application of specific algorithms or the determination of bio-optical provinces.

In Case II waters, the requirements in many cases for a regional solution to the algorithmic problem have long been known. The method presented here strove to provide a technique to retrieve quantitative algorithms for each chosen region. The forward model is represented by four components for absorption and three components for backscattering (each including water) where the proportionality factor (f) is also evaluated as a variable. The priority in all of the parameterisations of the

forward model is to allow the maximum variability of the non-chlorophyllous components.

This has been successfully achieved and the reproduction of reflectance through the forward model is to levels within the bounds of the uncertainty in the in-situ measured reflectance. This model is then used as a *motor* in the development of regional algorithms. To begin a large number of reflectance spectra are simulated from the model using lognormal probability distribution functions of the OACs as input. These simulated spectra are then inverted using multivariate statistical techniques (i.e. Principal Component Analysis) and a simple multiple regression is applied to relate the geophysical products to the transformed reflectance. The true strength of this method lies in the fact that, whilst the limitations of PCA (a linear method) in describing a non-linear system such as the co-variability of OACs in coastal waters is well acknowledged, the use of the log-normal PDF for each region limits the variability strictly to that representative of the natural population in the region considered, thus reducing the levels over which the simulations are made (approaching linearity). The method retrieved geophysical variables (CHL,TSM, YS) within the error levels (i.e. 25%) set down by NASA for the required retrieval accuracy of chlorophyll a in **Case I waters** (McClain 1995).

The method presented in chapter 3 limits itself to considering elastic processes, and did not take into account other contributions. A detailed study was therefore made to consider possible contributions from a number of processes including, fluorescence due to chlorophyll a, yellow substance and phycoerythrin Raman scattering and bottom reflectance. These were considered both with respect to the contribution of each process to the overall magnitude of reflectance, as well as through their contribution to the proposed inversion procedure through their effect on the computed eigenvectors. The dataset used for the parameterisation adequately covers extremes of many of the processes considered.

The following conclusions were made: Both chlorophyll and yellow substance may exhibit a significant contribution to the overall reflectance, 30% and 100% of the elastic signal respectively. Yellow substance however contributed only minimally to

the shape of the eigenvector. This is probably due to its very broadband emission spectra. The chlorophyll a fluorescence emission however has a significant effect on the eigenvectors considerably changing there shape.

In considering the cumulative contribution of in-elastic processes and bottom reflectance with respect to elastic processes, in Case II waters, it is shown that the contribution by the in-elastic signal is negligible below 650nm. This is true except in extreme cases of high yellow substance concentrations i.e. greater than 0.5 m^{-1} (at 400nm). Above 650nm this contribution rises quickly to 95%, suggesting that techniques such as those proposed in chapter 3 should ideally restricted themselves to wavelengths less than 650nm; a possible wavelength in the red is the channel at 620nm present both on the MOS and MERIS sensors.

In the final chapter a novel approach was considered to retrieve geophysical parameters from reflectances. The procedure was carried out on measured reflectances which were inverted to retrieve, using a two component description of the Volume Scattering phase Function, b_{bTOT} and the proportionality factor (f). Thus, the total absorption coefficient is deconvolved using the method presented in chapter 2. The derived a_{ph} can then be used to retrieve multiple pigment concentrations using published specific absorption spectra (Hoepffner and Sathyendranath 1993, Bidigare et. al. 1990). The inversion and deconvolution techniques were shown to work very well on an evaluation dataset considering outputs from the model at various levels i.e. TSM, a_{ys}, a_d, a_{ph}. Of the retrieved pigments the calculation accuracy of chlorophyll a was validated, and was shown to lie in a 30% error margin. The global validity of the model was verified (applicability to any region or any water type) and found to be acceptable. Potential applications of such a technique based on absolute reflectance were also considered in detail. These included spectral primary production modelling and chemotaxonomy. The results of this method are obviously heavily dependent on the assumption of the accuracy of the calculated of the water leaving radiance (L_w) but potentially hold many opportunities for future research.

6.2. Accomplishment of the Main goal and objectives

The use of optical remote sensing for the retrieval of quantitative products in investigations of coastal waters with the first generation of Ocean Colour sensors was limited. At the same time the qualitative synoptic potential of ocean colour data for studying coastal waters bodies was widely acknowledged and applauded. The second generation of Ocean Colour sensors provide an increased spectral resolution and radiometric quality, in conjunction with a decade of experience of marine optics and in-situ instrumentation to improve the role of Ocean Colour in quantitative coastal oceanography. The presented thesis has contributed to establishing the validity of this statement and it is hoped that it may fuel future studies in coastal optics and Ocean Colour remote sensing.

The key objectives have been achieved and were undertaken as follows. Firstly in order to *identify a minimum number of components .... and to gain detailed information on the spectral variability of the components influencing the spectral shape of reflectance i.e. through the absorption.* This involved an investigation of spectrally resolved data of all of the main components contributing to absorption for various different regions. Thus, a minimum number of components required to reproduce the total absorption from a summation of the individual contributions were found. Subsequently models were proposed capable of reproducing the equivalent spectral variance as found in the field data.

The second objective was to identify a simple methodology, which allowed the systematic development of regional algorithms for the retrieval of quantitative geophysical products. The methodology proposed a minimum amount of parameterisation to account for the regional variability of the in-water properties. This objective was achieved as follows: A forward model was developed based on a large amount of in-situ data relevant to the Inherent Optical Properties. The model was also verified with a validation dataset and showed to reproduce reflectance within acceptable error levels. The parameterisation of each region is based on input distributions for the simulated reflectance subsequently inverted with the Principal Component Analysis. The method was shown to accurately retrieve geophysical

quantities in Case II waters (with 30% accuracy). The sensitivity of the model to the omitted contribution of in-elastic processes and bottom reflectance was also considered. This contribution was found to have a negligible effect on the model if the wavelength 400-650 nm is adopted.

A final objective was to develop a novel technique to retrieve geophysical products from absolute magnitudes of measured reflectance based on the hypothesis that water leaving radiance (L_w) with better than 5% uncertainty can be assumed from current and future Ocean Colour sensors. This objective was also accomplished by combining the inversion of reflectance to retrieve a_{tot} based on a two component model of the VSF with an absorption deconvolution technique resulting from the spectral variance properties of the individual contributions to absorption. The model successfully underwent a severe validation at various stages of development. This model has the potential of producing many diverse geophysical and IOP outputs, which could prove to be of significant interest in a number of applications. In present study applications of the model to primary production modelling and taxonomic mapping were considered.

6.3. Applications of presented work

Application ultimately is the driving force in the development of algorithms or products. This is fundamentally because the applications command most of the available funding lines. Recently there has been more focused attention on coastal optics, compared to the 1980's when the incentive was mainly on basin scale or global scale processes. This has also been reflected in the funding lines, both from the military and from governmental intergovernmental organisations, and is therefore apparent in contemporary research.

In coastal areas the applications of synoptic instantaneous representations of the quantitative distribution of geophysical parameters are numerous. These for example may include eutrophication studies and more generally all studies related to coastal zone management, water quality monitoring, and impact assessment associated with terrestrial input to the coastal zone river plumes discharges. The complex nature of

sediment dynamics in coastal areas also contains many potential topics for quantitative Ocean Colour remote sensing including erosion deposition processes and modification of sediment dynamics due to the addition of anthropogenic defence structures.

However, to be able to transfer the geophysical data into information products that can be of use to coastal managers further work is required. There is in fact a delicate compromise to be dealt with on this topic. Whilst the spectral resolution and the models become more complex there is potential for the derived products to become more sophisticated but complex. Whilst the user often requires simpler products than may be initially imagined, they also need confidence limits for the products. It is in the estimation of this error that more energy needs to be invested if the methods presented in this thesis are to be considered as more than research tools. Activities to achieve this have now begun through projects such as COASTLOOC and COLORS, which are gathering high quality datasets (in European waters) to use both for parameterising the algorithms and models, and in validating the eventual products. Other projects (e.g. ICAMS) are attempting the real-time validation of standard derived products that then can be of immediate effective use by the appropriate user. Thus the ongoing activities are striving for this common goal and if the user community can be adequately integrated in this process then there is potential for success of the use of optical remote sensing in coastal studies and management.

6.4. Future work

The present study represents an ongoing research activity. Most of the methodologies presented here are still being investigated. In particular no remotely sensed images have been presented in the thesis. This is mainly because work is still ongoing to establish a reliable processing chain to account for the atmospheric correction for coastal areas retrieving water leaving radiances. Water leaving radiances are the fundamental physical quantity; the starting point of all of the tools presented in the current study.

Chapter 2 presented models and detailed information on the spectral variance for the individual components of absorption. The ongoing work on this topic involves several aspects. Firstly the validation of the methodology proposed to retrieve phytoplankton absorption from total absorption and the use of this technique in deconvolving in-situ measured total absorption i.e. AC-9, HISTAR. Secondly a verification of the parameterisation chosen for each of the components using new high quality IOP datasets (i.e. COASTLOOC) to verify spectral variance spectra. This will include the re-evaluation of a Bricaud et. al. (1995) type model for a_{ph} but for different circumstances (e.g. pheophytin a presence).

The parameterisation of the forward model (chapter 3) is now being verified for other regions to formulate a forward model applicable in all water types and based on the unique parameterisation of the three input parameters (CHL,TSM, YS); anomalous circumstances not covered by the model may be evidenced i.e. monospecific particle size distributions (blooms and/or plumes) which will be identified by a flag. As far as the regional parameterisation of the model is concerned, more automated solutions are being sort. This is because it is not always the case that large datasets of the OACs exist which allow to retrieve the PDF required to start the algorithm development procedure. A potential solution is the use of an Ocean Colour climatology of water leaving radiance based itself on a long time-series of satellite data and to use this with simple empirical algorithms to retrieve indicative PDF for the OACs for each region considered. This type of approach has shown interesting initial results and will undergo a severe validation test as a part of the ICAMS project where it will be tested in 4 different sites. The approach will also be compared for specific test areas with output from a multivariate technique applied to the TOA radiances (Neumann 1995) and a neural network based inversion technique (Doerffer 1997). Finally alternative techniques are being considered for the inversion of the simulated reflectance (in substitution of PCA). In particular these include non-linear multivariate techniques such as Blind Source Separation and Independent Component Analysis and non-linear mathematical optimization (i.e. Levenberg Marquardt).

The work presented in chapter 4 was intended to carry out a sensitivity analysis of the response of the forward model presented in chapter 3 to the presence of unaccounted for in-elastic processes. However it is apparent in certain environments the use of the in-elastic processes may be a means of retrieving geophysical parameters (a fact already well studied for CHL (Gower 1981)). This may be interesting for many reasons, including the ease in modelling the spectral shape of the emission spectra and perhaps more importantly the fact that unlike elastic processes in-elastic processes are related to the concentration through a linear relationship. Therefore with the advent in the near future of a spaceborne hyperspectral sensor with high spatial and spectral resolution and a high SNR (the ARIES (CSIRO)) sensor, a project is being prepared which will investigate the use of in-elastic processes coastal waters to retrieve geophysical concentrations.

Finally, chapter 5 presented a novel approach to retrieve geophysical parameters and inherent optically properties from the direct inversion of remotely sensed reflectances. There is obviously a requirement for detailed validation and a sensitivity analysis of L_w. Work is also being undertaken to consider the integration of the model in depth integrated primary production models similar to that proposed in the application section of chapter 5. This model is being configured at present to be used with SeaWiFS data using AVHRR SST for the parameterisation of the photosynthetic parameters. Ultimately the model is being prepared for MERIS and AATSR data to retrieve primary production estimates in coastal waters. The use of the MERIS sensor to perform this task has the added advantage of an option to select an alternative band set for limited periods, enabling the use of a specific band set specific for the retrieval of multiple pigments. This should allow for a more accurate retrieval of spectral information on pigment absorption and the diffuse attenuation coefficient both of fundamental importance in making accurate estimates of primary production in coastal waters.

Bibliography

Aiken, J., Moore, G., and Holligan, P. (1992). "Remote sensing of oceanographic biology in relation to global climate change." J. Phycol. **28**: 579-590.

Aiken, J., Moore,G.F., Trees,C.C., Hooker,S.B., and Clark,D.K. (1995). The SeaWiFS CZCS-Type Pigment Algorithm. Greenbelt, Maryland, NASA Tech. Memo.104566. **29:** 34pp.

Aiken, J., and Moore,G. (1997). Case 2 (S) Bright Pixel Atmospheric Correction, ESA PO-TN-MEL-GS-0005 ATBD 2.6**:** 14pp.

Aiken, J., and Moore,G. (1997). Photosynthetically Available Radiation (PAR), ESA PO-TN-MEL-GS-0005 ATBD 2.18**:** 5.

Antoine, D., and Morel,A. (1997). Atmosphere corrections Over the Ocean (Case 1 waters), ESA PO-TN-MEL-GS-0005 ATBD 2.7**:** 117pp.

Austin, R. W. (1979). Coastal zone color scanner radiometry. Ocean Optics VI, SPIE: 170-177.

Babin, M., Therriault, J.-C., and Legendre, L. (1991). "Potential Utilization of Temperature in Estimating Primary Production from Remote Sensing Data in Coastal and Estuarine waters." Est. Coastal and Shelf Sci. **33**: 559-579.

Babin, M., Morel, A., and Gentili, B. (1996). "Remote Sensing of sea surface Sun-induced chlorophyll fluorescence: consequences of natural variations in the optical characteristics of phytoplankton and the quantum yield of chlorophyll "a" fluorescence." International Journal of Remote Sensing **17**(12): 2417-2448.

Barale, V., Rizzoli,P.M., and Hendershott,M.C. (1984). "Remotely sensing the surface dynamics of the Adriatic Sea." Deep Sea Research **31**(12): 1433-1459.

Berthon, J., Dowell,M., Hoepffner,N., and Grossi,S. (1996). Retrieving chlorophyll and non chlorophyllous matter from ocean colour satellite data in Baltic "Case 2Y" waters. Ocean Optics XIII, Halifax, Nova Scotia, Canada, SPIE: 353-357.

Bidigare, R. R., Ondrusek,M.E., Morrow,J.H., and Kiefer,D.A. (1990). In vivo absorption properties of algal pigments. Ocean Optics, SPIE: 290-302.

Bishop, J. K. B., and Rossow,W.B. (1991). "Spatial and Temporal Variability of Global Surface Solar Irradiance." Journal of Geophysical Research **96**(C9): 16,839-16,858.

Blackman, R. B., and Tukey,J.W. (1957). The Measurement of Power Spectra, Dover Press.

Boxall, S. R., and Robinson,I.S. (1987). "Shallow sea dynamics from CZCS imagery." Advances in Space Research **7**(2): 37-46.

Bricaud, A., Morel,A., and Prieur,L. (1981). "Absorption by dissolved organic matter of the sea (yellow substance) in the UV and visible domains." Limnology and Oceanography **26**(1): 43-53.

Bricaud, A., and Morel,A. (1987). "Atmospheric corrections and interpretation of marine radiances in CZCS imagery: use of a reflectance model." Oceanologica Acta(SP): 33-49.

Bricaud, A., and Stramski,D. (1990). "Spectral absorption coefficients of living phytoplankton and nonalgal biogenous matter: A comparison between the Peru upwelling area and the Sargasso Sea." Limnology and Oceanography **35**(3): 562-582.

Bricaud, A., Babin,M., Morel,A., and Claustre,H. (1995). "Variability in the chlorophyll-specific absorption coefficients of natural phytoplankton: Analysis and parameterization." Journal of Geophysical Research **100**(C7): 13,321-13,332.

Bukata, R. P., Jerome,J.H., Bruton,J.E., Jain,S.C., and Zwick,H.H. (1981). "Optical water quality model of Lake Ontario. 1: Determination of the optical cross sections of organic and inorganic particulates in Lake Ontario." Applied Optics **20**(9): 1696-1703.

Cabaniss, S. E., and Shuman,M.S. (1987). "Synchronous fluorescence spectra of natural waters: tracing sources of dissolved organic matter." Mar. Chem. **21**: 37-50.

Campbell, J. W., and Esaias, W.E. (1983). "Basis for spectral curvature algorithms in remote sensing of chlorophyll." Applied Optics **22**(7): 1084-1093.

Campbell, J. W., and O'Reilly,J.E. (1988). "Role of satellites in estimating primary productivity on the northwest Atlantic continental shelf." Continental Shelf Research **8**: 179-204.

Campbell, J. W. (1995). "The lognormal distribution as a model for bio-optical variability in the sea." Journal of Geophysical Research **100**(C7): 13,237-13,254.

Carder, K. L., and Steward,R.G., (1985). "A remote-sensing reflectance model of a red-tide dinoflagellate off west Florida." Limnology and Oceanography **30**(2): 286-298.

Carder, K. L., Steward,R.G., Paul,J.H., and Vargo,G.A. (1986). "Relationships between chlorophyll and ocean color constituents as they affect remote-sensing reflectance models." Limnology and Oceanography **31**: 38-81.

Carder, K. L., Steward,R.G., Harvey,G.R., and Ortner,P.B (1989). "Marine humic and fulvic acids: Their effects on remote sensing of ocean chlorophyll." Limnology and Oceanography **34**(1): 68-81.

Carder, K. L., Hawes,S.K., Baker,K.A., Smith,R.C., Steward,R.G., and Mitchell,B.G. (1991). "Reflectance Model for Quantifying Chlorophyll "a" in the Presence of Productivity Degradation Products." Journal of Geophysical Research **96**(C11): 20,599-20,611.

Clark, D. K. (1981). Phytoplankton algorithms for the Nimbus 7 CZCS. Oceanography from Space. J. F. R. Gower, Plenum Press: 227-238.

Cole, B. E., and Cloern,J.E. (1984). "Significance of biomass and light availability to phytoplankton productivity in San Francisco Bay." Marine Ecology Progress Series **17**: 15-24.

Cole , B. E., and Cloern,J.E. (1987). "An empirical model for estimating phytoplankton productivity in estuaries." Marine Ecology Progress Series **36**: 299-305.

Comon, P. (1994). "Independent Component Analysis, a new concept?" Signal Processing **24**: 287-314.

Culver, M. E., and Perry, M.J., (1994). "Detection of phycoerythrin fluorescence in upwelling irradiance spectra." Eos Trans. AGU **75**(3): 233.

Culver, M. E., and Perry,J.P. (1997). "Calculation of solar-induced fluorescence in surface and subsurface waters." Journal of Geophysical Research **102**(C5): 10,563-10,572.

Dickey, T. D. (1991). "The emergence of concurrent high-resolution physical and bio-optical measurements in the upper ocean and their applications." Reviews of Geophysics **29**(3): 383-413.

Doerffer, R., and Fischer,J. (1994). "Concentrations of chlorophyll, suspended matter, and gelbstoff in case II waters derived from satellite coastal zone color scanner data with inverse modelling methods." Journal of Geophysical Research **99**(C4): 7457-7466.

Doerffer, R., and Schiller,H. (1997). Pigment index, sediment and gelbstoff retrieval from directional water leaving reflectances using inverse modelling technique, ESA PO-TN-MEL-GS-0005 ATBD 2.12**:** 83.

Dowell, M. D., and Kriebel,S.K.T. (1995). Land-Sea interaction: an AVHRR (NDVI), CZCS ocean colour "collage" for the Baltic region. The 21st Annual Conference of the Remote Sensing Society, The Remote Sensing Society: 985-987.

Dowell, M. D., Berthon,J.F., Hoepffner,N., and Grossi,S. (1996). Absorption modelling in Case II waters: the need to distinguish Coloured Dissolved Organic Matter from Non-Chlorophyllous Particulates. Ocean Optics XIII, Halifax, Nova Scotia, Canada, SPIE: 402-408.

Ehlin, U. (1981). Hydrology of the Baltic Sea. The Baltic Sea. A. Voipio, Elsevier Scientific Publishing Company. **30:** 123-133.

Ferrari, G. M., and Tassan,S. (1991). "On the accuracy of determining light absorption by "yellow substance" through measurements of induced fluorescence." Limnology and Oceanography **36**(4): 777-786.

Ferrari, G. M., and Mingazzini,M. (1995). "Synchronous fluorescence spectra of dissolved organic matter (DOM) of algal origin in marine coastal waters." Marine Ecology Progress Series **125**: 305-315.

Ferrari, G. M., and Dowell, M.D. (1998). "CDOM absorption characteristics with relation to fluorescence and salinity in coastal areas of the Southern Baltic Sea." Est. Coast. and Shelf Sci. **47**: 91-105.

Fischer, J., Doerffer,R., and Grassi,H. (1986). "Factor analysis of multispectral radiances over coastal and open ocean water based on radiative transfer calculations." Applied Optics **25**(3): 448-456.

Garver, S. A., Siegel,D.A., and Mitchell,B.G (1995). "Variability in near-surface particulate absorption spectra: What can a satellite ocean color imager see?" Limnology and Oceanography **39**(6): 1349-1367.

Gathman, S. G. (1983). "Optical properties of the marine aerosol as predicted by the Navy aerosol model." Optical Engineering **22**(1): 57-62.

Ge, Y. R., Gordon,H.R., and Voss,K.J. (1993). "Simulation of inelastic-scattering contributions to the irradiance field in the ocean: variation in Fraunhofer line depths." Applied Optics **32**(21): 4028-4036.

Giles-Guzman, A. D., and Alvarez-Borrego,S. (1996). "Covariance of the absorption of phytoplankton, colored dissolved organic matter, and detritus in case I waters, as deduced from the Coastal Zone Color Scanner bio-optical algorithm." Applied Optics **35**(12): 2109-2113.

Gohs, L., Dera J., Gedziorowska, D. Hapter, R., Jonasz, M., Prandke, H., Siegel., H., Schenkel, G., Olszewski, J., Wozniak, B., and Zalewski, M.S. (1978). Untersuchen zur Wechselwirkung zwischen de optische, physikalischen, biologischen, und chemischen Umweltfaktoren in der Ostsee aus den Jahren 1974, 1975 und 1976. Geod. Geophys. Veroff. Serie 4, 25.

Gordon, H. R., and Brown,O.B. (1973). "Irradiance reflectivity of a flat ocean as a function of its optical properties." Applied Optics **12**: 1549-1551.

Gordon, H. R., Brown,O.B., and Jacobs,M.M. (1975). "Computed Relationships Between the Inherent and Apparent Optical Properties of a Flat Homogeneous Ocean." Applied Optics **14**(2): 417-427.

Gordon, H. R. (1976). "Radiative transfer in the ocean: a method for determining absorption and scattering properties." Applied Optics **15**: 2611-2613.

Gordon, H. R. (1979). "Diffuse reflectance of the ocean: the theory of its augmentation by chlorophyll "a" fluorescence at 685 nm." Applied Optics **18**(8): 1161-1166.

Gordon, H. R., and Morel,A.Y. (1983). Remote Assessment of Ocean Color for Interpritation of Satellite Visible Imagery: A review. New York, Springer-Verlag.

Gordon, H. R., Brown,O.B., Evans,R.H., Brown,J.W., Smith,R.C., Baker,K.S., and Clark,D.K. (1988). "A Semianalytic Radiance Model of Ocean Colour." Journal of

Geophysical Research **93**(D9): 10,909-10,924.

Gordon, H. R., and Ding, K. (1992). "Self shading of in-water optical instruments." Limnol. Oceaogr. **37**: 491-500.

Gordon, H. R., and Wang,M. (1994). "Retrieval of water-leaving radiance and aerosol optical thickness over the oceans with SeaWiFS: a preliminary algorithm." Applied Optics **33**(3): 443-452.

Gower, J. F. R. (1980). "Observations of fluorescence of "in situ" chlorophyll "a" in Saanich inlet." Boundary-layer Meteorology **18**: 235-245.

Gower, J. F. R., Lin,S., and Borstad,G.A. (1984). "The information content of different optical spectral ranges for remote chlorophyll estimation in coastal waters." International Journal of Remote Sensing **5**: 349-364.

Green, S. A. (1992). Applications of fluorescence spectroscopy to environmental chemistry. MIT & Woods Hole, PhD., 228pp.

Green, S. H., and Blough,N.Y. (1994). "Optical absorption and fluorescence properties of chromophoric dissolved organic matter in natural waters." Limnology and Oceanography **39**: 1903-1916.

Gregg, W. W., and Carder,K.L. (1990). "A simple spectral solar irradiance model for cloudless maritime atmospheres." Limnology and Oceanography **35**(8): 1657-1675.

Haltrin, V. I., and Kattawar,G.W. (1993). "Self-consistent solutions to the equation of transfer with elastic and inelastic scattering in oceanic optics: I. Model." Applied Optics **32**(27): 5356-5367.

Haltrin, V. I., Kattawar,G.W., and Weidemann,A.D. (1996). Modeling of elastic and inelastic scattering effects in ocean optics. Ocean Optics XIII, Halifax, Nova Scotia, Canada, SPIE: 597-602.

Haltrin, V. I. (1997). Theoretical and Empirical Phase Functions for Monte Carlo Calculations of Light Scattering in Seawater. The Fourth International Conference of Remote Sensing for Marine and Coastal Environments, Orlando, Florida, ERIM: 509-651.

Harvey, G. R., Boran, D.A., Chesal, L.A., Tokar, J.M. (1983). "The structure of marine fulvic and Humic acids." Marine Chemistry **12**: 119-132.

Hawes, S. K., Carder,K.L., and Harvey,G.R. (1992). Quantum fluorescence efficiencies of fulvic and humic acids: effects on ocean color and fluorometric detection. Ocean Optics XI, SPIE: 212-223.

Hinton, J. C. (1990). "Application of eigenvector analysis to remote sensing of coastal water quality." International Journal Remote Sensing.: 1441-1460.

Hoepffner, N., Sathyendranath,S. (1991). "Effect of pigment composition on absorption properties of phytoplankton." Marine Ecology Progress Series **73**: 11-23.

Hoepffner, N., and Sathyendranath,S. (1992). "Bio-optical characteristics of coastal waters: Absorption spectra of phytoplankton and pigment distribution in the Western North Atlantic." Limnology and Oceanography **37**: 1660-1679.

Hoepffner, N., and Sathyendranath,S. (1993). "Determination of the Major Groups of Phytoplankton Pigments From the Absorption Spectra of Total Particulate Matter."

Journal of Geophysical Research **98**(C12): 22,789-22,803.

Hoge, F. E. (1994). "Asymmetrical spectral algorithms: oceanic-constituents sensitivities." Applied Optics **33**(33): 7764-7769.

Hooker, S. B., C.R. McClain, J.K. Firestone, T.L. Westphal, E-n. Yeh, and Y. Ge, (1994). The SeaWiFS Bio-Optical Archive and Storage System (SeaBASS), Part 1. Greenbelt, Maryland, NASA Tech. Memo.104566**:** 40pp.

Horstmann, U., and Hardtke,P.G. (1980). Transport Process of Suspended Matter, including Phytoplankton, studied from LANDSAT images of the Southwestern Baltic Sea. Oceanography from Space. J. F. R. Gower. New York, Plenum Press**:** 429-438.

Ignatius, H., Axberg,S., Niemisto,L., and Winterhalter,B. (1981). Quarternary geology of the Baltic Sea. The Baltic Sea. A. Voipio, Elsevier Scientific Publishing Company. **30:** 54-86.

Iturriaga, R. (1990). An in situ active fluorometer to measure coccoid cyanobacteria fluorescence. Ocean Optics X, SPIE: 346-354.

Jaquet, J. M., Tassan, S., Barale, V., and Sarbaji, M. (1998). "Bathymetric and bottom effects on CZCS chlorophyll like pigment estimation: data from the Kerkennah shelf (Tunisia)." International Journal of Remote Sensing(Ocean Project special issue): In Press.

Jerlov, N. G. (1951). Optical studies of ocean water, Report of Swedish Deep Sea Expedition**:** 1-59.

Jerlov, N. G. (1976). Marine Optics. Amsterdam, Elsevier.

Jonasz, M., Fournier,G. (1996). "Approximation of the size distribution of marine particles by a sum of log-normal functions." Limnology and Oceanography **41**(4): 744-754.

Kelley, J. C. (1976). Sampling the sea. Ecology of the Seas. D. H. Cushing, and Walsh,J.J. Oxford, Blackwell**:** 361-387.

Kirk, J. T. O. (1975). "A theoretical analysis of the contribution of algal cells to the attenuation of light within waters, II, Spherical cells." New Phytology **75**: 21-36.

Kirk, J. T. O. (1981). "Monte Carlo Study of the Nature of the Underwater Light Field in, and the Relationships between Optical Properties of, Turbid Yellow Waters." Aust.J.Mar. Freshwater Res.. **32**: 517-532.

Kirk, J. T. O. (1983). Light and Photosynthesis in aquatic ecosystems. Cambridge, Cambridge U. Press.

Kirk, J. T. O. (1984). "Dependence of relationship between inherent and apparent optical properties of water on solar altitude." Limnology and Oceanography **29**(2): 350-356.

Kirk, J. T. O. (1991). "Volume scattering function, average cosines, and the underwater light field." Limnology and Oceanography **36**(3): 455-467.

Kishino, M., Booth,C.R., and Okami,N. (1984). "Underwater radiant energy absorbed by phytoplankton, detritus, dissolved organic matter, and pure water." Limnology and Oceanography **29**(2): 340-349.

Kishino, M., Takahashi,M., Okami,N., and Ichimura,S. (1985). "Estimation of the spectral absorption coefficients of phytoplankton in the sea." Bull. Mar. Sci. **37**: 634.

Kopelevich, O. V., and Mezhericher,E.M. (1983). "Calculation of the Spectral Characteristics of Light Scattering by Sea Water." Izvestiya, Atmospheric and Oceanic Physics **19**(2): 144-149.

Krijgsman, J. (1994). Optical Remote Sensing of Water Quality Parameters: Interpretation of Reflectance Spectra. Delft, Delft University: 203pp.

Lazzara, L., Bricaud,A., and Claustre,H. (1996). "Spectral absorption and fluorescence excitation properties of phytoplanktonic populations at a mesotrophic and an oligotrophic site in the tropical North Atlantic (EUMELI program)." Deep-Sea Research I **43**(8): 1215-1240.

Lee, Z., Carder,K.L., Hawes,S.K., Steward,R.G., Peacock,T.G., and Davis,C.O. (1994). "Model for the interpretation of hyperspectral remote-sensing reflectance." Applied Optics **33**(24): 5721-5732.

Lutz, V. A., Sathyendranath,S., and Head,E.J.H. (1996). "Absorption coefficient of phytoplankton: regional variations in the North Atlantic." Marine Ecology Progress Series **135**: 197-213.

Maritorena, S., Morel,A., and Gentili,B. (1994). "Diffuse reflectance of oceanic shallow waters: Influence of water depth and bottom albedo." Limnology and Oceanography **39**(7): 1689-1703.

Marshall, B. R., and Smith,R.C. (1990). "Raman scattering and in-water ocean optical properties." Applied Optics **29**: 71-84.

McClain, C. R., Arrigo,K., Esaias,W.E., Darzi,M., Patt,F.S., Evans,R.H., Brown,J.W., Barnes,R.A., and Kumar,L. (1995). SeaWiFS Algorithms, Part1. NASA Technical Memorandum 104566, Greenbelt, Maryland, NASA: 1-45.

Mobley, C. D. (1994). Light and Water Radiative Transfer in Natural Waters, Academic Press.

Morel, A. (1974). Optical properties of pure water and sea water. Optical Aspects of Oceanography. N. G. Jerlov, and Nielsen,S., Academic Press: 1-24.

Morel, A., and Prieur,L. (1977). "Analysis of variations in ocean color." Limnology and Oceanography **22**(4): 709-722.

Morel, A. (1988). "Optical Modeling of the Upper Ocean in Relation to Its Biogenous Matter Content (Case I Waters)." Journal of Geophysical Research **93**(C9): 10,749-10,768.

Morel, A. (1991). "Light and marine photosynthesis: a spectral model with geochemical and climatological implications." Progress in Oceanography **26**: 263-306.

Morel, A., and Gentili,B. (1991). "Diffuse reflectance of oceanic waters: its dependence on Sun angle as influenced by the molecular scattering contribution." Applied Optics **30**(30): 4427-4438.

Morel, A., and Gentili,B. (1993). "Diffuse reflectance of oceanic waters. II. Bidirectional aspects." Applied Optics **32**(33): 6864-6879.

Morel, A., and Gentili,B. (1996). "Diffuse reflectance of oceanic waters. III. Implication of bidirectionality for the remote-sensing problem." Applied Optics

35(24): 4850-4862.

Mueller, J. L. (1976). "Ocean color spectra measured off the Oregon coast: characteristic vectors." Applied Optics **15**(2): 394-402.

Mueller, J. L., and Austin,R.W. (1995). Ocean Optics Protocols for Sea WiFS Validation, Revision1. Greenbelt, Maryland, NASA: 1-67.

Nehring, D. (1990). Eutrophication in the Baltic Sea. Marine Coastal Eutrophication. R. A. Vollenweider. Amsterdam, Elsevier: 673-682.

Nelson, J. R., and Robertson,C.Y. (1993). "Detrital spectral absorption: Laboratory studies of visible light effects on phytodetritus absorption, bacterial spectral signal, and comparison to field measurements." Journal of Marine Research **51**: 181-207.

Neumann, A., Krawczyk,H., and Walzel,T. (1995). A Complex Approach to Quantitative Interpretation of Spectral High Resolution Imagery. The Third Thematic Conference on Remote Sensing for Marine and Coastal Environments, Seattle, Washington: 641-652.

O'Reilly J. E., S. Maritorena, B. G. Mitchell, D. A. Siegel, K. L. Carder, S. A. Garver, M. Kahru and C. R. McClain. 1998. Ocean Color Chlorophyll Algorithms for SeaWiFS. J. Geophys. Res., **103(C11),** 24,937-24,953.

Philpot, W. D. (1987). "Radiative transfer in stratified waters: a single-scattering approximation for irradiance." Applied Optics **26**(19): 4123-4132.

Platt, T., Sathyendranath,S., Caverhill,C.M., and Lewis,M.R. (1988). "Ocean primary production and available light: further algorithms for remote sensing." Deep-Sea

Research **35**: 855-879.

Platt, T., and Sathyendranath,S. (1993). "Estimators of Primary Production for Interpretation of Remotely Sensed Data on Ocean Color." Journal of Geophysical Research **98**(C8): 14,561-14,576.

Pope, R. M., and Fry,E.S. (1997). "Absorption spectrum (380-700nm) of pure water. II. Integrating cavity measurements." Applied Optics **36**(33): 8710-8723.

Preisendorfer, R. W. (1976). Hydrologic Optics. Washington.D.C., U.S Department of Commerce. **1-6:** 1-218.

Prieur, L., and Sathyendranath,S. (1981). "An optical classification of coastal and oceanic waters based on the specific spectral absorption curves of phytoplankton pigments, dissolved organic matter, and other particulate materials." Limnology and Oceanography **26**(4): 671-689.

Roesler, C. S., Perry,M.J., and Carder,K.L. (1989). "Modeling in situ phytoplankton absorption from total absorption spectra in productive inland marine waters." Limnology and Oceanography **34**(8): 1510-1523.

Roesler, C. S., and Perry,M.J. (1995). "In situ phytoplankton absorption, fluorescence emission, and particulate backscattering spectra determined from reflectance." Journal of Geophysical Research **100**(C7): 13,279-13,294.

Sathyendranath, S., and Morel,A. (1983). Light emerging from the sea - Interpretation and uses in remote sensing, D. Reidel Publishing Company.

Sathyendranath, S., Prieur,L., and Morel,A. (1989). "A three-component model of ocean colour and its application to remote sensing of phytoplankton pigments in

coastal waters." Int. J. Remote Sensing **10**(8): 1373-1394.

Sathyendranath, S., and Platt,T. (1991). "Angular distribution of the submarine light field: modification by multiple scattering." Proc. R. Soc. Lond. A **433**: 287-297.

Sathyendranath, S., Platt,T., Horne,E.P.W., Harrison,W.G., Ulloa,O., Outerbridge,R., and Hoepffner,N. (1991). "Estimation of new production in the ocean by compound remote sensing." Nature **353**: 129-133.

Sathyendranath, S., and Platt,T. (1997). "Analytic model of ocean color." Applied Optics **36**(12): 2620-2629.

Simonds, J. L. (1962). "Application of Characteristic Vector Analysis to Photographic and Optical Response Data." Journal of the Optical Society of America **53**(8): 968-974.

Smith, R. C., and Baker,K. (1978). "The bio-optical state of ocean waters and remote sensing." Limnology and Oceanography **23**(2): 247.

Smith, R. C., and Wilson,W.H. (1981). Ship and satellite bio-optical research in the California Bight. Oceanography from space. J. F. R. Gower. New York, Plenum Press: 281-294.

Smith, R. C., Prezelin,B.B., Bidigare,R.R., and Baker,K.S. (1989). "Bio-optical modeling of photosynthetic production in coastal waters." Limnology and Oceanography **34**(8): 1524-1544.

Spinrad, R. W. (1986). "A Calibration Diagram of Specific Beam Attenuation." Journal of Geophysical Research **91**(C6): 7761-7764.

Spitzer, D., and Dirks,R.W.J. (1985). "Contamination of the reflectance of natural waters by solar-induced fluorescence of dissolved organic matter." Applied Optics **24**(4): 444-445.

Spitzer, D., and Dirks,R.W.J. (1987). "Bottom influence on the reflectance of the sea." International Journal of Remote Sensing **8**(3): 279-290.

Strickland, J. D. H., and Parsons,T.R. (1972). A Practical Handbook of Sea Water Analysis, Fish. Res. Board. Canada.

Sugimura, Y., and Suzuki,Y. (1988). "A High-Temperature Catalytic Oxidation Method for the determination of non-volatile dissolved organic carbon in seawater by direct injection of a liquid sample." Marine Chemistry: 105-131.

Sydor, M., and Arnone,R.A. (1997). "Effect of suspended particulate and dissolved organic matter on remote sensing of coastal and riverine waters." Applied Optics **36**(27): 6905-6912.

Talling, J. F. (1957). "The phytoplankton population as a compound photosynthetic system." New Phytology **56**: 133-149.

Tassan, S., and Sturm,B. (1986). "An algorithm for the retrieval of sediment content in turbid coastal waters from CZCS data." Int. J. Remote Sensing **7**(5): 643-655.

Tassan, S., and Ferrari,G.M. (1995). "An alternative approach to absorption measurements of aquatic particles retained on filters." Limnology and Oceanography **40**(8): 1358-1368.

Victorov, S. V. (1996). Regional Satellite Oceanography, Taylor & Francis.

Viollier, M., and Sturm,B. (1984). "CZCS Data Analysis in Turbid Coastal Water." Journal of Geophysical Research **89**(D4): 4977-4985.

Vodacek, A., Green,S.A., and Blough,N.V. (1994). "An experimental model of the solar-stimulated fluorescence of chromophoric dissolved organic matter." Limnology and Oceanography **39**(1): 1-11.

Vodacek, A., Hoge,F.E., Swift,R.U., Yungel,J.K., Peltrer,E.T., and Blough,N.V. (1995). "The use of in situ airborne fluorescence measurements to determine UV absorption coefficient and DOC concentration in surface waters." Limnology and Oceanography **40**(2): 411-415.

Vodacek, A., Blough, N.V., DeGrandpre, M.D., Peltzer, E.T., and Nelson, R.K. (1997). "Seasonal variation of CDOM and DOC in the Middle Atlantic Bight: terrestrial inputs and photooxidation." Limnol. Oceanogr. **42**(4): 674-686.

Walsh, J. J., Rowe,G.T., Iverson,R.L., and McRoy,C.P. (1981). "Biological export of shelf carbon is a sink of the global CO2 cycle." Nature **291**: 196-201.

Walsh, J. J., and Dieterle,D.A. (1988). "Use of Satellite Ocean Colour Observations to Refine Understanding of Global Geochemical Cycles." Scales and Global Change: 287-317.

Weidemann, A. D., Stavn,R.H., Zaneveld,R.V., and Wilcox,M.R. (1995). "Error in predicting hydrosol backscattering from remotely sensed reflectance." Journal of Geophysical research **100**(C7): 13,163-13,177.

Witek, z., Ochocki,S., Maciejowska,M., Pastuszak,M., Nakonieczny,J., Podgorska,B., Kownacka,J.M., Mackiewicz,T., and Wrzesinska-Kwiecien,M. (1997). "Phytoplankton primary production and its utilization by the pelagic community in

the coastal zone of the Gulf of Gdansk (southern Baltic)." Marine Ecology Progress Series **148**: 169-186.

Zaneveld, J. R. V. (1982). "Remotely sensed reflectance and its dependence on vertical structure: a theoretical derivation." Applied Optics **21**(22): 4146-4150.

Zaneveld, J. R. V. (1989). "An asymptotic closure theory for irradiance in the sea and its inversion to obtain the inherent optical properties." Limnology and Oceanography **34**(8): 1442-1452.

Zaneveld, J. R. V. (1995). "A theoretical derivation of the dependence of the remotely sensed reflectance of the ocean on the inherent optical properties." Journal of Geophysical Research **100**(C7): 13,135-13,142.

Zibordi, G., Barale, V., Ferrari, G.M., Hoepffner, N., van der Linde, D., Alberotanza, L., Cova, P., and Ramasco, C. (1995). Coastal Atmosphere and Sea Time-Series Project (CoASTS): an ocean colour remote sensing calibration/validation project. Third Thematic Conf. on Remote Sensing for Marine and Coastal Environments, Seattle: 96-100.

Zibordi, G., Berthon,J.F., Grossi,S., van der Linde,D., and Targa,C. (1997). Long-term in situ measurements supporting ocean colour cal/val activities. 1st International Workshop on MOS-IRS and Ocean Colour, Berlin: 5pp.

Appendix 2.A

Reprinted from

MARINE CHEMISTRY

AN INTERNATIONAL JOURNAL FOR STUDIES OF THE MARINE ENVIRONMENT

Marine Chemistry 55 (1996) 299–316

Relationship between the optical properties of chromophoric dissolved organic matter and total concentration of dissolved organic carbon in the southern Baltic Sea region

Giovanni M. Ferrari [a,*], Mark D. Dowell [b,1], Stefania Grossi [a], Cristina Targa [1,c]

[a] *Space Applications Institute, Marine Environment Unit J.R.C., I-21020 Ispra (Va), Italy*

[b] *Southampton Oceanography Centre, Department of Oceanography, University of Southampton, Waterfront Campus, European Way, Southampton, SO14 3ZH, UK*

[c] *University of Venice, Dipartimento di Scienze Ambientali, Campo Celestia 2737 / B, I-30123 Venice, Italy*

Received 17 November 1995; accepted 22 May 1996

ELSEVIER

ELSEVIER

Marine Chemistry 55 (1996) 299–316

MARINE CHEMISTRY

Relationship between the optical properties of chromophoric dissolved organic matter and total concentration of dissolved organic carbon in the southern Baltic Sea region

Giovanni M. Ferrari [a,*], Mark D. Dowell [b,1], Stefania Grossi [a], Cristina Targa [c]

[a] *Space Applications Institute, Marine Environment Unit J.R.C., I-21020 Ispra (Va), Italy*

[b] *Southampton Oceanography Centre, Department of Oceanography, University of Southampton, Waterfront Campus, European Way, Southampton, SO14 3ZH, UK*

[c] *University of Venice, Dipartimento di Scienze Ambientali, Campo Celestia 2737 / B, I-30123 Venice, Italy*

Received 17 November 1995; accepted 22 May 1996

Abstract

Absorption and fluorescence of chromophoric dissolved organic matter (CDOM) and dissolved organic carbon (DOC) measurements were performed during three oceanographic surveys in 1994 in the southern Baltic Sea (Polish area of the Baltic Proper). DOC was measured both by high-temperature catalytic oxidation (HTCO) and low-temperature oxidation (LTO) conventional persulphate methods. CDOM fluorescence was shown to be highly correlated with absorption, with the same regression parameters, despite the seasonal change in different hydrographic conditions and the fluorescence quantum yield variations (1.23 ± 0.07 in April and 0.97 ± 0.12 in September). The results show a good correlation between the optical parameters and DOC although $\sim 70\%$ of the DOC does not display significant absorption in the UV–visible range (350–750 nm). The non-absorbing DOC measured with HTCO method appears unaffected by seasonal changes. Consequently, total DOC can be predicted by optical methods using remote sensing techniques. The non-absorbing DOC measured by LTO method varies from 62% (April) to 76% (September), which implies that there is requirement for estimates on a seasonal basis.

Keywords: dissolved organic carbon; dissolved organic matter; Baltic Sea

1. Introduction

Chromophoric dissolved organic matter (CDOM) interacts with sunlight absorbing quanta in the same range as phytoplankton, thus subtracting from the water body radiant energy available for marine photosynthesis. Furthermore, in the surface waters, CDOM is involved in chemical, photochemical and microbial processes and that have been studied by several authors for the photodegradation to low-molecular-weight carbonyl compounds (Kieber et al., 1990; Miller, 1994); for the carbon gases (Miller, 1994) and for trace gases (Valentine and Zepp, 1993; Miller, 1994). CDOM optical properties such as absorbance and fluorescence can be used as tracers

* Corresponding author.

[1] Present address: Space Applications Institute, Marine Environment Unit J.R.C., 21020 Ispra (Va), Italy.

PII S0304-4203(96)00061-8

of dissolved organic carbon (DOC). In natural waters CDOM absorbs UV and visible light according to the energy of the electronic states of the molecule as well as to its intermediate vibrational or rotational levels. Aliphatic low-molecular-weight compounds with low number of π bonds such as carbohydrates, urea and many carbonyl compounds, which can also result from photodegradation or photobleaching in surface waters (Miller, 1994), do not absorb UV–visible light (350–750 nm) significantly. This means that the main part of the DOC pool is detectable by remote sensing methods only when it is constant or correlated with the absorbing DOC fraction. Mopper and Schultz (1993) categorised DOC in two fractions according to the lability toward chemical and photochemical oxidative degradation during DOC analysis, giving a more labile DOC (DOC_{lab}) and a more resistant DOC (DOC_{res}). DOC_{lab} is obtained by low-temperature oxidation method using persulphate (here named LTO) (Menzel and Vaccaro, 1964; Druffel et al., 1989; Suzuki and Tanoue, 1991). DOC_{res} is the difference between the measurement with the high-temperature method (here named HTCO) and that obtained with LTO.

The measurement of DOC concentration in natural waters has been an object of considerable controversy for some decades. Sharp (1993) has written an update on this problem summarizing the results of an inter-laboratory comparison to obtain an uniform DOC measurement. The reported results show that, if the blank correction is carefully performed, the difference between DOC concentration measured with HTCO and LTO methods are minimized (10–15%). Whilst for oceanic waters the differences range from a minimum of almost 0 (Hedges and Bergamaschi, 1992) to ~20% (Chen, 1992), for fresh waters the difference was found uniformly minimal (5–10%; Kaplan, 1992). However, the majority of the recent published data regard oceanic waters, open sea and not marginal or enclosed sea, coastal or estuarine areas. In these environments, the presence of chemically refractory material such as dissolved humic matter may be significant in the resulting measurements of DOC concentration dependent on the oxidative capacity of the analytical method used. The Baltic is an enclosed sea exhibiting pronounced characteristics of an estuarine environment (low salinity, high continental inputs) and consequently DOC concentration measured with the two methods described here may give different results.

These initial considerations, which are only a minimal part of the detailed knowledge of DOC in natural waters, allow the authors to comment on a problem recently addressed, involving the identification of parameters which can be easily collected and used as input for models describing the carbon cycle in the aquatic (marine) ecosystems (Bocastow and Maier-Reimer, 1991; Jackson, 1993). Large-scale studies of CDOM may be made using remote sensed data from active airborne sensors or from passive multispectral sensors in the near future when imagery from the forthcoming ocean colour sensors (e.g., SeaWiFS) will be available. CDOM must be acquired as absorption in UV–visible range, which is difficult to achieve because the low sensitivity of the measurement. In earlier works, Hoge et al. (1993), Green and Blough (1994), and Vodacek et al. (1995) demonstrated that CDOM absorption can be quantitatively retrieved from fluorescence measurements. The fluorescence emission maximum (excitation at 355 nm) was found to be well correlated with absorption coefficient at 355 nm despite the different marine water bodies analysed along the U.S. coast. Similar results were also obtained by Ferrari and Tassan (1991) in the Mediterranean.

In this study we have considered the relationships between absorption and fluorescence in the southern Baltic Sea, as well as a further investigation into the relationship of the CDOM absorption with DOC concentration measured with HTCO and LTO methods. This work will provide data for preparation of local algorithms for SeaWiFS in the Baltic Sea, through the formulation of optical models for the region where CDOM absorption is dominant with respect to the other optically-active substances (pure water, phytoplankton-like pigments and detritus) as illustrated in Fig. 1.

2. Material and methods

2.1. Study area and sampling

The area of investigation includes the Gulf of Gdansk, the Polish Coast as far as the Pomeranian Bay, and part of the open sea of the so-called Baltic

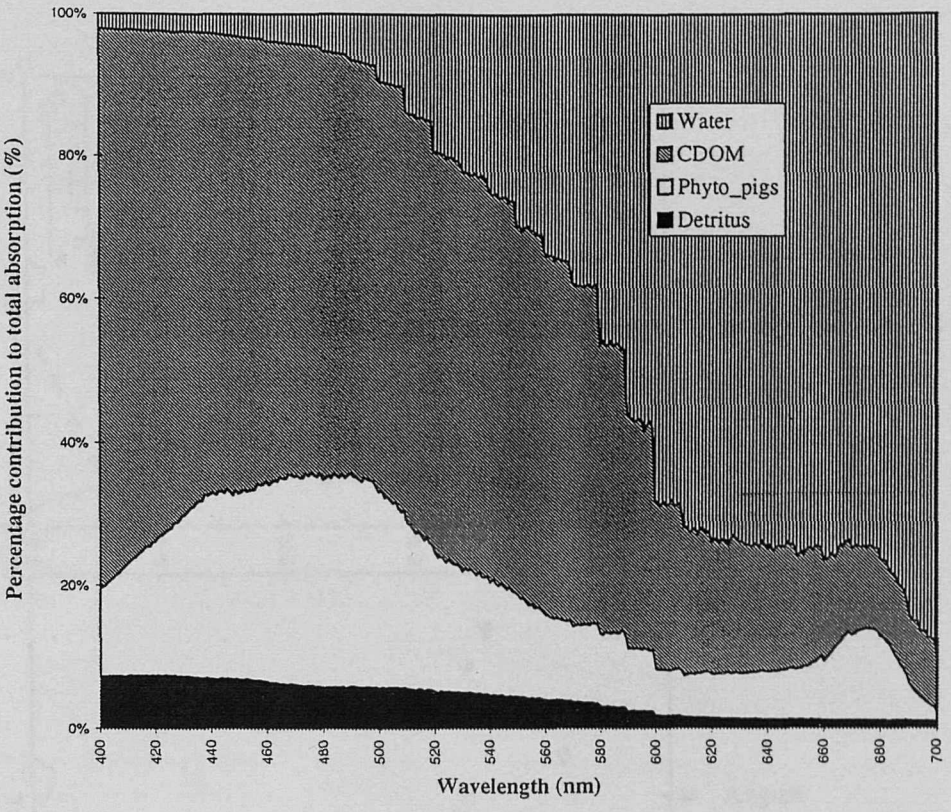

Fig. 1. Typical coastal water of the Baltic Sea (station 24, August 1994) illustrating the percentage contribution of different components (pure water, CDOM, phytoplankton pigments and detritus absorptions) to the total absorption of the water body. Phytoplankton-like pigment and detritus absorption were obtained using a method described in Tassan and Ferrari (1995).

Proper from 15 to 60 km from the shoreline (Fig. 2). The sampling area was defined in order to assess the full influence on the hydrobiological conditions of the basin considered by inputs from the main rivers the Vistula and Oder (which flow into the Gulf of Gdansk and the Pomeranian Bay, respectively), as well as the several small but significant inflows coming from the forested area along the Polish coast. A comparison between coastal areas and the open sea was made to evaluate the sources of CDOM both from the above-mentioned rivers as well as from the algal blooms, which occur frequently during spring in the coastal and offshore waters. This is shown by monthly colour composite of historical CZCS imagery for the southern Baltic Sea elaborated at the Joint Research Centre (JRC) at Ispra, Italy.

Sampling was performed three times in 1994: in April, during well-mixed water column conditions and with the maximum of freshwater inflow, in August and September during the summer period characterized by the stratified water masses, by a sharp thermocline and minimum river inflow. The survey consisted of 101 stations in total, some of which were repetitions of the same location during the three periods considered. The CDOM samples were collected on board of the Polish RV "Oceania" generally at three depths within the euphotic depth as indicated by CTD and fluorescence profiles. Fig. 2 shows the sampling areas and the position of the stations while Fig. 3 illustrates typical salinity and temperature profiles representing the water mass structures in three seasons (April, August and September) for the Gulf of Gdansk, the coastal zone and the open sea and Pomeranian Bay (surveyed in September).

The samples for CDOM were filtered through

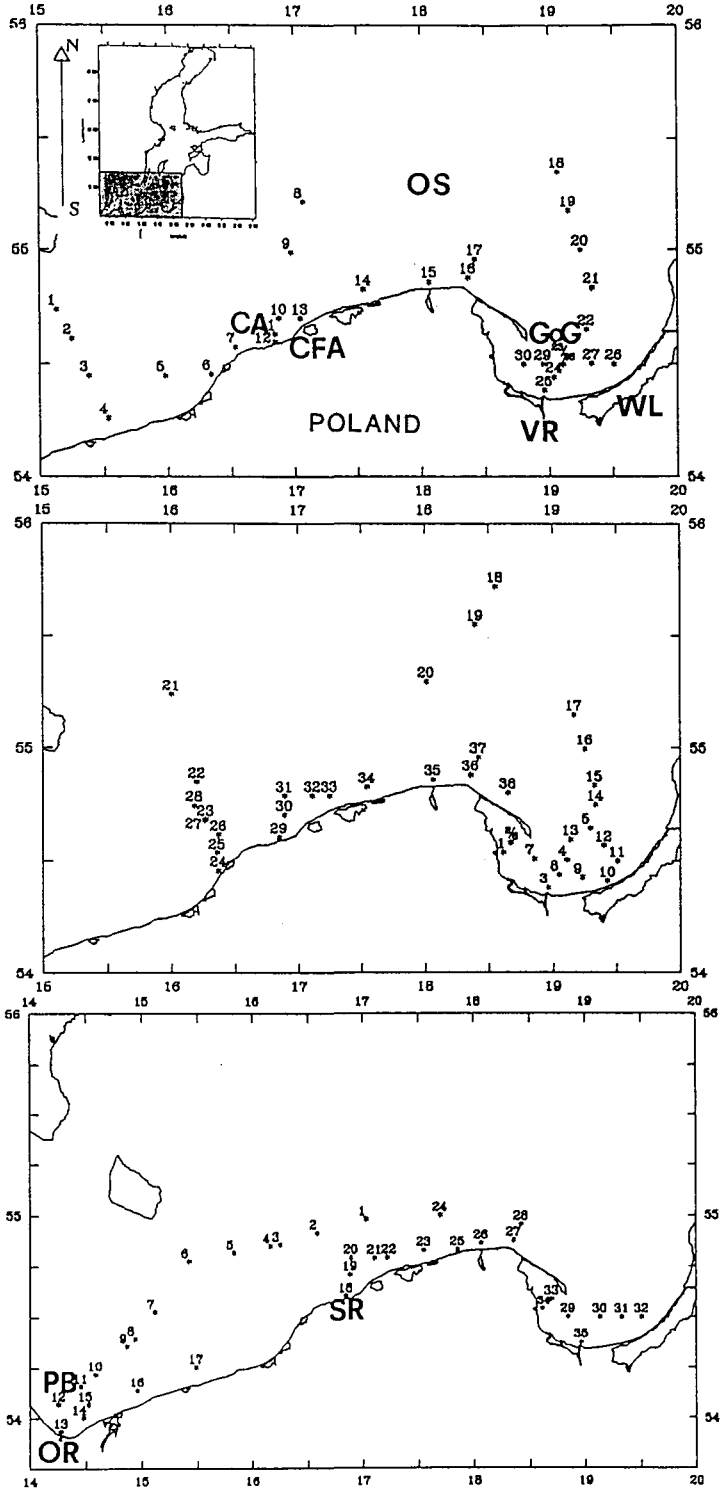
April
August
September
OS
CA
CFA
GoG
POLAND
VR
WL
SR
PB
OR
N
S

GFF filters and successively the filtrate was re-filtered through 0.22-μm Millipore membranes previously rinsed with Milli-Q water. This final filtrate was fixed with (0.5 ml for 100 ml of sample) a solution of 10 g/l sodium azide as bacteriostatic agent, and subsequently stored in 250-ml amber glass bottles at 4°C. The samples were analysed for absorption, fluorescence and DOC within one month of collection. Samples were collected at the pre-determined depths with a conventional 10-l Nansen bottle sampler and the surface sample was collected with a seawater conditioned polyethylene bucket.

2.2. *Fluorescence, absorption, quantum yield and* DOC *measurements*

2.2.1. *Fluorescence*

Fluorescence measurements were performed immediately after sampling (before fixation with sodium azide) with a Perkin Elmer LS50 spectrofluorimeter installed on board the vessel. The measurements were made in emission mode using the accepted excitation wavelength at 355 nm (Hoge et al., 1993) which corresponds to high-power-pulsed UV laser available for laser-induced fluorescence technique. The instrument has a xenon pulsed lamp and the excitation band is automatically corrected, for intensity fluctuations, with a reference photomultiplier supplied with a rhodamine dye correction curve. The wavelength reproducibility is ±0.5 nm. The fluorescence measurement is a modification of that described by Ferrari and Tassan (1991). The emission signal (430–450 nm) is normalised to an external standard constituted by the fluorescence peak height of a solution of quinine sulphate 0.01 mg/l in 1 *N* H_2SO_4 defined as 10 normalised fluorescence units:

$$Fs(\lambda) = F_s/F_{qs} \times 10$$

where Fs is the standardised fluorescence; F_s is the fluorescence of the sample, F_{qs} is the fluorescence of the quinine sulphate; and λ is the excitation wavelength at 355 nm. Milli-Q water is used as a blank and its contribution to fluorescence subtracted whilst for quinine sulphate fluorescence, a solution of 1 *N* H_2SO_4 is used as baseline. To account for any possible instrumental drift, quinine sulphate spectra were acquired two times per each day of sampling.

2.2.2. *Absorption*

The CDOM samples, fixed with sodium azide, were transported refrigerated to JRC at Ispra and measured with a Perkin Elmer Lambda19 dual beam spectrophotometer using 10-cm fused quartz cuvettes with Milli-Q water as a blank. The Lambda19 unit was used in the range 300–750 nm with a spectral resolution of 1 nm. The absorbance acquired was converted to absorption coefficient (m^{-1}) using the $a_{CDOM}(\lambda) = 2.3A(\lambda)/L$, were $A(\lambda)$ is the absorbance and L the pathlength of the optical cell in meters.

2.2.3. *Quantum yield*

Fluorescence quantum yield (Q.Y.) is an ancillary derived parameter which can provide further information for understanding the relative sources of CDOM. It expresses the quantum efficiency of the fluorescence with respect to the absorption. Q.Y. is computed, using a quinine sulphate reference, with the relationship (Green and Blough, 1994):

$$\Phi_s(\lambda) = \left[\int_{420}^{460} F_s(\lambda)\,d\lambda\, x a_{qs}(\lambda)\, x\Phi_{qs}\right] \Big/ \times \left[\int_{420}^{460} F_{qs}(\lambda)\,d\lambda\, x a_s(\lambda)\right]$$

where subscripts $_s$ and $_{qs}$ refer to the sample and quinine sulphate reference (0.5 mg/l in 0.1 *N* H_2SO_4 which gives an $a = 1.5\ m^{-1}$ at 355 nm), respectively; and $a(\lambda)$ is the absorption coefficient of each sample and where λ, in this case, is 355 nm. The integration of the fluorescence emission F (355 nm) is performed instrumentally between 420 and 460 nm. Φ_{qs} is typically 0.51. Q.Y. is dimensionless and its estimate is related to the uncertainties on the absorption measurement when this value is low. Q.Y. is normalized with quinine sulphate and there-

Fig. 2. Sampling areas and position of the stations in the three surveys of 1994: 7–17 April; 17–25 August and 5–15 September. The letters indicate: *OS* = open sea; *GoG* = Gulf of Gdansk; *VR* = Vistula River; *WL* = Wislany lagoon; *CFA* = coastal forested area; *CA* = coastal area; *SR* = Slupia River mouth; *PB* = Pomeranian Bay; *OR* = Oder River.

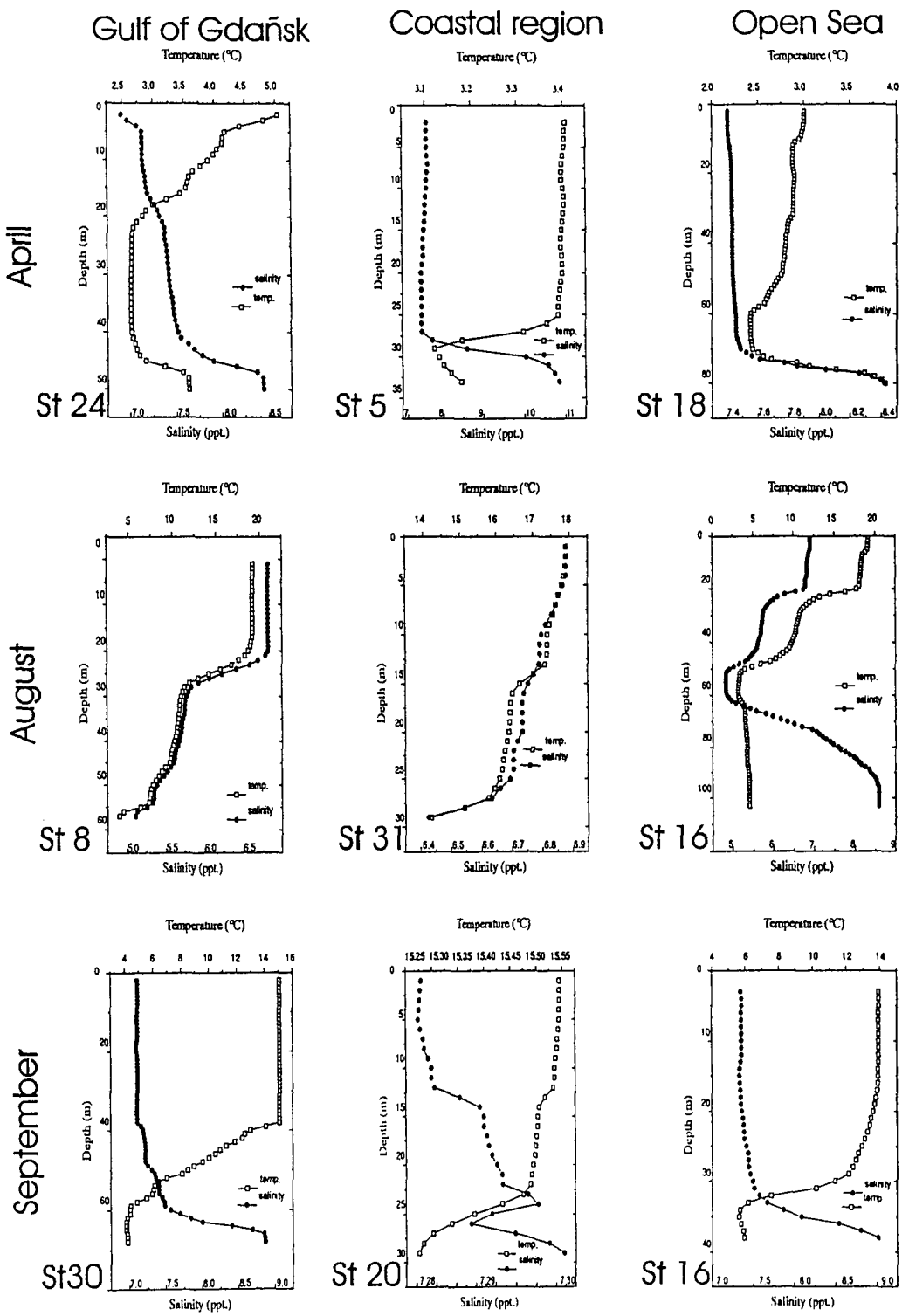
Gulf of Gdañsk
Coastal region
Open Sea
April
August
September
St 24
St 5
St 18
St 8
St 31
St 16
St30
St 20
St 16
Temperature (°C)
Depth (m)
Salinity (ppt.)
temp.
salinity

fore has the advantage of being independent on the instrument used. Generally, of the photons absorbed by a typical CDOM sample, ~ 1% is re-emitted as fluorescence (Green, 1992).

2.2.4. DOC *measurements*

Seawater samples collected with a 10-l Nansen bottle were stored in 15-l seawater-preconditioned polyvinylchloride (PVC) containers in order to reduce contamination. The filtration was performed under gentle vacuum (100 mbar) on a precombusted GFF filter rinsed with filtered seawater to eliminate the main part of particulate matter. This first filtrate was refiltered on a Millipore 0.22-μm membrane pre-rinsed with Milli-Q water. In each filtration the initial aliquot (~ 200 ml) was discarded to prevent any possible source of contamination by the filters. The final filtrate was therefore transferred to 250-ml amber glass bottle pre-rinsed with the same filtered seawater. During the August 1994 campaign, DOC samples were taken in duplicate. After addition of sodium azide the sample was stored at 4°C. The DOC analyses were performed at the JRC Ispra Institute of Environment for the HTCO method, and at the University of Venice for the LTO method.

2.2.4.1. HTCO *method.* For this measurement a Carlo Erba-Fisons TMC 480 analyser was used. This instrument consists of a high-temperature oxidation reactor thermoregulated at 1020°C. The inorganic carbon is first stripped after acidification with 0.5 *N* HCl solution and nitrogen as a purging gas to separate carbon dioxide from the sample. The liquid phase is driven through an automatic sample valve which injects 50 μl to the high-temperature reactor (a ceramic column filled with NiO). The combustion products are carried by nitrogen flow as carrier gas. Water is eliminated by a condenser while CO_2 is initially adsorbed by a chromatographic Poropak QS column thermostated at 100°C, and subsequently deadsorbed by a second carrier gas (nitrogen + hydrogen) and thus transported into the reduction reactor. CO_2 is reduced to methane in the presence of a copper–nickel catalyst at 400°C. The methane is measured with a flame ionisation detector (FID) whose signal is fed to a potentiometric chart recorder which has a response directly proportional to the amount of organic carbon present in the original sample. The relative instrumental response was determined with a calibration curve (which is linear in the range of our interest) obtained using reference samples of potassium biphthalate (Merck p.a., stock solution in Milli-Q water). The instrument has a range of detection within 83 to 83,000 μ*M* C. The blank was obtained with Milli-Q water and was found to be invariant with time and equal to 86.66 μ*M* C (±6.3 on 39 observations) and subtracted from each measurement. The instrumental blank appears high with respect to the other C analyzers however, resulting in a lower range of detection. A blank and a standard were performed every 10 sample measurements averaging 5 successive replicates to check the efficiency of the oxidation column which was changed when the standard response reduction was > 10%. The error of determination was estimated as ±1.95% with 95% confidence limits of 0 and ±5.2%. The estimate was derived from a population of 91 averages formed by four replicates of each sample. The 39 samples collected in the August survey were analysed in duplicate to check the effect of sampling on DOC determination. The percent deviation between the single observation and the average of the two replicates determined is shown here below:

Number of observations	± deviation	% of total population
16	(0–6%)	41
7	(6–10%)	18
11	(10–20%)	28
5	(> 20%)	12

Of the 39 duplicates, the average deviation was in ±11%. If the difference among the two replicates was > 10%, the minor value was chosen; for all other cases the average has been considered.

Fig. 3. Salinity and temperature (by CTD) profiles showing the different water masses and thermocline. In April in the Gulf of Gdansk (station 24), the relatively warm (4–5°C) surface water of the Vistula River is evident with respect to the cold deep water (2.5°C). In August, station 16 shows a complicated structure with two thermoclines due to the strong sun irradiance.

2.2.4.2. LTO *method.* These measurements were performed with a Auto Analyzer II of the Technicon Instrument Co., New York, which is able to detect DOC concentrations in the range between 33 and 830 μM C. As with the HTCO, the method requires the accurate removal of inorganic carbon by acidification. The procedure uses a purge rate of 500 ml/min, therefore implying a removal of up to 500 mg of inorganic carbon with minimal loss of volatiles. An aliquot of carbonate-free sample is mixed with a stream of sodium tetraborate and potassium persulphate and then subjected to UV radiation in a reactor at 37°C. When seawater is analyzed, hydroxylamine, hydrochloric and sulphuric acids are added to reduce the generated chlorine from sodium chloride. The resultant CO_2 is dialysed through a silicone rubber membrane and made to react with a weakly buffered phenolphthalein indicator whose colour variation is proportional to organic carbon concentration. The standards used were taken from a stock solution of potassium biphthalate (0.212 g/l) + 0.5 ml 1 N H_2SO_4. The calibration was linear in the range of measurement. The error of determination was found to be $\pm 2\%$ with 95% confidence limits of 0 and $\pm 3.8\%$ considering an average of 3 replicates for sample. The instrumental blank was performed each day with Milli-Q water and was found to be less than to the detection limit of the instrument and therefore not subtracted by the sample measurement.

2.2.5. Effect of sample storage and blank determination

The samples which were not directly measured on board, were stored, refrigerated (at 4°C) in amber glass bottles with addition of sodium azide. The effect of storage was tested to determine the maximum delay possible to perform absorption and DOC measurements. The results of this test lead to the conclusion that a storage time of up to three weeks is acceptable as described in a specific study by Ferrari (1990). Sodium azide does not affect CDOM absorption above 300 nm. Some blanks were taken during each cruise reproducing the sampling operations made using Milli-Q water. In terms of absorption the blanks obtained were negligible, while, for the DOC, values of 16 μM C were obtained using HTCO and 12.4 μM C using LTO, both significantly under the measurement limits of the instruments used.

Table 1
Data of the intercalibration test between HTCO and LTO carbon analyzers

Standard used	(μM C)	HTCO (μM C)	LTO (μM C)
K-biphtalate	622	629 (±1.9%)	630 (±2.5%)
K-biphtalate	415	448 (±2%)	414 (±2.5%)
K-biphtalate	207	208 (±1.8%)	210 (±2.5%)
D-glucose (+)	415	439 (±2%)	415 (±2%)
Humic acid	–	395 (±0.2%)	307 (±2%)
Humic acid	–	2075 (±1.5%)	1535 (±1.8%) [a]
Humic acid	–	4971 (±1.8%)	3735 (±1.5%) [a]
Humic acid	–	11,786 (±0.9%)	8134 (±1.5%) [a]
Phloroglucinol	–	197 (±2.9%)	134 (±2.3%)

Standard deviations are given in brackets.
[a] Measured after dilution.

2.2.6. Intercalibration test between HTCO *and* LTO *methods*

In order to check the oxidation capacity between the two C analyzers, an intercalibration test was performed using the following standards: potassium biphthalate (Merck p.a.), D-glucose(+) (99% HPLC grade, ACROS), humic acid (Fluka) and phloroglucinol (*1,3,5*-trihydroxybenzene) (Sigma). The results given by the test are shown in Table 1.

3. Results and discussion

The marine area investigated during the three cruises was arbitrarily subdivided into geographical regions to evaluate the effects of the terrestrial inflows. These were: (1) Gulf of Gdansk influenced by the Vistula River (with a maximum discharge in spring: 955 m^3/s; Mikulski, 1970; Voipio, 1981) and by sporadic injection of highly eutrophicated waters from the Wislany lagoon; (2) a coastal area along the Polish coast up to the Pomeranian Bay surveyed in September; (3) a so-called open sea not affected directly by continental waters. For these "zones" and for all the samples from each cruise the correlations between absorption and fluorescence have been considered. The results of these correlations are illustrated in Fig. 4 whilst the regression equations are shown in Table 2. Considering all samples collected at three different depths within the euphothic zone, the plots show high coefficient of

Table 2
Regression equations between absorption at 355 nm (a_{CDOM} 355), and fluorescence F_x, (F_x 355), using the methods described here for the data sets produced during the three oceanographic cruises in 1994 in the southern Baltic Sea

Subset description	Month	Number of samples	Regression equations	Correl. coeff.
Coastal area	Apr.	37	$a_{CDOM}(355) = 0.35(\pm 0.055) + 0.113(\pm 0.003)F_x(355)$	0.98
Gulf of Gdansk	Apr.	32	$a_{CDOM}(355) = 0.22(\pm 0.07) + 0.113(\pm 0.002)F_x(355)$	0.99
Gulf of Gdansk, except for stations 25 and 26	Apr.	27	$a_{CDOM}(355) = 0.43(\pm 0.14) + 0.104(\pm 0.008)F_x(355)$	0.99
All stations	Apr.	92	$a_{CDOM}(355) = 0.32(\pm 0.03) + 0.113(\pm 0.001)F_x(355)$	0.99
All stations	Aug.	97	$a_{CDOM}(355) = 0.54(\pm 0.03) + 0.102(\pm 0.002)F_x(355)$	0.99
Vistula River and river mouths	Aug.	9	$a_{CDOM}(355) = 0.021(\pm 0.42) + 0.116(\pm 0.006)F_x(355)$	0.99
All stations	Sep.	106	$a_{CDOM}(355) = 0.4(\pm 0.068) + 0.116(\pm 0.006)F_x(355)$	0.91
Pomeranian Bay	Sep.	12	$a_{CDOM}(355) = 0.28(\pm 0.58) + 0.127(\pm 0.028)F_x(355)$	0.86

correlation and regression equations have similar coefficients for the three periods despite the fact that quantum yields were different. Average Q.Y. (Table 3) was 1.3 in April, 1 in August and 0.99 in September. The coefficient B (slope), not affected by Q.Y. variations, was shown to be 0.113 in April, 0.102 in August and 0.116 in September whilst the coefficient A (intercept) gave 0.32 in April, 0.54, and 0.40 in August and September. Again considering the selected zones separately, we found no change in the coefficients which are of the same order as the all averaged data. For the subsets of the stations located in the open sea and in the Gulf of Gdansk (in September), no correlation was found, undoubtedly because of the low data variability. The data summarised in Table 4 suggest that CDOM, expressed here as absorption, is slightly variable with season in the open sea of the Baltic Proper, at least within the

Table 3
Averaged quantum yield data and chlorophyll + phaeophytin concentrations

Subset description	Month	Number of samples	Quantum yield (×100)	Chlorophyll [a,b] (mg/m^3)
Vistula River mouth	Apr.	5	1.56 (±0.05)	16.2 (±1.33)
Open sea	Apr.	23	1.23 (±0.07)	5.8 (±2.73)
Coastal area	Apr.	37	1.28 (±0.08)	4.9 (±1.74)
Gulf of Gdansk	Apr.	27	1.36 (±0.12)	8.89 (±4.7)
All stations	Apr.	92	1.3 (±0.1)	7.23 (±7)
All stations	Aug.	56	1 (±0.1)	2.19 (±1.4)
Open sea and other coastal areas	Aug.	18	1.02 (±0.06)	1.77 (±0.74)
Gulf of Gdansk	Aug.	35	0.96 (±0.06)	2.07 (±0.99)
Vistula and river mouths	Aug.	3	0.97 (±0.05)	7.9 (±4.5)
All stations	Sep.	106	0.99 (±0.12)	3.56 (±2.5)
Pomeranian Bay	Sep.	9	1.14 (±0.11)	5.6 (±1.43)
Oder plume [c]	Sep.	3	1.33 (±0.12)	14.3 (±7.5)
Slupia plume [d]	Sep.	20	1.1 (±0.14)	2.36 (±0.56)
Gulf of Gdansk	Sep.	15	0.92 (±0.09)	3.1 (±1.87)
Open sea and other coastal areas	Sep.	59	0.97 (±0.12)	3.19 (±1.1)

[a] Strickland and Parsons (1972) method.
[b] The data can be found in Ooms (1996).
[c] Oder plume refers to the station 13.
[d] Slupia plume refers to the stations 18, 19 and 20.

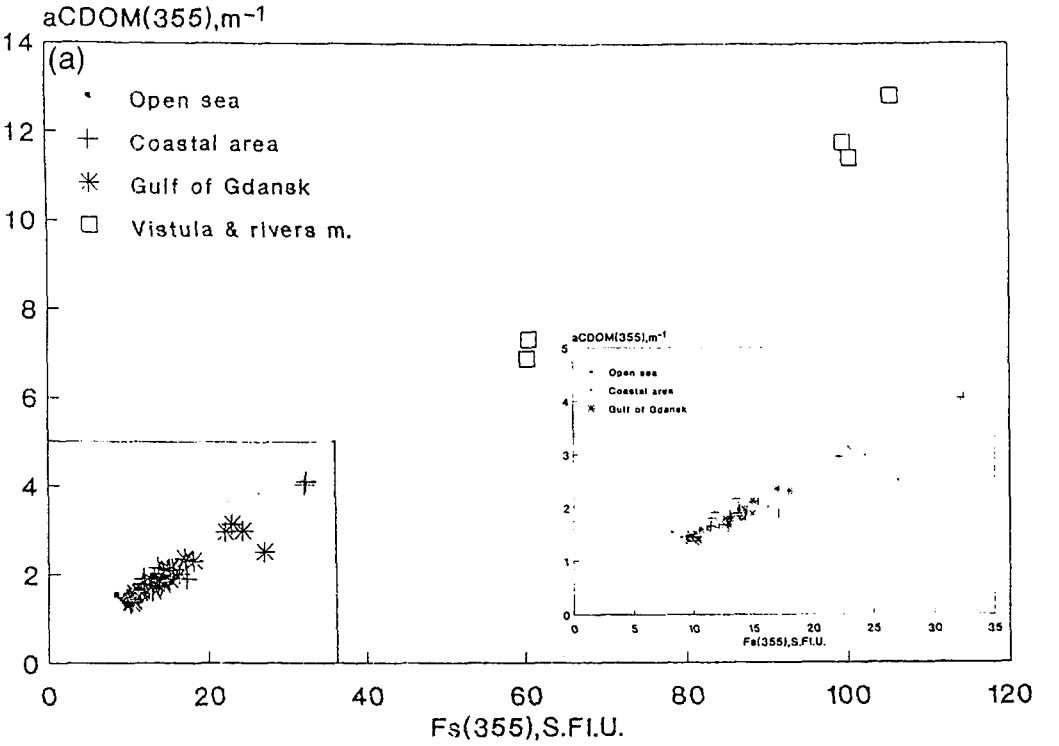
aCDOM(355),m-1
(a)
Open sea
Coastal area
Gulf of Gdansk
Vistula & rivers m.
Fs(355),S.FI.U.

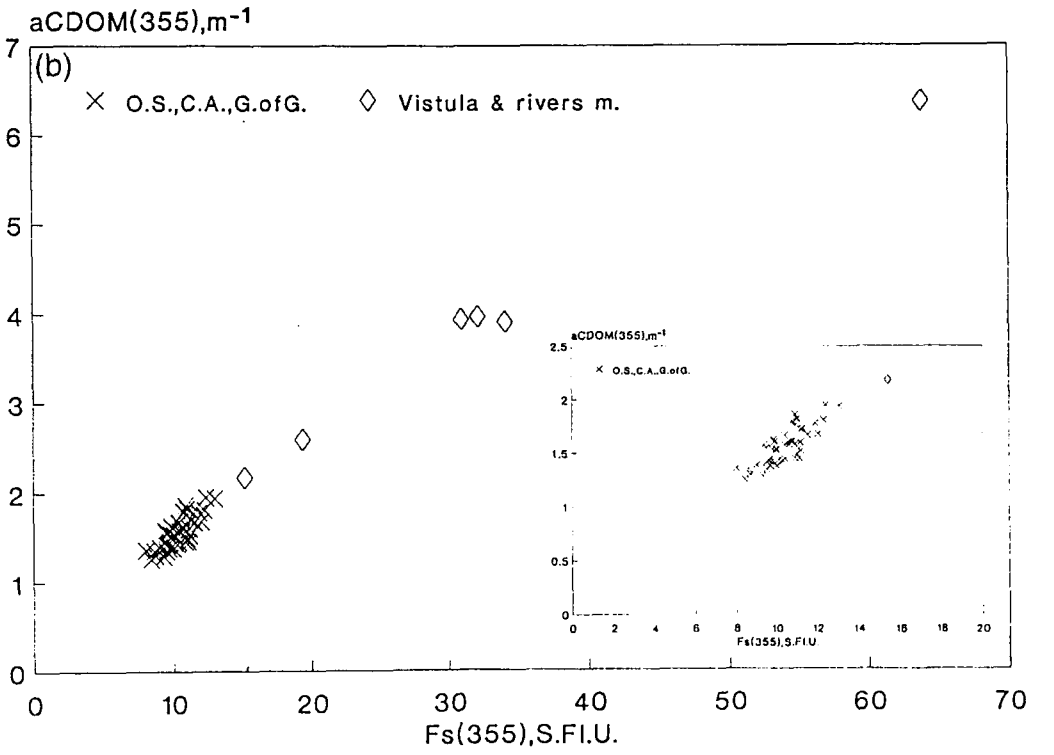
aCDOM(355),m-1
(b)
O.S.,C.A.,G.ofG.
Vistula & rivers m.
Fs(355),S.FI.U.

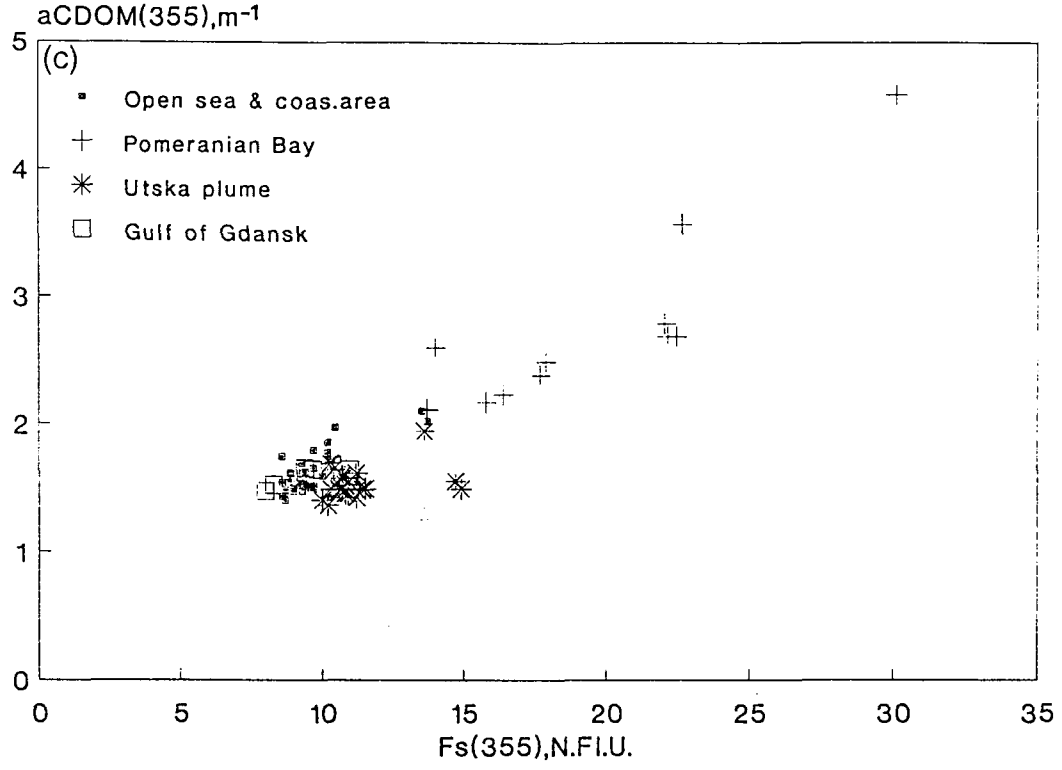

Fig. 4. Correlation plot of absorption coefficient (m^{-1}) of chromophoric dissolved organic matter at 355 nm [$a_{CDOM}(355)$] and fluorescence emission expressed in standardized fluorescence units [Fs(355), S.Fl.U.] (see explanation in the text): (a) April cruise; (b) August cruise; and (c) September cruises.

Table 4
Averaged *a*CDOM(355) values

Subset description	Month	Number of samples	$a_{CDOM}(355)$
Open sea	Apr.	23	1.44 (±0.32)
Coastal area	Apr.	37	1.96 (±0.55)
Gulf of Gdansk	Apr.	32	3.02 (±2.02)
All stations	Apr.	92	2.14 (±1.3)
All stations	Aug.	93	1.73 (±0.5)
Gulf of Gdansk	Aug.	59	1.77 (±0.22)
Vistula River and river mouths	Aug.	9	3.4 (±1.4)
Open sea	Aug.	25	1.4 (±0.08)
All stations	Sep.	106	1.75 (±0.45)
Pomeranian Bay	Sep.	12	2.67 (±0.67)
Slupia plume	Sep.	20	1.53 (±0.12)
Gulf of Gdansk	Sep.	15	1.77 (±0.27)
Open sea	Sep.	18	1.54 (±0.06)
Coastal area	Sep.	41	1.62 (±0.18)

investigated area. The strong contributions of all the river discharges (large and small) as well as marshes and lagoons affect marine CDOM in the coastal areas only in the spring when precipitation increases the land drainage both along the Polish forested coast and in the large drainage basin (agricultural and industrialised zone) of the Vistula River. Højerslev (1988) observed that substantial change in amount of suspended matter causes no significant change in CDOM concentration determined optically. He further stated that autochthonous CDOM formation in the region is negligible compared to the existing background concentration. The Q.Y. variability is mainly seasonal, linked to the algal blooms induced by the solar irradiation and by the full vertical circulation in the water column as well as, in

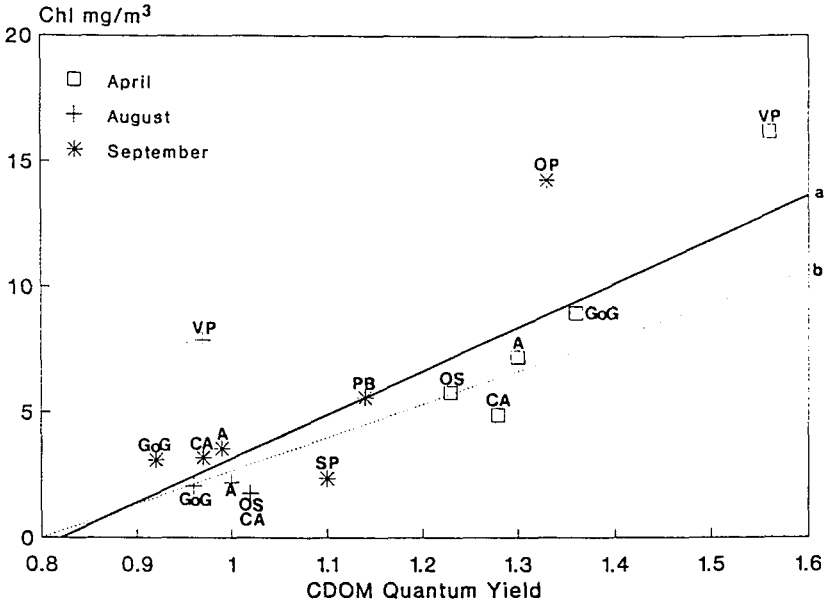

Fig. 5. Correlation plot of CDOM quantum yield (average) with the average chlorophyll-like pigment concentration for homogeneous subsets of data (Table 3). The symbols in the graph represent: *VP* = Vistula plume; *OP* = Oder plume; *GoG* = Gulf of Gdansk; *OS* = open sea; *PB* = Pomeranian Bay; *CA* = coastal area; *SP* = Slupia plume; *A* = average of the cruise. Line *a* expresses the best fit for all the points, line *b* the best fit excluding the Vistula and Oder plume stations.

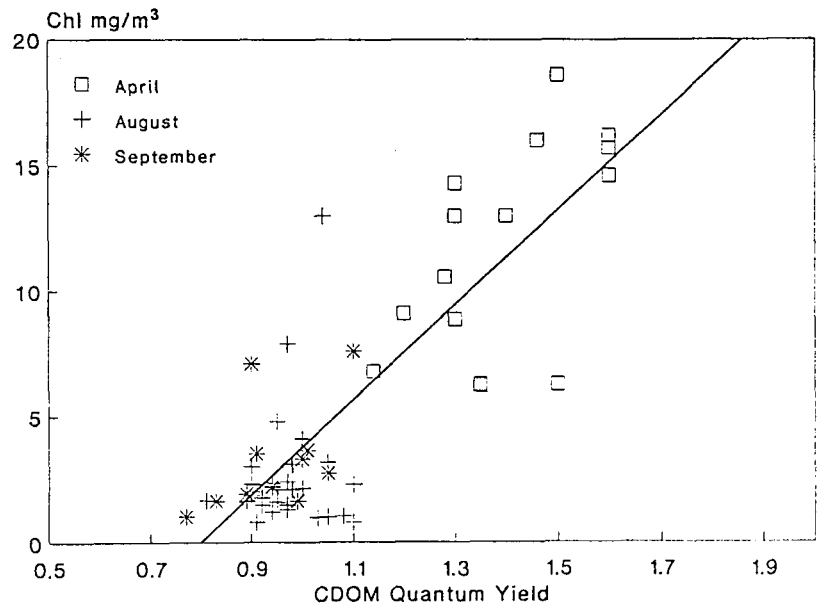

Fig. 6. Correlation plot and best-fit line between CDOM quantum yieldand chlorophyll-like pigment concentration for the Gulf of Gdansk. All samples for all cruises.

the Gulf of Gdansk and in the coastal zones, by nutrients and by fluorescent material transported by the rivers (see Vistula and river mouths in Fig. 4a and b).

Q.Y. affects only slightly the regression curves of a_{CDOM} vs. Fs. A positive correlation between average Q.Y. and the respective average of chlorophyll concentrations for the homogeneous zones was found as illustrated in Table 3. Fig. 5 shows two best-fit lines:

(a) for all the averages, with the regression equation:

$$[\text{Chl}] = -15.5(\pm 4.3) + 8.8(\pm 3.7)\ [\text{Q.Y.}]$$

with $r = 0.82$

(b) excluding Vistula and Oder plume stations, with the regression equation:

$$[\text{Chl}] = -10.2(\pm 2.6) + 13.1(\pm 2.3)\ [\text{Q.Y.}]$$

with $r = 0.87$

Fig. 5 seems to infer that dissolved matter with high Q.Y. (high fluorescence with respect to absorption) is frequent in spring during the intense algal growth and high continental inputs. If we use the individual data, we find a positive and significant correlation for the Gulf of Gdansk for all the seasons (Fig. 6) with the expression:

$$[\text{Chl}] = -15.3(\pm 1.9) + 19.0(\pm 1.7)\ [\text{Q.Y.}]$$

with $r = 0.82$

which is similar to the fit line *a* in Fig. 5. Due to the low variability of the parameters, no correlation has been found for the subset open-sea and coastal areas ($r = 0.53$ and 0.3, respectively).

The differences in DOC concentration found between HTCO and LTO methods are −33% for April, −21% for August and −22% for September. These differences are real and cannot be attributed to systematic sample contamination or analytical errors. The blanks were performed accurately and subtracted from the HTCO measurements. Excluding these effects, the differences can only be ascribed to the different oxidative capacity of the instruments with respect to the chemical structure of the dissolved organic matter. The intercalibration test (Table 1) has shown that potassium phthalate and glucose gave the same results while for the humic acid and the phloroglucinol we obtained from −20% to 26% and −32%, respectively, as difference between HTCO and LTO methods. The presence of considerable amount of dissolved humic matter of continental origin and substances of algal exudation or decay, may explain the DOC differences found especially in April during the strong river inflows and the intense algal growth. In addition to the dissolved humic matter, among the substances of algal production, the polyphenols are highly fluorescent, and thus explain the high quantum yield found in April (Table 3). Highly fluorescent substances in algal exudates and algal decay have been identified by several authors

Table 5
Averaged DOC (HTCO, LTO and DOC_{res}) concentations for the three cruises

Subset of description	Month	DOC HTCO	Number of samples	DOC LTO	Number of samples	DOC_{res}
Open sea	Apr.	435 (±54)	23	–	–	–
Coastal area	Apr.	488 (±45)	37	–	–	–
Gulf of Gdansk	Apr.	543 (±142)	32	–	–	–
All stations	Apr.	491 (±88)	92	341 (±105)	17	186 (±59)
All stations	Aug.	503 (±66)	60	400 (±72)	20	114 (±62)
Vistula River and river mouths	Aug.	616 (±82)	9	–	–	–
All stations	Sep.	474 (±51)	98	367 (±38)	29	102 (±40)
Pomeranian Bay	Sep.	529 (±58)	12	–	–	–
Slupia plume	Sep.	465 (±38)	16	–	–	–
Gulf of Gdansk	Sep.	438 (±31)	13	–	–	–
Open sea and other coastal areas	Sep.	472 (±46)	57	–	–	–

DOC_{res} = (DOC HTCO) − (DOC LTO).

(Craig and McLachlan, 1964; Sieburth and Jensen, 1969; Hellebust, 1974; Ferrari and Mingazzini, 1995). During the summer, under high solar irradiance, these substances can be photoalterated to less fluorescent products (Kouassi and Zika, 1990).

Average concentrations of DOC obtained both by the HTCO and LTO methods and the regression equations derived from the correlation with a_{CDOM} at 355 nm are presented in Tables 5 and 6, while Fig. 7a and b shows the dependency between the cited

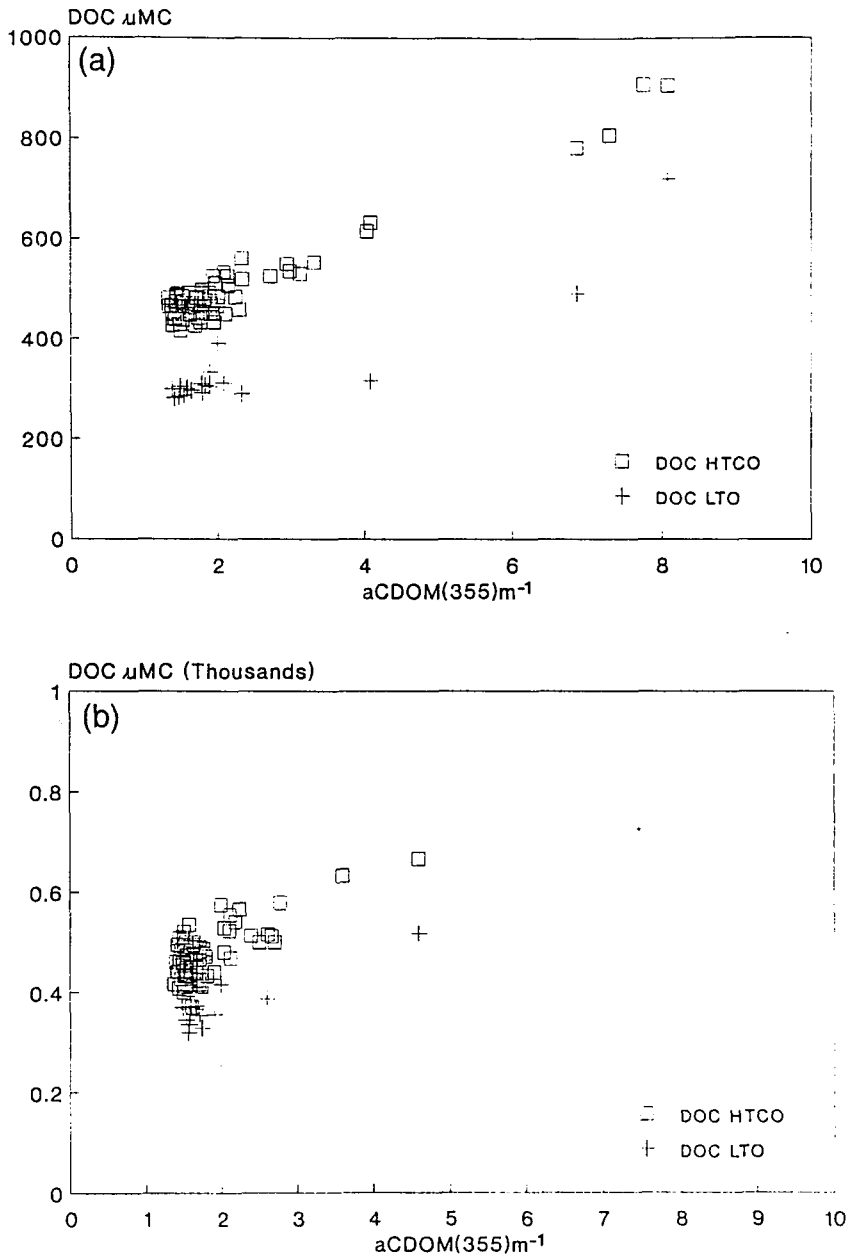

Fig. 7. a. Correlation plot of $a_{CDOM}(355)$ and DOC (μM C) measured by HTCO and LTO for April cruise.
b. The same for the September cruise.

Table 6
Regression equations between DOC concentration (HTCO and LTO) and $a_{CDOM}(355)$ for April and September cruises

Subset description	Month	Regression equation	Coeff. of corr., r
All stations	Apr.	DOC HTCO (μM C) = 357.3($\pm$5.13) + 64.9($\pm$2.03)$a_{CDOM}(355)$	0.90
All stations	Apr.	DOC LTO (μM C) = 211.6($\pm$18.3) + 50.9($\pm$5.8)$a_{CDOM}(355)$	0.96
All stations	Sep.	DOC HTCO (μM C) = 343.6($\pm$13.7) + 73.2($\pm$7.7)$a_{CDOM}(355)$	0.70
All stations	Sep.	DOC LTO (μM C) = 282.6($\pm$18.1) + 49.1($\pm$9.06)$a_{CDOM}(355)$	0.81

parameters for April and September surveys, respectively. For the August cruise the low variability in absorption of the sample population does not provide a regression line with an acceptable coefficient of correlation. However, if we superimpose the data points on the regression lines derived for the others two cruises, we observe that they appear to coincide with the best-fit lines identified for these data sets and therefore are considered as belonging to the same distribution (Fig. 8). The coefficient of correlation for HTCO and LTO are good for April (0.96 and 0.81, respectively) and acceptable for September (0.7 and 0.81, respectively) while the parameters A and B are similar for HTCO and different in the intercept for LTO (Table 6). This could mean that DOC obtained via HTCO can be estimated using the absorption (or fluorescence) properties of a small part of the total DOC. Furthermore, given that the average intercept derived by the linear expressions (Table 6) is 350 μM C, the non-absorbing/fluorescent (in the UV–visible range) DOC represents ~ 70% of the total DOC considered as an average of 214 observations for the whole survey performed. Similar results, in terms of fraction of non-absorbing DOC, were found by Vodacek et al. (1995) along a transect extending from the mouth of the Delaware Bay southeast to the Sargasso Sea.

Among the non-absorbing DOC substances, urea and sugars may represent the main fraction. Carbohydrates constitute the main part (up to 35%) of

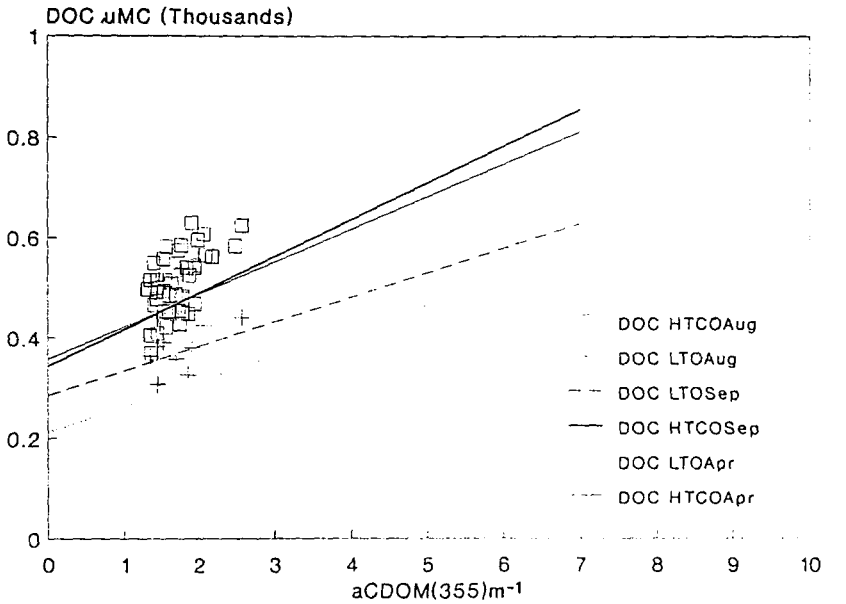

Fig. 8. Plot showing the best-fit lines for the correlation between $a_{CDOM}(355)$ and DOC (HTCO and LTO) for April and September where the points distribution of August is superimposed.

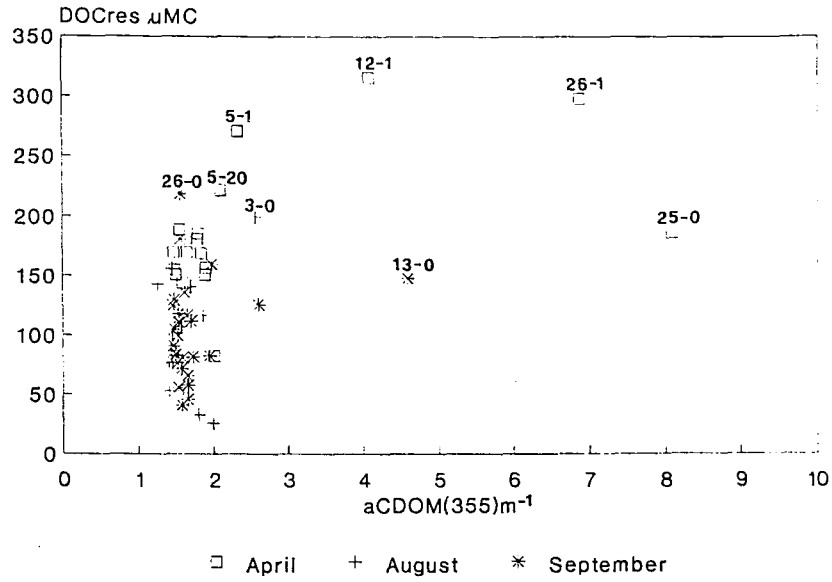

Fig. 9. Plot of the DOC_{res} with $a_{CDOM}(355)$ for all the stations where DOC LTO was measured.

dissolved organic matter (Benner et al., 1992) while monosaccharides contribute 35–50% of the dissolved carbohydrates. From HPLC specific measurements, dissolved monosaccharides seem dominated, in the Baltic Sea region, by glucose and fructose (Kerstan, 1994) which are not absorbing in the UV–visible region (350–750 nm).

The regression curves between a_{CDOM} and DOC obtained by LTO, present the same slope but different intercepts such as 211 and 282 μM C for April and September, respectively. This implies that the DOC LTO fraction represents a higher specific absorption in April with respect to September, when the averaged DOC LTO concentration is more or less the same as in August. Given that the samples have been collected only in the surface and within the euphotic layer, DOC LTO of September could be constituted by low or even non-absorbing biologically utilizable compounds such as sugars, urea, amino-acids, resulting also from photodegradation, rather than humic-type high-absorbing/fluorescent material dominant in brackish/fresh waters and in the deep marine waters (Druffel et al., 1989).

DOC_{res} appears to be uncorrelated with a_{CDOM} at 355 nm (Fig. 9). Because of the large continental contributions in April by the rivers of the forested Polish coast, by the Vistula River and Wislany lagoon, DOC_{res} is particularly high (as shown in Fig. 8) and represents the 33% of the total DOC measured (HTCO) in April whereas in August and September it is only ~ 20%. Interestingly the high value associated with the Wislany lagoon is possibly explained by a localised coastal jet characterised by a highly concentrated filaments visible on CZCS and AVHRR imagery and caused by the sporadic output of optically active material from the otherwise semi-stagnant lagoon (Semovski et al., 1995).

4. Conclusions

Despite the seasonal variability of the water column and the various geographical regions tested in the southern Baltic Proper, fluorescence, which is a more sensitive measurement than absorption and which could be acquired with good accuracy by airborne lidar active remote sensing (Hoge et al., 1993; Vodacek et al., 1995), has been shown to be useful for retrieving CDOM absorption coefficient in the Baltic Sea. Fluorescence quantum yield variations do not significantly affect the regression curves derived by the best fit. At this point the question remain as to whether or not CDOM absorption in the Baltic Sea can correctly predict DOC concentration

which is the most important parameter for marine carbon cycle studies. This study has shown that > 70% of the DOC measured by HTCO displays negligible absorption in the UV–visible range (350–750 nm). The non-absorbing carbon levels have been found to be similar both in spring during full vertical mixing of the water column and in late summer during stratified conditions. This invariant non-absorbing DOC allows the use of the remaining absorbing part to estimate total DOC. DOC, obtained with LTO method, correlates well with CDOM absorption/fluorescence but the non-absorbing DOC LTO varies with the season. It increases from the 62% (40–80%) in April to 76% (67–85%) in September according to the minor contribution of continental high-absorbing humic substances (high in spring) and to the increased presence of low-molecular-weight simple non-absorbing material produced by photodegradation. For this reason DOC LTO could be retrieved by optical methods, taking into account its seasonal behaviour that must be confirmed by further seasonal surveys in sites influenced by different continental sources. DOC_{res} concentration does not show dependence on light absorption and it seems linked to seasonal conditions. It is not clear, and is a planned area for future studies, if its diminution in summer is due to an increased microbial uptake (Carlucci et al., 1986; Kirchman et al., 1991) or to a reduced continental inflow. Further studies on the arguments treated in this article, will be addressed by the separation of absorbing and non-absorbing DOC using ultrafiltration and by subsequent biochemical analysis to determine the fraction available for the biological cycle.

Acknowledgements

The field work was carried out on board R.V. "Oceania" as part of a collaboration between the Institute of Oceanology, Polish Academy of Science, and the Institute for Remote Sensing Application, JRC Ispra. The authors would like to thank S. Kaczmarek, the captain and the crew of the R.V. "Oceania" for their support during the cruises. We also thank R. Hapter and M. Ostrowska for the chlorophyll analyses, F. Bo and R. D'Ippolito for the DOC measurements.

References

Benner, R., Pakulski, J.D., McCarthy, M., Hedges, J.I. and Hatcher, P.G., 1992. Bulk chemical characteristics of dissolved organic matter in the ocean. Science, 255: 1561–1564.

Bocastow, R. and Maier-Reimer, E., 1991. Dissolved organic carbon in modelling oceanic new production. Global Biogeochem. Cycles, 5(1): 71–85.

Carlucci, A.F., Shimp, S.L. and Craven, D.B., 1986. Growth characteristics of low-nutrient bacteria from the north-east and central Pacific Ocean. FEMS (Fed. Eur. Microbiol. Soc.) Microb. Ecol., 38: 1–10.

Chen, W., 1992. The measurement, production, and degradation of marine dissolved organic matter. Ph.D. Dissertation, Dalhousie University, Halifax, N.S.

Craig, J.S. and McLachlan, J., 1964. Excretion of coloured ultraviolet absorbing substances by marine algae. Can. J. Bot., 42: 23–33.

Druffel, E.R.M., Williams, P.M. and Suzuki, Y., 1989. Concentration and radiocarbon signatures of dissolved organic matter in the Pacific Ocean. Geophys. Res. Lett., 16: 991–994.

Ferrari, G.M. (Editor), 1990. Napoli 88 — Data catalogue. Comm. Eur. Commun., Joint Res. Cent., Ispra, S.P.I. 9015.

Ferrari, G.M. and Mingazzini, M., 1995. Synchronous fluorescence spectra of dissolved organic matter (DOM) of algal origin in marine coastal waters. Mar. Ecol. Progr. Ser., 125: 305–315.

Ferrari, G.M. and Tassan, S., 1991. On the accuracy of determining light absorption by "yellow substance" through measurement of induced fluorescence. Limnol. Oceanogr., 36(4): 777–786.

Green, S.A., 1992. Application of fluorescence spectroscopy to environmental chemistry. Ph.D. Thesis, Massachusetts Institute of Technology/Woods Hole Oceanographic Institution, Woods Hole, MA, Joint Prog. Oceanogr.

Green, S.A. and Blough, N.V., 1994. Optical absorption and fluorescence properties of chromophoric dissolved organic matter in natural waters. Limnol. Oceanogr., 39: 1903–1916.

Hedges, J.I. and Bergamaschi, B.A., 1992. Seawater carbon measurement. Nature (London), 339: 202.

Hellebust, J.A., 1974. Extracellular products. In: Steward N.D. (Editor), Algal Physiology and Biochemistry. University of California Press, Berkeley, CA, pp. 838–863.

Hoge, F.E., Vodacek, A. and Blough, N.V., 1993. Inherent optical properties of the ocean: retrieval of the absorption coefficient of chromophoric dissolved organic matter from fluorescence measurement. Limnol. Oceanogr., 38: 1394–1402.

Højerslev, N.K., 1988. Natural occurrence and optical effects of Gelbstoff. Copenhagen Univ., Geophys. Inst., Rep. No. 50.

Jackson, A.G., 1993. The importance of the DOC pool for primary production estimates. ICES Mar. Sci. Symp., 197: 141–148

Kaplan, L.A., 1992. Comparison of high-temperature and persulphate oxidation methods for determination of dissolved organic carbon in fresh waters. Limnol. Oceanogr., 37: 1119–1125.

Kerstan, E., 1994. Carbohydrates in the Baltic Sea. Proc. 15th Conf. on Baltic Oceanography, Sopot.

Kieber, R.J., Zhou, X. and Mopper, K., 1990. Formation of carbonyl compounds from UV-induced photodegradation of humic substances in natural waters: Fate of riverine carbon in the sea. Limnol. Oceanogr., 35: 1503–1515.

Kirchman, D.L., Suzuki, Y., Garside, C. and Ducklow, H., 1991. High turnover rate of dissolved organic carbon during spring phytoplankton bloom. Nature (London), 352: 612–614.

Kouassi, A.M. and Zika, R.G., 1990. Light-induced alteration of the photophysical properties of dissolved organic matter in seawater. Part I. Estimates of the environmental rates of the water fluorescence. Neth. J. Sea Res., 27(1): 25–32.

Menzel, D.W. and Vaccaro, R.F., 1964. The measurement of dissolved organic and particulate carbon in seawater. Woods Hole Oceanogr. Inst., Woods Hole, MA, Contrib. No. 1921.

Mikulski, Z., 1970. Inflow of river water to the Baltic Sea in the period 1951–1960. Nord. Hydrol., 4: 216–227.

Miller, W.L., 1994. Recent advances in the photochemistry of the natural dissolved organic matter, pp. 111–127. In: G.R. Helz et al. (Editors), Aquatic Sea Surface Photochemistry. Lewis, Boca Raton, FL.

Mopper, K. and Schultz, C.A., 1993. Fluorescence as a possible tool for studying the nature and water column distribution of DOC components. Mar. Chem., 41: 229–238.

Ooms, M.C. (Editor), 1996. Ulisse — Baltic 93–94 data catalogue. Comm. Eur. Commun., Joint Res. Cent., Ispra (in press).

Semovski, S.V., Hapter, R., Beszczyñska-Möller, A. Walczowsky, W., Darecki, M., Szczucka, J., Dowell, M.D. and Staoekiewicz, A., 1995. Remote sensing of mesoscale features in the Baltic coastal phytoplankton field: an analysis of the incorporation of contact observations and models. Proc. 3th Thematic Conf. on Remote Sensing for Marine and Coastal Environments, Seattle, WA, 18–20 Sept. 1995.

Sharp, J.H., 1993. The dissolved organic carbon controversy: An update. Oceanography, 6(2): 45–50.

Sieburth, J. and Jensen, A., 1969. Studies of algal substances in the sea, II. The formation of Gelbstoff (humic material) by exudates of phaeophyta. J. Exp. Mar. Biol. Ecol., 3: 275–289.

Strickland, J.D. and Parsons, T.R. 1972. A practical handbook of sea-water analysis. Bull. Fish. Res. Board Can., No. 167.

Suzuki, Y. and Tanoue, E., 1991. Dissolved organic carbon enigma — implication for ocean margin. In: R.C.F. Mantoura, J.M. Martin and R. Wollast (Editors), Ocean Margin Processes in Global Change. Dahlem Workshop, Wiley, New York, NY, pp. 18–23.

Tassan, S. and Ferrari, G.M., 1995. An alternative approach to absorption measurements of aquatic particle retained on filters. Limnol. Oceanogr., 40(8): 1358–1368.

Valentine, R.L. and Zepp, R.G., 1993. Formation of carbon monoxide from photodegradation of terrestrial dissolved organic carbon in natural waters. Environ. Sci. Technol., 27: 409–412.

Vodacek, A., Hoge, F.E., Swift, R.N., Yungel, J.K., Peltrer, E.T. and Blough, N.V., 1995. The use of in situ airborne fluorescence measurements to determine UV absorption coefficient and DOC concentration in surface waters. Limnol. Oceanogr., 40 (2): 411–415.

Voipio, A., 1981. The Baltic Sea. Elsevier, Amsterdam, 418 pp. (see especially p.125).

Appendix 2.B

Estuarine, Coastal and Shelf Science (1998) 47, 91–105
Article No. ec970309

CDOM Absorption Characteristics with Relation to Fluorescence and Salinity in Coastal Areas of the Southern Baltic Sea

G. M. Ferrari[a] and M. D. Dowell[b,c]

[a]*Space Application Institute, Marine Environment Unit, Joint Research Centre, Ispra, Italy*
[b]*Department of Oceanography, University of Southampton, U.K.*

Received 30 July 1997 and accepted in revised form 27 October 1997

Chromophoric dissolved organic matter (CDOM) absorption measurements and their relationship with fluorescence and salinity are presented for a highly dynamic coastal environment. The results were obtained in the context of seasonal cruises in 1994 in the southern Baltic Sea. They encompass the large gradient of geophysical parameters existing in the environment considered.

Comparison of different methods for the normalization of CDOM fluorescence are considered. The method suggested here gives a linear relationship between fluorescence and absorption for the whole data set, where CDOM absorption has a range of 1·4–12·8 m^{-1} with an average of 2·26 m^{-1} at 355 nm. Establishing CDOM absorption and fluorescence relationships is useful because absorption could therefore be inferred from fluorescence measurements which can be acquired more rapidly and with greater sensitivity than absorption.

A significant relationship was identified between CDOM absorption and salinity in surface waters. The dependency of these two variables is especially evident in spring during periods of vertical mixing and large input from continental runoff, reflecting the potential of CDOM absorption to be used as a passive tracer of freshwater input. Accurate CDOM absorption measurements are also of use in the definition of remote sensing algorithms and in reflectance and model development and validation.

Keywords: fluorescence; salinity; CDOM; remote sensing; Baltic Sea

Introduction

Chromophoric dissolved organic matter (CDOM) is the main contributor to light absorption, in the blue region of the spectrum, in the Baltic Sea (Højerslev, 1988). This contribution implies that the active radiation available for the phytoplankton is greatly reduced. Furthermore these circumstances are detrimental to the accurate determination of chlorophyll by ocean colour satellite sensors (Tassan, 1988; Carder *et al.*, 1989; 1991; Ferrari & Tassan, 1992). Moreover, CDOM absorption coefficient has been retrieved during winter, in low chlorophyll conditions, in the Middle Atlantic Bight using historical CZCS data by Hoge *et al.* (1995). The ocean remote sensing (R/S) community has recently focused much attention on the study of marginal and semi-enclosed basins, which often show anomalous and unique geophysical and hydrographical properties (Victorov, 1996). To accommodate for the special requirements of these regions, specific or local algorithms must be formulated. In order to develop and validate these local R/S algorithms for the next generation of sensors (SeaWiFS, OCTS, MOS, MODIS and MERIS), a detailed and precise series of CDOM measurements has been made in the Polish coastal region of the Baltic Sea. The absorption coefficient of CDOM is typically evaluated at a specific wavelength, λ (e.g. 355 nm coinciding with the currently used pulsed frequency tripled Nd:YAG excitation laser) using:

$$\mathrm{aCDOM}(\lambda) = \mathrm{aCDOM}(\lambda o) \times e^{S(\lambda - \lambda o)} \qquad (1)$$

where aCDOM is expressed in m^{-1} and S (nm^{-1}) is the spectral slope dependent on the type of CDOM present (Kieber *et al.*, 1990; Green & Blough, 1994). The absolute quantity of CDOM (in terms of mg l^{-1}) is not usually required in R/S algorithm studies, although initial attempts of CDOM quantification were coincidentally made in the Baltic Sea (Nyquist, 1979). The authors have chosen to present their CDOM quantities in optical units as currently adopted by the R/S community. Many current bio-optical models of oceanic/coastal waters for

[c]Present address: Marine Environment Unit, Space Application Institute, Joint Research Centre, Ispra, Italy.

0272-7714/98/010091+15 $30.00/0

quantifying chlorophyll in the presence of CDOM involved the separate estimation of CDOM absorption (Carder *et al.*, 1991; Lee *et al.*, 1994, 1996). Chromophoric dissolved organic matter absorption can be an important parameter for predicting dissolved organic carbon (DOC) concentration in the water column when the relationship between the two parameters exists and it is known. According to Stewart and Wetzel (1981), absorption alone provides correct predictions of DOC for labile materials (with low molecular weight). Other optical parameters, such as fluorescence, are poor predictors due to the greater level of internal quenching and shielding in compounds of a larger apparent molecular weight. Dissolved organic carbon is recognized as a significant contributor in present carbon exchange models of water productivity (Bacastow & Maier-Reimer, 1991; Jackson, 1993), especially relating to the fraction of DOC used as nutrients. As reported in recent work (Ferrari *et al.*, 1996), a good relationship between CDOM absorption (355 nm) and DOC has been found in the southern Baltic Sea despite the fact that the majority of DOC (up to 70%) does not absorb light in UV visible range.

The adsorption of CDOM may be measured directly using a spectrophotometer or may be inferred from fluorescence measurements (which can be acquired more rapidly and with a greater sensitivity than absorption). This technique has been developed and adapted with the use of airborne fluorescence laser-induced measurements in mind (Bristow *et al.*, 1981; Hoge & Swift, 1981; Hoge *et al.*, 1993). A marked and consistent relationship between absorption and emission fluorescence has been found by Hoge *et al.* (1993) for numerous marine areas around the U.S. coastline. This study, as well as other less recent works, shows that despite the numerous sources of CDOM and the different characteristics of these sources, there appears to be a consistent and marked correlation between CDOM absorption and fluorescence emission. However, it is important to note that not all of the previous data are directly comparable. This is due to the different methodologies used and, in particular, the use of various radiometric standards. Ferrari and Tassan (1991) used the Raman signal of a separate Milli-Q water sample to normalize the fluorescence measurements whilst Hoge *et al.* (1993) used the fluorescence to Raman peaks ratio of the sample which is further ratioed to an external standard such as quinine sulphate. In the approach discussed by Ferrari and Tassan (1991), the Raman signal of the separate sample was used to allow the instrumental decay to be monitored and regulated (lamps, photo multiplier etc.). Furthermore, in this case, the authors corrected both the Raman and the sample emission signals for the self-absorption of the fluorescent light which is shown to be important at high concentrations.

This study has been focused on different objectives:
(1) To obtain accurate CDOM absorption data at the levels found in the southern Baltic Sea, which are approximately 10 times higher than the values for the U.S. coasts shown by Hoge *et al.* (1993). Additionally, to verify whether the general protocol proposed in the above cited work is applicable to the Baltic Sea waters or if the particular CDOM concentrations found in this sea require a specific procedure.
(2) To investigate the relationship between CDOM absorption and salinity. This relationship is considered as it could prove extremely useful in R/S investigations of coastal zones. The reason for this is that a well-established correlation between an optically active component, quantifiable by R/S techniques, and a physical parameter (i.e. salinity), could therefore be used as a logical indicator of hydrography in those highly dynamic regions.

Site, materials and methods

Biological measurements and particularly CDOM samples were collected in April, August and September 1994 during detailed surveys with a particular orientation towards the development of R/S algorithms. This series of ship campaigns was planned as the result of collaboration between the J.R.C. (Joint Research Centre) in Ispra (Italy) and the P.A.S. (Polish Academy of Science) in Sopot (Poland). The station locations of the two cruises are shown in Figure 1. The sampling was performed in three distinct zones:

(1) Open sea (stations made at a distance over 15 km from the coastline).
(2) Coastal zone (stations made within the 15 km band from the coastline).
(3) Gulf of Gdansk and Pomeranian Bay strongly influenced by the Vistula and the Oder rivers respectively.

These different zones were delimited according to the presumed (different) inputs of CDOM. The geophysical characterization of these different zones and therefore the differentiation of the various CDOM provinces are the objectives of a further investigation. In the open sea, the salinity varies between 7·3 and 7·6. In this zone the CDOM belongs to the pool of the background dissolved organic matter of the Baltic Sea which is a result of the biochemical degradation of organic matter either formed *in situ* or transported. The coastal zone is an area in which the quantities of CDOM are influenced by the input of numerous small

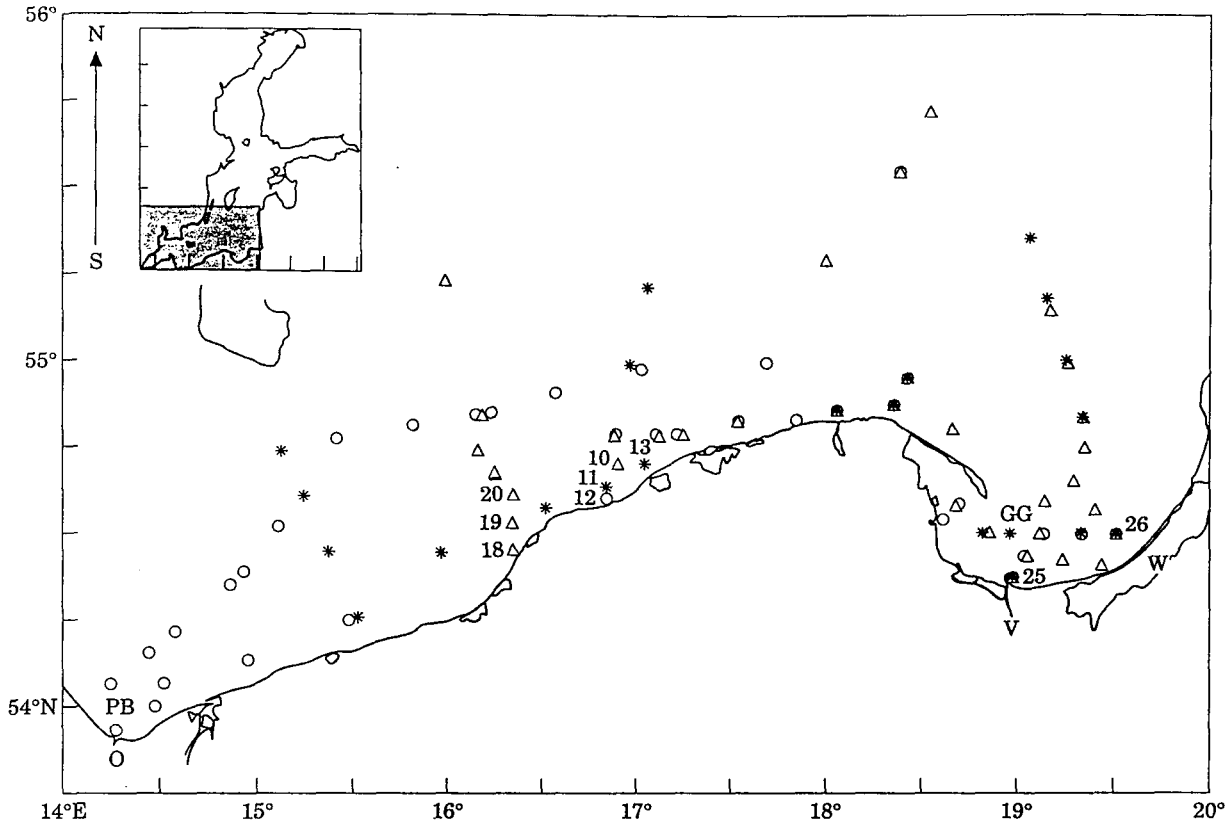

FIGURE 1. Test site (the Baltic Sea) geographic areas covered during the cruise of 1994. PB, Pomeranian Bay; GG, Gulf of Gdansk; O, Oder river; V, Vistula river; W, Wislany lagoon. Stations 10, 11, 12, 13, 25 and 26 of April as well as 18, 19 and 20 of September cruises, cited in the text. *, April; △, August; ○, September 1994.

rivers which drain an intensive coastal forested area. The Gulf of Gdansk and the Pomeranian Bay were separated because of its unique CDOM properties caused by the high inputs from the river Vistula (mean discharge 954 $m^3\ s^{-1}$), whose large drainage basin (approximately 193 910 km^2 with mean annual runoff of 4·92 $dm^3\ s^{-1}\ km^2$) consists mainly of arable land and industrialized areas (power plants etc.). These zones were identified as logical and justifiable subsets of the whole data set. The cruises were planned in order to survey different biological situations exhibiting the highest gradient possible. Hydrographically the seasonality of the water columns state proved to be also quite diverse. April is clearly characterized by vertical water mixing and extended coastal blooms in the Gulf of Gdansk and in the Pomeranian Bay. In the Gulf of Gdansk, the blooms are produced mainly by diatoms (Witex, 1993). In August and September the marine conditions are affected by greater solar irradiation generating a stratified water column. During this period the influence if river inflows are less important whilst the local precipitation reaches its maximum levels (Ehlin, 1981). Less affected by continental inputs during this period, the primary production appears distributed, within the basin, in small but well-identifiable bloom distributions as shown in monthly colour composites from historical CZCS data (1979–1985) for the southern Baltic Sea.

During all cruises, salinity was acquired with a Guildline 87104-CTD. Chromophoric dissolved organic matter absorption samples were collected using a 10 l Nansen bottle at a minimum of three depths. These samples were then filtered through 0·22 μm Millipore membrane and the filtrate was stored in glass ambered bottles. An inhibitor of aerobic bacterial growth (0·1 ml of 10 mg l^{-1} Na N_3) was added to the samples, which were stored in a dark environment at 4 °C. The absorption measurements were performed within 1 week of the end of the campaign in accordance with guidelines set down following storage test results as described by Ferrari (1990). The filtrates of the 0·22 μm membrane were also used for the fluorescence emission measurements, which were performed directly on board the vessel. These fluorescence measurements were made using a Perkin Elmer LS-50 spectrofluorimeter.

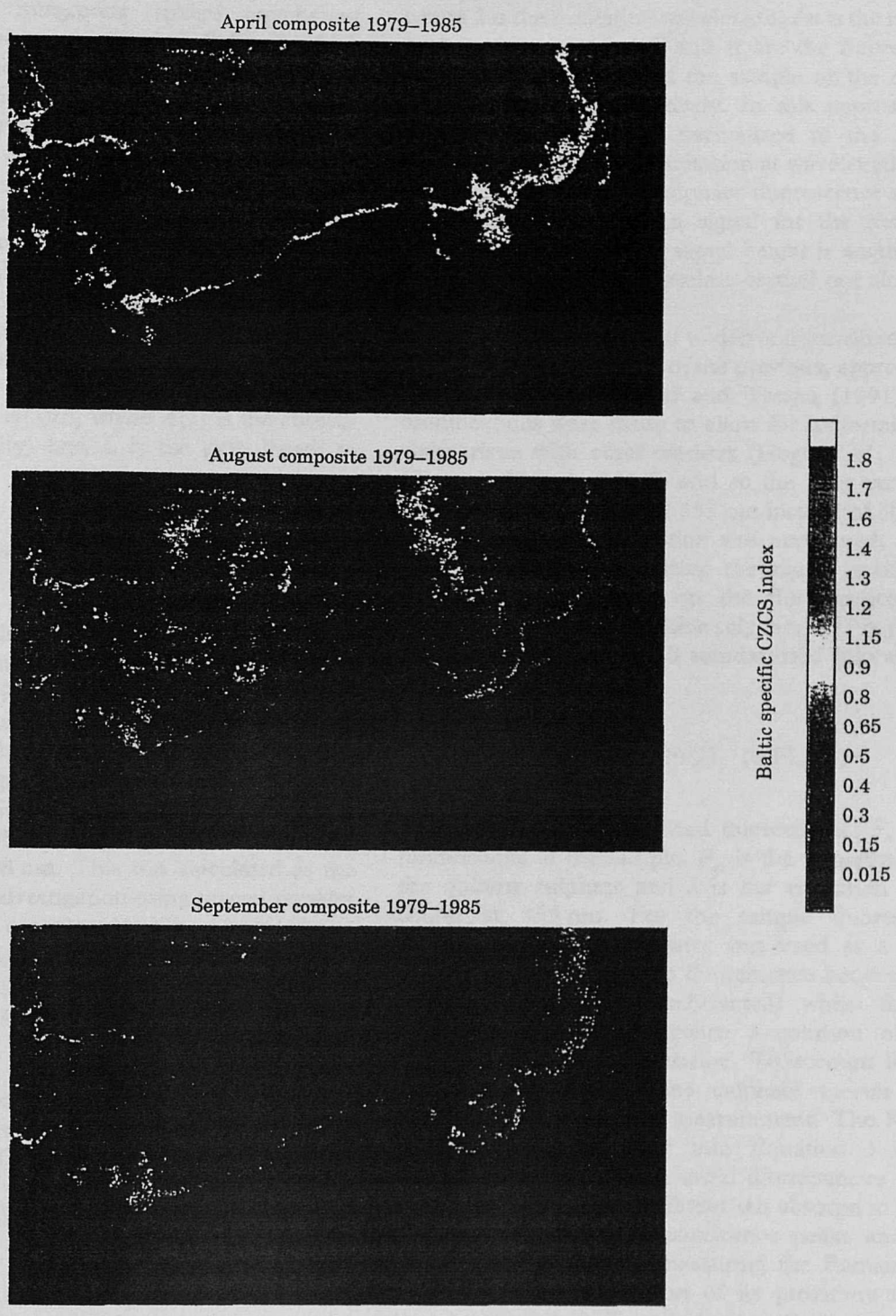

FIGURE 2. CZCS colour composite historical data (1979–1985) for southern Baltic Sea of April, August and September. The colour scale indicates chlorophyll-like pigment concentration obtained with conventional algorithms (Sturm, 1993).

Absorption measurements

The samples of CDOM filtered through 0·22 μm membranes with addition of NaN_3 were transported from the harbour in Gdansk to the J. R. C. in Ispra. A Perkin Elmer Lambda 19 dual beam spectrophotometer was used to retrieve the absorption spectra of the samples. The instrument is equipped with a

60 mm diameter integrating sphere attachment supplied with a photomultiplier and PbS cell which permits measurements in the spectral range 200–2500 nm. Correction for the difference in beam efficiency is performed automatically. Both 4 and 10 cm quartz cells were used to analyse the samples, with Milli-Q water as the blank. In this case the Lambda 19 unit was used in the range 300–750 nm, with a spectral resolution of 1 nm. A comparison of the results shows that the values obtained using the standard compartment without integrating sphere and the 10 cm quartz cell show no significant difference. Absorbance was converted into absorption coefficient (m-1) using the expression $aCDOM(\lambda)=2{\cdot}3 \times A(\lambda)/L$, where $A(\lambda)$ is the absorbance (optical density) and L is the path length in metres.

Fluorescence measurements

In order to be able to compare the present data with others reported in literature, a fluorescence excitation wavelength at 355 nm was used. This was identified by Hoge *et al.* (1993) as the most suitable band corresponding to high power pulsed UV laser line available both for shipboard and airborne laser fluorescence spectroscopy. However, it is important to emphasize that the ideal excitation wavelength, that is the wavelength at which the most efficient emission is associated, is at 308 nm. This was calculated as the result of a prescan investigation using several samples of natural dissolved organic matter in seawater. Emission fluorescence measurements were performed, immediately after sampling, with a Perkin Elmer LS 50 installed on board the vessel. The instrument has a xenon pulsed lamp and the excitation band is automatically corrected with a reference photomultiplier supplied with a rhodomine dye correction curve. The spectral ranges of the instrument are 200–800 nm and 200–900 nm for the excitation and emission monochromators, respectively. The wavelength reproducibility is 0·5 nm.

Fluorescence data analysis

The analysis followed two methods:

(1) The fluorescence standardization developed by Hoge *et al.* (1993), which uses a solution of 0·01 mg l^{-1} of quinine (qs) in 1 N H_2SO_4 is defined as 10 normalized fluorescence units (N.FL.U.) and is expressed by the formula:

$$([F_s/R_s]/[F_{qs}/R_{qs}]) \times 10 = Fn(\lambda) \quad \text{(N.FL.U.)} \qquad (2)$$

where λ is the excitation wavelength, Fn is the normalized fluorescence and F and R are the fluorescence and the Raman signal of the sample or the quinine sulphate sample, respectively. In this approach the CDOM fluorescence is normalized to the Raman signal generated by the excitation at wavelength λ and relative to the quinine sulphate fluorescence as normalized to water Raman signal for the excitation wavelength. The Raman signal height is acquired by an interpolation of the baseline carried out along the tail of the main peak.

(2) The second method to derive normalized fluorescence is a modification of the previous, approaching that described by Ferrari and Tassan (1991). The modifications were made to allow for uniformity, the comparison with other workers (Hoge *et al.*, 1993; Green & Blough, 1994), and so the light excitation wavelength was chosen at 355 nm instead of 308 nm. Fluorescence standardization was performed, in this investigation, by normalizing the signal (main peak height at 430–450 nm) on the fluorescence peak height of a solution of quinine sulphate 0·01 mg l^{-1} in 1 N H_2SO_4 defined as 10 standardized fluorescence units (S.FL.U.):

$$(F_s/F_{qs}) \times 10 = Fs(\lambda) \quad \text{(S.FL.U.)} \qquad (3)$$

where Fs is the standardized fluorescence, F_s is the fluorescence of the sample, F_{qs} is the fluorescence of the quinine sulphate and λ is the excitation wavelength at 355 nm. For the sample fluorescence measurements Milli-Q water was used as a blank (the water contribution to fluorescence between 430 and 450 nm was also subtracted) whilst for the quinine sulphate fluorescence a solution of 1 N H_2SO_4 was used as a baseline. To account for the instrumental drift, quinine sulphate spectra were acquired for each day of measurement. The Raman signal is not introduced into Equation 3 as an internal standard so as to avoid discrepancies which would arise due to the different self absorption of the Raman and the main fluorescence peaks and also due to the difficulty in measuring the Raman peak which is distorted because of its proximity to the broad main peak. To avoid this effect, instead of diluting the very high absorbing samples as suggested by Green and Blough (1994), the authors preferred to measure the high fluorescence signal and then to correct it for the superimposed effect of the absorption of the exciting radiation. The method uses the correction factor as suggested by Duursma and Rommet (1961) and described by Ferrari and Tassan (1991).

Results

As commented in the introduction, CDOM is the main contributor to light absorption, in the blue region of the spectrum, in the Baltic Sea. The contribution can be illustrated by considering the spectral range 400–500 nm, in which CDOM absorbs approximately three times more than the photosynthetic particles. Figure 3 illustrates absorption spectra averaged from the coastal stations 10, 11 and 13 for the April 1994 cruise. Phytoplankton and detritus absorption were obtained using the *in vivo* technique (Tassan & Ferrari, 1995) while for pure water absorption data was used from the literature (Smith & Baker, 1981).

Table 1 summarizes the CDOM absorption (at 355 nm) data averaged for geographical site and for season, the spectral slopes (S) in the range 355–420 and 400–600 nm, and the salinity values. The general relationship between salinity and CDOM absorption is illustrated in [Figure 4(a)]. The data, considered as a whole, seem not to demonstrate a general conservativity of CDOM; in fact particular stations need to be considered separately such as the mouth of the Wislany Lagoon which is a high productivity basin (see Figures 1 and 2) with high CDOM release in to the Gulf of Gdansk. The CDOM absorption data of August do not display a dependency on salinity since they are probably less affected by continental CDOM inputs. The samples collected at the euphotic depth in the Gulf of Gdansk have low salinity because the halocline (at 20–25 m) coincides with the euphotic depth (Ooms, 1996). Chromophoric dissolved organic matter absorption of 1·1 m^{-1} at 355 nm can be considered as a background level of the Baltic Proper [Figure 4(b)]. The level seems invariant and it has been measured at 100 m (station 5 in the Gulf of Gdansk) in unmixed high density water (8·5 units at

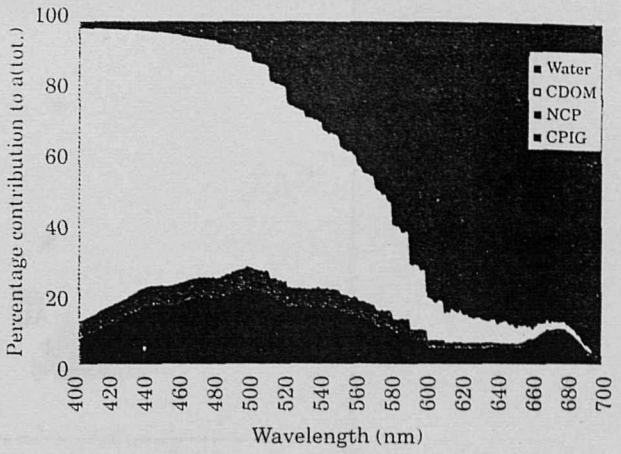

FIGURE 3. Typical coastal water absorption for the southern Baltic Sea illustrating the percentage contribution of optically active components: pure water, chromophoric dissolved organic matter (CDOM), phytoplankton pigments (CPIG) and detritus (NCP), to the total absorption of the water body. Average of stations 10, 11 and 13 of April.

TABLE 1. Lists of stations and parameter statistics: geographic site, sampling period, station number, absorption values, spectral fluorescence values using both methods, absorption values (355 nm), spectral slopes (to be considered as negative) S1, obtained for the wavelength range 355–420 nm, S2 for the range 400–600 nm and the salinity

Subset description	Month (1994)	Number of samples	aCDOM(355) (m^{-1})	S1 (nm^{-1})	S2 (nm^{-1})	Salinity
Open sea	April	23	1·44(±0·32)	0·0199(±0·001)	0·0187(±0·0007)	7·4 (±0·02)
Coastal area	April	37	1·96(±0·55)	0·0193(±0·0007)	0·0184(±0·0008)	7·33(±0·2)
Gulf of Gdansk	April	32	3·02(±2·02)	0·020 (±0·0005)	0·0193(±0·0014)	6·49(±1·35)
All stations	April	92	2·14(±1·3)	0·0197(±0·0008)	0·0189(±0·0008)	7·01(±0·92)
All stations	August	97	1·73(±0·5)	0·0197(±0·0008)	0·0194(±0·0008)	6·62(±0·45)
Gulf of Gdansk	August	63	1·77(±0·22)	0·0199(±0·001)	0·0193(±0·0008)	6·59(±0·35)
Vistula and rivers mouth	August	5	3·40(±1·4)	—	—	—
Open sea and coastal areas	August	25	1·40(±0·08)	0·0201(±0·001)	0·0195(±0·0007)	6·67(±0·57)
All stations	September	106	1·75(±0·45)	0·0180(±0·001)	0·0190(±0·001)	7·14(±0·43)
Pomeranian Bay	September	12	2·67(±0·67)	0·0175(±0·0007)	0·0184(±0·0005)	6·52(±0·69)
Slupia plume	September	20	1·53(±0·12)	0·0187(±0·001)	0·0187(±0·001)	7·21(±0·16)
Gulf of Gdansk	September	15	1·77(±0·27)	0·0175(±0·0013)	0·0192(±0·0012)	6·96(±0·35)
Open sea	September	18	1·54(±0·06)	0·0178(±0·001)	0·0192(±0·0012)	7·5 (±0·15)
Coastal area	September	41	1·62(±0·18)	0·0188(±0·0007)	0·0194(±0·0009)	7·2 (±0·38)

CDOM; chromophoric dissolved organic matter.

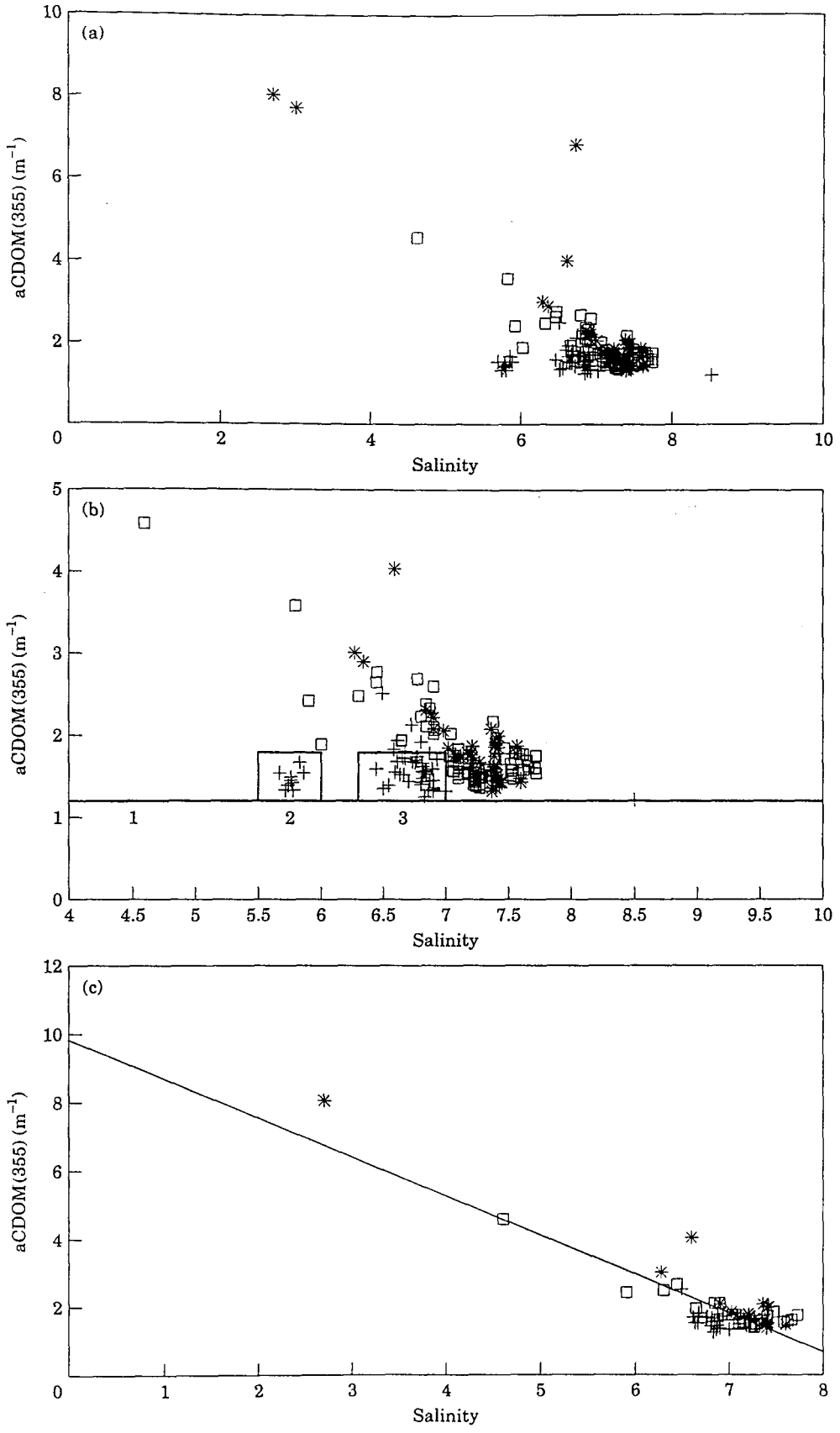

FIGURE 4. (a) Regression plot of aCDOM (355) *vs* salinity for all samples and depths. (b) as (a) excluding the data with aCDOM >5 m^{-1} and indicating: (1) the aCDOM background; (2) the euphotic depth samples (August), and (3) all the samples of August. (c) the same for all the surface samples (r, correlation=0·89). *, April; +, August; □, September 1994. CDOM, chromophoric dissolved organic matter.

TABLE 2. Lists of stations and parameter statistics: geographic site, sampling period, stations number, fluorescence quantum yield and fluorescence values: N.FL.U. obtained with method 1 and S.FL.U. obtained with method 2 as outlined in the text

Subset description	Month (1994)	Number of samples	Quantum yield (× 100)	N.FL.U.	S.FL.U.
Open sea	April	23	1·23(± 0·07)	8·26(± 0·64)	9·79(± 0·39)
Coastal area	April	37	1·28(± 0·08)	11·77(± 4·3)	13·6 (± 4·7)
Gulf of Gdansk	April	32	1·41(± 0·2)	27·3 (± 34·4)	28·37(± 29·2)
All stations	April	92	1·3 (± 0·1)	15·4 (± 20·6)	16·8 (± 17·8)
All stations	August	60	1·0 (± 0·1)	11·9 (± 10·5)	12·7 (± 8·3)
Vistula and rivers mouth	August	9	1·14(± 0·11)	27·9 (± 22·1)	25·2 (± 17·3)
All stations	September	106	0·99(<0·12)	9·4 (± 3·2)	11·11(± 3·7)
Pomeranian Bay	September	12	1·19(± 0·14)	15·86(± 5·9)	17·7 (± 6·7)
Slupia plume[a]	September	20	1·1 (± 0·14)	9·1 (± 1·4)	11·2 (± 1·2)
Gulf of Gdansk	September	15	0·92(± 0·09)	9·6 (± 2·5)	9·3 (± 1·1)
Open sea and other coastal areas	September	59	0·97(± 0·12)	8·17(± 0·8)	9·78(± 1·05)

[a]Slupia plume refers to the stations 18, 19 and 20.
N.FL.U., normalized fluorescence units.
S.FL.U., standardized fluorescence units.

4 °C). When considering only the surface water for all the surveys, a significant dependency of aCDOM on salinity is observed (r=0·89) as shown in [Figure 4(c)] so reflecting the conservative properties of CDOM in surface waters. The correlation should be considered as acceptable when the very low salinity gradients of the Baltic sea (2–8) with respect to the other seas (0–37) is taken into account and also the irregular distribution of the points. The derived regression equation is:

$$\text{aCDOM}(355) = 9{\cdot}87(\pm 0{\cdot}5) - 1{\cdot}15(\pm 0{\cdot}07)\ [\text{SAL}] \quad (4)$$

where SAL is the salinity in practical salinity units. Table 2 shows the averaged (per area and per season) fluorescence data obtained following the two different methods described. In addition to the variables discussed above, the data set presented also includes an estimate of quantum yield computed using the relationship (Green & Blough, 1994):

$$\varphi_s(\lambda) = [F_s(\lambda) \times a_{qs} \times \varphi_{qs}]/[a_s(\lambda) \times F_{qs}] \quad (5)$$

where subscripts s and qs refer to the sample and quinine sulphate reference (0·5 mg l^{-1} in 0·1 N H_2SO_4 which give an a_s=1·5 m^{-1} at 355 nm), respectively and $a(\lambda)$ is the absorption coefficient of each of the samples where λ in this case is 355 nm. The integration of the fluorescence emission, F (355 nm) is performed instrumentally between 420 and 460 nm. The quantum yield φ_{qs} is typically 0·51. Values for the slope S1 (shown in Table 1) are measured in the range 355–420 nm. In this range all of the samples show a signal measurable with good accuracy, whereas at the longer wavelengths the signal is low and may be affected by subparticle (less than 0·22 μ) residual scattering. S2 is measured in the spectral range 400–600 nm subtracting, when existing, the baseline at 600 nm. This residual absorption is generally attributed to the subparticle backscattering. This correction is not applied in case of high CDOM absorption values (>2·5 m^{-1} at 355 nm) of stations located close to the river mouths, rich in soluble humic matter where the absorbance is measurable even at 700 nm. For April stations no. 13, 25 and 26 (see Figure 1) and for a solution of humic acid (Fluka), the absorption at 600 nm represented 2–3% of that at 355 nm. The slope S1 has been found largely invariant despite the different sample collection areas and highly varying CDOM absorption. A seasonal change is evident for the samples collected in September where the slope is slightly lower. This variation, at the end of the summer, may reflect an effect due to photobleaching of the CDOM structure in the surface layer (Miller, 1994; Zhou & Mopper, 1997) considering that the averaged solar irradiation, measured during the cruises with a Kipp-Zonen CM-5 pyranometer, had mean values of 600 for April, 715 for August and 560 W m^{-2} for September measured at 1100h GMT (Ooms, 1996). The constant nature of the spectral slope S (0·0197 ± 0·0008) in spring-summertime allows extrapolation the absorption at 412 nm which is the dedicated band sensitive to CDOM absorption of the SeaWiFS satellite sensor. The data from September would suggest

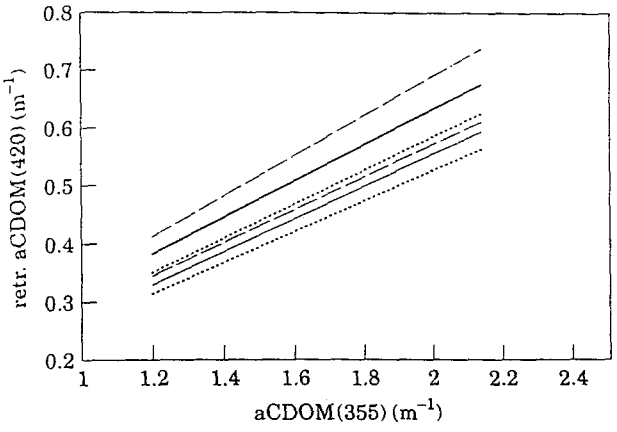

FIGURE 5. Derivation of aCDOM at 420 nm from the data at 355 nm, using S=0·0197 (average of April and August data) and S=0·018 (September data) with the respective standard deviations. ——, slope 0·0197; · · ·, SD; ——, slope 0·018; – – –, SD. CDOM, chromophoric dissolved organic matter.

the need to use a different slope (0·0177 ± 0·0014) in such extrapolation, although, with respect to 0·0197, the error would be ~12%, with an overlapping of the respective error bands as shown in Figure 5.

For all the samples the relationship between aCDOM at 355 nm and the corresponding optimal fluorescence emission at 430 nm (excited at 355 nm) are shown in Figures 6 and 7. The fluorescence, measured using the first method as defined by Hoge *et al.* (1993) and expressed by Equation 2, shows a linear dependency with the absorption as illustrated in Figure 6 (a–d). Similarly, Figure 7(a–d) show the same relationships with the fluorescence measured with the second method (according to Equation 3).

The CDOM absorption can be derived from equations of the form:

$$\text{aCDOM}(355) = A + B\,Fn(355) \qquad (6)$$

when the fluorescence is normalized with method 1 or:

$$\text{aCDOM}(355) = A + B\,Fs(355) \qquad (7)$$

when the fluorescence is standardized with method 2.

Table 3 lists various values for the intercepts, slopes (A and B), relative standard deviations and correlation coefficients for selected subsets within the data set. These include the entire data set (all stations and all depths) for April, August and September 1994. The lack of data in the aCDOM=0–1·3 m^{-1} range, is important in the statistical output of the intercepts and is reflected in the relative standard deviations. However, the values for slope B and their relative standard deviations (mean=3%) show a greater consistency. The correlation coefficients shown in Tables 3 and 4 are also extremely high apart from those of the open sea where no significant correlation was found. This is, however, explained by the fact that there is almost no variability in the fluorescence and aCDOM when this data set is considered independently. Furthermore it was found, when the best fit line for the whole data set was compared to a best fit line for the subset excluding the higher values from stations 25 and 26, that the slope was essentially the same for both method 1 and method 2. Additionally, using method 2, the relationship was the same even when the higher values (for samples from river mouths and their vicinities) were excluded. These differences in the two methods can be explained by the fact that in method 2, the fluorescence data were corrected for the self-absorption effect as described in Ferrari and Tassan (1991). This correction is particularly sensitive for the fluorescence data obtained ratioing to the Raman signal (method 1) because the Raman peak, which is difficult to extract from the spectrum especially for samples with high levels of aCDOM, must be corrected. Conversely the correction is more effective and has greater accuracy for the fluorescence data processed using method 2 which uses only the main fluorescence peak for standardization.

Discussions and conclusions

The results show that CDOM absorption values are significantly correlated with the salinity in surface waters. The dependency is especially evident throughout the water column in spring during periods of increased vertical mixing and with a large input from continental runoff, and also in other seasons, at stations located at the mouths of rivers. On the other hand, if the summertime situation is considered, with strong stratification on the water column, the salinity appears to be independent of the level of CDOM absorption which displays little variability (1·77 ± 0·5 and 1·75 ± 0·45 m^{-1} at 355 nm, for August and September, respectively), as well as in correspondence of strong hydrographic vertical discontinuity such as the halocline and thermocline. The significance of the correlation between CDOM absorption and salinity found in surface waters, lies in the fact that from the point of view of remote sensing, only the surface layer is observed by the remote sensors in the bands used for CDOM detection. Therefore the

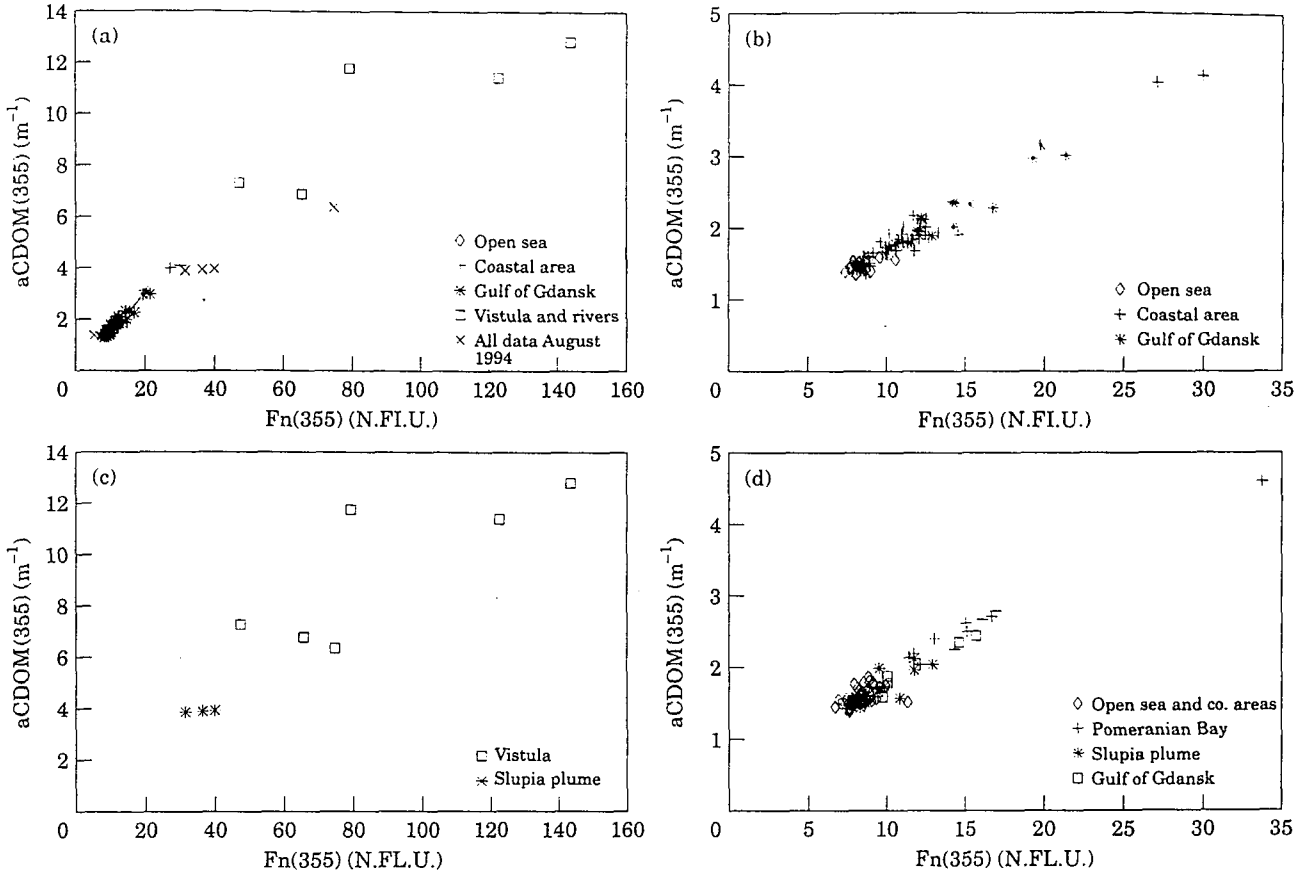

FIGURE 6. (a) Regression plot of aCDOM *vs* Fn (355) calculated using method 1 (Hoge *et al.*, 1993) for all stations of April and August subdivided per geographic site. (b) as (a) excluding the data of August and these of the rivers plumes. (c) as (a) with only the data of the river plumes. (d) as (a) regarding the data of September. CDOM, chromophoric dissolved organic matter; N.FL.U., normalized fluorescence units.

semi-conservative nature of CDOM with respect to salinity would imply that its use as a passive tracer of fresh water input and therefore local hydrography in this region is supported. It is however obvious that although this relationship exists, it is purely a local relationship which does not coincide with the more general relationships identified to date (Doerffer *et al.*, 1995). This is undoubtedly due to the high gradient of CDOM in the Baltic and relatively low gradient of salinity, which is the inverse condition found in other European marine coastal waters.

The spectral slope S (Equation 1) obtained between 355 and 420 nm, has been found to have a slight seasonal dependency; 0·0197 (± 0·0008) in April and August 0·0177 (± 0·0014) for September, but it seems to be independent of the geographical site. Moreover, the spectral absorption characteristics of CDOM are not strictly dependent on the various sources and on the total amount of CDOM for the area investigated. S can therefore be used to extrapolate CDOM absorption at 412 nm, with an error varying from 4·5 to 5·4% for the slope S=0·0197 and from 6·5 to 9% for the slope S=0·0177 according to the respective standard deviations (Figure 5), when it is difficult to derive it directly because of the low instrumental sensitivity in the case of 'sea truth' investigation for local/seasonal algorithms development. The results presented in this study confirm that CDOM absorption can be derived from standardized fluorescence measurements using a general expression that appears to be valid for diverse marine and coastal waters. Data coming from different environments in different seasons can be described by a single expression relating fluorescence to absorption. In fact using method 2, the values of the slope B (Table 4) are 0·113 (± 0·001), 0·102 (± 0·002) and 0·116 (± 0·006) for all of the stations in April, August and September, respectively. The intercepts A show a larger variability, mainly due to the lack of low aCDOM data (0–1 m^{-1}), while a general observation is that, if the high river values are removed, the intercept increases. This variation can be explained by

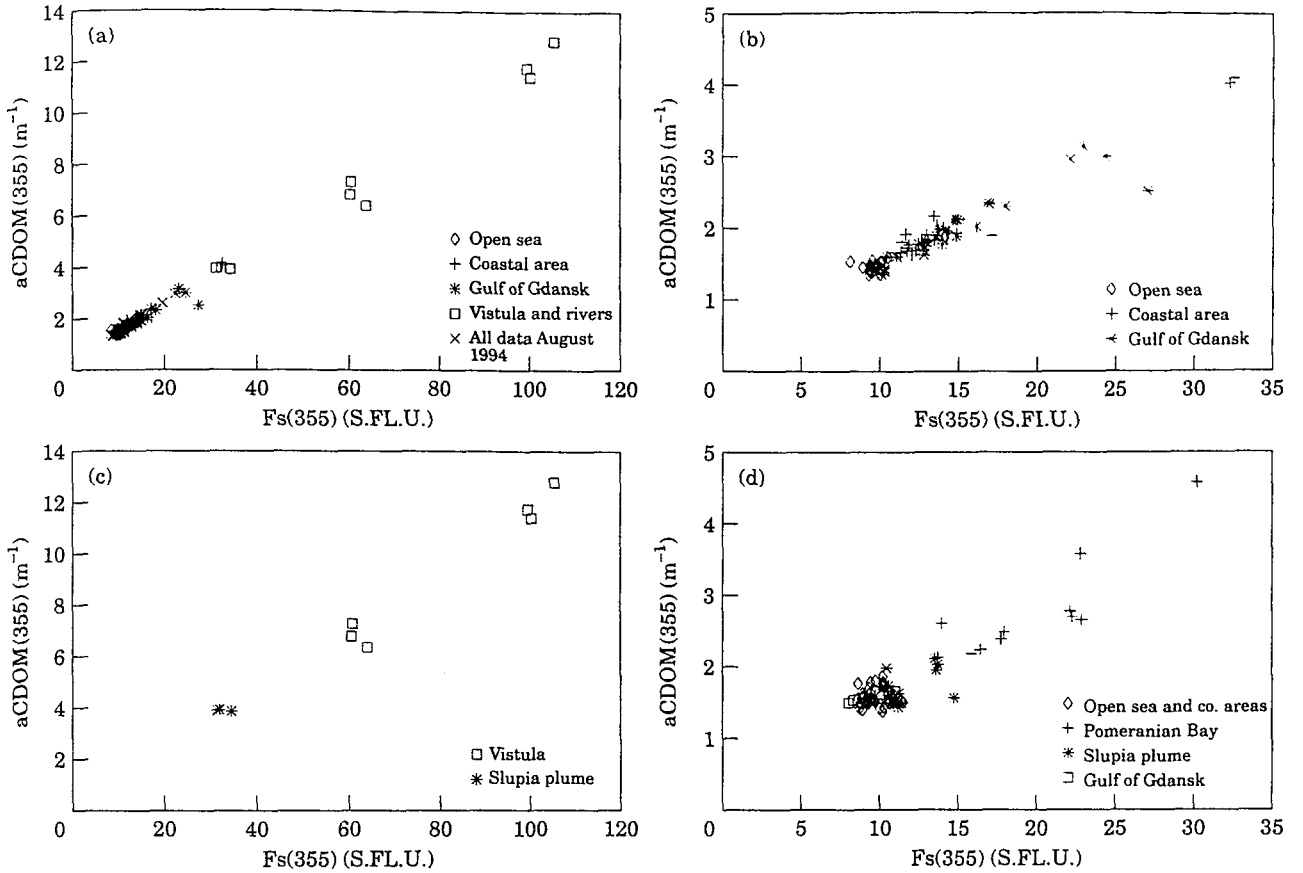

FIGURE 7. (a), (b), (c) and (d). As Figure 6, using the data calculated with method 2 introduced in this work. CDOM, chromophoric dissolved organic matter; S.FL.U., standardized fluorescence units.

the diminished contribution to the CDOM pool due to riverine and estuarine sources which are characterized by a high quantum yield of CDOM (see Table 2). The quantum yield data explain the high intercepts of the regression analysis for all of the stations of August (A=0·54) and September (A=0·4) with an averaged quantum yield of 1 and 0·99 respectively, whereas the averaged intercept for the April was lower (0·32) and the relative quantum yield was 1·2. Using method 1 the slope B varies from 0·078 (± 0·002) in August to 0·125 (± 0·037) in September (Table 3). The considerations made above on the intercepts for method 2 are also valid for method 1 for the subset excluding the highly fluorescent values; this discrepancy is due to the possible overestimation of the fluorescence and also to the limited number of samples in this set [Figure 6(c)].

This result confirms the capability and adequacy of both the methods to calculate the absorption coefficient using a simple fluorescence equation, despite the different properties of a variety of CDOM absorptions. However, for the Baltic Sea as well as for other enclosed and semi-enclosed seas and coastal regions characterized by high levels of CDOM, the method defined by Hoge require a correction for the self absorption effect, especially for the water Raman peak when values of CDOM are greater than 3 m^{-1} at 355 nm. Furthermore, dilution of highly fluorescent/absorbent samples are not appropriate since the fluorescence responses, because of the self absorption, have been found non-linear with respect to dilution. The update method originally proposed by Ferrari and Tassan (1991), here referred to as method 2 allows the whole range of fluorescence and absorption values to be described by a linear equation which has high correlation coefficients (Table 4). Given that method 2 has covered an extended area of the Baltic proper including the river plumes, it can be proposed to obtain CDOM absorption data to be used to validate direct or inverse radiative transfer numerical models to generate, among the other water components or water leaving radiances, CDOM absorption and at least DOC concentrations. The estimation of total DOC concentration through CDOM absorption is

TABLE 3. Coefficient A and B with respective standard deviations and r of correlation of the regression equations between CDOM absorption at 355 nm and fluorescence calculated by method 1

Subset description	Month (1994)	Number of samples	Regression equations	Correlation coefficient (r)
Open sea	April	23		0·44
Coastal area	April	37	aCDOM(355)=0·46(±0·059)+0·124(±0·005)Fn(355)	0·97
Gulf of Gdansk	April	32	aCDOM(355)=0·93(±0·178)+0·093(±0·004)Fn(355)	0·62
Gulf of Gdansk except the stations 25 and 26	April	27	aCDOM(355)=0·42(±0·089)+0·127(±0·007)Fn(355)	0·96
All stations	April	121	aCDOM(355)=0·79(±0·06)+0·094(±0·025)Fn(355)	0·97
All stations	August	97	aCDOM(355)=0·87(±0·03)+0·078(±0·002)Fn(355)	0·98
Vistula and rivers mouth	August	9	aCDOM(355)=1·8(±0·12)+0·08(±0·015)Fn(355)	0·89
All stations	September	106	aCDOM(355)=0·54(±0·036)+0·125(±0·037)Fn(355)	0·98
Pomeranian Bay	September	12	aCDOM(355)=0·87(±0·092)+0·11(±0·005)Fn(355)	0·98

TABLE 4. Coefficient A and B with respective standard deviations and r of correlation of the regression equations between CDOM absorption at 355 nm and fluorescence calculated by method 2

Subset description	Month	Number of samples	Regression equations	Correlation coefficient (r)
Open sea	April 1994	23		0·4
Coastal area	April 1994	37	aCDOM(355)=0·35(±0·055)+0·113(±0·003)Fs(355)	0·98
Gulf of Gdansk	April 1994	32	aCDOM(355)=0·22(±0·07)+0·113(±0·002)Fs(355)	0·99
Gulf of Gdansk except the stations 25 and 26	April 1994	27	aCDOM(355)=0·43(±0·14)+0·104(±0·008)Fs(355)	0·99
All stations	April 1994	121	aCDOM(355)=0·32(±0·03)+0·113(±0·01)Fs(355)	0·99
All stations	August 1994	97	aCDOM(355)=0·54(±0·03)+0·102(±0·002)Fs(355)	0·99
Vistula and rivers mouth	August 1994	9	aCDOM(355)=0·021(±0·42)+0·116(±0·006)Fs(355)	0·99
All stations	September 1994	106	aCDOM(355)=0·4(±0·068)+0·116(±0·006)Fs(355)	0·91
Pomeranian Bay	September 1994	12	aCDOM(355)=0·28(±0·58)+0·127(±0·028)Fs(355)	0·86
North Sea and Atlantic Coasts	April 1997	>100	aCDOM(355)=0·06(±0·058)+0·14(±0·003)Fs(355)	0·98

possible only when the non-absorbing DOM is constant or a low variable in the environment studied. This aspect is, at present, poorly investigated and requires further study. Recent works have demonstrated that relative to the areas and seasons investigated, CDOM absorption (or CDOM fluorescence) can be used to infer DOC concentration (Vodacek *et al.*, 1995; Ferrari *et al.*, 1996). This opens the possibility for using R/S products (active or passive aCDOM on large areas) to assess DOC concentration in surface marine waters. The potential of CDOM as passive tracer, in the study area considered, was illustrated inferring that synoptic thematic maps of surface CDOM absorption should provide a good indication of surface patterns and especially of freshwater dispersion.

Acknowledgements

The authors would like to thank S. Boxall (University of Southampton), S. Kaczmarek (Polish Academy of Science) and S. Tassan (JRC Ispra) for their support and useful suggestions during the preparation of the manuscript. The fieldwork was carried out onboard RV *Oceania* as part of a collaboration between the institute of Oceanology, Polish Academy of Science and the Institute for Remote Sensing Applications, JRC Ispra.

References

Bascastow, R. & Maier-Reimer, E. 1991 Dissolved organic carbon in modelling oceanic new production. *Global Biogeochemical Cycles* **5**, 71–85.

Bristow, M., Nielsen, D., Bundy, D. & Furtek, R. 1981 Use of water Raman emission to correct airborne laser fluorosensor data for effects of water optical attenuation. *Applied Optics* **20**, 2889–2906.

Carder, K. L., Steward, R. G., Harvey, G. R. & Ortner, P. B. 1989 Marine humic and fulvic acids and their effects on the remote sensing of ocean chlorophyll. *Limnology and Oceanography* **34**, 68–81.

Carder, K. L., Hawes, S. K., Baker, K. A., Smith, R. C., Steward, R. G. & Mitchell, B. F. 1991 Reflectance model for quantifying chlorophyll *a* in the presence of productivity degradation products. *Journal of Geophysical Research* **96**, 20 599–20 611.

Doerffer, R., Sorensen, K. & Aiken, J. 1995 MERIS: potential for coastal zone application. *Proceedings of the 21st Annual Conference of the Remote Sensing Society*. pp. 166–175.

Duursma, K. E. & Rommet, J. W. 1961 Interpretation mathematique de la fluorescence des eaux douces, saumatres et marines. *Netherlands Journal of Sea Research* **1** (3), 391–405

Ehlin, U. 1981 Hydrology of the Baltic Sea. In *The Baltic Sea*. (Voipio, A., ed.). Elsevier Scientific Publishers, pp. 125–134.

Ferrari, G. M. (ed.) 1990 Napoli 88—data catalogue CEC *Jt. Res. Centre Rep.* S.P.I.90.15. 148 pp.

Ferrari, G. M. & Tassan, S. 1991 On the accuracy of determining the light absorption by ' yellow substance ' through measurement of induced fluorescence. *Limnology and Oceanography* **36**, 777–786.

Ferrari, G. M. & Tassan, S. 1992 Evaluation of the influence of yellow substance absorption on the remote sensing of water quality in the Gulf of Naples: a case study. *International Journal of Remote Sensing* **12**, 2177–2189

Ferrari, G. M., Dowell, M. D., Grossi, S. & Targa, C. 1996 Relationship between optical properties of chromophoric dissolved organic matter and total concentration of dissolved organic carbon in the Southern Baltic Sea region. *Marine Chemistry* **55**, 299–316.

Green, S. A. & Blough, N. V. 1994 Optical absorption and fluorescence properties of chromophoric dissolved organic matter in natural waters. *Limnology and Oceanography* **38**, 1903–1916.

Hoge, F. E. & Swift, R. N. 1981 Airborne simultaneous spectroscopic detection of laser-induced water-Raman backscatter and fluorescence from chlorophyll a and other naturally occurring pigments. *Applied Optics* **20**, 3197–3205.

Hoge, F. E., Vodacek, A. & Blough, N. V. 1993 Inherent optical properties of the ocean: retrieval of the absorption coefficient of chromophoric dissolved organic matter from fluorescence measurements. *Limnology and Oceanography* **38**, 1394–1402.

Hoge, F. E., Williams, M. E., Swift, R. N., Yungel, J. K. & Vodacek, A. 1995 Satellite retrieval of the absorption coefficient of chromophoric dissolved organic matter in continental margins. *Journal of Geophysical Research* **100**, 24 847–24 854

Højerslev, N. K. 1988 Natural occurrences and optical effects of Gelbstoff, *Copenhagen University Report* 50. 30 pp.

Jackson, G. A. 1993 The importance of DOC pool for primary production estimates. *ICES Marine Science Symposium* **197**, 141–148.

Kieber, R. J., Zhou, Z. & Mopper, K. 1990 Formation of carbonyl compounds from UV-induced photodegradation of humic substances in natural waters: Fate of riverine carbon in the sea. *Limnology and Oceanography* **37** (7), 1503–1515.

Lee, Z., Carder, K. L., Hawes, S. K., Steward, R. G., Peacock, T. G. & Curtiss, O. D. 1994 Model for the interpretation of hyperspectral remote-sensing reflectance. *Applied Optics* **33**, 5721–5732

Lee, Z., Carder, K. L., Peacock, T. G., Davis, C. O. & Mueller, J. L. 1996 Method to derive ocean absorption coefficients from remote-sensing reflectance. *Applied Optics* **35**, 453–462.

Miller, W. L. 1994 Recent advances in the photochemistry of natural dissolved organic matter. *Aquatic Sea Surface Photochemistry* (Helz, G. R. *et al.*, eds). Lewis, pp. 111–127.

Nyquist, G. 1979 *Investigation of Some Optical Properties of Sea-water with Special Reference to Lignin Sulfonate and Humic Substances.* Thesis at Department of Analysis and Marine Chemistry. University of Goteborg.

Ooms, M. C. (ed.) 1996 Ulisse. Baltic 93–94 data catalogue. *Commission of European Communities, Joint Research Centre*, 21020 Ispra (Va). Italy. S.P.I.96.29.

Smith, R. C. & Baker, K. S. 1981 Optical properties of clearest natural waters. *Applied Optics* **20**, 177–184.

Stewart, A. J. & Wetzel, R. G. 1981 Asymmetrical relationships between absorbance, fluorescence, and dissolved organic carbon. *Limnology and Oceanography* **26**, 590–597.

Sturm, B. 1993 CZCS data processing algorithms. In *Ocean Colour: Theory and Application in a Decade of CZCS Experience.* (Barale, V. & Schlittenhardt, P., eds) Kluwier Academic Publishers, Dordrech (NL), pp. 95–116.

Tassan, S. 1988 The effect of dissolved ' yellow substance ' on the quantitative retrieval of chlorophyll and total suspended sediment concentration from remote measurement of water colour. *International Journal of Remote Sensing* **9** (4), 787–797.

Tassan, S. & Ferrari, G. M. 1995 An alternative approach to absorption measurements of aquatic particles retained on filters. *Limnology and Oceanography* **40** (8), 1358–1368

Victorov, S. 1996 *Regional Satellite Oceanography*. Taylor & Francis.

Witex, Z. (ed.) 1993 Marine Biology (9). Structure and function of marine ecosystem in the Gdansk Basin on the basis of studies performed in 1987. *National Scientific Committee on Oceanic Research* PAW Gdansk (Poland).

Vodacek, A., Hoge, F. E., Swift, R. N., Yungel, J. K., Peltzer, E. T. & Blough, N. V. 1995 The use of in situ and airborne fluorescence measurements to determine UV adsorption coefficients and DOC concentrations in surface waters. *Limnology and Oceanography* **40**, 411–415.

Zhou, X. & Mopper, K. 1997 Photochemical production of low-molecular-weight carbonyl compounds in seawater and surface microlayer and their air-sea exchange. *Marine Chemistry* **56**, 201–213.

Appendix 2.C

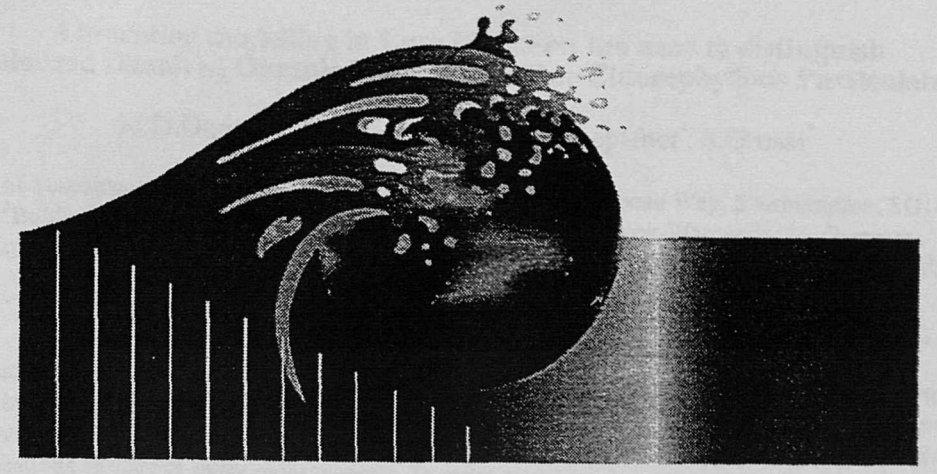

Reprinted from

OCEAN OPTICS XIII

22–25 October 1996
Halifax, Nova Scotia, Canada

SPIE Volume 2963

Absorption modelling in Case II waters: the need to distinguish Coloured Dissolved Organic Matter from Non-Chlorophyllous Particulates.

M.D.Dowell[1*], J-F.Berthon[2*] and N.Hoepffner[*], S.Grossi[*]

[1]University of Southampton, Southampton Oceanography Centre, European Way, Southampton, SO14 3HZ, UK
[2]Baltic Sea Research Institute, Seestrasse 15, D-18119 Rostock-Warnemünde, Germany.
[*]Marine Environment Unit, Space Applications Institute, JRC Ispra Site, TP272, Ispra, I-21020, (VA), Italy.

ABSTRACT

The presented study examines, for substantial datasets in different Case II waters, the variability of the spectral absorption of Non Chlorophyllous Particles (NCP) and Coloured Dissolved Organic Matter (CDOM). The investigation has considered the validity of the currently proposed modelling of the absorption of these two components as a single variable, in applications to Case II water environments. In order to encompass a broad range of environmental situations (within coastal Case II waters) in the comparison of NCP and CDOM absorption spectra, two very different sites were selected. The locations investigated were the Southern Baltic Proper and a site in the Northern Adriatic close to the Italian coast. These two regions differ both in their basic oceanographic properties and in their relative proportions of Optically Active Components (OAC). Furthermore, the datasets considered illustrate the variability at different scales in both space and time, combining a series of seasonal oceanographic campaigns in the Baltic with a complete annual timeseries of monthly measurements at a fixed point in the Adriatic. The analysis has shown that, in the selected European Case II waters, the observed variability of the spectral absorption of NCP and CDOM, both with respect to each other as well as to the total absorption, are independent. It is therefore suggested that, in the frame of Reflectance modelling in Case II waters, attention must be placed on accounting for NCP and CDOM individually when defining the absorption segment.

Keywords: Absorption modelling, Case II waters, Inherent Optical Properties, Coloured Dissolved Organic Matter, Non Chlorophyllous Particles, Baltic, Adriatic.

1. INTRODUCTION

A general formulation relating Reflectance (R) to the Inherent Optical Properties: absorption (a) and backscattering (b_b) was defined by Gordon et. al.[1] through Monte Carlo simulation:

$$R = f \times \frac{b_b}{a + b_b}$$

in general a >> b_b (except in very turbid sediment laden waters e.g. certain parts of the Northern Sea) and therefore, as described by Morel and Prieur[2] $R=f*b_b/a$ where these authors found f to be equal to 0.33 (this value has since proven to be variable[3] and dependent on water composition and illumination conditions).
The absorption segment of the above relationship has it's own budget, comprising of n components which are linearly related so that:

$$a_{TOT}(\lambda) = \sum_{i=1}^{n} ai(\lambda)$$

where the overall budget has been shown to be adequately described by the following components in different investigations (e.g. Sathyendranath et. al. 1989[4]):

$$a_{TOT}(\lambda) = a_{CPIG}(\lambda) + a_{NCP}(\lambda) + a_{CDOM}(\lambda) + a_w(\lambda)$$

the subscripts TOT, CPIG, NCP, CDOM and w refer to different sections of the absorption segment namely Total, Chlorophyll like Pigments, Non-Chlorophyllous Particulates, Coloured Dissolved Organic Matter and water respectively. Some authors have tried to refine this differentiation even further such as Bukata[5] who proposed a four component model excluding water which he also differentiated the NCP fraction into organic and inorganic particulates.

However, recently several authors have proposed what have been termed as two component models[6,7] in which the modelisation of the absorption of the above relationship is defined by two components CPIG and DP (Detrital Products),

where DP are a combination of NCP and CDOM. These modelisations of absorption were principally defined for Case I (oceanic) waters however there validity must also be tested in Case II (coastal) waters. The principle rational behind the grouping together of these two components in the above mentioned model is that apart from the fact (purely by the definition of Case I waters) that in the open ocean these two components covary implicitly with CPIGS, a fact which has recently been explicitly used[8] in defining an expression for retrieving DP in Case I waters, is that these two components are very similar spectrally in their absorption properties. More specifically both of these components can be adequately (or have been shown to be to date) described by an exponential decay fit (e.g. Roesler (1995)[9]), although recent comparisons with Target Factor Analysis[10] have shown that the RMS error on the determinations of the fit can be improved, with such techniques.

The principle objective of the current study is to present a series of quality datasets for different geographic regions in predominantly Case II waters (although the Adriatic platform is considered as being in certain seasons Case I). The data are continuous measurements of spectral absorption in the range 400 to 700nm for CPIG, NCP and CDOM. These datasets will therefore allow the authors to accomplish the following analyses. An investigation and description of the variability of spectral shape and amplitude for the two sites selected (Baltic and Adriatic) of the three components (CPIG, NCP and CDOM). Subsequently, considerations will be made on the contribution of each of the components to the total a(λ) budget, considering site and seasonal variations. Finally the best exponential fits for all CDOM and NCP spectra are determined and a study, of both the slope and a specific value of absorption for the two types of spectra through analyses of variance and covariance for the two locations, is undertaken.

2. METHODS, SITES AND SAMPLING

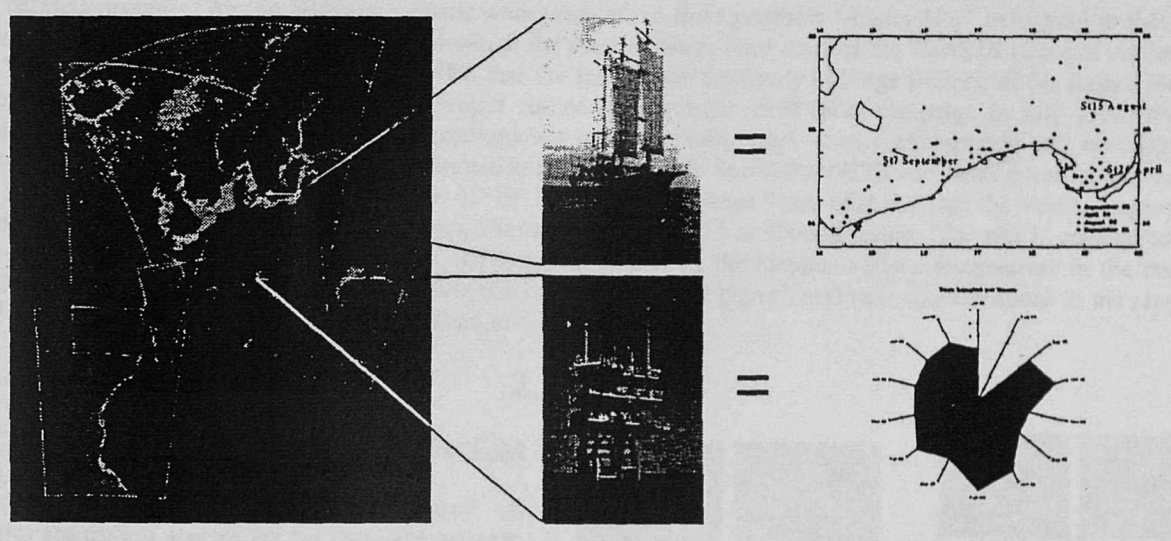

Figure 1: CZCS 7 year composite showing sites, station maps and sampling times

2.1. Methods

The samples for CDOM were filtered through 0.22μm Millipore filters and were stored in glass amber bottles at 4°C with the addition of 0.5ml of NaN_3 (sodium azide) as an inhibitor of anaerobic growth all samples were analyzed within one week of collection (within time determined by predefined protocol[11]). A Perkin Elmer Lambda 19 dual beam spectrophotometer with a 10 cm quartz cuvette was used to determine the absorption spectra of the sample (MilliQ water was used as a blank). In the investigations described here the measurements were made in the range 350 to 700nm, with a spectral resolution of 1nm. Absorbance was subsequently converted into absorption coefficient (m^{-1}) using the expression:

$$a_{CDOM}(\lambda) = 2.3 \times A(\lambda) / L$$

where A(λ) is the Absorbance (optical density) and L is the pathlength in metres (i.e. L=0.1 in our analyses).

Absorption measurement for CPIG and NCP were not carried out with the standard solvent extraction process for pigment removal on glass fibre filters, but an alternative approach specifically designed for Case II waters was used to account for possibly high suspended sediment concentrations. The filtrations were made on Whatmann GFF (Glass Fibre Filters), the samples were then frozen in liquid nitrogen and put in the freezer at -20°C on return to the laboratory. The measurements were made as for the CDOM with a Perkin Elmer Lambda 19 dual beam spectrophotometer equipped with a 60mm integrating sphere , so as to remove the spurious contribution to the measured absorption caused by the sample backscattering. The Chlorophyll pigment spectra was extracted from the total particulate absorption spectra by bleaching the sample with a NaClO solution allowing for a depigmentation of the particles. The pigment spectra is therefore obtained by subtracting the bleached Non-Chlorophyllous Particles from the total absorption spectra. Further details on this alternative technique are given by Tassan and Ferrari[12] .The absorption spectra of the particles retained on the filter are converted into an equivalent particle suspension absorption, using an empirical expression defined in the above mentioned study:

2.2. Sites and Sampling

The dataset presented here for the Southern Baltic Region (as shown in Figure 1) are the result of a collaborative agreement between the Institute of Oceanology of the Polish Academy of Science and the then Institute for Remote Sensing Applications (now Space Applications Institute (SAI)) of the Joint Research Centre in Ispra. Four cruises were carried out on-board *r/v Oceania* one in September 1993 and three in 1994 (April, August and September). Station positions (as in Figure 1) were not fixed before the campaigns, and a principle aim was to collect a dataset representing the largest possible gradients in the measured parameters in order to adequately characterize the notable contribution by terrestrial inputs as well as the marine autochtonous contribution.

The datasets presented for the Northern Adriatic were taken at the fixed platform *"Acqua Alta"* belonging to the Italian National Research Council. The project under which the measurements were made is the CoASTS (Coastal Atmosphere and Sea Time-Series) project[13] between SAI JRC and the Institute for the Study of Large Masses, of the Italian National Research Council in Venice. The CoASTS project started in September 1995 (pilot campaign in July 1995) and will continue until September 1997. Monthly campaigns are made involving high quality atmospheric and oceanographic (bio-optic) measurements to support calibration/validation activities for SeaWiFS, OCTS and MOS ocean colour sensors. The site itself is at the geographic position lat. 45°19' long. 12°30' at about 30km offshore from the Venice Lagoon. The region is, depending on the prevailing currents, characterised by Case I or Case II waters. The site is considered to be well representative of the entire Adriatic Sea. Some typical values for the location include temperature in the range 4-26°C, salinity: 32-36 ppt., chlorophyll concentrations in the range 0.1-2 mg/m^3, sediment concentrations in the range 1-5 g/m^3 and CDOM absorption coefficients at 400nm of 0.07-0.45m^{-1}.

3. RESULTS

3.1. The variability of shape and magnitude of the three components

Figure 2 represents specific and normalised (at 440nm) absorption spectra for the three components. For both the considered sites these show a reasonable degree of variability both in magnitude and for the CDOM and NCP spectra in shape as well. However, the NCP and CDOM spectra do appear to maintain the standard exponential decay general attributed to them. In the CPIG spectra there is less variability in the overall shape and the largest variability in overall magnitude seems to be at the two peaks in the blue 443nm and in the red at about 670 nm. The slight deviation from the mean trend of the CPIG absorption spectra which occurs around 420nm for some particular stations seems to coincide samples during highly productive circumstance.

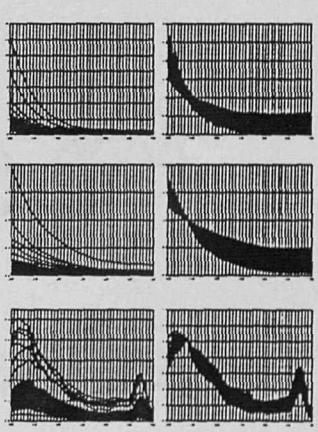

Figure 2a: Baltic absorption spectra

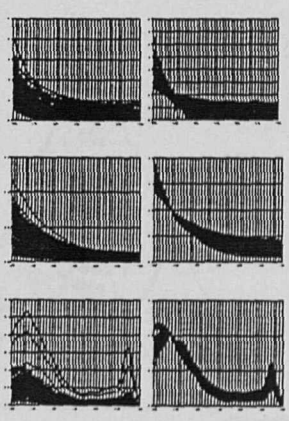

Figure 2b: Adriatic absorption spectra

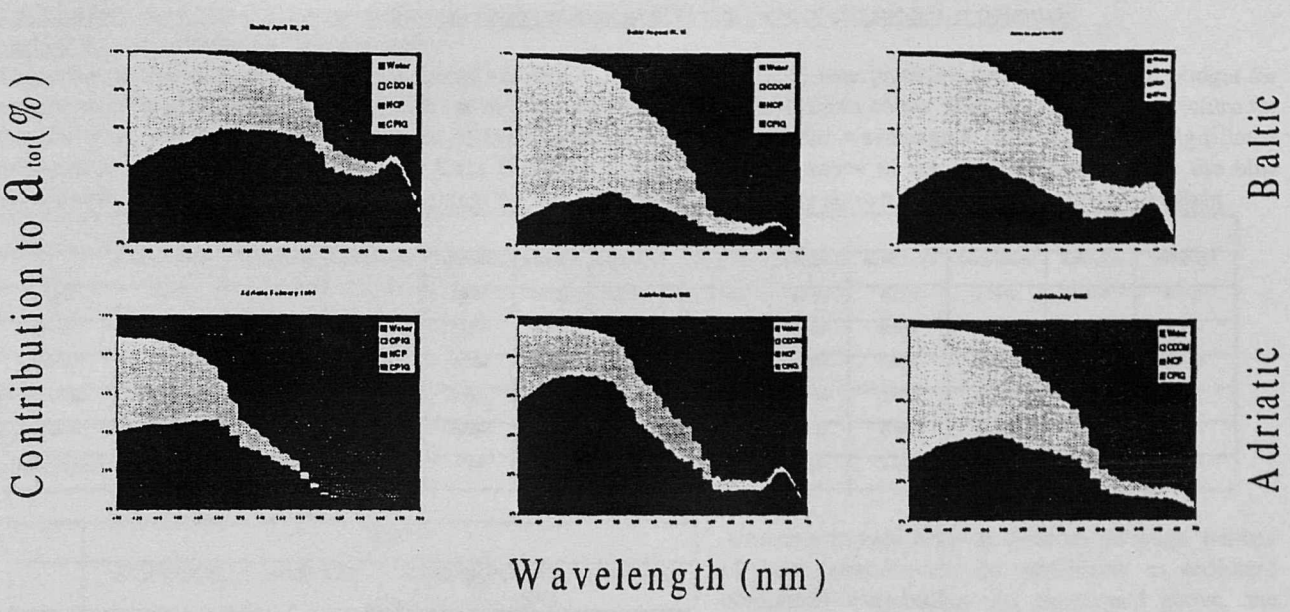

Figure 3: % contribution to the total absorption of the three components

3.2. The relative contribution of the three components to the total absorption

Figure 3 shows plots illustrating the contribution of the three components to the total absorption as a percentage of the total absorption including water (three for the Baltic and three for the Adriatic). The stations included as Baltic examples have been highlighted on the map in Figure 1. Several significant points are quite obvious from these plots: firstly it is apparent that there exists a large variability in the contribution of the individual components to the total absorption. These differences are apparent both on seasonal and geographical (for the Baltic) scales. The dominant component in total absorption budget may vary significantly from one season to another. For example, although CDOM is the dominant constituent in the Baltic, the plot for station 26 in April would seem to suggest that there is a significant contribution by the NCP as well especially in the green area of the spectrum. For the Adriatic plot, an interesting combination is presented. In each of the graphs shown (February, March and July) different dominant constituents are observed. Thus, this highlighting the strong seasonal variation in the absorption budget, with NCP absorption dominating in the Winter month (February), CPIG absorption in spring during the bloom period and CDOM absorbing more during the summer.

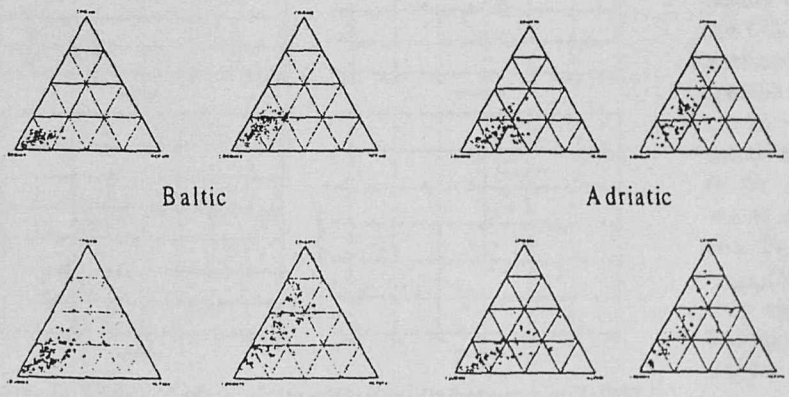

Figure 4: Ternary plot for the two sites

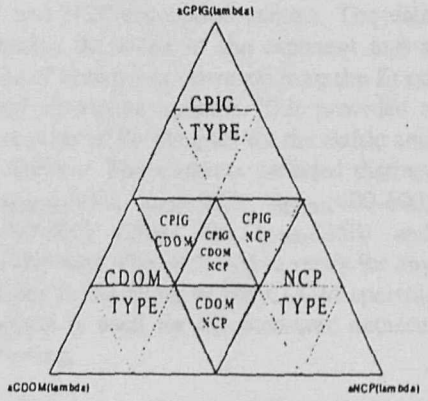

Figure 4 b proposed classification

3.3. Mixture plots: considerations on the absorption budget in different parts of the spectra, a potential method for sub-classifying Case II waters

The investigation using ternary/mixture plots has shown to be most useful in interpretations of the absorption budget for specific wavelengths here coinciding with (or near to) channels from typical ocean-colour sensors .The general picture for the two sites would seem to prominence of the variability shown in the red wavelengths (this may be of significant importance in Reflectance modelling of Case II coastal waters). The dominance of the CDOM absorption at the blue wavelength for the Baltic and to a lesser extent for the Adriatic is quite clearly shown. For both sites, there is a slight

	Baltic						Adriatic					
	A350(CDOM)	S350(CDOM)	A400(CDOM)	S400(CDOM)	A400(NCP)	S400(NCP)	A350(CDOM)	S350(CDOM)	A400(CDOM)	S400(CDOM)	A400(NCP)	S400(NCP)
Mean	3.2763	0.0212	1.1668	0.0188	0.1528	0.0116	0.3498	0.0186	0.1406	0.0176	0.0478	0.0135
Std. Dev.	3.9888	0.0017	1.5682	0.0029	0.2178	0.0026	0.1683	0.0029	0.0583	0.0044	0.0252	0.0026
Variance	15.9107	0.0000	2.4594	0.0000	0.0474	0.0000	0.0283	0.0000	0.0034	0.0000	0.0006	0.0000
Minimum	1.3871	0.0183	0.4781	0.0081	0.0353	0.0049	0.1372	0.0106	0.0520	0.0101	0.0070	0.0088
Maximum	30.2913	0.0280	12.1913	0.0254	1.7977	0.0168	1.0282	0.0281	0.3746	0.0258	0.1267	0.0191
Coeff. of Variation	1.2175	0.0806	1.3441	0.1548	1.4251	0.2288	0.4810	0.1585	0.4145	0.2487	0.5271	0.1898

	Baltic	
	aCDOM(400) vs. aNCP(400)	SCDOM(400-600) vs. SNCP(400-600)
No. Obs.	88	88
F	51.85	3.21
Fcrit	1.42	1.42
	Adriatic	
	aCDOM(400) vs. aNCP(400)	SCDOM(400-600) vs. SNCP(400-600)
No. Obs.	64	64
F	5.35	2.89
Fcrit	1.52	1.52

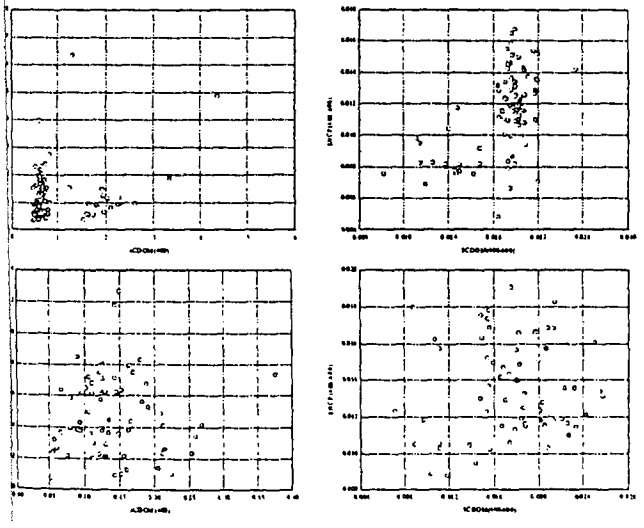

Figure 5: 1Scatter plots of the relationship between aCDOM and aNCP

tendency toward NCP at 550nm, although neither of these locations can be considered as sediment dominated waterbodies. As mentioned above, the plot for 670nm shows the largest degree of variability for the datasets considered although the values are concentrated on the CDOM CPIG side of the plot. Ensuing the use of mixture plots in this investigation, it is suggested that, their use may be useful for classification purposes. This technique, already proposed by Prieur and Sathyendranath[14] for a generic marine classification, has here shown its value in sub-classifying Case II waters. Figure 4b shows the proposed classification scheme using the nomenclature adopted in this investigation.

3.4. The variance of a_{CDOM} and a_{NCP} and their covariance with a_{TOT}

Figure 5 shows tables and graphs illustrating the results from the statistical analysis carried out on the CDOM and NCP absorption spectra. The data analysed involve the slope of the exponent and a specific value of absorption retrieved from the fit on the measured absorption spectra. This provided a substantial data set of 88 samples for the Baltic and 64 for the Adriatic. The datasets included distinct values of $a_{CDOM}(400)$, $a_{NCP}(400)$, $S_{CDOM}(400\text{-}600)$ and $S_{NCP}(400\text{-}600)$ values for $a_{CDOM}(350)$ and $S_{CDOM}(350\text{-}400)$ were also included to verify for any large variations in the slope of the CDOM spectra. The exponential fit used for the measured datasets was the following:

$$a_{CDOM}(\lambda) = a_{CDOM}(\lambda_o) \times e^{(-S(\lambda-\lambda_0))} + C$$

for CDOM, and:

$$a_{NCP}(\lambda) = a_{NCP}(\lambda_0) \times e^{(-S(\lambda-\lambda_0))}$$

for NCP. Here λ_0 and S refer to the values of the specific absorption coefficient and the slope respectively. The value C in the fit for CDOM absorption represents a constant included to improve the fit, and which is proportional to the baseline occurring in the red part of the spectra. This feature is not included in the subsequent analysis as it is interpreted as being an artifactual contribution resulting from instrumental noise or very fine particles (in fact this feature is further minimized by refilteration through 0.1μm nucleopore filter).The results from the statistical analysis indicate some very clear findings, namely that there is little or no common relationship in variability between the both the specific value of absorption and the slopes of the two datasets (NCP and CDOM). This is shown under many different forms, principally by the large scatter shown in the plots and the results from the F-test in which the calculated values of F are consistently higher than F_{crit} there rejecting the null hypothesis (varCDOM=varNCP).

4.CONCLUSIONS AND FUTURE WORK

4.1.Conclusions

The presented study has shown the need to independently describe the contributions to the total absorption budget of surface Case II waters by NCP and CDOM. The ranges means and standard deviations found are is some cases substantially different to those presented in literature, indicating that allocating a mean slope in the modelisation of the absorption of these parameters may represent a considerable source of error. The results have further shown the importance of these two components in the composition of Case II waters, where either of these constituents can prove to be dominant in the budget of the total absorption. The analyses of the variance coefficients has shown that it is incorrect to assume the covariability of the two components or that there is a seasonal variability as there are strong gradients in the variables considered for the two datasets showing no relationship whatsoever (within 95% confidence levels).

The results from the ternary/mixture plots has indicated the potential of 670nm, and the red part of the spectra in general, in describing and differentiating the different components (this has already indirectly been observed in Case II waters through the development of empirical algorithms[15]). This fact is obviously of considerable importance in the formulation of models for water bodies exhibiting a large degree of variability of the three components. However, assurances must be given on data quality for this part of the spectra, with considerations made on noise and contamination effects.

Therefore in conclusion the results would infer that it is necessary to account for NCP and CDOM absorption distinctly when developing forward reflectance models for waters determined as being Case II. And that although a balance must be maintained between the accuracy of the definition of each individual component in the forward reflectance model with the minimisation of the unknowns in the IOPs for inversion. The considerable importance of terrigenous and atmospheric inputs, both particulate and dissolved, mean that is these coastal regions for an accurate determination and characterisation of the OACs it may be more significant to give priority to the description of the variability of the of NCP and CDOM components and to limit the number of variables used to define the CPIG absorption. In fact it has already been shown[9] that in models dealing with localized areas which are necessary for these types of Case II waters the CPIG absorption can be adequately defined by a mean spectra and variability at one specific wavelength, Figure 2 here shows this as a possible solution for both the Adriatic and the Baltic spectra.

4.2. Future work

The presented study involves only a first part of a thorough investigation of the absorption budget in the two regions considered. Further investigations will include topics such as investigations of diverse models representing the spectral characteristics of each of the components including approaches similar to that suggested by J. Krijgsman[10] (Target Factor Analysis). A further direction in which the work will progress is a verification that the absorption calculated by the sum of the three components presented here sufficiently describes the total absorption for the areas presented (as well as others). An initial verification of the calculation of the absorption budget could be made through a simple closure experiment using a submersible multispectral absorption meter and comparing the result from this to the summation of the analyses made on the individual components as described here

5. ACKNOWLEDGMENTS

The authors wish to thank all the people who participated in the two activities which were fundamental in creating the datasets used in this investigation. In particular to the staff of the Institute of Oceanology of the Polish Academy of Science and the crew of *r/v Oceania* for the work in the Baltic and G.M.Ferrari for his work on the Baltic datasets, and to G. Zibordi responsible for coordinating the CoASTS project and D. van der Linde for his numerous trips to the platform.

6. REFERENCES

1. H. R. Gordon, O. B. Brown and M. M. Jacobs, "Computed relationships between the inherent and apparent optical properties in a flat homogeneous ocean", *Appl. Optics.* **14(2)**, 417-427. (1975).

2. A. Morel and L. Prieur, "Analysis of variations in ocean color", *Limnol. Oceanogr.* **22**, 709-722 (1977).

3. A. Morel and B. Gentili, "Diffuse reflectance of oceanic waters. II Bidirectionnal aspects", *Appl. Optics, vol.* **32**, no. 33 6865-6879 (1993).

4. S. Sathyendranath, L. Prieur and A. Morel, "A three-component model of ocean colour and its application to remote sensing of phytoplankton in coastal waters." *Int. J. Remote Sensing*, vol. **10**, No. 8, 1373-1394. (1989)

5. R. P. Bukata, J. H. Jerome, J. E. Bruton, S. C. Jain and H. H. Zwick, "Optical water quality model of Lake Ontario. 1: Determination of the optical cross sections of organic and inorganic particulates in Lake Ontario". *Appl. Opt.* **20**(9), 1696-1703, (1981)

6. K. L. Carder, S. K. Hawes, K. A. Baker, R. C. Smith, R. G. Steward and B. G. Mitchell. "Reflectance model for quantifying chlorophyll a in the presence of productivity degradation products", *J. Geophys. Res.* **96**, 20599-20611 (1991).

7. J. Aiken, G. F. Moore, C. C. Trees, S. B. Hooker and D. K. Clark, "The SeaWiFS CZCS-Type Pigment Algorithm." NASA Tech. Memo. 104566, Vol. 29, S. B. Hooker and E. R. Firestone, Eds., NASA Goddard Space Flight Center , Greenbelt, Maryland, 34 pp., (1995).

8. A. D. Giles-Guzmán and S. Alvarez-Borrego, "Covariance of the absorption of phytoplankton, colored dissolved organic matter, and detritus in case I waters, as deduced from the Coastal Zone Color Scanner bio-optical algorithm.", *Appl. Opt.*, **35**(12), 2109-2113, 1996.

9. C.S. Roesler and M.J. Perry, "In situ phytoplankton absorption, fluorescence emission, and particulate backscattering spectra determined from reflectance." *J. Geophys. Res.*, vol. **100**, No. C7,pp. 13279-13294. (1995)

10. J. Krijgsmann, *Optical Remote Sensing of Water Quality Parameters: Interpretation of Reflectance Spectra.* Delft University Press-I11. Thesis Delft University of Technology, p.198. (1994)

11. G. M. Ferrari and S. Tassan, "On the accuracy of determining light absorption by 'yellow substance' through measurement of induced fluorescence." *Limnol. Oceanogr.*, **36**, 777-786, (1991)

12. S. Tassan and G. M. Ferrari, "An alternative approach to absorption measurements of aquatic particles retained on filters", *Limnol. Oceanogr.* **40**, 1358-1368 (1995).

13. G. Zibordi, V. Barale, G. M. Ferrari, N. Hoepffner, D. van der Linde, L. Alberotanza, P. Cova and C. Ramasco, "Coastal Atmosphere and Sea Time-Series Project (CoASTS): an ocean colour remote sensing calibration/validation project." Proc. of Third Thematic Conf. on Remote Sensing for Marine and Coastal Environments, Seattle, Vol. II, pp. 96-100. (1995)

14. L. Prieur and S. Sathyendranath, "An optical classification for coastal and oceanic waters based on specific spectral absorption curves of phytoplankton pigments, dissolved organic matter , and other particulate materials." *Limnol. Oceanogr.*, **26**(4), pp.671-689. (1981)

15. H. Siegel, M. Gerth and M. Beckert. "The variations of optical properties in the Baltic Sea and algorithms for the application of remote-sensing data", Ocean Optics XII, *SPIE* **2258**, 894-905 (1994).